An Investigation into the Importance of T2 Relaxation and Echo Time Choice for Accurate Metabolite Biomarker Quantification

Dominic Alexander Carlin

A thesis submitted to the University of Birmingham
for the degree of DOCTOR OF PHILOSOPHY

Institute of Cancer and Genomics Sciences
College of Medical and Dental Sciences
University of Birmingham
September 2016

UNIVERSITYOF
BIRMINGHAM

University of Birmingham Research Archive

e-theses repository

Abstract

Metabolite concentrations are fundamental biomarkers of disease. With increasing interest in personalised medicine, this work assessed the accuracy of non-invasive metabolite quantification with magnetic resonance spectroscopy (MRS) using a combination of simulations, phantom and in vivo data. No optimal echo time (TE) was found for measuring a range of key metabolites with quantification accuracy generally influenced more by data quality than TE choice. The T2 relaxation times of water and metabolites with MRS dominated by a singlet could be estimated using 2 TEs and were found to be significantly different in paediatric brain tumours compared with normal brain, varying between tumour types. The T2 relaxation times of paediatric brain tumours were significantly shorter at 3T compared with 1.5T. Metabolite concentrations for individual patients were most affected by changes in the T2 relaxation time of water which is quick to measure. A clinical JPRESS protocol was developed which aids assignment of overlapping metabolites using changes of MRS with TE. Overall, measurement of MRS with a short TE reduces inaccuracies associated with variability in metabolite T2 and does not tend to lead to worse quantification of overlapping resonances. Further improvements in concentration accuracy can be obtained by measuring case-specific water T2.

Declaration

I declare that the work presented in this thesis is entirely my own.

The following aspects of this thesis were performed in collaboration:

1) Dr Martin Wilson developed the TARQUIN software used for quantification of in vivo and in vitro magnetic resonance spectroscopy (MRS) data.

2) Dr Brian Soher, Dr Karl Young, Dr Philip Semanchuk and Dr David Todd developed the VESPA software used for metabolite spectrum simulation in Chapters 4 and 7.

3) Dr Ben Babourina-Brooks assisted with visual inspection of MRS spectra at short and long echo time for inclusion in the T2 relaxation time analysis of Chapter 5.

4) MRI and MRS of paediatric brain tumours were acquired by radiographers in the Radiology Department at Birmingham Children's Hospital.

5) The MRS protocol for congenital adrenal hyperplasia (CAH) was decided in collaboration with Dr Emma Webb, Dr Amanda Wood and Professor Andrew Peet.

6) MRI and MRS investigations of CAH and healthy controls, used in Chapter 6, were acquired by radiographers at Birmingham University Imaging Centre. Data were collated and made available by Lucy Elliott and Dr Emma Webb.

Acknowledgements

Table of Contents

List of Figures

List of Tables

1. INTRODUCTION

Magnetic resonance imaging (MRI) is a method used regularly for structural imaging of the brain producing detailed images which enables identification of abnormalities and diagnoses for a range of conditions. While MRI is typically interpreted following qualitative expert review by radiologists, there is a move towards the use of quantification to yield imaging biomarkers.

Imaging biomarkers provide an objective measurement of indicators of pathogenic processes (Biomarkers Definitions Working Group., 2001). MRI biomarkers have become widely-used in healthcare and are used to determine response to treatment, through tumour size, in oncology (Eisenhauer et al., 2009) and to assess atrophic brain changes in neurodegenerative disease (Risacher and Saykin, 2013). However, conventional MRI is limited in its ability to provide information on tissue properties. For example, conventional MRI provides little information about metabolism, perfusion and cellularity which can be used to improve patient management. Structural imaging is therefore increasingly complemented with advanced imaging techniques which provide this information (Koh and Thoeny, 2010; Peet et al., 2012). However, the difficulties associated with the provision of protocols which determine imaging biomarkers in an accurate, reproducible manner in a clinically acceptable timescale mean biomarkers have not been widely adopted in clinical practice.

Advanced imaging techniques, such as ^{1}H magnetic resonance spectroscopy (MRS), have identified a range of potential imaging biomarkers (Oz et al., 2014). However, before an

imaging biomarker can be used for widespread clinical decision making it requires technical validation and an assessment of the precision of measurement. This thesis investigates how the quantification accuracy of MRS is affected by a number of experimental factors.

1.1 Introduction to MRS

MRS has been used in the assessment of a number of disorders in the brain including brain tumours (Howe et al., 2003; Panigrahy et al., 2006; Peet et al., 2012), HIV/AIDS (Descamps et al., 2008), traumatic brain injury (Brooks et al., 2001) and neurodegenerative disease (Gujar et al., 2005; Oz et al., 2014a). MRS can be incorporated into MRI investigations using the same equipment used for structural imaging and is a non-invasive method for measurement of the chemical composition of tissue. Information is extracted from a region of interest (ROI) called a voxel. MRS can either be collected from one voxel location, termed single voxel spectroscopy (SVS), or can be collected from multiple voxel locations, known as Magnetic Resonance Spectroscopic Imaging (MRSI) or Chemical Shift Imaging (CSI).
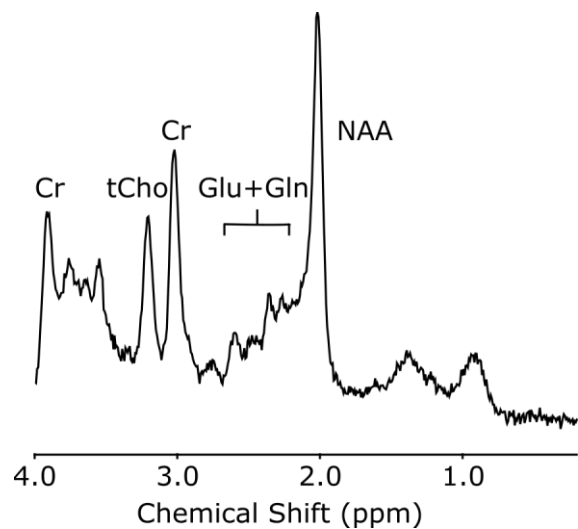
Figure 1-1: Example MRS of normal brain at TE 35 ms and the peak positions of N-acetylaspartate (NAA), creatine (Cr), choline (tCho), glutamate (Glu) and glutamine (Gln).

MRS data is displayed as a spectrum of peaks representing the various chemicals present in the voxel (Figure 1-1). These chemicals can be grouped into small molecules involved in metabolism, known as metabolites, and larger molecules such as lipids and macromolecules. Each metabolite has a characteristic spectral appearance and metabolites can be identified by their pattern of peaks at specific positions on the horizontal axis which has units of parts per million (ppm) (Govindaraju et al., 2000). The intensity of a peak indicates how much of the metabolite is present in the voxel, with larger peaks indicative of higher concentrations.

The MRS spectrum is a combination of the signals produced by resonating hydrogen atoms or protons. The appearance of an MRS spectrum is determined not just by the concentrations of the metabolites present but their chemical structure. A single peak resonance, called a singlet, is produced when the hydrogen atoms producing the signal are said to be uncoupled. However, when the hydrogen atoms of a metabolite interact with each other through a process called J-coupling, a complex arrangement of MRS peaks, called a multiplet, is produced.

The MRS spectral appearance will also depend on a number of acquisition parameters. One of the most important of these is the echo time (TE). While the appearance of singlets will remain the same, regardless of the TE used, the appearance of multiplets will change with TE because of J-evolution Figure 1-2.
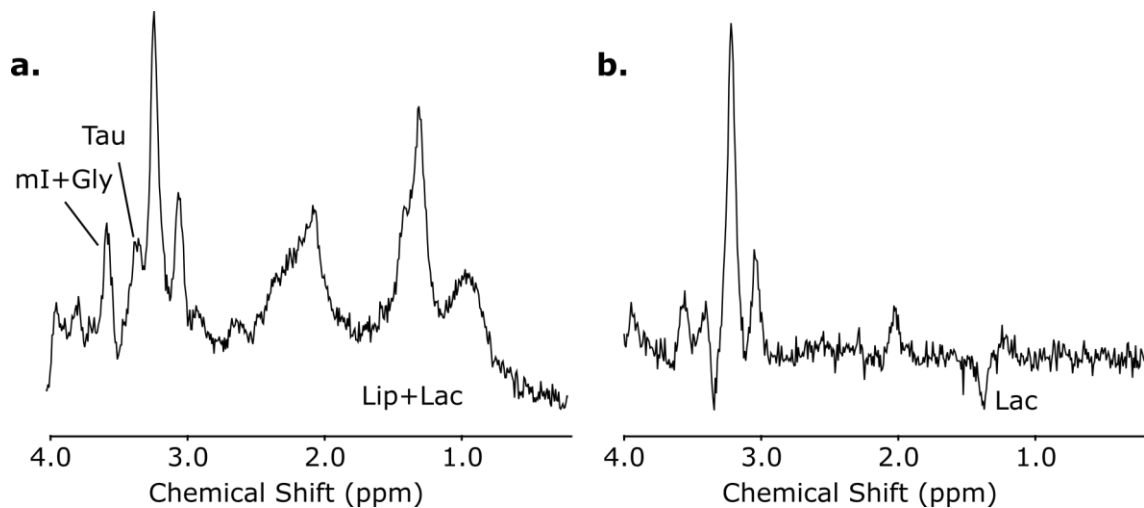
Figure 1-2: Example MRS spectra of paediatric brain tumour at a) TE 35 ms and b) TE 135 ms. The lactate (Lac) doublet appears inverted at 135 ms due to J-evolution.

An MR spectrum can be assessed in either a qualitative (McRobbie et al., 2007) or quantitative manner (Graaf, 2007; Mukherji, 1998). The following metabolites are amongst the most studied in clinical MRS. The main identifying feature of N-acetylaspartate is a large single peak at 2.01 ppm. The peak at 3.20 ppm is a combination of glycerophosphocholine (GPC), phosphocholine (PCh) and free choline, these are typically grouped together and reported as total choline (tCho) in clinical MRS. Total creatine (Cr) presents as two single peaks at 3.02 and 3.90 ppm on MRS, and is a combination of creatine and phosphocreatine, while glycine (Gly) has a single peak at 3.54 ppm on MRS. Gly can be difficult to distinguish from myo-Inositol (mI) using MRS. mI is a complex metabolite with its main resonances between 3.50 and 3.60 ppm. Lactate (Lac) can be identified by its doublet at 1.31 ppm, this doublet is inverted at a long TE of 135 ms (Figure 1-2). Glutamate (Glu) and glutamine (Gln) are two chemically similar metabolites, each producing a broad group of resonances between 2.00 and 2.50 ppm. The sum of glutamate and glutamine concentrations is often reported as a single measurement (Glx).

Metabolites are involved in physiological processes and each have a specific biological significance. NAA is the most prominent peak in MRS of normal brain and is a marker of neuronal integrity; it is often reduced in a range of brain diseases (Gujar et al., 2005). tCho is a marker of cell proliferation and membrane disruption. tCr is a marker of energy metabolism, while Lac, the end point of anaerobic glycolysis, is an indicator of abnormal energy metabolism (Veech, 1991). mI is a pentose sugar which plays an important role in osmoregulation of the central nervous system (Fisher et al., 2002). Gly is an antioxidant and inhibitory neurotransmitter and Glu is an excitatory neurotransmitter, while Gln is an amino acid precursor is a storage form of Glu (Panigrahy et al., 2010a).

The concentration of these metabolites is known to vary in a number of disease states, including paediatric brain tumours and neurodegenerative disease (Mukherji, 1998). Metabolite concentrations measured with MRS are therefore potentially important imaging biomarkers which could inform future clinical decision making.

While knowledge of altered metabolism and the chemical composition of disease states is potentially important for clinical decision making and drug development, MRS has not been widely adopted in the clinic. MRS remains predominantly a research tool in the technical validation domain of the Imaging Biomarkers Roadmap (O'Connor et al., 2016) for a number of reasons. Firstly, when compared to structural imaging, which radiologists have years of training and experience of, the complicated spectrum of peaks that MRS produces is less readily interpreted than anatomical images.

Secondly, the most common MRS technique, SVS, collects data from a relatively large single volume of size 6 mL and greater with an acquisition time of 3-5 minutes (Oz et al., 2014).

While MRI and MRS are complementary techniques, the voxel size, spatial resolution and acquisition time compare poorly to MRI which can acquire whole coverage of the brain in 5-10 minutes (Ellingson et al., 2015). The multi-voxel technique, MRSI, provides larger anatomical coverage and information on tissue heterogeneity from smaller volumes of 1 mL and below; however, MRSI is less quantifiable, provides information on fewer metabolites than SVS due to its reduced signal, and is acquired at the expense of longer acquisition times (Posse et al., 2013). SVS is therefore the more commonly used MRS method in the clinical environment. With technological advancements in the form of the improved signal-to-noise from higher field strengths clinically and reduced acquisition times due to compressed sensing (Geethanath et al., 2012) and parallel imaging (Birch et al., 2015), MRSI is now becoming more applicable in the clinical environment.

A further advance in the field of MR imaging comes in the form of chemical exchange saturation transfer imaging (CEST). CEST utilises the change in signal that occurs due to the exchange of protons with hydrolysable functional groups with bulk water, to produce contrast based on metabolite concentrations while retaining the spatial resolution of MRI. As a developing technique, metabolites identified using MRS could be used to determine future imaging targets for CEST and to validate its results in a number of disease states (Cai et al., 2013; Haris et al., 2011; Ray et al., 2016).

1.2 Introduction to Paediatric Brain Tumours

Brain tumours account for approximately a quarter of all cancers in children (Cancer Research UK, 2015) and are the most common solid tumour in children (Bleyer, 1999; Office for National Statistics, 2016). Paediatric brain tumours are the leading cause of death in

children's cancer with a 10-year survival rate of approximately 68% (Cancer Research UK, 2015).

The gold standard for diagnosis is from histopathological examination of tissue. Tissue samples are stained with haematoxylin and eosin to assess morphology and with immunohistochemical stains for cell and tissue specific markers. These stains are used to identify tumour type and associated grade according to the World Health Organisation (WHO) system (Louis et al., 2016). The WHO classification in paediatric brain tumours is graded on a scale of I-IV, with higher grades associated with increased aggressiveness and a poorer prognosis.

Approximately two-thirds of paediatric brain tumours are diagnosed from histology with the remaining third of paediatric brain tumours are diagnosed on clinical and imaging grounds. The development and validation of non-invasive imaging methods for diagnosis and identification of prognostic biomarkers for these tumours would therefore represent a substantial advance for clinical management of these patients.

1.2.1 Tumours Diagnosed By Histopathology
<u>Astrocytomas</u>

Pilocytic astrocytomas (PA) are the most common paediatric brain tumour. They are grade I glial tumours which most often present in the cerebellum (Gan and Haas-Kogan, 2010). PA have a good prognosis with a 5-year overall survival over 90% (Dodgshun et al., 2016). Primary treatment of PA consists of maximal resection, with chemotherapy and radiotherapy administered when the majority of the tumour has not been resected.

Grade II to IV astrocytomas fall on a spectrum of disease. In contrast to the stable PA which do not progress, grade II and III astrocytomas can progress to higher grades and progression of these tumours has been linked to levels of citrate (Blüml et al., 2011). While glioblastoma is the most common grade IV astrocytoma in adults they are rare in children. Despite treatment with surgery, radiotherapy and chemotherapy, these tumours tend to have a very poor prognosis (Fangusaro, 2012).

Medulloblastomas

Medulloblastomas are grade IV tumours that present in the cerebellum. The overall five-year survival rate is over 70% (Packer et al., 2013); however, varying prognosis is associated with a number of distinct histological and genetic subgroups (Louis et al., 2016). Medulloblastoma treatment is stratified by risk and treatment primarily consists of maximal safe resection followed by craniospinal radiotherapy and chemotherapy. The combination of tumour and treatment can lead to later life cognitive deficits and identification of lower risk tumours could therefore improve future quality of life.

Ependymomas

Ependymomas are the third most common paediatric brain tumour and make up 6-10% of all childhood brain tumours (Smyth and Rubin, 2010). Two thirds of ependymomas present in the posterior fossa. Treatment currently involves maximum surgical resection followed by either chemotherapy or radiotherapy. The only current prognostic marker used clinically is the extent of resection (Vaidya et al., 2012). However, distinct molecular subgroups with prognostic significance have emerged recently (Pajtler et al., 2015).

1.2.2 Other Tumours

In cases where tissue samples are not available, they are often described in terms which describe their location and their likely underlying biology. Tumours diagnosed on imaging grounds can include the following.

Optic Pathway Glioma

Optic pathway gliomas (OPG) are often associated with mutations in the neurofibromatosis-1 gene (Listernick et al., 2007). The vast majority, but not all, of OPG diagnosed with histopathology are PA. OPG have a survival rate of over 90%. Despite their good overall prognosis, some OPG have multiple episodes of progression (Kelly and Weiss, 2013). These are treated with chemotherapy, radiotherapy and surgery (Goodden et al., 2014).

Diffuse Intrinsic Pontine Glioma

Diffuse intrinsic pontine gliomas (DIPG) are a rarer form of glial tumours which present in the brain stem. DIPG are grade IV tumours and have a poor prognosis with a mean survival of less than 12 months (Hargrave et al., 2008). Resection of DIPG is not typically possible due to their location. DIPG are now increasingly biopsied, they are often lower grade tumours but rapidly progress to high grade, with molecular subgroups having been identified (Grill et al., 2012; Puget et al., 2012).

As not all patients will have tissue biopsy and the processing time of histopathology results, non-invasive imaging methods could facilitate improved clinical outcomes through early diagnosis and earlier administration of treatment.

1.2.3 Imaging of Brain Tumours

T1-weighted and T2-weighted imaging are the two most common structural imaging modalities used in MR to differentiate between anatomical structures. T1 and T2-weighted imaging exploit differences in tissue density and relaxation rates of tissue types to create contrast between tissue types. A full description of T1 and T2 relaxation is provided in Chapter 2. Structural imaging is performed at multiple time points to confirm the presence of a mass, to aid diagnosis and to assess the extent of resection following surgery. Structural imaging is subsequently performed at regular intervals to monitor treatment response and for tumour surveillance.

Determination of tumour size, location and blood-brain barrier status from structural imaging is often enough to make diagnosis and immediate clinical decisions (Panigrahy and Blüml, 2009) However, paediatric brain tumours represent a heterogeneous group and diagnosis and determination of optimal biopsy sites is not always possible from imaging alone. The ability to increase confidence in these areas would therefore be welcomed. Furthermore, structural imaging is limited in its ability to predict survival (Hargrave et al., 2008) and some tumours of the same grade and tumour type are known to have differing survival (Krishnatry et al., 2016). Identification of quantitative biomarkers of diagnosis and prognosis is becoming increasingly important and would allow treatment stratification according to risk (Dufour et al., 2011; Zacharoulis and Moreno, 2009).

A number of quantitative MR methods have become available which could provide quantitative biomarkers. Texture analysis provides an avenue for quantitative analysis of conventional structural MRI, representing the image as mathematical features which can

successfully discriminate between paediatric brain tumour types (Fetit et al., 2015; Orphanidou-Vlachou et al., 2014; Rodriguez Gutierrez et al., 2014).

A range of quantitative advanced imaging techniques are also available and these enable investigations of tumour metabolism, cellularity and perfusion. Diffusion weighted imaging provides information about water diffusion in tissue, giving an indication of the cellularity of the tumour. Apparent diffusion coefficients (ADC) are significantly different between tumour types, with PA having higher ADC values than the more cellular medulloblastomas and ependymomas and the ADC of ependymomas was higher than that of medulloblastomas (Rumboldt et al., 2006). In the posterior fossa, ADC histograms correctly classified 80% of ependymomas, 100% of astrocytomas and 94% of medulloblastomas (Bull et al., 2012). Perfusion imaging enables identification of neo-angiogenesis in tumours. Increased perfusion was predictive of shorter survival in DIPG (Hipp et al., 2011), whilst reduction of cerebral blood volume during radiotherapy treatment was predictive of increased survival in gliomas (Cao et al., 2006).

1.2.4 MRS of Adult and Paediatric Brain Tumours

While perfusion and diffusion imaging provide valuable prognostic and diagnostic markers, they provide no information about tumour metabolism. MRS is one method capable of investigating tumour metabolism. Preoperative short-TE MRS of untreated paediatric brain tumours revealed differences in metabolite concentrations between tumour types (Panigrahy et al., 2006), with differences in the metabolite concentrations also seen between astrocytoma, ependymoma and medulloblastoma and between tumours and normal brain (Davies et al., 2008a). Multivariate analysis also identified key differences in the metabolite profiles for the three tumour types, with the three classifiers presented

accurately classifying 93-95% of cases (Davies et al., 2008a). In a large multi-centre study, the use of two echo times was found to have a balanced accuracy rate of 98% for classification of the same tumour types (Vicente et al., 2013). Interestingly, the use of two echo times for classification was also found to significantly improve classification performance.

Automatic pattern recognition has been used to cluster spectra according to their pathology in adult brain tumours (Tate et al., 2006). This decision support system successfully classified 81 out of 91 brain tumours, helping to resolve diagnosis in borderline cases, and was a significant improvement over the use of MRI alone. Decision support systems based on preoperative MRS outperformed MRI evaluation alone in the diagnosis of grade III adult astrocytomas and had no negative effect on radiologists' predictions (Julià-Sapé et al., 2012).

A number of metabolites measured with MRS have been identified as prognostic biomarkers. The tCho/NAA ratio was found to predictive of survival in DIPG (Steffen-Smith et al., 2011a). In addition to the tCho/NAA ratio, tCho and Lac were all found to be significantly different between survivors and non-survivors in paediatric brain tumours (Marcus et al., 2007). The same study concluded that tCho + 0.1Lac was an independent predictor of survival and that MRS biomarkers predict survival better than standard histopathology. Levels of NAA and Gln have been observed to predict improved survival, with lipids and scyllo-Inositol associated with poor survival in paediatric brain tumours (Wilson et al., 2013). A risk model combining lipids, Scy and Gln predicted survival with a similar accuracy to histological grading (Wilson et al., 2013). High levels of lipids are also associated with poor survival (Crawford et al., 2009) and grade (Murphy et al., 2003) in adult brain tumours.

Gly has also been identified as a feature of high grade in paediatric brain tumours (Davies et al., 2010a). However, whilst grade is associated with prognosis, tumours of the same type and grade can belong to molecular subgroups which have very different outcomes (Taylor et al., 2012). MRS provides an avenue to investigate molecular subgroups and retrospective analysis of medulloblastomas determined that metabolite profiles could distinguish between the sonic hedgehog and group 3/4 subgroups (Blüml et al., 2015). Furthermore, Citrate (Cit), a metabolite that has been suggested as increased in DIPG (Seymour et al., 2008), was also identified in a subgroup of grade II paediatric astrocytomas with aggressive behaviour (Blüml et al., 2011). In a small study of pilocytic astrocytomas, lower levels of ml were observed in pre-treatment MRS of tumours which progressed compared to those where disease was stable (Harris et al., 2008a). MRS has also been used in adult brain tumours to detect 2-hydroxyglutarate (Choi et al., 2012), a biomarker associated with isocitrate dehydrogenase mutations (Dang et al., 2009) and improved survival in adult gliomas (Cohen et al., 2013).

MRS can also be used as a tool for monitoring response to treatment. Optic pathway gliomas, where tumours are often incompletely resected (Nicolin et al., 2009), were found to have significantly lower ml levels at follow up in tumours that had progressed compared with initial MRS (Harris et al., 2008a). A reduction in Cit has been observed in DIPG following radiation therapy (Seymour et al., 2008). DIPG patients with an increase in tCho/NAA between imaging time points were at significantly greater risk at death than those with stable or reduced levels (Steffen-Smith et al., 2011a). In adult brain tumours, changes in normalised tCho between week 4 of radiotherapy and post-radiotherapy were predictive of survival (Quon et al., 2011). While a reduction in tCho was closely matched to reductions in

tumour volume (Murphy et al., 2004). Finally, changes over 14 months of the MRS profiles of

grade II gliomas treated with temozolomide are related to outcome (Guillevin et al., 2011).

1.3 Introduction to Neurodegenerative Disease

Treatment of brain tumours with radiotherapy can affect brain structure and function

(Padovani et al., 2012; Parihar and Limoli, 2013). This loss of function or structure of cells

with the central nervous system is called neurodegeneration. In addition to

neurodegeneration following treatment, it can also arise in children as a result of inherited

metabolic disorders. Neurodegeneration is associated with a number of other disease states,

including amyotrophic lateral sclerosis (ALS); dementias, such as Alzheimer's disease;

Huntington's disease and multiple sclerosis

1.3.1 Imaging of Neurodegenerative Disease

Structural MRI is typically used to assess local and global volume changes (Risacher and

Saykin, 2013), however diagnosis of neurodegenerative diseases can be difficult due to

similar clinical presentations and diagnosis is often only confirmed post-mortem (Mok et al.,

2004). Therapies for neurodegenerative disease tend to treat only the symptoms without

affecting the cause of the disorder; however neuroscience advances could facilitate the

development of therapies to treat the underlying condition (Stoessl, 2012). Brain volume

losses, particularly of grey matter, correlate with cognitive impairment in multiple sclerosis

(De Stefano et al., 2014) and CSF volume in Huntington's disease is associated with disease

progression and severity (Squitieri et al., 2009). In Alzheimer's disease (AD), hippocampal

volume loss in AD has been identified as an early potential indicator of AD pathology.

However, regional brain volume changes occur even in elderly people who are unlikely to be

presymptomatic of neurodegenerative disease (Fjell et al., 2013). Identification of

biomarkers of disease and prognosis which can be monitored is therefore required.

Diffusion tensor imaging (DTI) probes tissue microstructure, providing a measure of tissue

integrity. In AD, reduced fractional anisotropy (FA) and increased diffusion relative to normal

brain has been observed in white matter (Stebbins and Murphy, 2009). Reduced white

matter integrity is also associated with Parkinson's disease (Auning et al., 2014) and

Huntington's disease (Poudel et al., 2014).

Neuroimaging advances could lead to the early detection of preclinical neurodegenerative

diseases, enabling improved clinical outcomes following treatment at an early stage.

1.3.2 MRS of Neurodegenerative Disease

Alzheimer's disease (AD), a form of dementia, is one of the most studied neurodegenerative

diseases with MRS. While much of the following discussion will focus on AD, a number of

these findings are typical of neurodegenerative diseases and cognitive decline, particularly

for dementias (Kantarci, 2013). NAA has been identified as a significant biomarker of

neurodegenerative disease due to its role in neuronal integrity. In longitudinal studies of

Alzheimer's patients, a decrease in NAA levels was associated with severity (Adalsteinsson et

al., 2000; Kantarci et al., 2008), however reductions in NAA levels were not accompanied by

changes in grey matter volume (Kantarci et al., 2008). In addition to reduced NAA, an

increase in mI (Kantarci et al., 2000; Miller et al., 1993; Oz et al., 2011) and decreased Glu

(Oz et al., 2011; Rupsingh et al., 2011; Unschuld et al., 2012) have been observed in a

number of AD studies. A reduction in NAA accompanied by an increase in mI has also been

observed in Huntington's disease (Sturrock et al., 2015)

Metabolite biomarkers could provide early indicators of disease in AD. The increase of mI

levels in AD has been seen to appear early in presymptomatic individuals with familial AD,

prior to structural changes (Kantarci et al., 2010)).

MRS has been used as a tool for monitoring treatment and disease progression. A temporary

increase in NAA for patients treated with donepezil, relative to patients treated with

placebo, suggested that donepezil could potentially have protective effects in AD (Krishnan

et al., 2003). Further evaluation with MRS of donepezil treatment observed lower levels of

NAA, tCho and mI/Cr after four months of treatment, with decreased levels of tCho and

mI/Cr possibly suggesting a positive treatment effect (Bartha et al., 2008). Changes in

metabolite levels have also correlated with cognition scores following treatment, with

increases in Glu following galantine treatment associated with improved cognitive

performance (Penner et al., 2010). In multiple sclerosis, an increase in the mI/NAA ratio was

significantly associated with decreasing brain volume and disability evolution (Llufriu et al.,

2014).

1.4 Introduction to MRS Quantification

While MRS can be interpreted in a qualitative manner, the association of metabolite

concentrations with prognosis and their role in non-invasive diagnosis and treatment

monitoring show that quantified MRS metabolite biomarkers and can potentially become a

powerful tool for clinical decision making. Quantification of MRS can be performed by either

calculating the area under the curve of the MRS peak or by fitting the whole spectrum using

prior knowledge using software such as LCModel (Provencher, 2001a) and TARQUIN (Wilson

et al., 2011a). The two main ways of expressing quantified MRS data are as metabolite ratios

and as absolute concentrations. While metabolite ratios will reduce errors associated with

partial volume contamination with CSF, they can be confounded by unexpected changes in metabolite levels, giving no indication of why the ratio has changed. Furthermore, metabolite ratios are less reproducible than absolute concentrations (Minati et al., 2010), break down when the denominator is small and can be less sensitive to abnormalities than absolute concentrations (Simister et al., 2002). Quantification of MRS, using water as an internal reference with known concentration values, enables absolute concentrations to be reported (R. Kreis et al., 1993). The use of absolute concentrations in combination with pattern recognition techniques has also been shown to improve classification accuracy when compared with pattern recognition based on whole spectrum appearance (Opstad et al., 2007).

While up to 35 brain metabolites can be quantified in vitro (Govindaraju et al., 2000), far fewer can be detected in vivo. Ex vivo and in vitro investigations, such as high-resolution magic angle spinning (HR-MAS), can be performed at high field strengths that are not available for clinical studies. HR-MAS uses the high field strengths available to improve line shape and linewidth, improving peak assignment in brain tumour tissue samples (Barton et al., 1999).

A number of factors can affect the accuracy of metabolite quantification in vivo. The signal-to-noise ratio (SNR) and spectral resolution of clinical MRS is poor when compared with high field HR-MAS. Unambiguous peak assignment of metabolites is therefore restricted to a few metabolites in vivo. This is typically due to the spectral overlap of peak resonances, with coupled metabolites often overlapping considerably, while metabolites present in very small concentrations can be difficult to distinguish from the background noise due to SNR.

Though low metabolite concentrations and spectral overlap can affect visual assignment of MRS peaks in vivo, quantification of MRS is reproducible and reliable (Mullins et al., 2008). However, coupled metabolites typically have higher coefficients of variation. Nonetheless, metabolite concentrations measured with LCModel and TARQUIN correlate well with tissue concentrations estimated from HR-MAS (Opstad et al., 2010; Wilson et al., 2009b).

When measured as absolute concentrations with reference to water, quantitative estimates of metabolite concentrations will also depend on a phenomenon called T2 relaxation T2 relaxation describes the MRS signal decay with echo time and a full description of T2 relaxation, and the MR theory relevant to the work in the thesis, is provided in Chapter 2.

The difference in the T2 relaxation decays of water and metabolite is known to affect metabolite quantification, with the effect becoming more pronounced at longer echo times (Yamamoto et al., 2015a). The discrepancy between the T2 relaxation times of water and metabolite is illustrated schematically for typical examples in Figure 1-3.
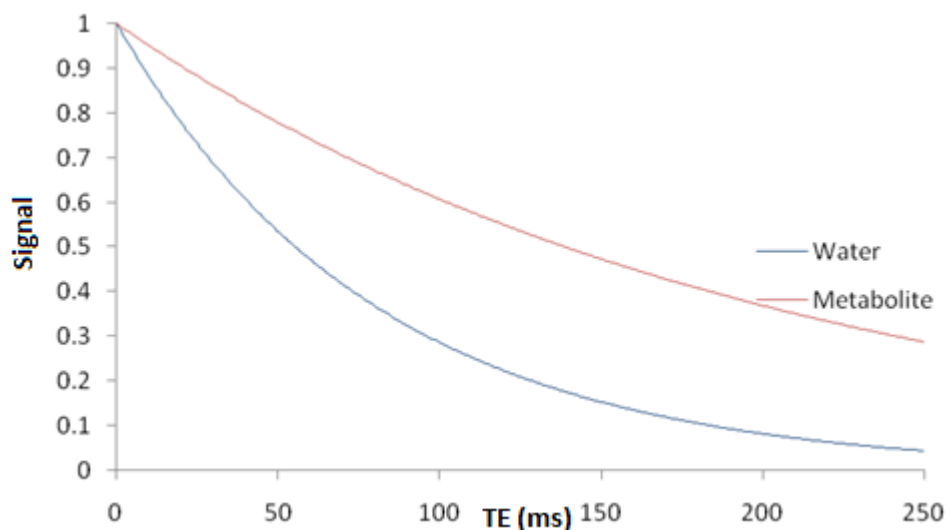
Figure 1-3: T2 relaxation decays of water and metabolite normalised to 1.

To acquire data without T2 relaxation decay is not currently possible in a clinical setting due to the technical limitations of clinical MR scanners. TARQUIN and LCModel account for T2 relaxation by assuming T2 values typical of normal adult brain at 1.5 T. However, T2 relaxation times are known to change with age (Kirov et al., 2008a), vary in regions of the brain (Ganji et al., 2012a) and are reduced at higher field strengths (Träber et al., 2004a). The accuracy of metabolite quantification will therefore depend on how well T2 relaxation, in addition to spectral overlap and data quality, is dealt with in the MRS analysis.

1.5 Challenges of MRS Quantification

Following the advent of field strengths of 3 T and higher, the acquisition of structural and advanced imaging in the same session is becoming possible in clinically feasible timeframes. With an increasing desire for personalised medicine, metabolite concentrations should be evaluated in prospective multi-centre clinical trials which link metabolite biomarkers to clinical outcomes. However, a number of factors are known to affect metabolite quantification and an investigation into how these factors affect metabolite quantification accuracy on a case-by-case basis is therefore required.

The SNR and spectral resolution of in vivo MRS is poor at clinical field strengths when compared with ex vivo HR-MAS. Data quality is known to affect quantification accuracy at 1.5 and 4 T with accuracy improving with SNR (Bartha et al., 2000); however an assessment of quantification accuracy at 3 T has not been performed. With an increasing body of evidence that coupled metabolites are potential prognostic biomarkers (Cohen et al., 2013; Harris et al., 2008a; Wilson et al., 2014, 2013), accurate quantification of them becomes more important.

Coupled metabolites can be difficult to detect using conventional short-TE MRS due to their lower signal intensity and significant spectral overlap with other metabolites. Various methods have been proposed to improve their detection and measurement. One common method is to use an optimised echo time. Optimised TEs exploit the J-evolution of coupled metabolites to enhance the signal intensity of a particular metabolite relative to neighbouring resonances. While optimised TEs may improve the visual identification of coupled metabolites, there is limited evidence that they improve measurement accuracy. An assessment of how the J-modulation and spectral overlap of coupled metabolites affects metabolite quantification would therefore be welcomed.

Metabolite quantification at optimised TEs could also be confounded by T2 relaxation times with differences in the T2 values of water and metabolites having a greater effect at long TEs (Yamamoto et al., 2015a). Furthermore, relaxation times are also known to vary significantly between normal brain and pathology (Isobe et al., 2002; Li et al., 2008; Madan et al., 2015a; Sijens and Oudkerk, 2002). Whilst T2 relaxation times are known to affect quantification, there has been little formal assessment of how T2 variation affects metabolite quantification on a case-by-case basis at short-TE. Research has instead focused on how T2 differences will affect metabolite ratios (Li et al., 2008) and quantification at long echo times (Yamamoto et al., 2015a).

J-resolved spectroscopy (JPRESS) has also been proposed to reduce the spectral overlap of metabolites at clinical field strengths. While optimised TEs exploit the J-evolution of coupled metabolites to improve metabolite detection at a single TE, JPRESS exploits J-evolution differences over many TEs to spread the spectrum into a second dimension. Though JPRESS

can reduce the spectral overlap of coupled metabolites, it is characterised by long acquisition times and its analysis is not a straightforward task. The development of a clinical JPRESS protocol and postprocessing pipeline could therefore increase its utility in the clinical setting.

Given the range of acquisition protocols and analysis methods available, a systematic assessment of the various factors that affect metabolite quantification would help inform future protocol design and aid the validation of metabolite biomarkers in clinical trials and clinical practice. Providing this information would be a major advance towards the widespread use of MRS biomarkers for clinical decision making.

1.6 Aim
To assess the importance of echo time and T2 relaxation in accurate metabolite biomarker quantification

1.7 Objectives:
- To investigate the effect of J-evolution and T2 relaxation on metabolite quantification using simulations, phantoms and volunteers (Chapter 4).

- To assess how the T2 relaxation times of metabolites and water vary between normal brain and pathology at 1.5T and 3T (Chapters 5 and 6).

- To investigate how the accuracy of metabolite quantification at 1.5 and 3T is affected by changes in T2 relaxation times (Chapters 5 and 6).

- To assess how many echo times need to be collected to estimate the T2 relaxation time of water at 3T(Chapter 6)

- To develop a clinical protocol and processing pipeline for JPRESS at 3T and to implement it clinically in childhood brain tumours (Chapter 7).

1.8 Thesis Organisation

Chapter 2 introduces the essential theory of MRS and its acquisition. The process of MRS quantification and analysis is also described in Chapter 2 along with further discussion of the factors that will affect MRS quantification. The general methods described in this work are then described in Chapter 3.

The importance of echo time choice on accurate metabolite quantification is investigated in Chapter 4 using a combination of simulations, phantoms and volunteers. Three echo times are assessed using three spectral models and volunteer data. Simulated data is used to determine whether there is a single optimal echo time for accurate metabolite quantification. Whilst simulations allow an investigation into how spectral quality affects metabolite quantification, considerations such as T2 relaxation were not modelled. The influence of T2 relaxation time and echo time choice is therefore investigated using phantoms and volunteers.

Chapter 5 presents a retrospective study of MRS data collected at 1.5 T using two echo times. T2 relaxation times are estimated in paediatric brain tumours and in normal age-matched controls. The variation of T2 relaxation times between tumour types and between tumour and normal brain is assessed. Metabolite quantification accuracy is assessed by correcting metabolite concentrations using case-specific T2 relaxation times and comparing to concentrations which have been corrected using various combinations of water and metabolite T2 relaxation times.

Chapter 6 focuses on metabolite quantification and the need for case-specific T2 relaxation times at 3 T. A multi-TE MRS sequence is presented for quick estimation of the water T2

relaxation time. T2 relaxation times of common paediatric brain tumours are compared from 1.5 and 3 T cohorts. The use of case-specific and literature T2 relaxation times for relaxation correction in paediatric brain tumours is compared. Water and metabolite T2 relaxation times are estimated from two echo times in the brain of adults with congenital adrenal hyperplasia and age-matched healthy controls. The importance of case-specific metabolite and water T2 relaxation times is assessed at 3 T.

As a logical extension to the use of two echo times, a clinical protocol for the 2D J-resolved spectroscopy technique JPRESS is developed and optimised in Chapter 7. Clinical use of JPRESS has historically been limited by the long acquisition times associated with it. A protocol and processing pipeline which reduces the acquisition time from 40 minutes to 6 minutes is presented. This protocol and processing pipeline is assessed in four children with brain tumours.

2. INTRODUCTION TO NUCLEAR MAGNETIC RESONANCE

Nuclear magnetic resonance (NMR) has important applications in research and clinical use:

magnetic resonance imaging (MRI) and magnetic resonance spectroscopy (MRS). This

chapter introduces the essential theory behind the NMR phenomenon and its application to

MRS. A more detailed account of the theory is described in the following references (Graaf,

2007; Hore, 1989; Keeler, 2010). This chapter also details the acquisition and quantification

of MRS in a clinical and research setting.

2.1 NMR Theory

2.1.1 Nuclear Spin

All nuclei have the intrinsic properties of mass, charge, magnetism and spin. It is nuclear spin

upon which nuclear magnetic resonance (NMR) is founded.

Isotope	Nuclear Spin	Gyromagnetic Ratio (MHz / Tesla)	Natural Abundance (%)
^{1}H	1/2	42.58	99.985
^{3}He	1/2	-32.43	1.4 x 10-4
^{13}C	1/2	10.71	1.108
^{19}F	1/2	40.05	100
^{23}Na	3/2	11.26	100
^{31}P	1/2	17.24	100

Table 2-1: Nuclear spin, gyromagnetic ratio and natural abundance of selected nuclei.

Table 2-1 presents some of the NMR properties of selected nuclei which are present in vivo.

Hydrogen is the most abundant nucleus with a non-zero nuclear spin in the human body.

The high natural abundance of ^{1}H, its high gyromagnetic ratio, γ, and high sensitivity make it

a convenient target for MRI and MRS.

2.1.2 Nuclear Spins in Magnetic Field

[1]H nuclei possess a magnetic moment related to its spin. In the absence of an external magnetic field, the magnetic moments are randomly distributed (Figure 2-1a).
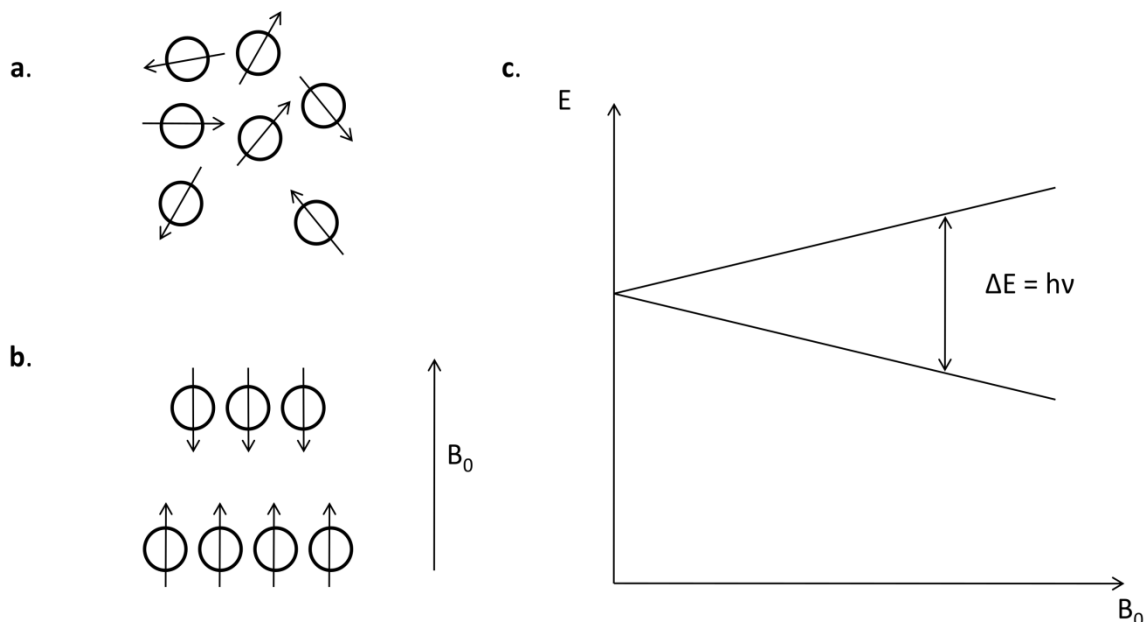
Figure 2-1: Dipole moment orientation in a) the absence of a magnetic field and b) in the presence of a magnetic field. c) The nuclear spin energy between the parallel and antiparallel states for a spin ½ nucleus as a function of magnetic field strength.

In the presence of a magnetic field, B_0, the spins will rotate around B_0 with the speed of precession, ω_0 (rad s[-1]), given by the Larmor equation:

$$\omega_0 = \gamma B_0 \qquad \text{(Equation 2-1)}$$

with the spins of the nuclei aligning in either parallel (↑) or antiparallel (↓) to B_0 (Figure 2-1b). The parallel and antiparallel spins are separated by an energy gap given by:

$$\Delta E = \bar{h}\omega_0 \qquad \text{(Equation 2-2)}$$

and the population of each state is given by:

$$N_\uparrow = N_\downarrow e^{\Delta E / k_b T}$$

Where $N_\uparrow$ is the number of spins parallel to the field, $N_\downarrow$ is the number of spins antiparallel, k_b is the Boltzmann constant and T is the temperature.

Nuclei aligned parallel to the magnetic field are at a lower energy level, resulting in more spins in this state (Figure 2-1). This is called the equilibrium or ground state. By virtue of having more nuclear spins aligned parallel to the external field, a net magnetisation occurs in the same direction as B_0. This is described as longitudinal magnetisation, M_z, along the z-axis by convention and this is the basis of MR signals. As the dipole moments are distributed randomly on the x-y plane, there is no transverse magnetisation and the dipole moments are not in phase with each other (Figure 2-2a).
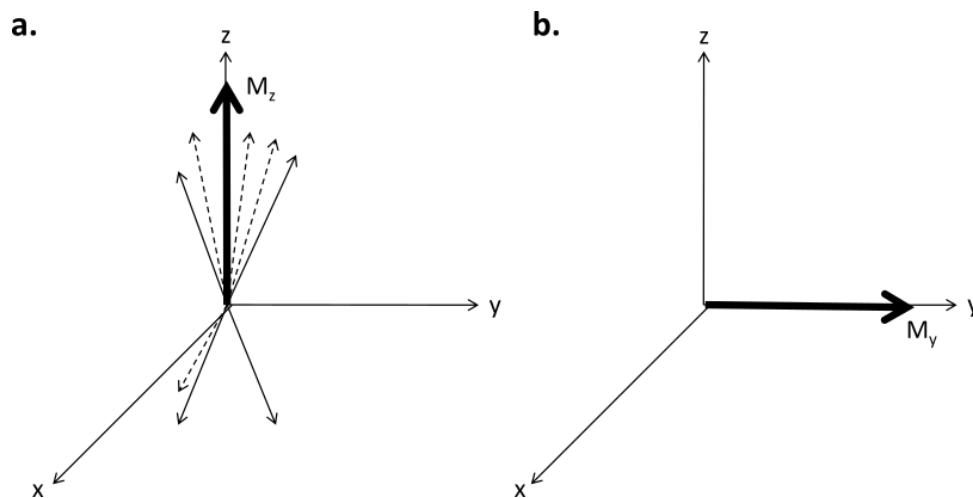
Figure 2-2: Phase orientation of spins at a) thermal equilibrium, where phases are randomly distributed, and the net magnetisation is longitudinal only and b) following application of RF pulse such that all spins are coherent (i.e. have the same phase) and magnetisation is in the transverse plane.

When a radiofrequency (RF) pulse is applied of Larmor frequency, ω_0, protons are excited from the low energy ground state to a high energy state. The net magnetisation is tipped

towards the transverse x-y plane and the nuclear spins become coherent (Figure 2-2b).

When the RF pulse is removed, the now transverse magnetisation rotates around B_0 and

induces an electromotive force (emf) on the surrounding receiver coils.

As the transverse magnetisation rotates around B_0, the nuclear spins dephase, losing phase

coherence, and the emf signal induced on the receiver coils decays exponentially with time.

The signal induced on the receiver coils is called the free induction decay (FID) and is

displayed in Figure 2-3.
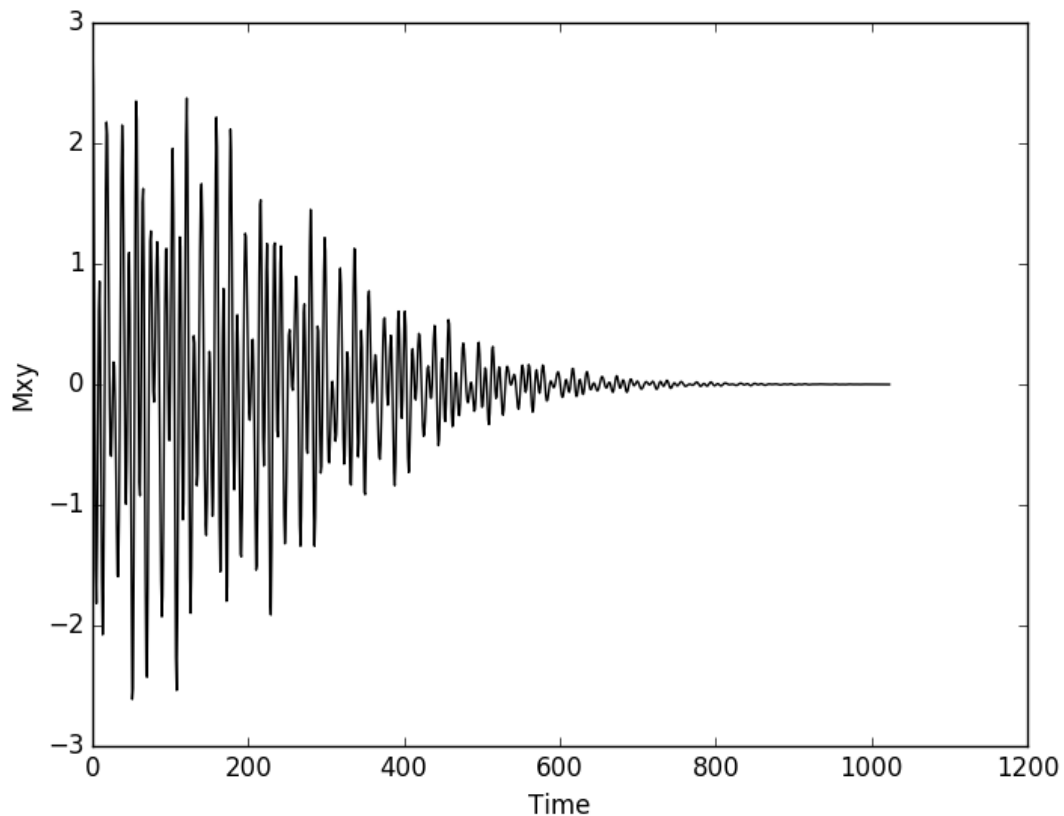
Figure 2-3: The free induction decay induced by transverse magnetisation.

2.1.3 Relaxation

The loss of transverse magnetisation is called T2 relaxation and it is caused by the exchange

of energy between spins. In practice, due to inhomogeneities in B_0 the decay of transverse

magnetisation is quicker than would be expected from T2 decay alone. The contribution of T2 can be separated from the effect of B_0 inhomogeneity through the generation of spin-echoes. The T2 relaxation time constant is determined by the amount of time it takes for the magnetisation to decay to 37% of its original value (Figure 2-4).

$$M_{xy} = M_0 e^{-t/T_2}$$
(Equation 2-4)

In addition to the decay of the transverse magnetisation, in the absence of the RF pulse the magnetisation will also return to its equilibrium state with magnetisation only present in the longitudinal plane. This process is called T1 relaxation. The T1 relaxation time is the time it takes for the longitudinal magnetisation to recover 63% of its initial magnetisation after being tipped into the x-y plane (Figure 2-4).

$$M_z = M_0(1 - e^{-t/T_1})$$
(Equation 2-5)

Differences in the T1 and T2 relaxation times of different tissue types are exploited in MRI to produce anatomical images. The influence of T1 and T2 relaxation on MRS is further discussed later in this chapter.
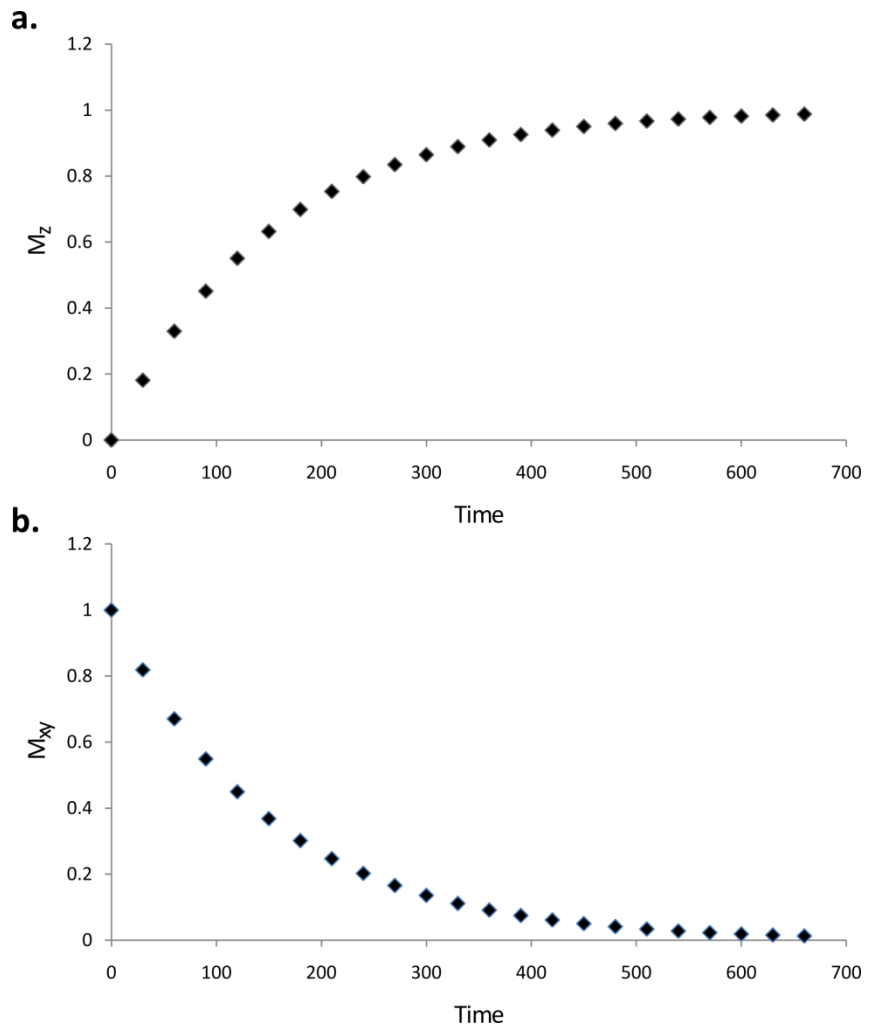
Figure 2-4: The decay of a) longitudinal (T1) and b) transverse (T2) relaxation.

2.2 MRS Theory
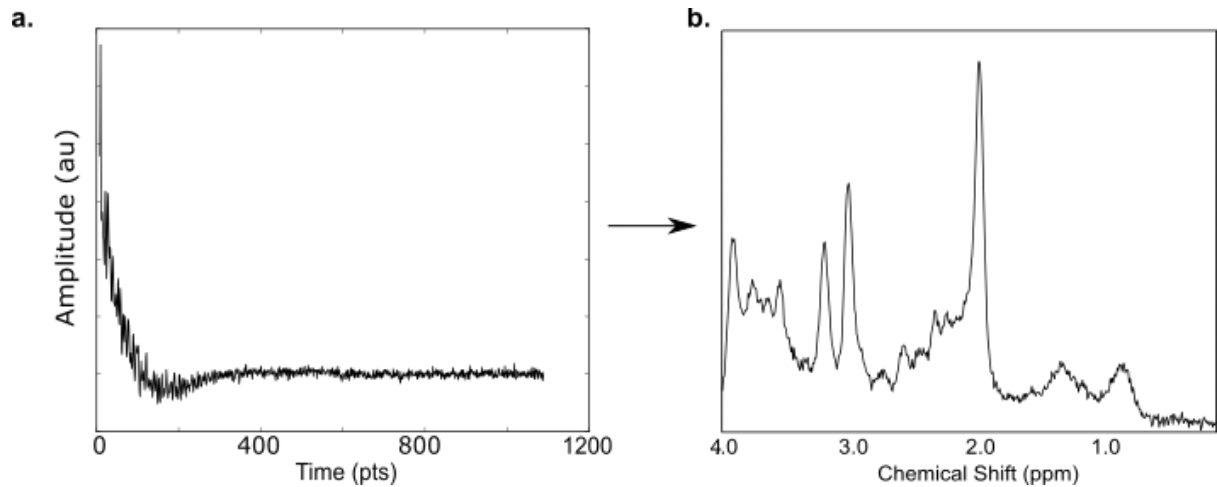
Figure 2-5: a) The free induction decay induced by in vivo MRS in the time domain and b) the frequency domain spectrum following a Fourier Transform.

The FID acquired by in vivo MRS is a combination of signals induced by small molecules involved in metabolism, called metabolites, and by larger molecules such as lipids and macromolecules. A Fourier Transform converts the FID from the time domain to the frequency domain, producing a spectrum of peaks (Figure 2-5). Metabolites have different chemical structures and experience slightly different magnetic fields which cause small alterations in resonant frequencies (Equation 2-1). This allows identification of metabolites by their characteristic spectroscopy. The spectral appearance of metabolites is governed by two chemical properties: chemical shift and J-coupling.

2.2.1 Chemical Shift

In the presence of an applied magnetic field B_0, the electrons orbiting the nucleus induce a small magnetic field, $B_{induced}$, which opposes B_0 and the nucleus is said to be 'shielded'. The amount of shielding experienced by a nucleus changes the local magnetic field that the nucleus experiences. While the size of the induced field is small – typically around 10^{-6} times smaller than B_0– the difference in shielding experienced by the nuclei of a molecule is large

enough to cause observable shifts in the resonance frequencies as determined by the Larmor equation (Equation 2-1).

To allow comparison between different field strengths, the chemical shift, σ, is typically reported in parts per million (ppm). The ppm unit is independent of field strength and is given by:

$$\sigma = \frac{\nu - \nu_{ref}}{\nu_{ref}} \times 10^6 \qquad \text{(Equation 2-6)}$$

Magnetically equivalent nuclei – those that experience the same shielding and same local magnetic field – can be grouped together and resonate at the same energy. As is seen in Figure 2-6, glycine has two magnetically equivalent protons which produce a single MRS peak at 3.54 ppm. Creatine has a group of three protons which resonates at 3.02 ppm and a group of two protons which produces a peak at 3.91 ppm. The intensity of a resonance peak is proportional to the number of protons in that group. Therefore the creatine peak at 3.02 ppm is 1.5x more intense than the peak at 3.91 ppm.
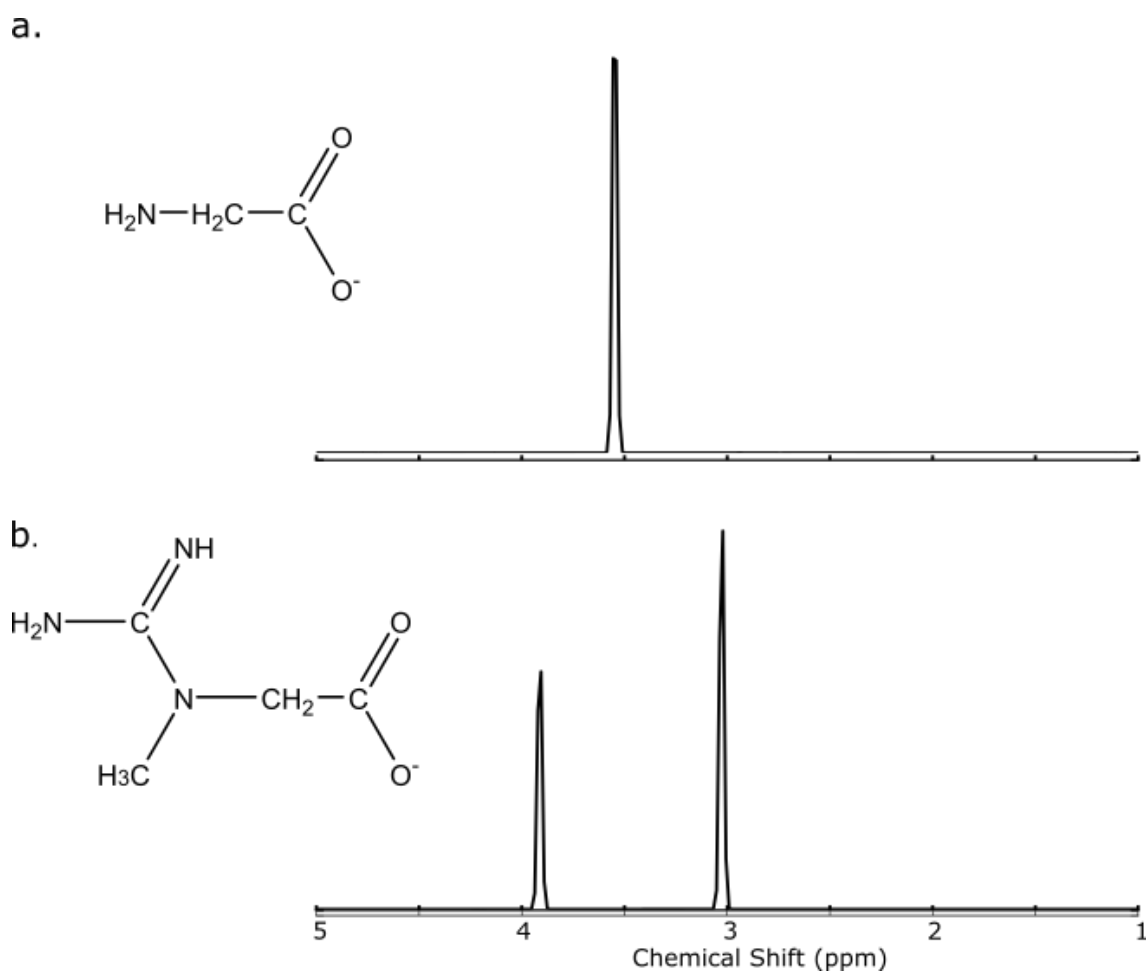
Figure 2-6: The chemical structure and spectrum of a) glycine and b) creatine at 3 Tesla. Each spectrum has been simulated using VESPA at an echo time of 0 ms.

2.2.2 J-coupling

Until this point, magnetic resonance has been treated in a semi-classical manner, stating that the spins will align either parallel or anti-parallel to the magnetic field. Strictly, spin is the intrinsic angular momentum, $\mathbf{I}$, of a nuclei and it is a quantum mechanical property. As before, the angular momentum of a ^1H nuclei can only exist in two discrete states: +1/2 and -1/2 which are known as the α and β states respectively. The α and β states correspond to two energy eigenstates; however, the system is not restricted to these eigenstates but is a superposition of the two energy eigenstates.

The spin Hamiltonian H_0 for a ^{1}H nuclei describes its energy and is proportional to I_z:

$$H_0 = \omega_0 I_z$$

(Equation 2-7)

With eigenstates corresponding to the energy of the system given by:

$$H_0 |\alpha> = +\frac{1}{2}\omega_0 |\alpha>$$

(Equation 2-8)

$$H_0 |\beta> = +\frac{1}{2}\omega_0 |\beta>$$

(Equation 2-9)

Unlike chemical shift, which depends on magnetic field strength, J-coupling is independent of the applied magnetic field B_0. J-coupling arises because the electrons of nuclei with non-zero spin can influence each other through chemical bonds.

The energy, E, of J-coupling is expressed as:

$$E = J_{AX}\boldsymbol{I_A}\boldsymbol{I_X}$$

(Equation 2-10)

Where J_{AX} is called the coupling constant between the two nuclei, A and X, and I_A and I_X represent the angular momentum of the spins.

The magnitudes of the chemical shift difference between nuclei (Δv) and the coupling constant, J, determines the appearance of the spectrum. When $\Delta v >> J$, the spins are said to be weakly coupled.

Lactate is a weakly coupled metabolite and its spectrum can be understood by considering the energy states that each group can take Figure 2-7. The three H atoms of the methyl group each have the same chemical shift and are each coupled to the methine proton with a coupling constant of 6.93 Hz. The methine proton can be in either the α state or the β state. The energy difference between the α and β states leads to a splitting of the resonance into

two peaks of equal heights called a doublet (Equation 2-8, Equation 2-9). Similarly, the

methine proton has a chemical shift of 4.10 ppm and is coupled to the three methyl Hs.

Extending this argument, the methine resonance is split into four peaks (called a quartet)

with an intensity ratio of 1:3:3:1.
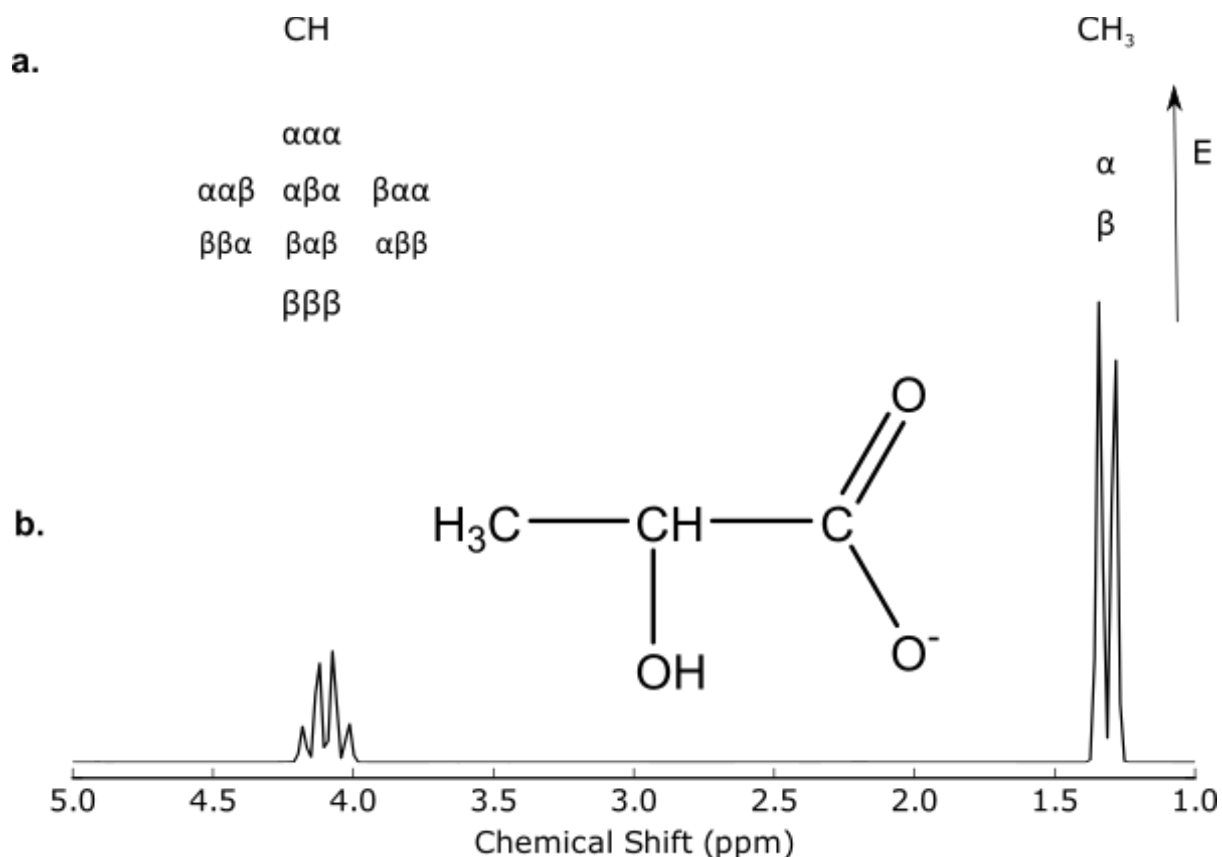
Figure 2-7: a) The energy level diagram and splitting experienced due to J-coupling and b) the
chemical structure and spectroscopy of lactate at 3 Tesla.

Whilst the spectra of weakly coupled molecules can be easily understood in this manner, the

same is not true for strongly coupled molecules. Strong coupling is said to occur when Δν is

of the same order as J.

Under strongly coupled conditions, the energy levels for a pair of spin 1/2 nuclei, A and B, do

not belong to well defined states of spin. The J-coupling interaction mixes the states $\alpha_A\beta_B$

and $\beta_A\alpha_B$ and modifies their energies, leading to a more complex pattern with deviations in the weakly coupled pattern of peak intensities and position. The effects of strong coupling are shown for a two spin system in Figure 2-8. As the two resonances move closer together, the intensity of the inner peaks increases and the outer peaks reduce in size. This intensity distortion of the resonances is sometimes called the roofing effect and can aid the detection of strongly coupled metabolites. For systems with more than two spins, such as glutamate, more peaks than would be expected under the weak coupling limit can appear. For this reason, it is necessary to use computer simulations which describe the system using the Hamiltonian, the chemical shifts and coupling constants to predict the spectral appearance.
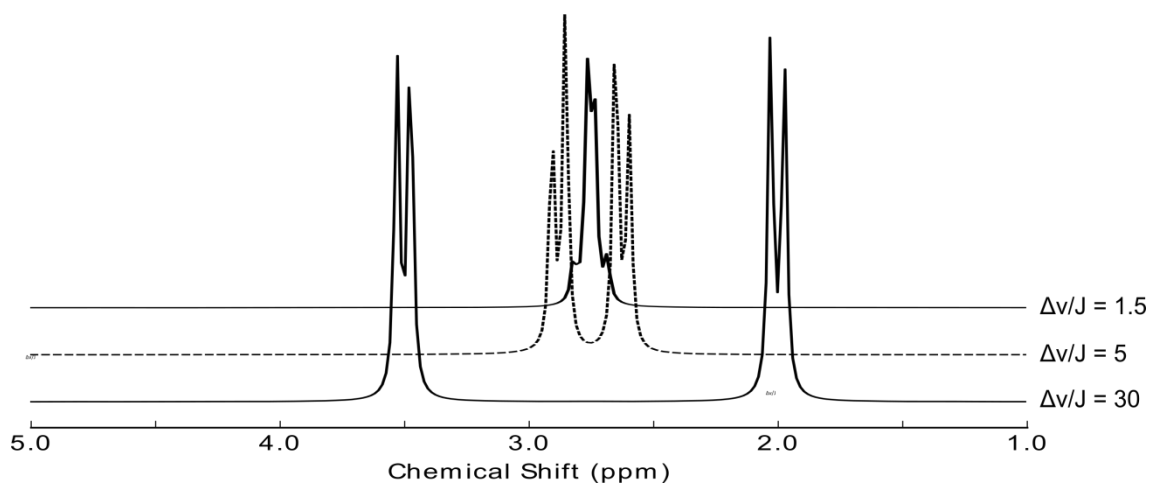
Figure 2-8: Simulated spectra for two coupled spin 1/2 nuclei for a range of Δν/J

2.3 MRS Acquisition

2.3.1 Volume Selection

MRS acquisition schemes can be described as either single voxel or multi-voxel. These phrases describe how many regions of interest MRS is acquired from. Single voxel spectroscopy (SVS) is collected from one region of interest and is the focus of this thesis.

MRS is acquired following the acquisition of anatomical MRI. The three planes of the anatomical image are used to define the voxel. The voxel should be placed carefully to avoid bone, scalp and air which can reduce spectral quality or introduce unwanted lipid signals. In the case of brain tumours, care should also be taken to avoid placing the voxel over adjacent normal brain as prominent signals from normal brain, for example NAA, can confound results.

2.3.2 Shimming

Imperfections in the magnetic field B_0 lead to equivalent nuclei experiencing slightly different magnetic fields. A consequence of this is that equivalent nuclei resonate at different frequencies and this leads to a broadening of the metabolite peaks. The broadening of metabolite peaks has the effect of reducing spectral resolution which can make distinguishing different metabolite peaks difficult. Shimming is performed to reduce the B_0 inhomogeneity over the voxel. This is done by orientating shim coils to produce a magnetic field that compensates for B_0 inhomogeneity.

2.3.3 Water Suppression

Approximately two-thirds of the human body is composed of water. Consequently the concentration of water is substantially larger than that of metabolites in the voxel. This leads to an MRS water signal which is approximately 10,000 times greater than that of metabolites. The water signal is suppressed in order to obtain useful metabolite spectroscopy (Castillo et al., 1996). In this thesis the water is suppressed using the chemical shift selective (CHESS) method (Haase et al., 1985). CHESS selectively excites the water molecules present and a spoiler gradient is applied to dephase the excited spins.

2.3.4 Acquisition Methods

Volumes are excited using pulse sequences with slice selective pulses which are designed to acquire data only from that volume. This is accomplished by eliminating signals from outside the signal through phase cycling of the RF pulses and by using sufficiently large crusher gradients. Various pulse sequences exist and the choice of pulse sequence and acquisition parameters will often depend on the goals of the experiment. This section describes some of the acquisition parameters and conventional single voxel pulse sequences used in MRS.

Key acquisition parameters include the number of signal averages (NSA), the repetition time (TR) and the echo time (TE) (Figure 2-9). To maximise the acquired MRS signal, a pulse sequence is often applied multiple times with the resulting signals averaged. The number of times a pulse sequence is repeated is given by the NSA. The TR describes the time between the start of one pulse sequence and the beginning of the next. The choice of TR will influence the amount of signal acquired and should be informed by the T1 relaxation times of water and metabolites.

The TE is defined as the time between the first 90° pulse and the signal acquisition. The spectrum acquired will depend on the choice of TE. The use of a short TE, used in this thesis to describe echo times of approximately 30-40 ms, helps to maximise the number of MRS signals observed by minimising the effect of T2 relaxation. Broad resonances from macromolecules and lipids are present in short-TE MRS, the combination of these broad resonances is often called the macromolecular baseline. Because of their short T2 relaxation times relative to metabolites, lipids and macromolecules are not present in MRS at long-TE (135 ms in this thesis), producing a flat baseline.

37
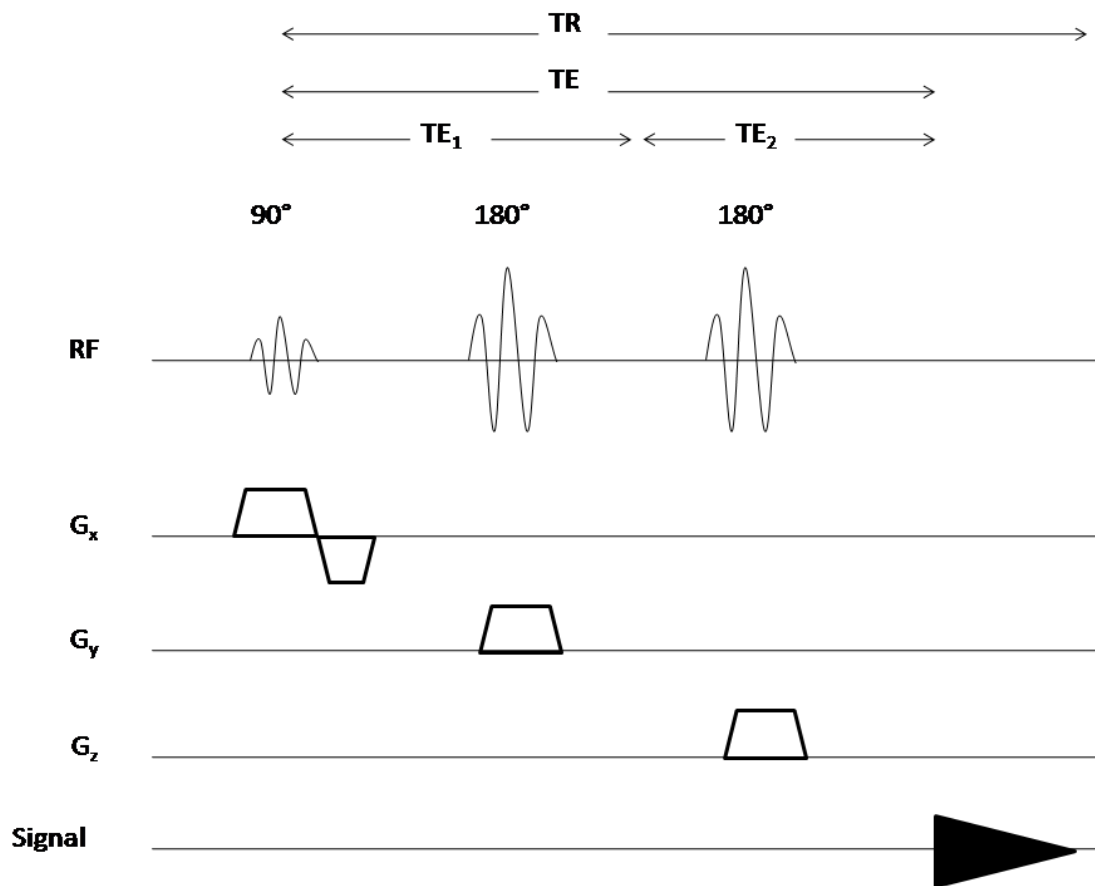
Figure 2-9: Simplified PRESS pulse sequence.

STEAM uses three 90° pulses to stimulate an echo and is able to achieve very short-TEs

(Frahm et al., 1989). Like STEAM, the PRESS pulse sequence (Figure 2-9) consists of three RF

pulses. It is a double spin echo technique that consists of a 90° pulse followed by two

refocusing 180° pulses to create a spin echo (Bottomley, 1987). The TE of the PRESS

sequence is described by TE_1 and TE_2 , with TE_1 defined as double the time the 90° pulse and

first 180° pulse and TE_2 describing the remaining period of the echo time. Optimised (TE_1,

TE_2) echo time spacing can be used to improve detection of coupled metabolites (Choi et al.,

2012, 2011a; Snyder and Wilman, 2010a).

Chemical shift displacement errors arise because molecules resonate at different frequencies. The volume of interest excited by pulse sequences such as PRESS will therefore differ for each resonance. Chemical shift displacement errors can also lead to signal cancellation for coupled resonances due to anomalous J-modulation and errors increase with field strength (Lange et al., 2006). LASER is a technique which uses the large bandwidth of adiabatic RF pulses to produce a uniform excitation profile, therefore reducing chemical shift displacement errors (Garwood and DelaBarre, 2001). While LASER reduces the influence of chemical shift displacement and other technical challenges that occur at field strengths of 3 T and above (Zhu and Barker, 2011), it is not available on all MR scanners. Of the two widely available sequences across vendors and field strengths described here, PRESS and STEAM, PRESS is the most widely used MRS sequence in the clinical environment and is used in this thesis as a compromise between SNR, multiplet dephasing and reduced baseline interference.
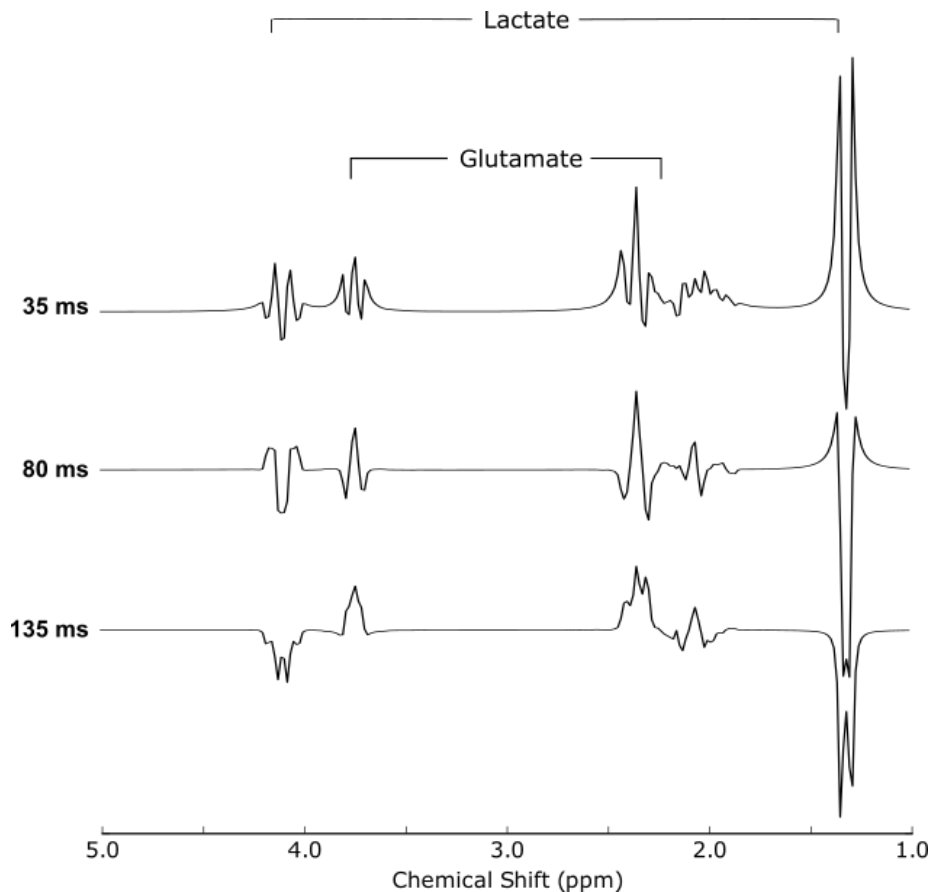
Figure 2-10: J-modulation of lactate and glutamate with increasing echo time.

JPRESS is also used in this thesis. JPRESS is a two-dimensional spectroscopy technique (Ryner et al., 1995; Thomas et al., 1996) based on the PRESS pulse sequence. JPRESS is collected at multiple echo times, keeping TE1 constant (Figure 2-9), and exploits the change in coupled spin systems with echo time (Figure 2-10) to spread the spectrum into two dimensions. This reduces the spectral overlap of metabolite compared to conventional short-TE PRESS.

2.4 MRS Quantification

2.4.1 Introduction to Metabolite Quantification

The simplest method of quantifying metabolites is through integration of the peaks. This approach is limited to simple spectra without overlapping resonances. Single value

decomposition (SVD) can also be used to decompose the spectrum into a series of resonances. The constructed series of resonances is described as a fit to the data. The quality of a fit to the data can be assessed by inspection of the residual signal (Figure 2-11). However, whilst SVD produces a fit which may look adequate on visual inspection, it does not have a biochemical basis. This can lead to resonances from the same metabolite appearing out of phase with each other or having the wrong relative peak intensities. These approaches may be adequate for single peaks at long-TE where the baseline is flat following T2 relaxation. However, with an increasing trend towards using short-TE and the added spectral complexity of short-TE, more sophisticated methods are required. This is particularly important as short-TE spectroscopy contains coupled metabolites, lipids and macromolecules which can be of importance in pathology. Quantification which has a biochemical basis and utilises prior knowledge is therefore key.

Quantification of the whole spectrum using prior knowledge can be performed using software packages such as LCModel (Provencher, 1993) and TARQUIN(Wilson et al., 2011b). These use a linear combination of metabolite, macromolecule and lipid signals, called a basis set, to model the signal. Basis sets can be made using experimentally acquired data or through simulations. Experimental basis sets are acquired from phantom data using the pulse sequence and protocol that will be used for MRS investigations. Phantoms are typically prepared with high metabolite concentrations, in the region of 100 mM, to ensure high SNR spectra are collected. While experimentally acquired basis sets can account for experimental factors, such as eddy currents and spatial profiles, they can be time consuming to obtain as phantom data is needed for every metabolite and protocol under investigation.

41

Furthermore, phantoms can be expensive to build and should be acquired at a physiological

temperature which is a non-trivial task.
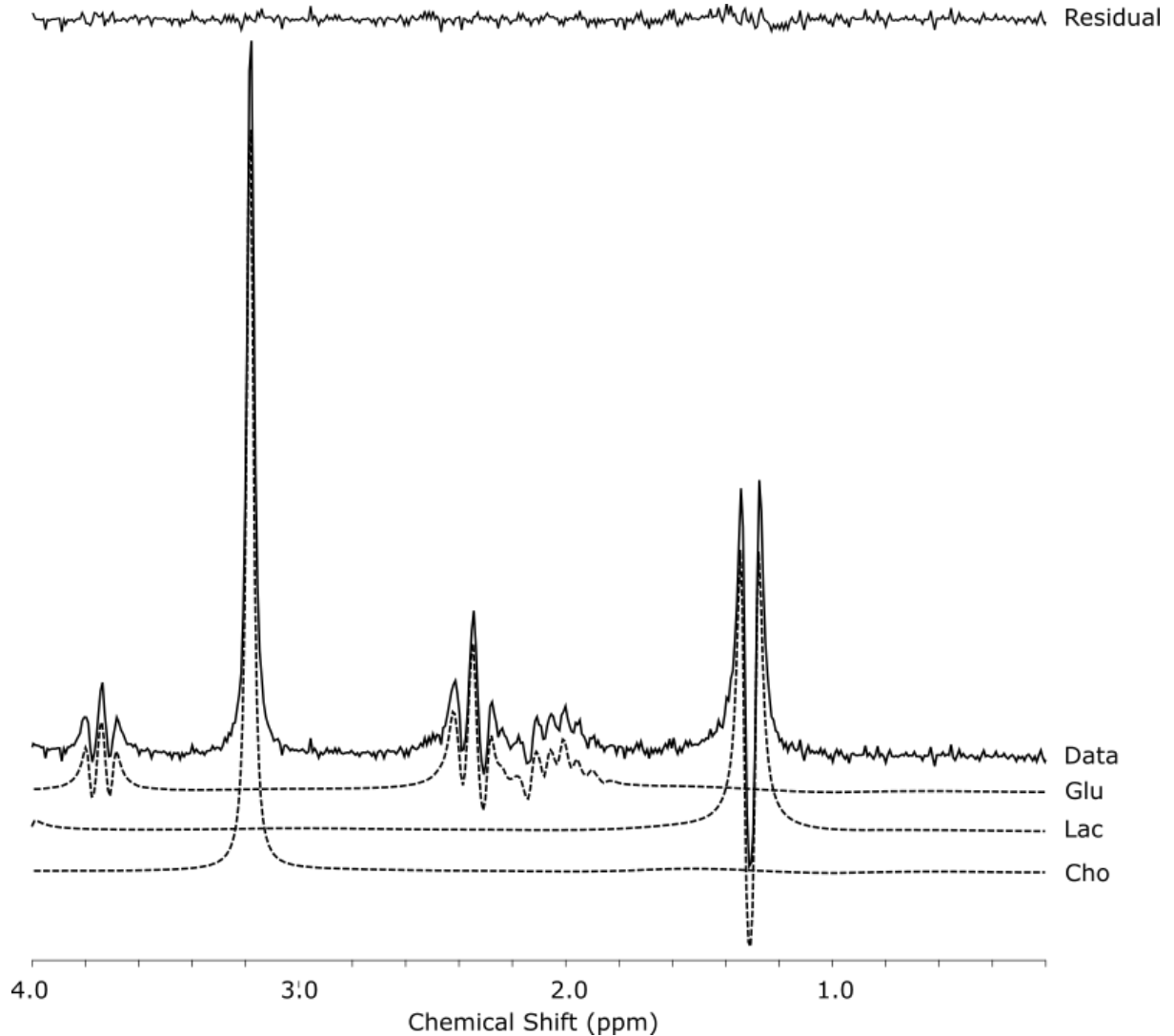
Figure 2-11: Experimentally acquired data from a phantom containing choline (Cho), glutamate (Glu) and lactate (Lac) fitted with TARQUIN using a simulated basis set.

Simulation of the basis sets using density matrix formalism is therefore an attractive

proposition. The advantage of simulated basis sets is that they are noiseless and free of

artifacts. Furthermore, variations in echo time are easily dealt with by simulations as they do

not require the acquisition of additional experimental basis sets. TARQUIN, the analysis

package used in this thesis, employs simulated basis sets.

2.4.2 Basis Set Simulation

A priori knowledge of the chemical shift and coupling constants of a molecule is used to simulate their spectral appearance. Simulation of metabolites is performed following a quantum mechanical assessment of density matrices and is described in full by Levitt (Levitt, 2008). A density matrix describes the energy levels and populations of a spin system.

The system is assumed to begin in thermal equilibrium, given by an initial density matrix $\boldsymbol{\rho}(0)$. Pulse sequences are modelled as RF pulses followed by time delays. The Hamiltonian dictates the free evolution dynamics of a spin system and is determined by considering the molecule's chemical shifts and the J-couplings between spins.

The evolution of the density matrix, $\boldsymbol{\rho}(t)$, under different Hamiltonians, **H**, is such that:

$$\boldsymbol{\rho}(t) = e^{-iHt}\,\boldsymbol{\rho}(0)e^{+iHt}$$ (Equation 2-11)

This enables calculation of the spin-system response to any pulse sequence and can include the effects of magnetic field gradients, delays and the RF pulse shapes used if they are known. Providing accurate prior knowledge is used, simulations of metabolite spectra agree extremely well with experimentally acquired data for both coupled and uncoupled spin-systems. Furthermore, the density matrix formalism approach is equally suitable for both strongly and weakly coupled systems. This is shown in Figure 2-11 where the weakly coupled lactate and the strongly coupled glutamate have been fitted using a simulated basis set.

2.4.3 Metabolite Quantification with TARQUIN

2.4.3.1 Preprocessing
TARQUIN is a fully automatic package for quantification of MRS data (Wilson et al., 2011b). The algorithm preprocesses the data, simulates the basis set and then fits the data in the

time domain. The initial time domain points are truncated to remove the fast decaying components of the FID therefore reducing the influence of baseline components on the fit. The residual water signal is removed by Hankel singular value decomposition. A reference spectrum of synthesised peaks – for example, NAA, tCho and Cr in normal brain – is used to correct for frequency drifts and the data is automatically phased to prevent out of phase peaks.

2.4.3.2 Processing

The remaining signal is modelled in the time domain by a basis set containing metabolites, lipids and macromolecules. Metabolite sets are modelled using published values (Govindaraju et al., 2000) whilst lipids and macromolecules are modelled using estimated parameters (Provencher, 2001b). TARQUIN then modifies the basis signals to account for small differences in the lineshape and frequency due to slight experimental differences in the resonant molecules. A non-negative least squares projection is then used to estimate the signals of the experimental data, fitting in the time domain. Soft constraints on the ratios of NAA/NAAG and of various lipid/lipid and macromolecule/molecule are applied to the signal amplitudes to improve fitting stability and reduce overfitting.

Concentrations are reported with reference to water (Roland Kreis et al., 1993) after accounting for the differences in the T2 relaxation times of water and metabolites. While concentrations are calculated with reference to an unsuppressed water signal, they can also be reported as a ratio to another metabolite present in the spectrum. However ratios can provide only limited information about the metabolic changes that occur. Consider a decrease in the NAA/Cr ratio. This could signify any of a decrease in NAA, an increase in Cr,

alterations to both NAA and Cr or a change in the T2 relaxation times of either or both of the

metabolites involved. For this reason, concentrations are presented as absolute values.

2.4.4 Errors in Quantification

Any quantification method will be subject to error and uncertainty. Errors in metabolite

concentration estimates are typically reported as Cramér-Rao lower bounds (CRLBs)

(Cavassila et al., 2001, 2000). CRLBs represent the lower limit of the measurement error and

are calculated following inversion of the Fisher matrix, **F**, and are given by the following

(Graaf, 2007):

$$\sigma \geq CRLB = \sqrt{\boldsymbol{F^{-1}}}$$
(Equation 2-12)

Where **F** is given by

$$\boldsymbol{F} = \frac{1}{\sigma^2}(\boldsymbol{P^T D^H D P})$$
(Equation 2-13)

and σ is the standard deviation of the noise, **P** is the prior knowledge matrix holding

derivates of one parameter with respect to another, and **D** holds the partial derivatives of

the model function with respect to the parameters in question.

As such, the CRLB will increase with both spectral overlap and noise. Strictly the CRLBs

reported are only approximate measures as they are not calculated using an exactly known

model (Graaf, 2007). Using an exact model is not practical for in vivo data as the nature of

the macromolecular baseline is not precisely known. Differences in how LCModel and

TARQUIN determine the baseline will therefore mean that CRLB estimates will vary between

software packages. Furthermore, estimates of the noise are measured in the time domain by

TARQUIN and in the frequency domain by LCModel and this could also lead to differences in

CRLB values between the two programs.

The use of CRLBs is becoming increasingly controversial for use in MRS studies (Kreis, 2016; Near et al., 2013; Tisell et al., 2013). CRLBs are generally reported as a percentage relative to the estimated concentration. The relative CRLBs have been used to aid exclusion of poor quality spectra and a maximum CRLB threshold of 50% has been recommended (Oz et al., 2014). However, as a relative measure, this means that metabolites present at low concentrations – as is typically the case with NAA in paediatric brain tumours – will inherently have higher CRLBs regardless of fit quality. The use of thresholds can therefore lead to the false exclusion of good quality data. For this reason CRLBs should be used with caution and be accompanied by visual inspection of the spectrum and fit quality by experienced spectroscopists.

2.4.5 Factors Affecting Metabolite Quantification

Whilst the estimated concentrations are subject to error due to data quality, spectral overlap and imperfect fitting models, they are also subject to error due to assumptions made when postprocessing the data. Metabolite concentrations are calculated based on the following equation:

$$Conc = \frac{signal_{amp} * water_{conc} * water_{att}}{water_{amp}}$$

(Equation 2-14)

Where $water_{att}$ describes the difference in relaxation times between water and metabolites. As the concentration of water in vivo is approximately 10,000 times greater than that of metabolites, proton density estimates can give an indication of the concentration of water, $water_{conc}$. Previous imaging data indicates that the proton density of tumour is between 1.25 and 1.32-times greater than that of normal white matter and is between 1.03 and 1.14-fold

greater than that of grey matter. Concentrations determined using the 43,300 mM concentration of grey matter are therefore likely to be underestimated by 3-14%.

By default, TARQUIN assumes the water signal has been collected from a homogenous voxel consisting of just white matter. White matter, grey matter and cerebrospinal fluid (CSF) are known to have different water concentrations (Roland Kreis et al., 1993), while the water content of brain tumours is not well known. Furthermore, the voxel will rarely contain only one of these components. Segmentation of the voxel into its different components should be performed to obtain the most accurate concentration values in normal brain (Gasparovic et al., 2006a).

In brain tumours, intravoxel heterogeneity can arise due to the presence of necrosis and cysts. Previous studies have shown that metabolite concentrations are inversely proportional to the diffusion measure of cellularity (Khayal et al., 2008), ADC, and the reduction in cell density that is associated with necrosis will lead to an overall reduction in all metabolite concentrations. While care should be taken to avoid placing the MRS voxel over necrotic regions, the reduction in metabolite concentrations will cancel through the use of ratios, and this is an option for investigating abnormality using the multi-voxel MRSI (Raschke et al., 2014).

However, as described earlier, ratios can be confounded by changes in relaxation times. Molecules can relax at different rates depending on their microenvironment and the field strength. Accounting for the relative signal reductions of water and the molecule under investigation is therefore important when reporting absolute concentrations. TARQUIN accounts for differences in T2 relaxation time with the parameter W_{att}:

$$W_{att} = \frac{exp(-TE/T2_{water})}{exp(-TE/T2_{metabolite})}$$ (Equation 2-15)

By default W_{att} assumes a short echo time and T2 relaxation times typical of normal brain at

1.5 T. However, T2 relaxation times are known to change with field strength (Träber et al.,

2004b) and alter with pathology (Isobe et al., 2002; Li et al., 2008; Madan et al., 2015a;

Sijens and Oudkerk, 2002). A new W_{att} value should therefore be calculated when

quantifying data at long-TE, higher field strength or from pathology.

The T2 relaxation time of tissue water in adult brain tumours has previously been shown to

be elevated from 70-100 ms in normal brain to 175 ms at 1.5 T (Isobe et al., 2002) and 150

ms at 3 T (Madan et al., 2015). The change in tissue water relaxation times in brain tumours

can lead to metabolite concentration estimates using TARQUIN's default settings to

underestimate by approximately 30% and 35% at 1.5 and 3 T respectively at short-TE.

Furthermore, a previous study has demonstrated that by not adequately accounting for T2

relaxation, metabolite concentration estimates can be increased 7-fold at a TE of 288 ms

(Yamamoto et al., 2015). However, paediatric brain tumours are biologically distinct from

their adult counterparts (Gilheeney and Kieran, 2012) and estimates of T2 relaxation specific

to paediatric brain tumours would be welcome.

While the influence of T1 relaxation times on metabolite concentrations is small compared

to T2 relaxation (Gasparovic et al., 2006), T1 relaxation times will also affect concentration

estimates. The proportional differences between water and metabolite T1 relaxation times

are much smaller than those of T2 relaxation (Mlynárik et al., 2001; Stanisz et al., 2005).

While there is limited information on the T1 of tissue water in paediatric brain tumours, an

early study indicated that the T1 of tissue water in brain tumours is comparable to that of

grey matter (Just and Thelen, 1988) and there are no observed differences in the metabolite

T1 relaxation times between normal brain and pathology (Li et al., 2008; Sijens and Oudkerk,

2002) or between field strengths (Träber et al., 2004). Assuming T1s of 1200 and 1400 ms at

1.5 and 3 T respectively for tissue water and a constant metabolite T1 of 1350 ms,

concentration estimates are likely to be underestimated by 6% at 1.5 T and overestimated

by 2% at 3 T when repetition times of 1500 ms and 2000 ms are assumed.

Overall, T2 relaxation times lead to the most significant source of error in metabolite

concentration estimation, though T1 relaxation can cancel some of this effect. T2 relaxation

times can be estimated by acquiring MRS at two echo times and this approach has been

shown to provide complementary information and improve classification of paediatric brain

tumours (Vicente et al., 2013). Furthermore, with long-TEs becoming more commonly used

clinically (Choi et al., 2012), the errors associated with T2 relaxation time are compounded.

For these reasons, T2 relaxation is investigated as a major source of error in metabolite

quantification ahead of proton density and T1 relaxation effects in this thesis.

3. METHODS

3.1 Simulations

Simulations are a powerful research tool that can greatly enhance our understanding of MR spectroscopy. In this thesis, the spectral appearance of various in vivo metabolites at 3 T (127.8 MHz) was simulated for a range of echo times. All simulations were calculated using VESPA (Soher et al., 2011). VESPA is based on the GAMMA library (Smith et al., 1994) and simulates metabolite appearance using published literature values of chemical shift and J-coupling values (Govindaraju et al., 2000).

Spectra were simulated assuming an Ideal PRESS pulse sequence (PRESS Ideal) at various echo times (Figure 2-9). PRESS Ideal simulates hard 90 and 180 degree pulses and does not account for the specific, vendor-specific pulse shapes used when acquiring real data. The first echo time spacing (TE_1) of the pulse sequence was kept constant at 10 ms for all experiments, such that (TE_1 + TE_2) = TE was (10 + 25 ms) for TE = 35 ms and (10 + 40 ms) for TE = 50 ms.

Spectra were exported as jMRUI text with a Lorentzian lineshape of FWHM of 1 Hz. The sweep width and number of data points were 2000 Hz and 1024 respectively.

The real and imaginary components of the FID corresponding to each metabolite and echo time combination were read into Python from the jMRUI text outputs using code written in house.

3.1.1 Simulation of PRESS

The 1H spectral appearance of N-acetylaspartate (NAA), creatine (Cr),

glycerophosphocholine (GPC), phosphocholine (PCh), glutamate (Glu), glutamine (Gln),

glycine (Gly), lactate (Lac) and myo-Inositol (ml) were simulated at echo times of 35, 80 and

135 ms. These metabolites were combined into various spectral model systems to assess the

importance of echo time choice for metabolite quantification

To create the synthesised spectrum for each model, the FIDs corresponding to each

metabolite were summed to create the overall FID of the spectrum. A residual water peak

was added to simulate incomplete water suppression and random Gaussian noise was

applied to the FID and the spectrum was line broadened. The resulting FID data was written

into a DICOM file for analysis with TARQUIN (Wilson et al., 2011). Spectra were modelled

under controlled conditions to assess only the influence of the spectral overlap of

metabolites on metabolite quantification. Overlap of lipid and macromolecular resonances

and inaccurate baseline modelling is also likely to impair metabolite quantification accuracy

(Birch et al., 2016).

3.1.2 Simulation of JPRESS spectra

The JPRESS appearances of 20 metabolites which can be observed in vivo were simulated to

aid identification of metabolites. JPRESS was simulated for alanine (Ala), asparate (Asp),

citrate (Cit), creatine (Cr), γ-Aminobutyric acid (GABA), glucose (Glc), glutamine (Gln),

glutamate (Glu), glutathione (Glth), glycine (Gly), glycerophosphocholine (GPC), hypotaurine,

lactate (Lac), myo-Inositol (ml), N-acetylaspartate (NAA), phosphocholine (PCh), scyllo-

Inositol (Scy) and taurine (Tau).

To simulate the dataset, the FIDs of each metabolite were calculated for 18 echo times ranging from 42 ms to 297 ms in 15 ms increments. A relaxation penalty given by $\exp(-TE/250)$ was applied to each FID. The FIDs corresponding to each echo time were then combined and Fourier Transformed in two dimensions to produce the JPRESS spectrum.

To assess the utility of JPRESS for discrimination between overlapping metabolites, JPRESS was also simulated for the following spectral models: NAA, Glu and Gln; mI and Gly; and GPC, PCh, Tau and Scy.

3.2 MRS Acquisition

Ethical approval was obtained for all studies and informed consent was granted. Single voxel MRS was acquired in a paediatric brain tumour cohort at Birmingham Children's Hospital at 1.5 and 3 T and from a congenital adrenal hyperplasia (CAH) population at Birmingham University Imaging Centre, with 1.5 T data collected using a Siemens Symphony Magnetom NUM4 scanner and 3 T data acquired using a Phillips Achieva scanner. Age matched controls were also collected for both cohorts.

Spectroscopy was collected using either a single echo time (TE) or multiple TEs using a point-resolved spectroscopy sequence (PRESS) (Bottomley, 1987). Where multiple TEs were collected, the spectroscopy sequences were linked as a parameter series to ensure the receiver gain stayed constant. MRS followed conventional imaging which consisted of T1 and T2-weighted imaging, with T1-weighted images also collected post contrast for the brain tumour studies.

All MRS at 1.5 T was acquired with 35 ms short-TE and 135 ms long-TE and a TR of 1500 ms. At 3 T, the core protocol consisted was collected at short 36-41 ms TE and water

unsuppressed data collected at 18 TEs spaced equally between 42 and 297 ms. A TR of 2000 ms was used for each acquisition. Data was also collected in the CAH cohort at a long-TE of 135 ms.

A subset of paediatric brain tumours had JPRESS collected at 3 T from a 30 x 30 x 30 mm voxel. The JPRESS protocol consisted of water suppressed data collected at 18 TEs with equal spacing of 15 ms between 42 and 297 ms. A TR of 2000 ms was used and the NSA/TE was 8.

3.3 Processing

3.3.1 Voxel Segmentation

A T1-weighted image of the brain was converted from DICOM to NIfTI using MRICron (Rorden and Brett, 2000). The T1-weighted image was skull stripped using the FSL (Smith et al., 2004) tool BET to remove extra-cerebral tissues such as skin, bone and the eyeballs (Smith, 2002). A mask of the spectroscopy voxel was created and segmentation was performed using the FSL tool FAST to determine the amount of grey matter (GM), white matter (WM) and cerebrospinal fluid (CSF) present in the voxel (Zhang et al., 2001).

Metabolite Quantification

Metabolite concentrations were initially quantified with TARQUIN v4.3.8 using the internal basis set 1H brain + Cit, Glth, Gly. The following metabolite, lipid and macromolecule signals were included in the basis set: Ala, Asp), GABA, GPC, Glc, Gln, Glth, Glu, Gly, mI, Lac, NAA, N-acetylaspartylglutamate (NAAG),PCh, phosphocreatine (PCr), Scy, Tau, lipids at 0.9, 1.3 (a+b) and 2.0 ppm and macromolecules at 0.9, 1.2, 1.4, 1.7 and 2.0 ppm.

The water attenuation parameter, W_{att}, was set to 1 and the water concentration was assumed to be 43,300 mM, the same as grey matter, unless otherwise stated.

3.3. T2 Relaxation Estimation

The metabolite signal amplitudes estimated by TARQUIN were fitted to a monoexponential decay curve to estimate the T2 relaxation times of metabolites. The T2 relaxation time of water was estimated from either two TEs collected at 35-41 and 135 ms or from five TEs collected between 42 and 112 ms with 15 ms spacing between TEs.

Concentration Correction for Relaxation Effects

Metabolite concentrations in brain tumours were corrected for relaxation effects by multiplying initial concentration estimates by W_{att}. W_{att} is calculated using estimates of the relaxation times and is calculated for brain tumours using:

$$W_{att} = \frac{exp(-TE/T2_{water})}{exp(-TE/T2_{metabolite})}$$ (Equation 3-1)

For normal brain, the reported metabolite concentrations were corrected for relaxation effects in accordance with the method detailed by Gasparovic et al (Gasparovic et al., 2006b). The volume estimates of grey matter, f_{GM_v}, white matter, f_{WM_v}, and cerebrospinal fluid, f_{CSF_v}, from image segmentation were used to estimate the water attenuation factor in normal brain, given by:

$$W_{att} = \frac{f_{GM}R_{GM} + f_{WM}R_{WM} + f_{CSF}R_{CSF}}{(1 - f_{CSF})R_{met}}$$ (Equation 3-2)

Where R_{GM}, R_{WM}, R_{CSF} and R_{met} describe the relaxation of GM, WM, CSF and the metabolites respectively and f_{GM}, f_{WM} and f_{CSF} describe the MR-visible water densities of these volumes. A full description of these parameters is described in the following reference (Gasparovic et al., 2006b).

For MRS data collected at multiple echo times, the spectroscopy was quantified at each TE and subsequently corrected for relaxation effects. The mean concentration of the estimates at all echo times is reported.

3.4 Quality Control

The location of MRS voxels was assessed on conventional MRI to confirm the voxel was placed away from bone, scalp and air. For paediatric brain tumour cases, voxel placement was also assessed to confirm that the voxel was placed over the solid enhancing component and that normal brain was not included.

MRS was included in the data analysis following visual inspection of the spectrum for spectral artifacts. Visual inspection was also used to assess the presence of tNAA, tCho and tCr and confirm the TARQUIN fit to these resonances. In addition to visual inspection, quantified estimates of spectral quality were used for quality control. Broad peaks can hinder accurate metabolite quantification, therefore spectra with a water peak full width half maximum line width greater than 10 Hz were excluded from the analysis. Spectra with a signal to noise ratio less than 4 were also excluded.

3.5 Statistical Analysis

All statistical analysis was performed with Python with statistical significance was declared for $P < 0.05$. Paired and unpaired Student's t-tests and non-parametric Mann-Whitney U-tests were used to compare metabolite concentrations and T2 relaxation times between tissue types. Analysis of variance (ANOVA) tests were used to compare between multiple groups.

Estimated metabolite concentrations were compared by calculating the percentage

difference between the two values:

$$Percentage\ Difference = 100 \times \frac{(Concentration_1 - Concentration_2)}{(Concentration_1 + Concentration_2)/2}$$ (Equation 3-3)

In cases where the actual concentration was known, the percentage error was used:

$$Percentage\ Error = 100 \times \frac{(Concentration_{est} - Concentration_{act})}{Concentration_{act})}$$ (Equation 3-4)

4. INFLUENCE OF ECHO TIME CHOICE ON METABOLITE QUANTIFICATION

4.1 Introduction

Metabolite concentrations are fundamental biomarkers. The metabolite profile of an MRS spectrum can demonstrate differences between both normal brain and brain tumours and between tumour types (Davies et al., 2008b; Panigrahy et al., 2010b). Quantified metabolite concentrations can also be used for non-invasive diagnosis (García-Gómez et al., 2009; Preul et al., 1996), treatment monitoring (Harris et al., 2008b; Steffen-Smith et al., 2011b) and treatment planning (Pirzkall et al., 2009).

MRS has historically focused on metabolites with large singlets without significant spectral overlap and lactate. However, there is emerging evidence that two pairs of metabolites are important in childhood brain tumours. The first pair, glutamate (Glu) and glutamine (Gln), are coupled metabolites, each with multiple resonances spread between 2.0 and 2.5 ppm. In high grade cerebellar tumours, Gln was found to be significantly lower and Glu was found to be significantly higher, when compared with low grade tumours (Davies et al., 2008b)

The second pair of metabolites is glycine (Gly) and myo-Inositol (mI). Gly presents as a single peak at 3.55 ppm and elevated levels are associated with an increase in grade (Davies et al., 2010b). The most prominent mI resonance is also at 3.55 ppm. High levels of mI are indicative of low tumour grade in brain tumours while low levels of mI have been found in tumours which would later progress (Harris et al., 2008b).

While the introduction of clinical field strengths of 3 T improves the dispersion of metabolites, reducing spectral overlap, there is still significant overlap between the

metabolites in each pair. This has led to the design of numerous acquisition protocols, each aimed at optimising measurement of a specific metabolite.

Acquisition methods proposed for measurement of coupled metabolites vary in complexity; however one of the simplest is to acquire MRS using an optimised TE. Using the chemical shift and J-coupling values of a metabolite, the spectral appearance of metabolites can be simulated at a range of echo times. By evaluating the spectral overlap with other metabolites and calculating the metabolite yield at each echo time, an echo time optimised for metabolite quantification can be proposed where overlapping resonances are minimised. Echo times of 40 ms (Mullins et al., 2008) and 80 ms (Schubert et al., 2004a) have been proposed for Glu, whilst an echo time of 110 ms has been proposed for measurement of Gln (Snyder and Wilman, 2010b). An echo time of 160 ms has been proposed for simultaneous measurement of myo-Inositol and glycine (Choi et al., 2011b).

Though optimal echo times have been proposed to improve metabolite quantification, there is limited evidence that they improve the accuracy of metabolite quantification. Accurate metabolite quantification requires correction for T2 relaxation effects and correction for T2 relaxation becomes more important at longer echo times (Yamamoto et al., 2015b). However, the effects of T2 relaxation times on accurate quantification have not been extensively assessed.

In this chapter, a combination of simulations, phantoms and volunteer data is used to assess three spectral models. The model systems of Glu, Gln and NAA, and Gly, mI and Cho are used to investigate quantification of pairs of metabolites with overlapping resonances of similar intensities. A model system containing the major metabolites typical of normal brain

is also used. The aims of this chapter are to investigate the influence of J-coupling evolution with echo time and the importance of T2 relaxation times on accurate metabolite quantification. The chapter is presented in two sections, the first deals with the effect of echo time in simulations with T2 relaxation excluded and the second investigates the effects of both J-coupling and T2 relaxation using phantoms and volunteers.

4.2 Quantification of Simulated Metabolite Spectra

4.2.1 Methods and Materials for Simulation Experiments

Three model systems containing various combinations of metabolites were assessed. The models were as follows:

1) Glu, Gln, NAA with a ratio of 1:1:1

2) mI, Gly, phosphocholine (PCh), GPC with a ratio of 2 : 1 : 1 : 1

3) Brain: NAA, Cho, Cr, Glu, mI, Lac with a ratio of 12.5 : 3 : 10 : 12.5 : 7.5 : 5

Models 1 and 2 were used to investigate pairs of metabolites important in paediatric brain tumours which can lead to contrasting clinical outcomes (Peet et al., 2012). The ratios were chosen to produce peaks of equal intensity for Glu and Gln in model 1 and for mI and Gly in model 2. Model 3 was chosen to assess concentrations that are typically seen in vivo (Govindaraju et al., 2000).

<u>Simulations</u>

Simulations of the three model systems were produced at three echo times to assess the influence of J-modulation and spectral overlap on metabolite quantification. A complete description of the process of simulating metabolite spectra is provided in Chapter 3.

Metabolite spectra were simulated at 3T using VESPA (Soher et al., 2011). Spectra were simulated at echo times of 35, 80 and 135 ms with a TE_1 of 10 ms using an ideal PRESS sequence. Individual metabolite spectra were exported as text files with 1024 data points, a sweep width of 2000 Hz and a Lorentzian lineshape with a line width of 1 Hz.

The free induction decays generated for each metabolite were read into Python. The metabolites were combined and weighted into various spectra according to the models detailed above. These idealised spectra did not include the presence of lipids or macromolecules and relaxation effects were not simulated.

Noise was added to the noiseless spectrum to simulate SNR levels of 25, 15 and 5 and spectra were line broadened to a linewidth of FWHM of 3 Hz by applying an exponential decay apodisation function in the time domain. A second set of spectra with identical metabolite combinations and SNR was also generated and line broadened to a FWHM of 7 Hz to assess the effect of shim on quantification.

A new noise seed was created for each spectrum and the resulting spectrum was converted in to DICOM format for analysis with TARQUIN.

The metabolite spectra were referenced to a simulated water spectrum and the metabolite concentration simulated was verified by quantifying a noiseless spectrum containing only one metabolite.

The simulated spectra were analysed with TARQUIN with created basis sets which contained only the metabolites present in the spectrum. The results for each simulation run were recorded. The simulations were run until the mean metabolite concentration for each

metabolite in the model had converged on a value. The convergence point was mathematically defined as the point at which the mean metabolite concentration over all simulation runs did not deviate by more than 0.01 mM from the convergence point for 50 successive points.

The mean concentrations measured for each metabolite were compared to the simulated concentration to assess the accuracy of metabolite quantification. The percentage error and root mean square (rms) percentage errors of estimated concentrations compared with the simulated concentrations were calculated for each simulation run to investigate the precision and accuracy of metabolite quantification.

4.2.2 Results of Simulation Experiments

4.2.2.1 Data Quality and Metabolite Quantification at 3 T
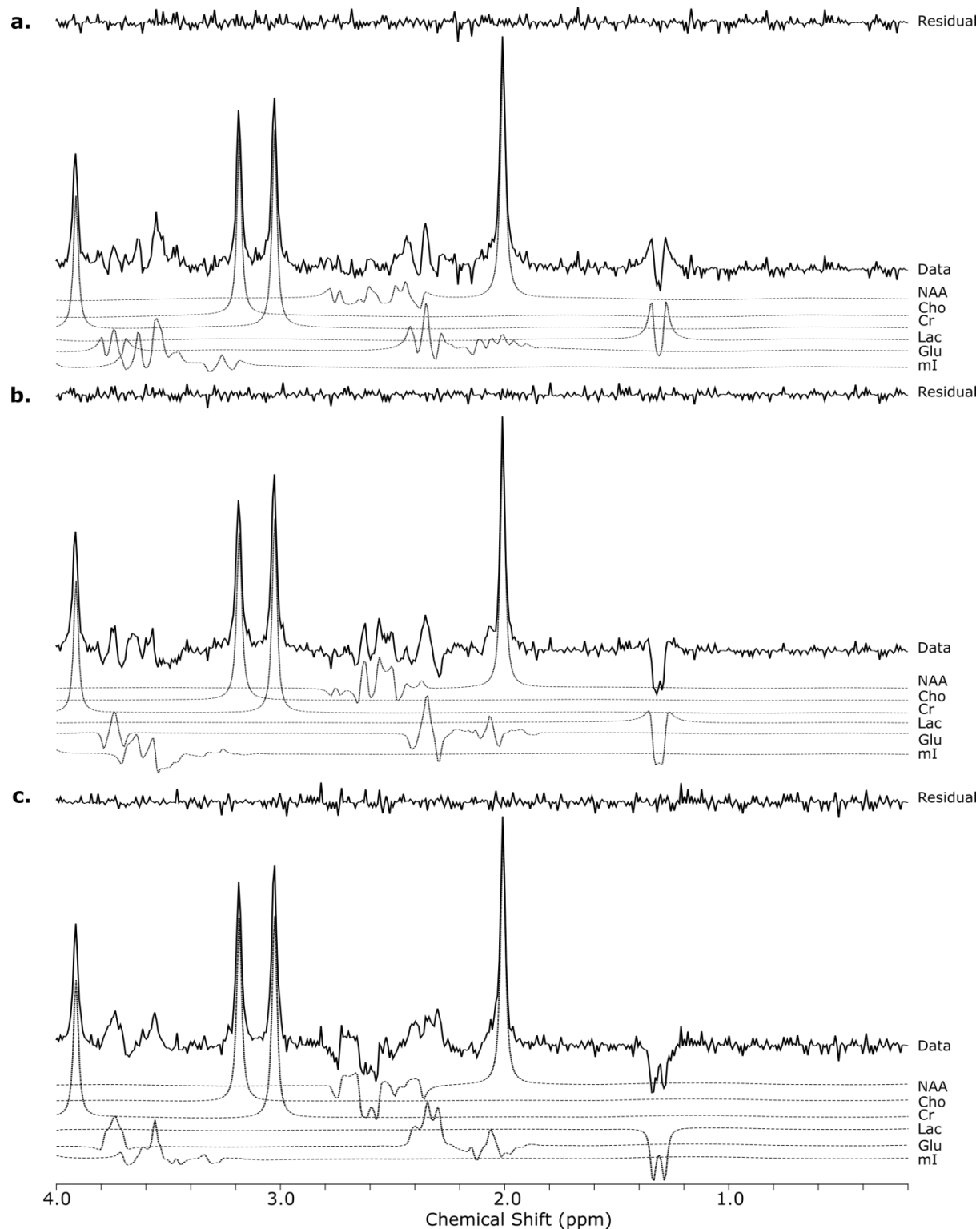
Figure 4-1: Simulated metabolite spectra and TARQUIN fits of the brain model system including NAA, Cho, Cr, Lac, Glu and mI at TEs a) 35 ms, b) 80 ms and c) 135 ms with SNR 25 and FWHM 3 Hz.

Figure 4-2: Simulated metabolite spectra and TARQUIN fits of the brain model system including NAA, Cho, Cr, Lac, Glu and mI at TEs a) 35 ms, b) 80 ms and c) 135 ms with SNR 5 and FWHM 7 Hz.

TE (ms)	**FWHM 3 Hz, SNR 5**			**FWHM 3 Hz, SNR 15**			**FWHM 3 Hz, SNR 25**		
	NAA	Cho	Cr	NAA	Cho	Cr	NAA	Cho	Cr
35	12.34 ± 1.28	2.94 ± 0.40	9.96 ± 1.09	12.49 ± 0.63	2.96 ± 0.19	9.98 ± 0.53	12.50 ± 0.40	2.97 ± 0.13	9.93 ± 0.33
80	12.27 ± 1.16	2.97 ± 0.38	10.00 ± 1.08	12.36 ± 0.54	2.98 ± 0.18	10.01 ± 0.49	12.39 ± 0.33	2.99 ± 0.11	10.00 ± 0.32
135	12.29 ± 1.52	2.94 ± 0.48	10.01 ± 1.35	12.47 ± 0.64	2.97 ± 0.20	9.98 ± 0.55	12.45 ± 0.36	2.97 ± 0.12	9.92 ± 0.32

TE (ms)	**FWHM 7 Hz, SNR 5**			**FWHM 7 Hz, SNR 15**			**FWHM 7 Hz, SNR 25**		
	NAA	Cho	Cr	NAA	Cho	Cr	NAA	Cho	Cr
35	12.43 ± 1.20	2.95 ± 0.37	9.89 ± 1.01	12.30 ± 0.62	2.90 ± 0.18	9.65 ± 0.49	12.28 ± 0.37	2.89 ± 0.11	9.60 ± 0.30
80	12.19 ± 1.02	2.96 ± 0.35	9.96 ± 0.96	12.10 ± 0.47	2.93 ± 0.16	9.78 ± 0.45	12.06 ± 0.26	2.92 ± 0.08	9.73 ± 0.24
135	12.30 ± 1.08	2.97 ± 0.36	9.99 ± 0.93	12.07 ± 0.49	2.91 ± 0.16	9.68 ± 0.40	11.90 ± 0.32	2.86 ± 0.10	9.54 ± 0.27

Table 4-1: Mean ± SD metabolite concentration for NAA (12.5 mM), Cho (3 mM) and Cr (10 mM) in the brain model system.

The brain model system, which contains NAA, Cho, Cr, Glu, mI and Lac at physiological concentrations, was simulated at TEs of 35, 80 and 135 ms. Representative spectra with SNR 25 and linewidth 3 Hz and SNR 5 and linewidth 7 Hz are shown in Figures 4-1 and 4-2. The system was simulated with different metabolite linewidths and SNRs to evaluate the effect that changes in experimental conditions has on metabolite quantification. Different noise seeds were applied to each simulation run and each run was analysed with TARQUIN. The spectral appearance of NAA, Cho and Cr is dominated by large single peak resonances. The mean and standard deviation of the concentrations estimated by TARQUIN for these metabolites is presented in Table 4-1. As the SNR increased, the standard deviation of the concentration estimate decreased. The mean concentrations were less accurate with a linewidth of 7 Hz compared with the mean at 3 Hz, however the standard deviation was smaller.

The root mean square (RMS) percentage error of the estimated concentration is presented for NAA, Cho and Cr in Figure 4-2. The RMS percentage errors reduced with increasing SNR and were smaller with a linewidth of 3 Hz. The average RMS percentage error for an SNR of 5 was 11.5% for NAA, Cho and Cr. The average RMS percentage errors were 5.6% and 4.1% for SNRs of 15 and 25 respectively.

Overall, the mean estimated metabolite concentrations improved with narrow linewidths and increasing SNR. Metabolites with prominent singlet peaks without significant spectral overlap could be measured with an error of 5% with an SNR $\geq$ 15.
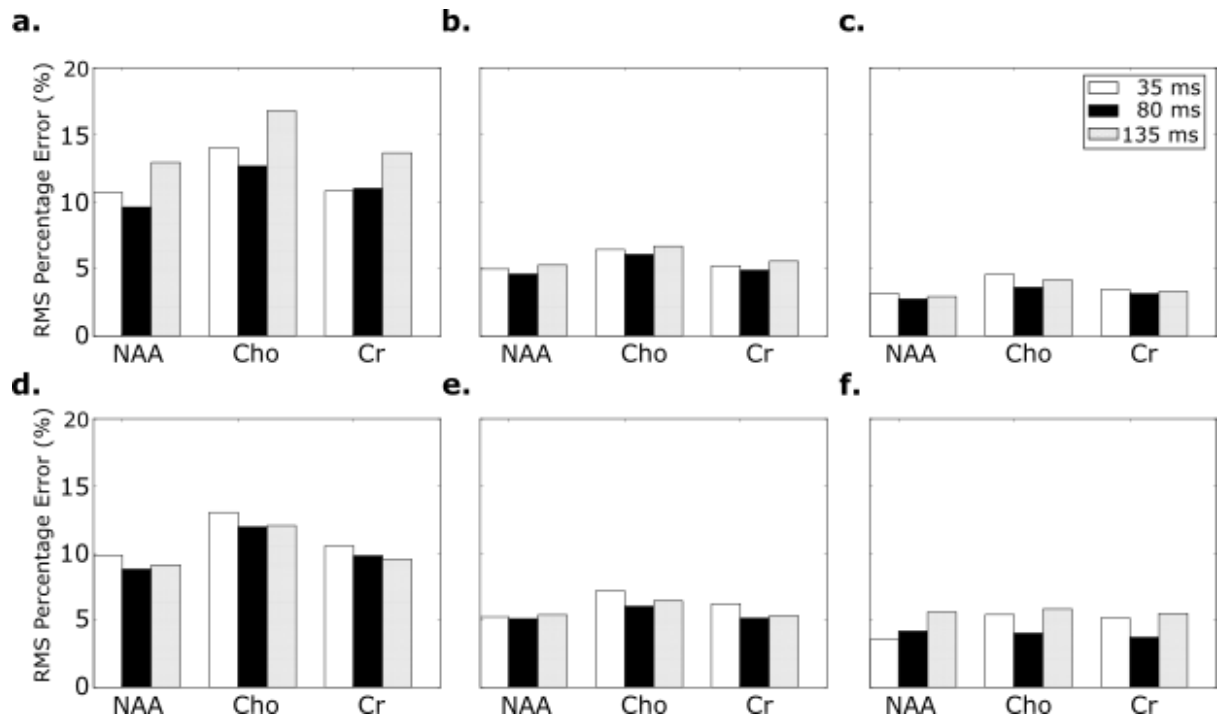
Figure 4-3: Root mean square (RMS) percentage error from the simulated concentration for N-acetylaspartate (NAA), choline (Cho) and creatine (Cr) in the brain model system with SNRs and FWHMs of a) SNR 5; FWHM 3 Hz; b) SNR 15, FWHM 3 Hz; c) SNR 25, FWHM 3 Hz; d) SNR 5, FWHM 7 Hz; e) SNR 15, FWHM 7 Hz; f) SNR 25, FWHM 7 Hz

4.2.2.2 Quantification of Coupled Metabolites and the Effect of Spectral Overlap

Whilst NAA, Cho and Cr present with large single MRS peaks to facilitate quantification, Glu, mI and Lac have complex spectral appearances. The mean and standard deviation of the estimated Glu, mI and Lac concentrations in the brain model system are presented in Table 4-2. As for NAA, Cho and Cr, the lowest standard deviations were found with an SNR of 25. Figure 4-3 presents the RMS percentage errors from the simulated concentrations for Glu, mI and Lac in the brain model system. The RMS percentage errors were significantly larger for Glu, mI and Lac compared to NAA, Cho and Cr at SNR 25 and FWHM 3 Hz (3.5% vs 10.9%, Student's t-test, t = -6.8, P = 0.0001).

	FWHM 3 Hz, SNR 5			FWHM 3 Hz, SNR 15			FWHM 3 Hz, SNR 25		
TE (ms)	Glu	mI	Lac	Glu	mI	Lac	Glu	mI	Lac
35	12.20 ± 4.43	7.06 ± 1.84	4.94 ± 1.96	12.14 ± 2.54	7.17 ± 1.07	4.84 ± 1.12	12.26 ± 1.57	7.20 ± 0.66	4.86 ± 0.73
80	12.00 ± 3.91	7.26 ± 2.40	4.82 ± 1.26	11.78 ± 2.23	7.44 ± 1.29	4.90 ± 0.66	11.72 ± 1.44	7.59 ± 0.81	4.89 ± 0.42
135	12.28 ± 2.90	7.45 ± 3.18	5.00 ± 1.30	12.30 ± 1.26	7.37 ± 1.56	5.02 ± 0.59	12.29 ± 0.70	7.50 ± 0.95	5.04 ± 0.35

	FWHM 7 Hz, SNR 5			FWHM 7 Hz, SNR 15			FWHM 7 Hz, SNR 25		
TE (ms)	Glu	mI	Lac	Glu	mI	Lac	Glu	mI	Lac
35	11.80 ± 3.78	6.85 ± 1.57	4.91 ± 1.82	11.67 ± 1.76	6.87 ± 0.74	4.69 ± 0.91	11.71 ± 1.05	6.87 ± 0.46	4.73 ± 0.57
80	11.21 ± 3.49	7.27 ± 1.99	4.73 ± 1.10	10.66 ± 2.02	7.35 ± 0.99	4.70 ± 0.59	10.34 ± 1.22	7.41 ± 0.69	4.66 ± 0.34
135	11.96 ± 1.85	7.12 ± 2.06	4.95 ± 0.87	11.80 ± 0.96	6.79 ± 0.98	4.90 ± 0.45	11.72 ± 0.64	6.67 ± 0.58	4.81 ± 0.32

Table 4-2: Mean ± SD metabolite concentration for Glu (12.5 mM), mI (7.50 mM) and Lac (5 mM) in the brain model system.
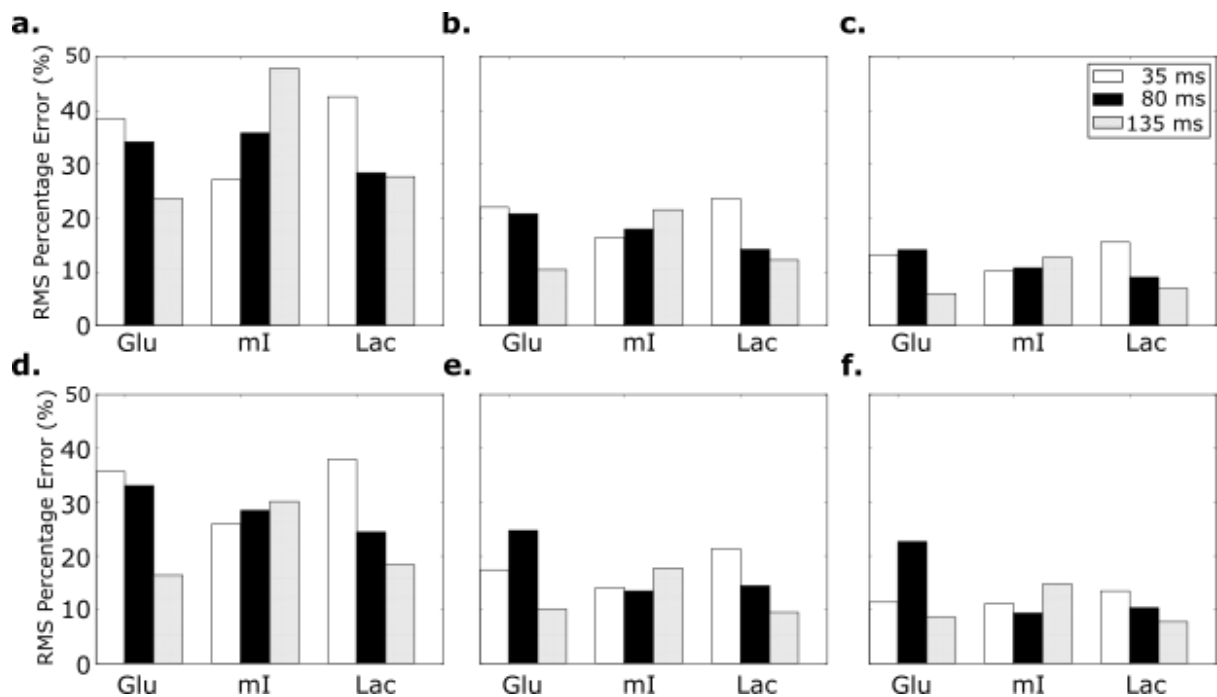
Figure 4-4: Root mean square (RMS) percentage error from the simulated concentration for glutamate (Glu), myo-Inositol (mI) and lactate (Lac) in the brain model system with SNRs and FWHMs of a) SNR 5; FWHM 3 Hz; b) SNR 15, FWHM 3 Hz; c) SNR 25, FWHM 3 Hz; d) SNR 5, FWHM 7 Hz; e) SNR 15, FWHM 7 Hz; f) SNR 25, FWHM 7 Hz

Two additional spectral model systems were simulated to assess the effect of overlapping metabolite resonances on metabolite quantification. The NAA, Glu and Gln model and the GPC, PCh, mI and Gly model are shown in Figure 4-4 and Figure 4-5 respectively. The mean and standard deviations concentration estimates are presented in Table 4-3 and Table 4-4. The RMS percentage errors for the NAA, Glu and Gln are shown in Figure 4-6 and for tCho (GPC + PCh), mI and Gly in Figure 4-7.

The RMS percentage errors for NAA and Glu in the brain and in the NAA, Glu, Gln model systems were compared. The increase of spectral overlap due to the presence of Gln did not lead to a change in RMS percentage errors for NAA (6.3% vs 6.4%; Student's t-test, t = 0.62, *P*

= 0.62) or Glu (20.1% vs 20.1%; t = -0.04, *P* = 0.96) when the RMS percentage errors were

averaged over all TEs and all experimental conditions.
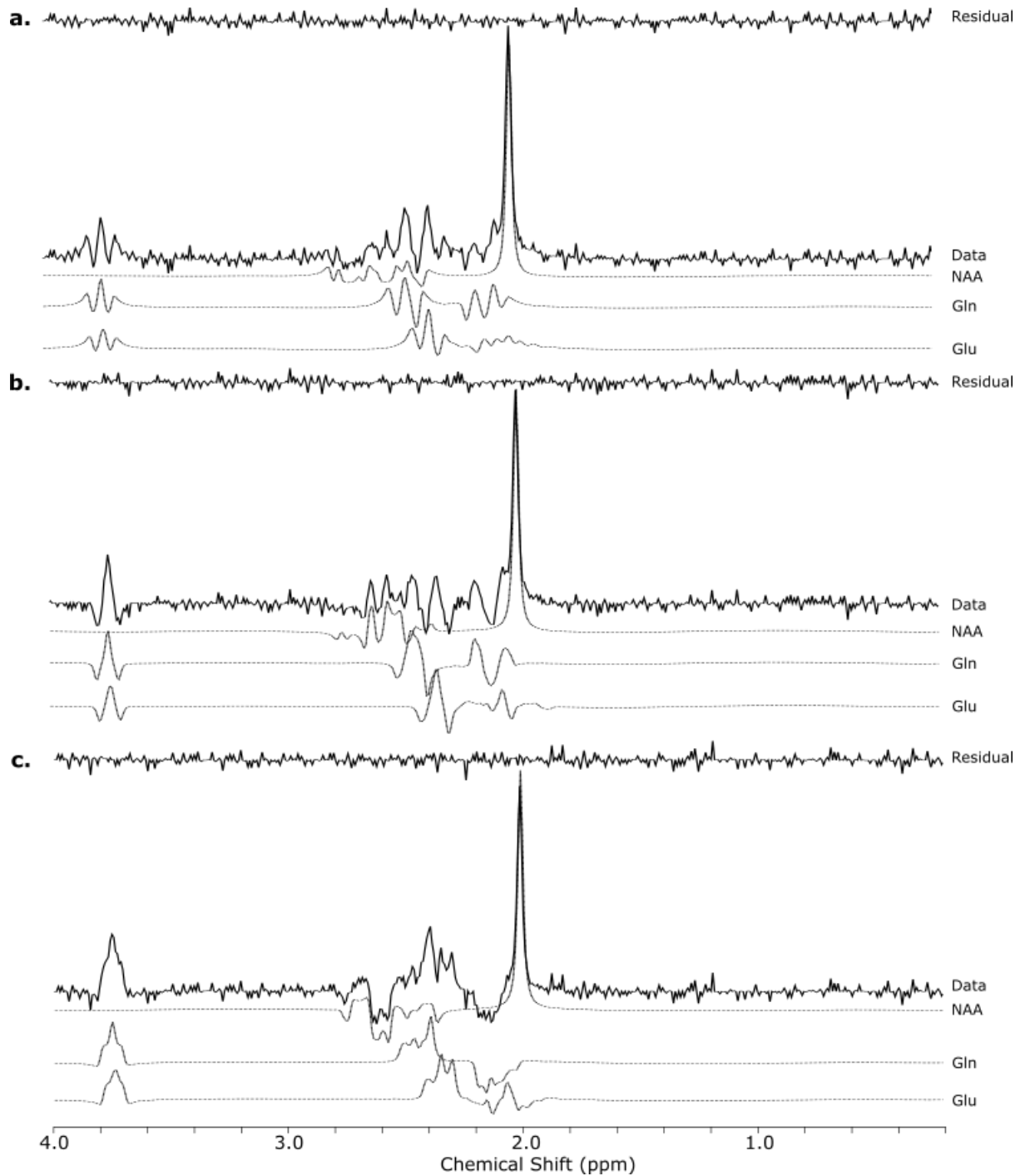
Figure 4-5: Simulated metabolite spectra and TARQUIN fits of the NAA, Glu, Gln model system at TEs a) 35 ms, b) 80 ms and c) 135 ms with SNR 25 and FWHM 3 Hz.
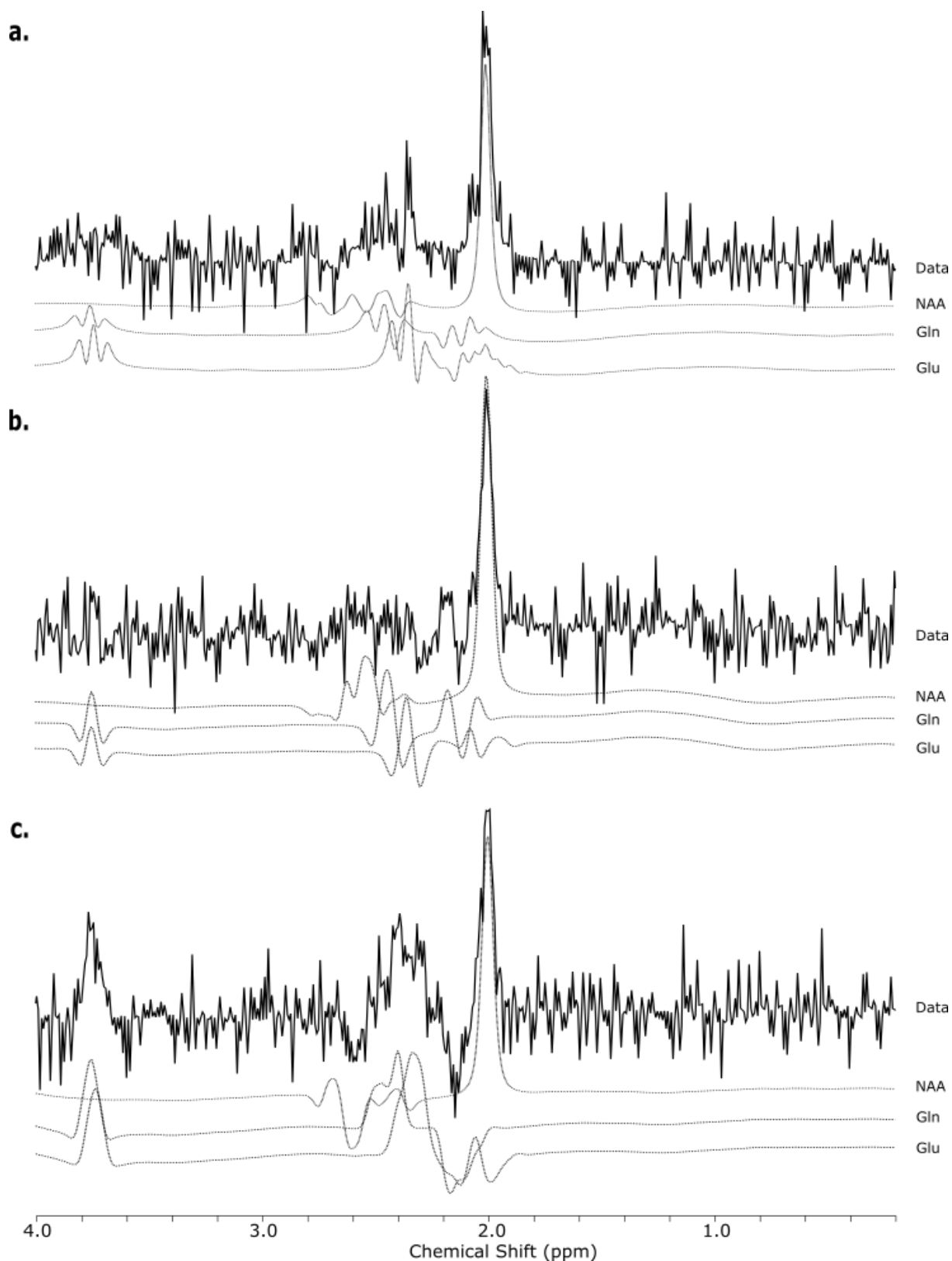
Figure 4-6: Simulated metabolite spectra and TARQUIN fits of the NAA, Glu, Gln model system at TEs a) 35 ms, b) 80 ms and c) 135 ms with SNR 5 and FWHM 7 Hz.
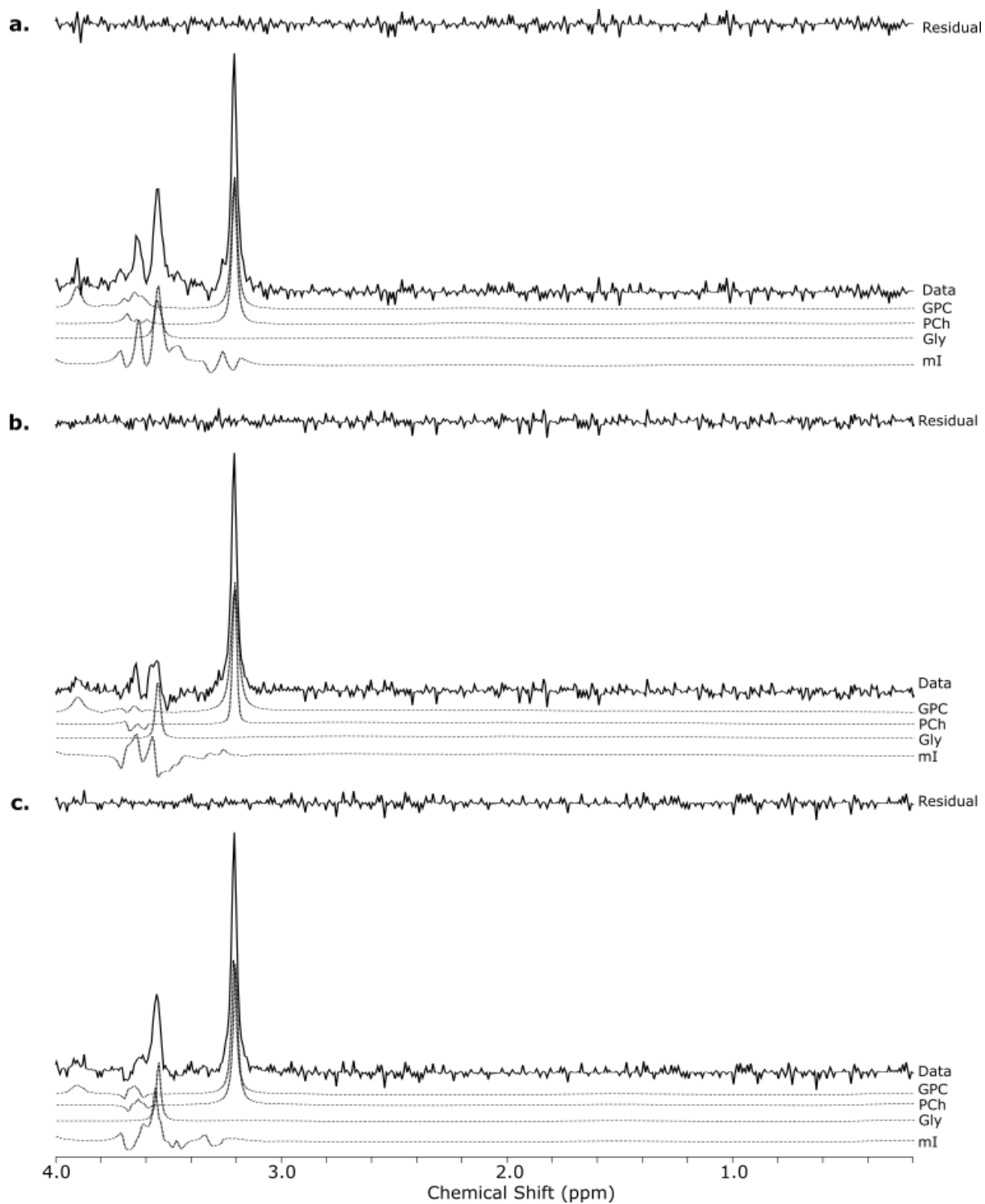
Figure 4-7: Simulated metabolite spectra and TARQUIN fits of the GPC, PCh, Gly and mI model system at TEs a) 35 ms, b) 80 ms and c) 135 ms with SNR 25 and FWHM 3 Hz.
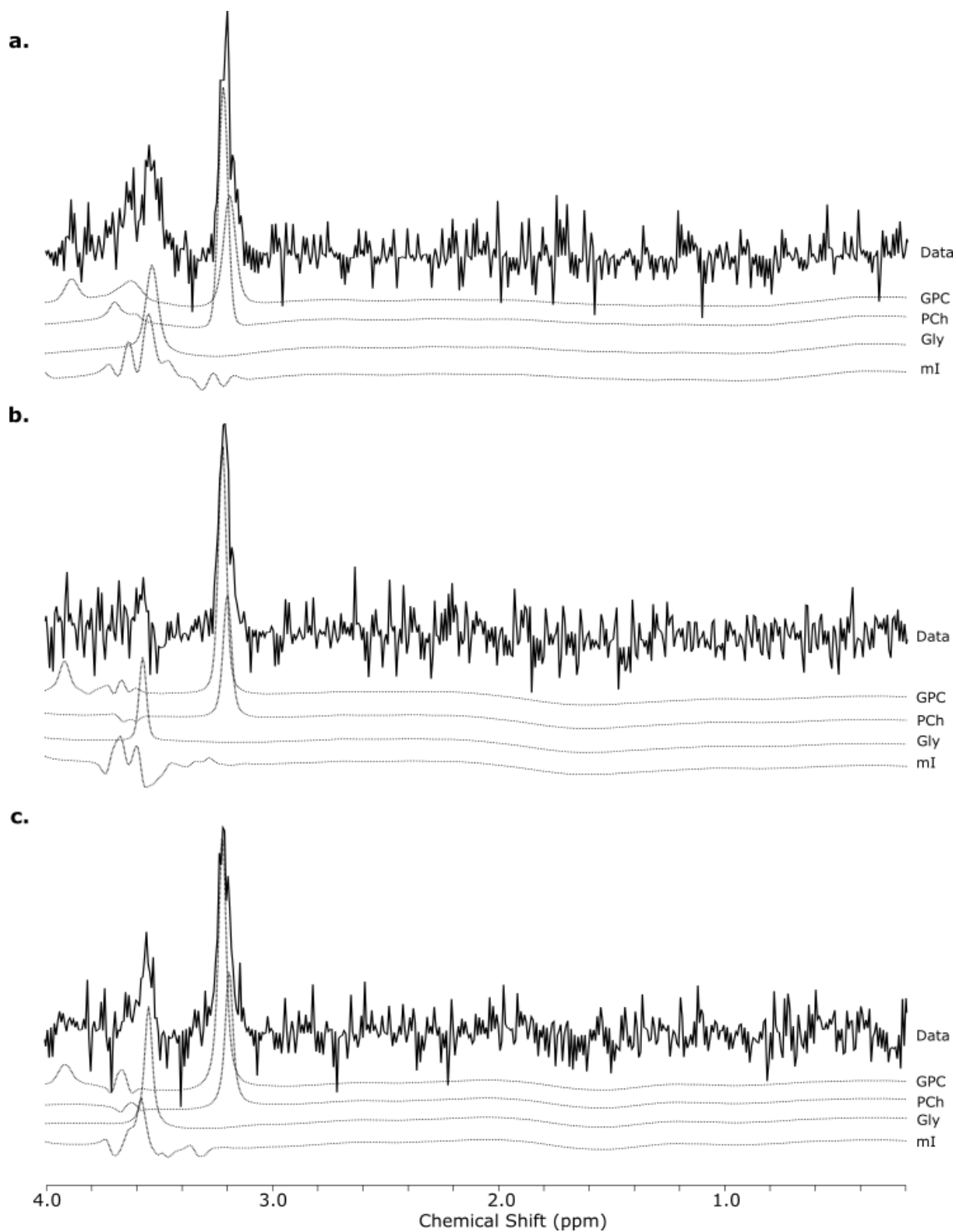
Figure 4-8: Simulated metabolite spectra and TARQUIN fits of the GPC, PCh, Gly and mI model system at TEs a) 35 ms, b) 80 ms and c) 135 ms with SNR 5 and FWHM 7 Hz.

	FWHM 3 Hz, SNR 5			FWHM 3 Hz, SNR 15			FWHM 3 Hz, SNR 25		
TE (ms)	NAA	Glu	Gln	NAA	Glu	Gln	NAA	Glu	Gln
35	0.98±0.11	0.99±0.36	0.98±0.37	0.99±0.06	0.99±0.20	0.98±0.23	1.00±0.04	0.98±0.13	1.00±0.17
80	0.98±0.10	0.94±0.33	0.96±0.25	1.00±0.05	0.93±0.19	0.96±0.15	1.00±0.03	0.96±0.13	0.98±0.09
135	0.98±0.10	0.98±0.22	0.98±0.19	0.98±0.05	0.98±0.11	1.01±0.09	0.99±0.03	0.98±0.07	1.02±0.06
	FWHM 7Hz,SNR5			FWHM 7Hz,SNR15			FWHM 7Hz,SNR25		
TE(ms)	NAA	Glu	Gln	NAA	Glu	Gln	NAA	Glu	Gln
35	1.00±0.09	0.98±0.31	0.98±0.36	1.00±0.05	0.98±0.15	0.99±0.21	1.00±0.03	0.98±0.10	1.00±0.13
80	1.00±0.09	0.93±0.31	0.96±0.23	0.99±0.05	0.92±0.18	0.92±0.14	0.99±0.03	0.89±0.12	0.91±0.09
135	0.98±0.08	0.99±0.18	0.99±0.15	0.95±0.04	0.95±0.09	0.98±0.07	0.93±0.03	0.93±0.05	0.98±0.04

Table 4-3: Mean ± SD metabolite concentration for the Glu (1 mM), Gln (1 mM) and NAA (1 mM) model system.

	FWHM 3 Hz, SNR 5			FWHM 3 Hz, SNR 15			FWHM 3 Hz, SNR 25		
TE(ms)	tCho	mI	Gly	tCho	mI	Gly	tCho	mI	Gly
35	0.94±0.10	1.98±0.67	0.92±0.43	0.99±0.04	1.99±0.33	0.94±0.22	0.99±0.03	2.00±0.20	0.97±0.14
80	0.93±0.10	2.00±0.64	0.90±0.32	0.97±0.05	2.03±0.35	0.93±0.18	1.00±0.03	1.98±0.23	0.96±0.11
135	0.93±0.10	2.09±0.93	0.84±0.43	0.97±0.05	2.04±0.54	0.92±0.26	0.99±0.03	2.10±0.39	0.93±0.18
	FWHM 7Hz, SNR 5			FWHM 7 Hz, SNR 15			FWHM 7 Hz, SNR 25		
TE(ms)	tCho	mI	Gly	tCho	mI	Gly	tCho	mI	Gly
35	0.98±0.07	1.98±0.48	0.91±0.33	0.98±0.04	1.96±0.26	0.95±0.19	0.98±0.03	1.94±0.18	0.97±0.15
80	0.97±0.07	1.88±0.54	0.87±0.29	0.98±0.04	1.98±0.25	0.94±0.14	0.99±0.03	1.97±0.16	0.95±0.09
135	0.97±0.07	2.07±0.76	0.86±0.38	0.99±0.04	2.13±0.47	0.90±0.22	0.99±0.03	2.05±0.37	0.94±0.17

Table 4-4: Mean ± SD metabolite concentration for the tCho (1 mM), mI (2 mM) and Gly (1 mM) model system, where tCho = GPC (0.5 mM) + PCh (0.5 mM).
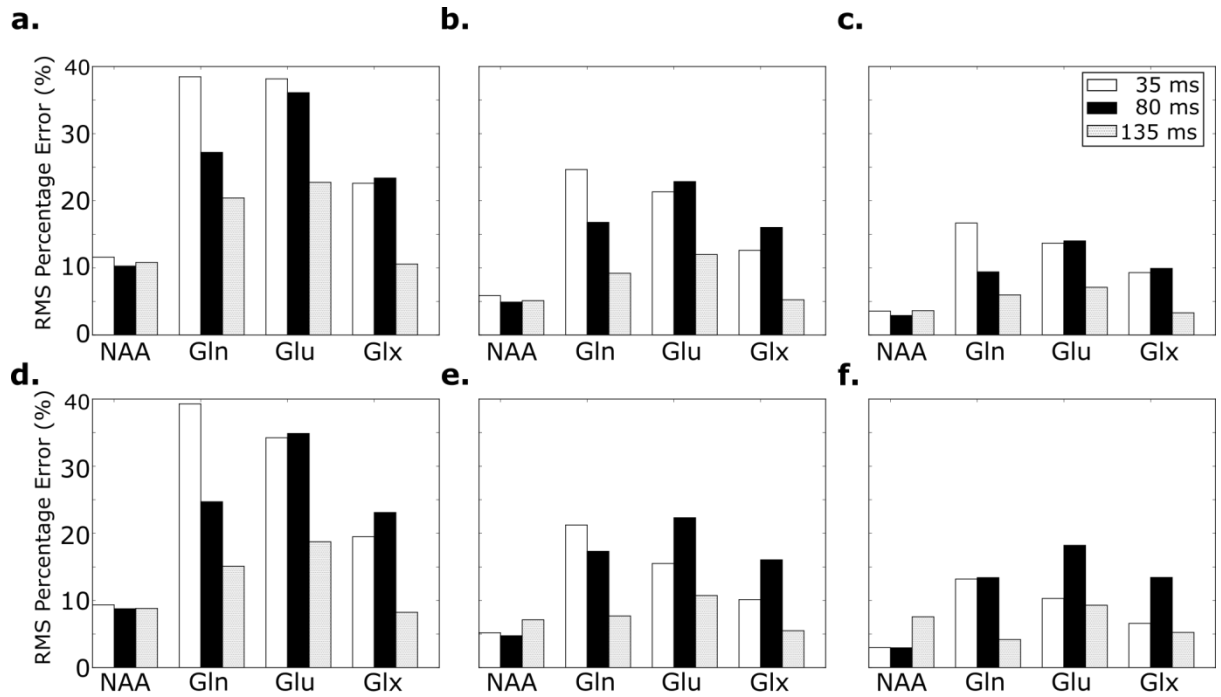
Figure 4-9: Root mean square (RMS) percentage error from the simulated concentration for NAA, Glu, Gln and Glx, where Glx = Glu + Gln, with SNRs and FWHMs of a) SNR 5; FWHM 3 Hz; b) SNR 15, FWHM 3 Hz; c) SNR 25, FWHM 3 Hz; d) SNR 5, FWHM 7 Hz; e) SNR 15, FWHM 7 Hz; f) SNR 25, FWHM 7 Hz
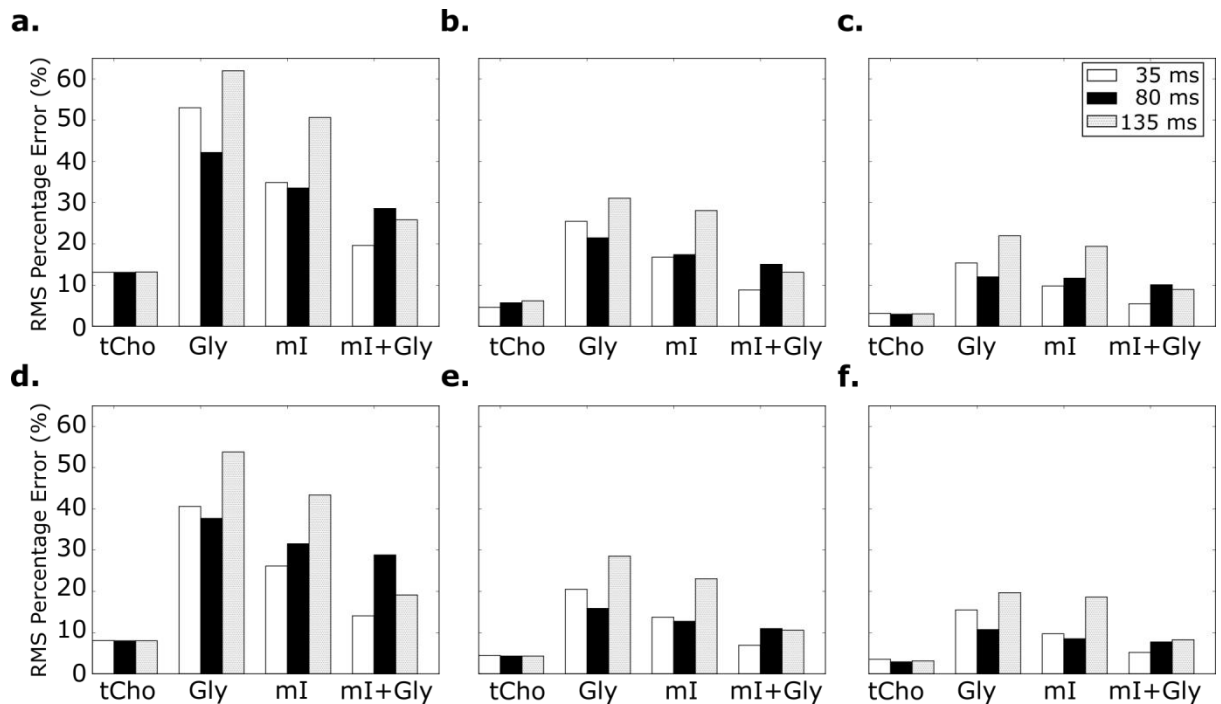
Figure 4-10: Root mean square (RMS) percentage error from the simulated concentration for tCho, mI, Gly and mI + Gly, where tCho = GPC + PCh, with SNRs and FWHMs of a) SNR 5; FWHM 3 Hz; b) SNR 15, FWHM 3 Hz; c) SNR 25, FWHM 3 Hz; d) SNR 5, FWHM 7 Hz; e) SNR 15, FWHM 7 Hz; f) SNR 25, FWHM 7 Hz

The RMS percentages for Cho and mI in the brain and in the tCho, mI and Gly model systems were also compared. There was a small, but not significant, increase in the RMS percentage error of mI in the presence of Gly (21.7% vs 22.7%; Student's t-test, t = 0.71, P = 0.54), when the RMS percentage errors were averaged over all TEs and all experimental conditions.

There was a significant increase in the RMS percentage error of tCho compared with Cho (8.2% vs 6.2%, Student's t-test, t = 5.98, P = 10^{-5}). At SNR 25 and FWHM 3 Hz, the RMS percentage errors of GPC were 21%, 27% and 28% at TEs 35, 80 and 135 ms respectively. For PCh, the RMS percentage errors were 21%, 27% and 30%. The RMS percentage error of Gly was larger than the RMS errors of both mI and tCho, but smaller than those of GPC and PCh.

The accuracy of metabolite quantification was worse for multiplets compared to metabolites with singlet peaks without significant spectral overlap. The presence of additional, but not total, spectral overlap did not significantly affect quantification accuracy; however, the accuracy of quantification was poorest for the metabolites with near total overlap of resonances (Gly, GPC, PCh).

4.2.2.3 Accuracy of Metabolite Quantification at Different Echo Times
The spectral appearance of Glu, Gln, mI and Lac changes considerably with echo time due to J-modulation. The three model systems were simulated at echo times of 35 ms, 80 ms and 135 ms to determine whether quantification accuracy depends on echo time choice.

For NAA, Cho and Cr, the RMS percentage errors were similar at each of the three TEs. The RMS percentage errors were smallest for Glu and Gln at TE 135 ms with 80 ms having smaller RMS errors for Gln compared with 35 ms. The RMS percentage errors were smallest

for Gly using a TE of 80 ms and worst with a TE of 135 ms. For mI, the RMS percentage errors were smallest for 35 and 80 ms.

When the RMS percentage errors were averaged over all metabolites and all model systems for SNR 25 and linewidth 3 Hz, the mean RMS percentage error was 9.7% at 35 ms, 8.3% at 80 ms and 8.8% at 135 ms.

4.2.3 Summary of Findings

There was not a single optimal echo time for accurate metabolite quantification of all metabolites. Instead the accuracy of metabolite quantification depended largely on the SNR and linewidth of the data. Metabolites with prominent single peaks, without significant spectral overlap, could be quantified to within 10% of their simulated concentrations at SNRs of 15 and above. The quantification accuracy of coupled metabolites did not change when additional, but not total, spectral overlap was introduced. The quantification accuracy was worst for metabolites with near total overlap of resonance peaks.

The three spectral model systems provided a means for investigating the effects of spectral overlap and J-modulation on metabolite quantification. However, experimental factors such as T2 relaxation, macromolecular baseline and differences between the basis set and experimentally acquired data were not modelled.

4.3 Metabolite Quantification of Experimentally Acquired Spectra

4.3.1 Methods

4.3.1.1 Phantoms
Phantom Preparation

All experimental data were acquired on a clinical 3.0 T Phillips Achieva scanner (Phillips Medical Systems, Best, the Netherlands) equipped with a 32-channel 1H Phillips head coil.

The braino phantom contained 12.5 mM NAA, 12.5 mM Glu, 10 mM Cr, 7.5 mM mI, 5 mM Lac, 3 mM Cho. 1 g of sodium azide was added as a biocide to prevent the growth of bacterial organisms. 1 mL/L of gadolinium was added to each phantom as a relaxation agent to shorten the T1 relaxation time. The pH of the phantom was adjusted to 7.2 in line with healthy tissue.

Data Acquisition

A cubic 25 x 25 x 25 mm voxel placed in the centre of the phantom (Figure 4-8).
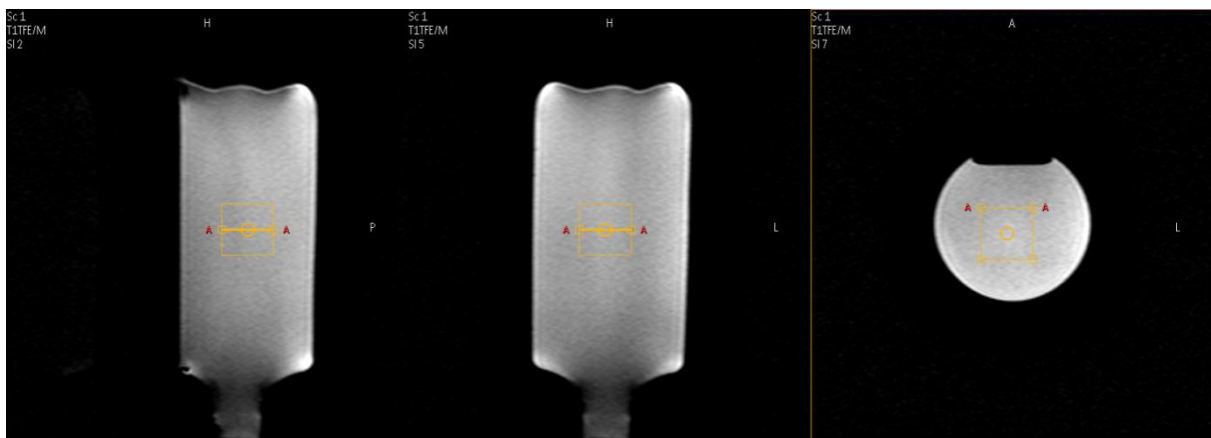
Figure 4-11: Typical placement of a 25x25x25 mm voxel in a phantom.

Spectroscopy was acquired using three sequences:

- PRESS: TE 35 ms, TR 2s, NSA 128

- 3 TEs: TE 35, 80 and 135 ms, with a TR of 2s and NSA 128. The three echo times were linked as a parameter series to prevent changes in the receiver gain.

- 18 TEs: 18 equally spaced TEs from 35-290 ms with 15 ms spacing. The TR was 2s and the NSA per TE was 8. The 18 echo times were linked as a parameter series to prevent changes in the receiver gain.

Data were acquired at room temperature.

Data Processing

Metabolite concentrations were initially quantified at each echo time with TARQUIN v4.3.8 using a basis set containing only the metabolites present in the phantom. Metabolite concentrations were referenced to an unsuppressed water signal and a pure water concentration of 55556 mM was assumed. The water attenuation parameter was fixed to 1.00 to neglect relaxation effects in the TARQUIN analysis.

T2 Estimation

Water and metabolite T2 relaxation times, $T2_w$ and $T2_m$ respectively, were estimated by fitting the signal amplitudes from each echo time to a monoexponential decay curve. The T2 relaxation times were estimated from both the JPRESS and 3TE acquisitions.

Concentration Correction for Relaxation Effects

The metabolite concentration at each echo time was corrected by multiplying the concentration by an attenuation factor, W_{att}, that accounts for the relaxation of the water

and metabolite signals. Metabolite concentrations were only corrected for relaxation effects where non-negative T2 relaxation times were estimated. Metabolites where negative T2 relaxation times were estimated were not assessed.

The metabolite concentration reported for phantoms is the mean of the concentrations from all echo times collected in that sequence.

Analysis and Statistics

The estimated mean metabolite concentrations were compared to the known phantom concentration. The percentage error and rms percentage error from the known phantom concentration were calculated.

Statistical comparisons were performed using a Student's t-test and statistical significance was declared for $P < 0.05$.

4.3.1.2 Volunteers
Data Acquisition

Informed consent was obtained from 5 healthy adults (4 males and 1 female) with a mean age of 26 ± 2 years. In four cases a voxel of size 25 x 25 x 25 mm was placed over parietal white matter. In the fifth case a cubic voxel of size 25 x 25 x 25 mm was placed in occipito-parietal grey matter across the midline to investigate the influence of cerebrospinal fluid (CSF).

Spectroscopy data were acquired using the same three sequences used for the phantoms.

Data Processing

Segmentation was performed using FSL (Smith et al., 2004) to determine the amount of grey matter (GM), white matter (WM) and CSF present in the voxel. A full description of steps taken for segmentation is presented in Chapter 3.3.1. Metabolite concentrations were quantified with TARQUIN v4.3.8 using the 1H brain + Glth, Cit, Gly internal basis set. The water attenuation factor was set to 1 and the water concentration was set to that of pure water, 55,556 mM.

T2 determination

The metabolite signal amplitudes were fitted to a monoexponential decay curve.

The water T2 relaxation time of the 3 TEs sequence was fitted to a monoexponential decay curve. To negate the influence of CSF components on T2 relaxation, only the water signal collected from the first five TEs of the 18 TEs sequence were fitted to a monoexponential decay.

Concentration Correction for Relaxation Effects

The reported metabolite concentrations were corrected for relaxation effects in accordance with the method detailed by Gasparovic et al (Gasparovic et al., 2006b) using literature values for T2 relaxation times. A comparison is also made to values corrected using the estimated W_{att} assuming monoexponential decay of the data acquired.

The metabolite concentration reported for volunteers is the mean of the concentrations from all echo times collected in that sequence.

4.3.2 Results
Example spectra at TEs 35, 80 and 135 are given for the braino phantom (Fig 4-12), NAA/Glu/Gln phantom (Fig 4-13), tCho/ml/Gly phantom (Fig 4-14) and healthy volunteer (Fig 4-15).
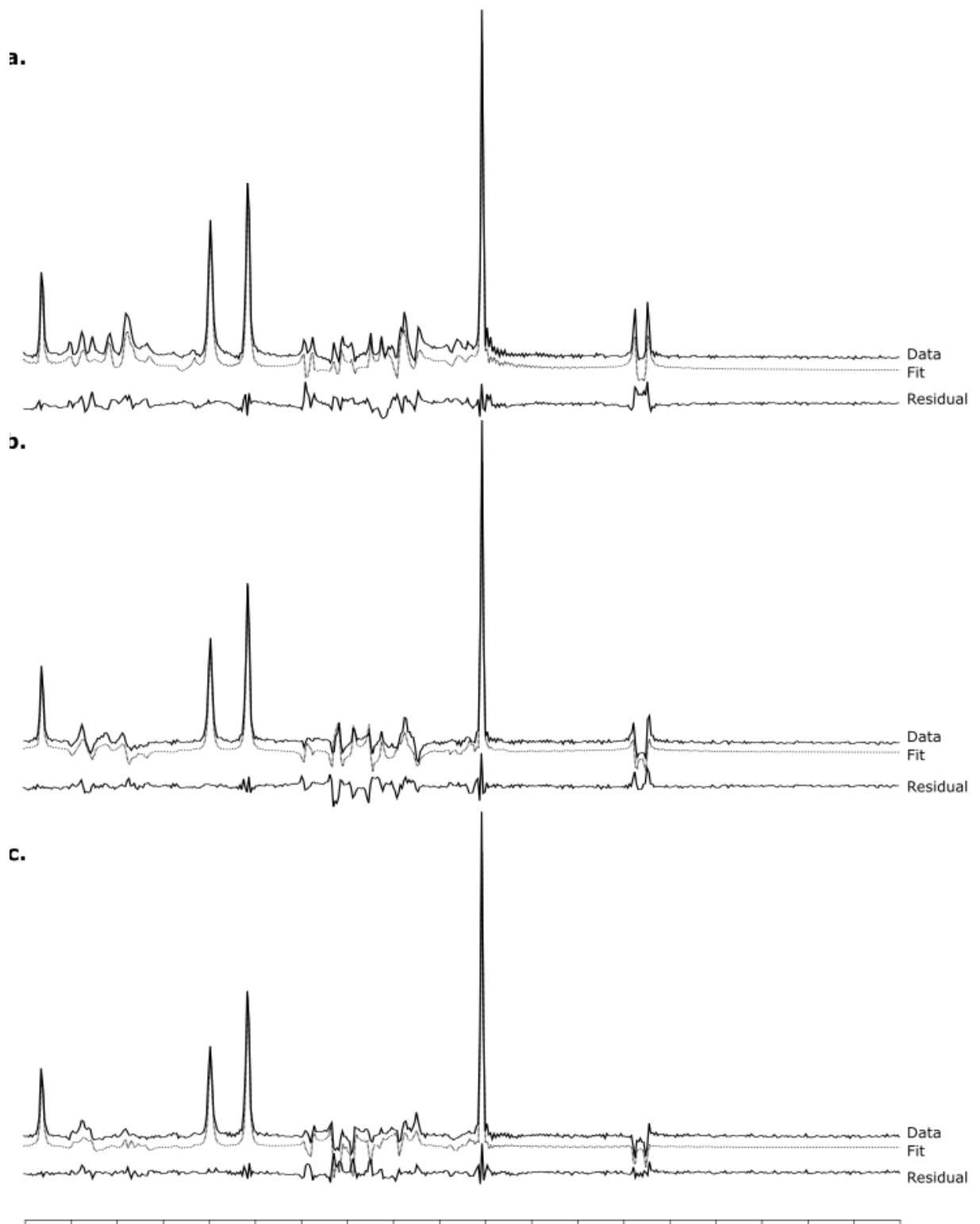
Figure 4-12: Example phantom data and TARQUIN fits of the braino model system at TEs a) 35 ms, b) 80 ms and c) 135 ms.
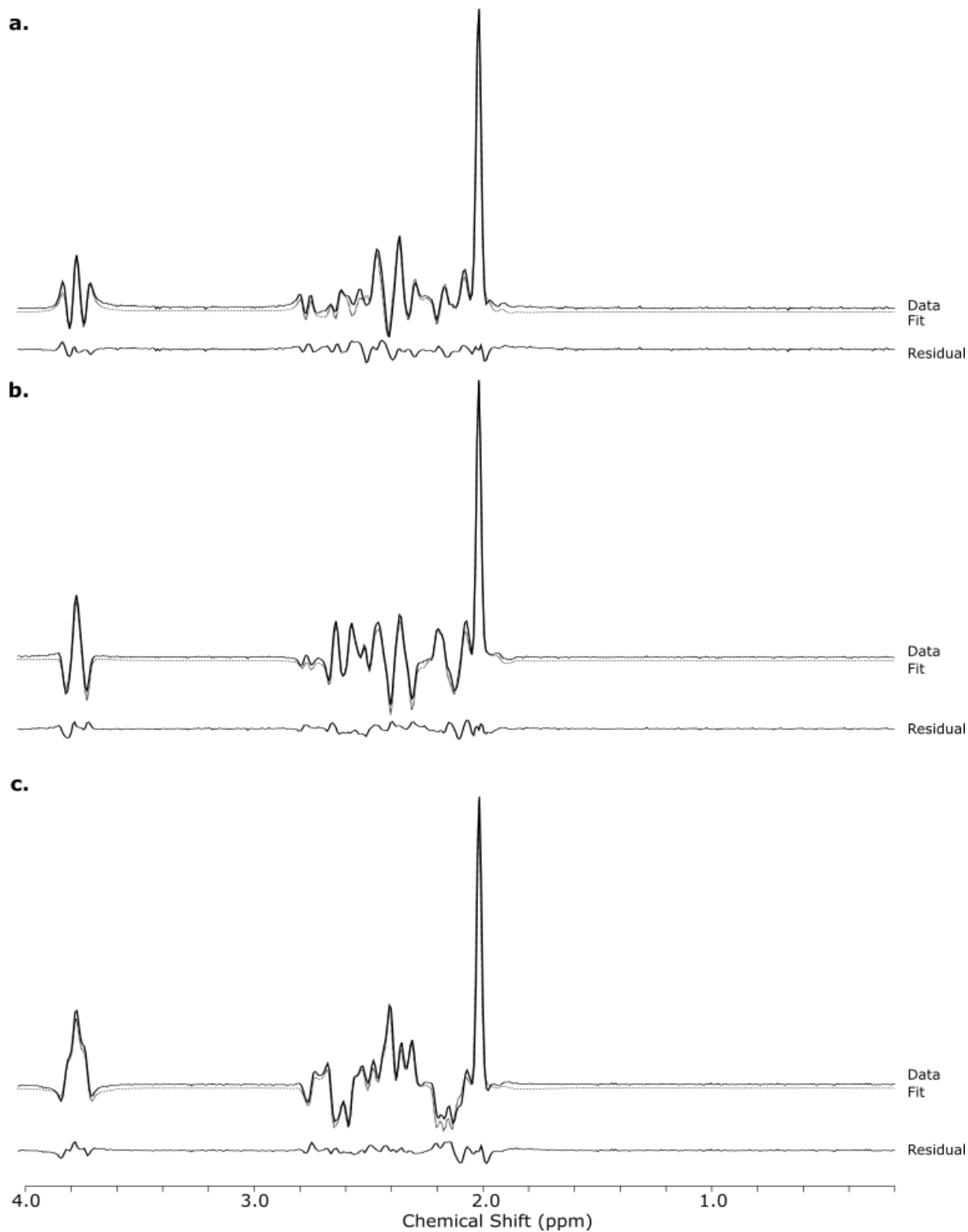
Figure 4-13: Example phantom data and TARQUIN fits of the NAA, Glu, Gln model system at TEs a) 35 ms, b) 80 ms and c) 135 ms.
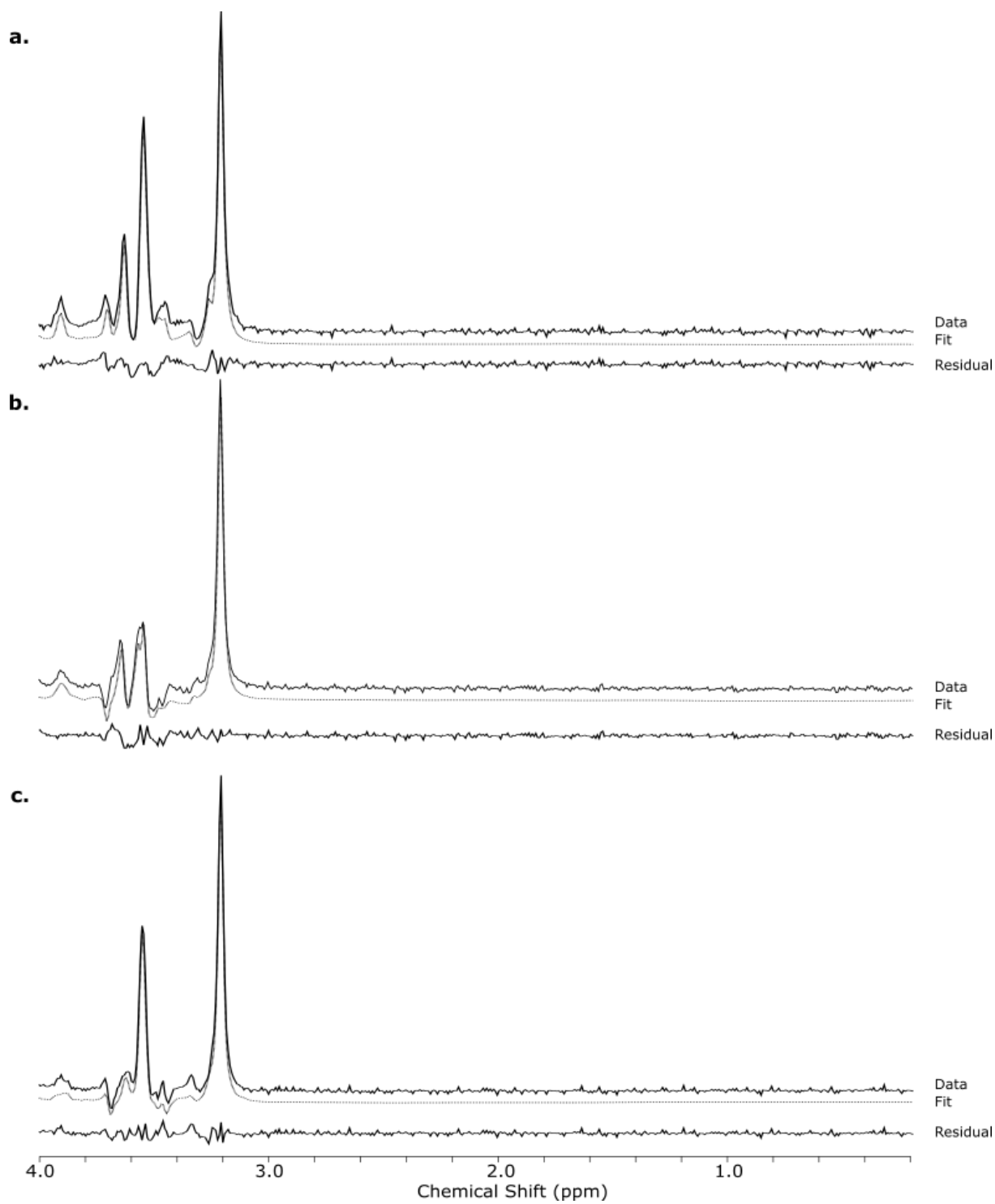
Figure 4-14: Example phantom data and TARQUIN fits of the GPC, PCh, Gly and mI model system at TEs a) 35 ms, b) 80 ms and c) 135 ms.
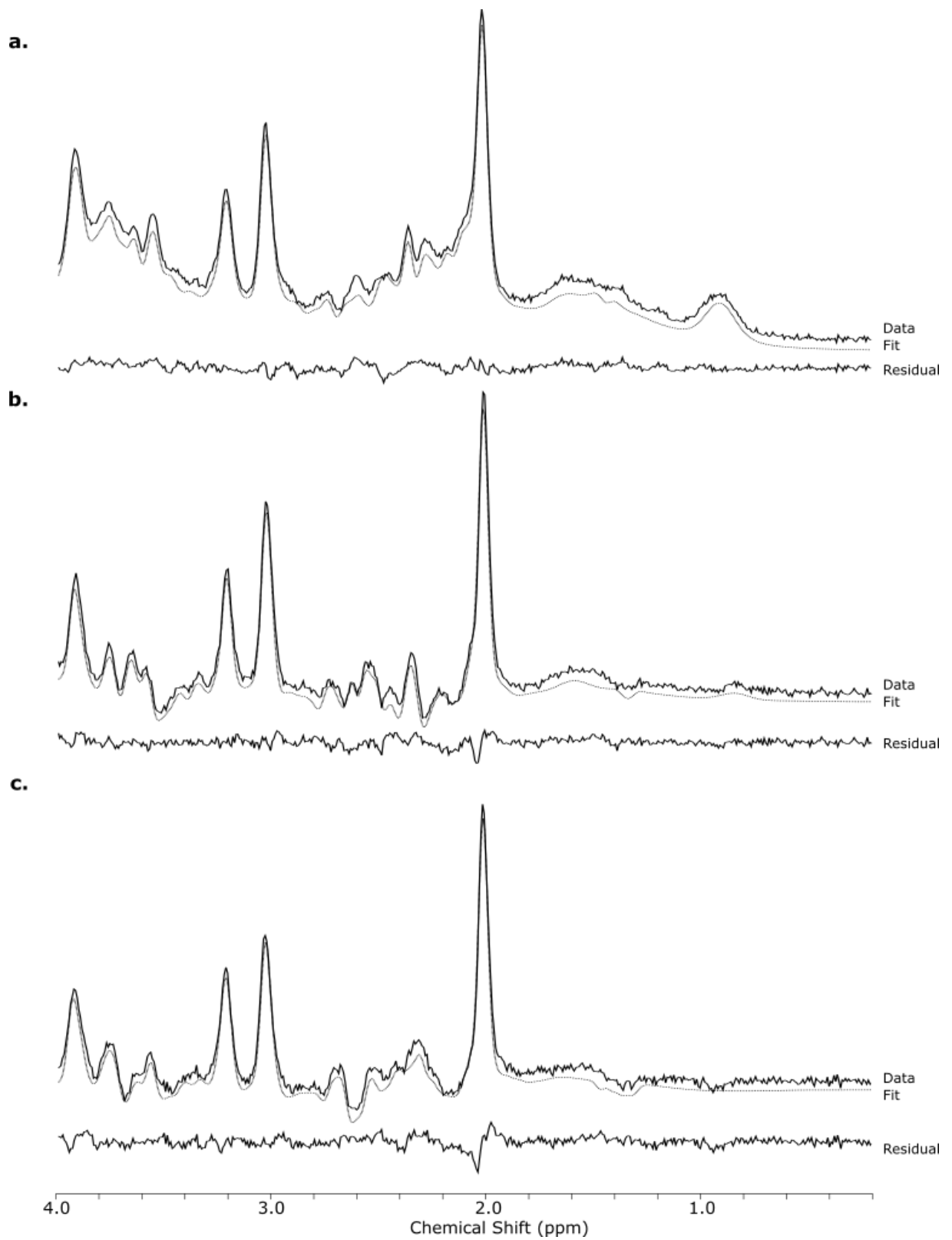
Figure 4-15: Example phantom data and TARQUIN fits of healthy parietal white matter at TEs a) 35 ms, b) 80 ms and c) 135 ms.

<u>4.3.2.1 T2 Relaxation</u>

Knowledge of the T2 relaxation times of water and metabolites is required for accurate quantification of metabolite concentrations. The T2 relaxation times for tNAA, tCho and tCr are presented for the braino phantom in Table 4-5 and volunteer in Table 4-6. T2 relaxation times have been calculated using 2 TEs (35 and 135 ms) and using 18 TEs spaced between 35 and 290 ms. Representative T2 relaxation fits for tNAA, tCho and tCr estimated from 18 TEs are presented for phantom and volunteer data in Figure 4-9.

	T2 ± SD (ms) – Braino Phantom			
	NAA	Cho	Cr	Water
2 TEs	560 ± 50	194 ± 9	323 ± 10	278 ± 4
18 TEs	524 ± 89	203 ± 6	318 ± 24	279 ± 2

Table 4-5: T2 relaxation times for NAA, Cho, Cr and water in the braino phantom, estimated using 2 TEs (35 and 135 ms) and 18 TEs. (n=4)

	T2 ± SD (ms) – Volunteer			
	tNAA	tCho	tCr	Wat
2 TEs	288 ± 40	201 ± 10	141 ± 12	64 ± 1
18 TEs	272 ± 23	208 ± 7	141 ± 12	69 ± 10

Table 4-6: T2 relaxation times for tNAA, tCho, tCr and water in healthy volunteer, estimated using 2 TEs (35 and 135 ms) and 18 TEs. (n=4)

The mean T2 values for tNAA, tCho and tCr estimated using 2 TEs and using 18 TEs were not significantly different in either phantom or volunteer. A Pearson correlation coefficient of 0.95 (P = 0.03) was found between the T2 values of tNAA, tCho and tCr estimated with 2 TEs and the relaxation times estimated with 18 TEs. There was not a significant difference in the mean T2 relaxation times estimated using the two methods in either phantoms (Student's t-test, t = 0.80, P = 0.42) or volunteers (t = 0.6, P = 0.53).
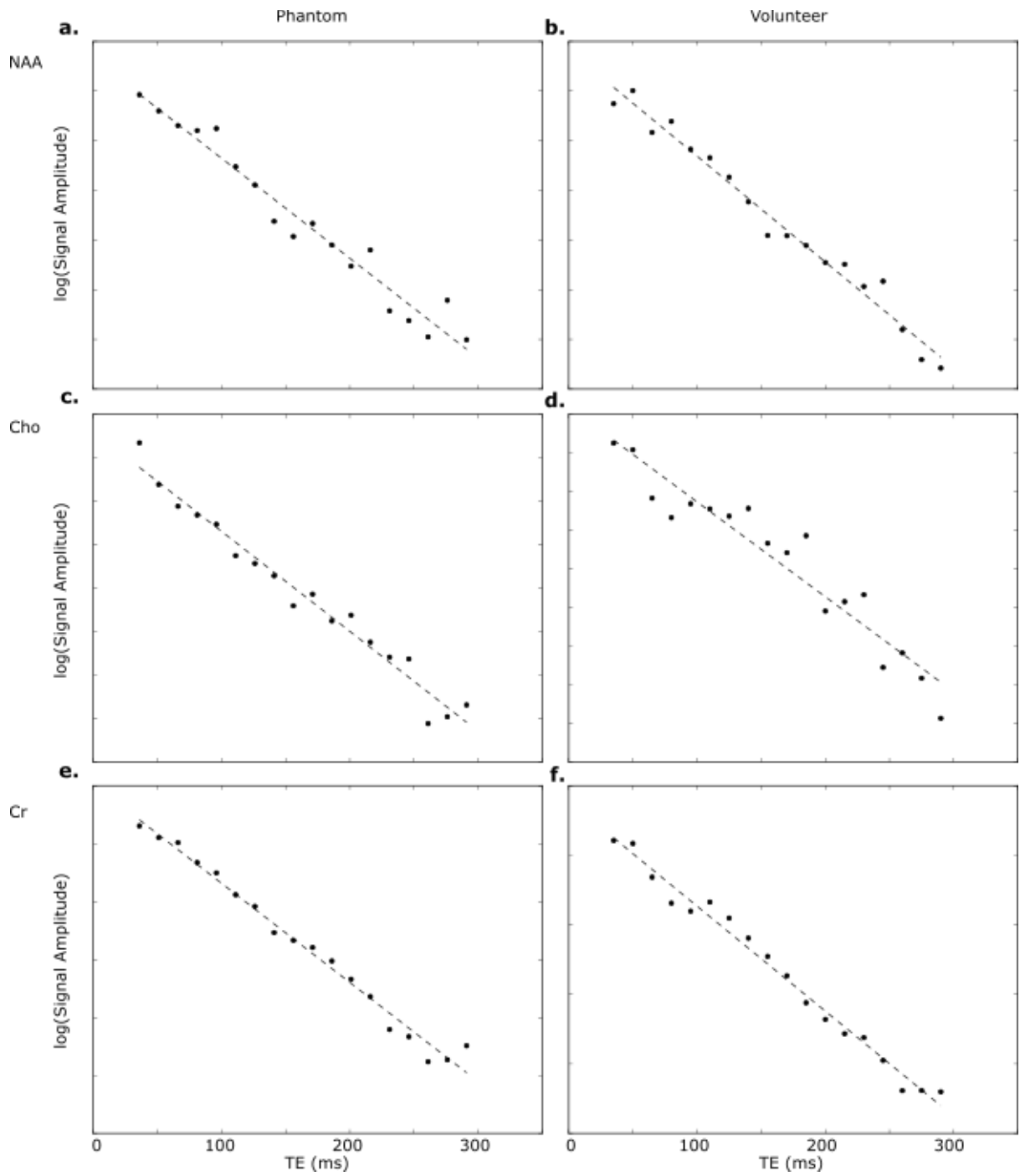
Figure 4-16: T2 relaxation decay for (t)NAA in a) phantom and b) volunteer; (t)Cho in c) phantom and d) volunteer; and (t)Cr in e) phantom and f) volunteer.

T2 relaxation times were estimated for Glu, mI and Lac in the braino phantom (Table 4-7) and volunteers (Table 4-8). Representative fits to 18 TEs are presented in Figure 4-10. There was a significant difference in the T2s estimated from 2 TEs and estimated from 18 TEs in the phantom (Student's t-test, t = 5.4, P = 10^{-5}) and in volunteers (t = -3.78, P = 0.001).

T2 (ms) –Braino Phantom			
	Glu	mI	Lac	Water
2 TEs	118 ± 17	77 ± 11	86 ± 4	278 ± 4
18 TEs	197 ± 20	142 ± 9	-3500 ± 2500	279 ± 2

Table 4-7: T2 relaxation times for Glu, mI, Lac and water in the braino phantom, estimated using 2 TEs (35 and 135 ms) and 18 TEs. (n=4)

T2 (ms) –Volunteer			
	Glu	mI	Lac	Water
2 TEs	86 ± 7	138 ± 9	100 ± 4	64 ± 1
18 TEs	184 ± 25	225 ± 52	50 ± 200	69 ± 10

Table 4-8: T2 relaxation times for Glu, mI, Lac and water in healthy brain, estimated using 2 TEs (35 and 135 ms) and 18 TEs. (n=4)

The T2 relaxation times of tNAA, tCho and tCr estimated from two TEs were comparable with the T2 values estimated using 18 TEs in both phantom and volunteer. In contrast, the T2 values estimated varied considerably between the two methods.
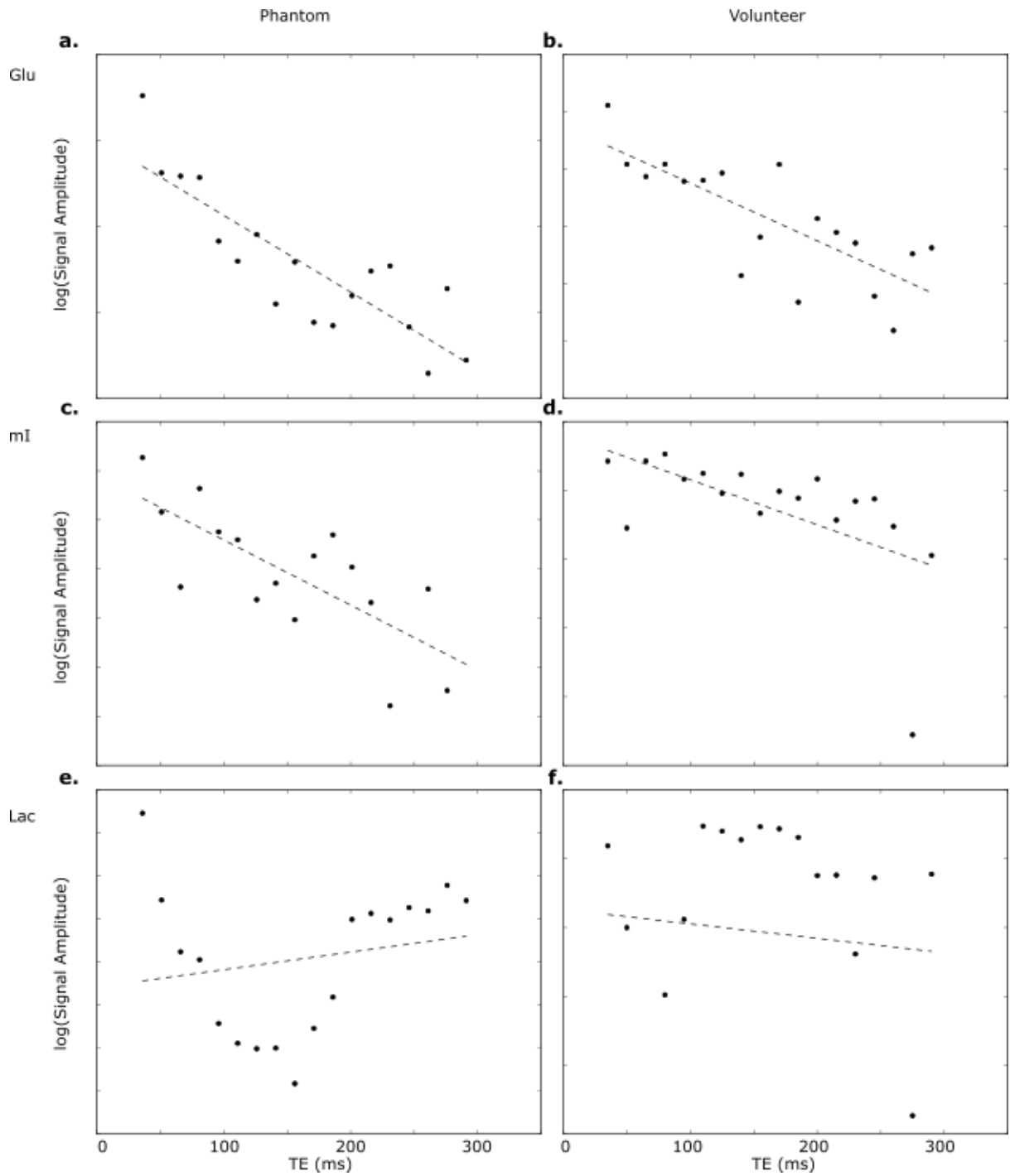
Figure 4-17: T2 relaxation decay for Glu in a) phantom and b) volunteer; mI in c) phantom and d) volunteer; and Lac in e) phantom and f) volunteer.

The T2 relaxation time of water was estimated in the braino phantom (Table 4-7) and

volunteers (Table 4-8). Monoexponential fits to the water signal are shown for phantom and

volunteer data in Figure 4-11.
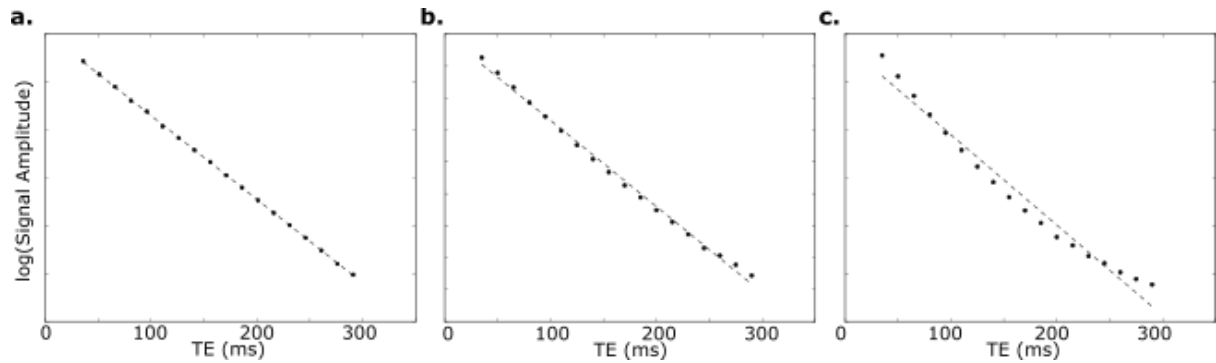
Figure 4-18: Example semi-log T2 decays of water in a) phantom, b) parietal grey matter with CSF approximately 1% of the voxel and c) occipito-parietal lobe with CSF approximately 18% of the voxel. Dashed line represents a monoexponential fit to the data.

The presence of CSF in acquisition voxels led to a multi-exponential decay of the water signal

in vivo. A biexponential signal composed of varying amounts of CSF and WM was simulated

to assess the influence that CSF could have on T2 estimates (Table 4-9).

CSF F	Number of TEs Fitted To			
	8 TEs	5 TEs	3 TEs	2 TEs
0.90	96.81	87.64	85.91	84.32
0.95	83.06	78.43	77.58	76.80
0.97	77.76	74.96	74.46	74.02
0.99	72.57	71.63	71.48	71.33

Table 4-9: Estimated T2 from a monoexponential fit to the first n TEs of a simulated signal (18 TEs, 35-290 ms with 15 ms spacing between TEs). The signal was composed of two components, analogous to CSF and WM, with varying amounts of CSF (T2 = 1300 ms), given by CSF F, with the remaining fraction composed of WM (T2 = 70 ms), such that CSF F + WM F = 1.

The T2 decay of the simulated signal arising from WM, as fitted to a monoexponential decay,

was overestimated more as CSF F increased. Fitting the first 5 TEs or fewer of the multi-TE

water scan to a monoexponential decay can minimise the effect of CSF on the T2

measurement.

The T2 relaxation times estimated from 2 TEs (35 ms and 135 ms) and estimated from 18 TEs

were comparable for metabolites with prominent singlets without significant spectral

overlap and for water in both phantom and normal brain. The signal decay of water in vivo

was not monoexponential and increasing the amount of CSF in the voxel increased the multi-

exponential behaviour of the decay curve. Estimating the T2 relaxation time of water with a

maximum TE ≤ 135 ms reduced the influence of long T2 components on T2 estimation. The

T2 relaxation times of coupled metabolites estimated from 2 TEs and 18 TEs were not

comparable and there was a large variability in metabolite quantification at different echo

times for couple metabolites.

4.3.2.2 Metabolite Concentrations Corrected for T2 Relaxation in Phantoms

Estimated T2 relaxation times were used to correct the metabolite concentration estimates

of the braino phantom at TEs of 35, 80 and 135 ms. The corrected concentrations of NAA,

Cho and Cr are shown in Figure 4-12. There was not a significant difference in the

concentrations of NAA, Cho and Cr estimated at the three echo times.
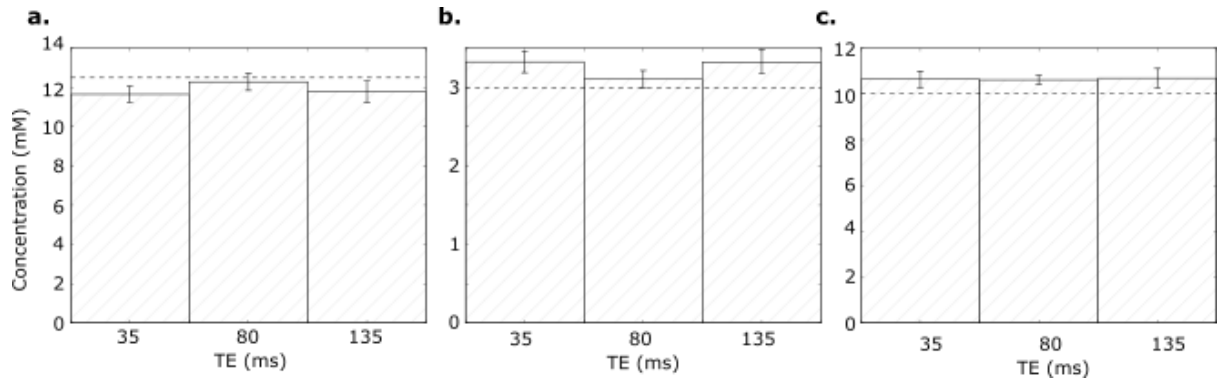
Figure 4-19: Mean ± SEM concentrations corrected for T2 relaxation of a) NAA (12.5 mM), b) Cho (3mM) and c) Cr (10 mM) in the braino phantom. Dashed line represents the phantom concentration.

Concentration estimates at TEs 35 ms, 80 ms and 135 ms are shown for Glu, mI and Lac in Figure 4-13. The mean concentration of Glu estimated at 135 ms was significantly smaller than that at 35 and 80 ms (Student's t-test: t = 4.04, P = 0.001 and t = 5.84, $P = 10^{-5}$ respectively). The mean concentration of mI estimated at 135 ms was significantly smaller than that at 35 (t = 4.16, P = 0.001) and 80 ms (t = 3.99, P = 0.001). The mean concentration of Lac estimated at 80 ms and 135 ms were significantly smaller than that at 35 ms (t = 4.91, $P = 10^{-4}$ and t = 5.50, $P = 10^{-4}$ respectively).
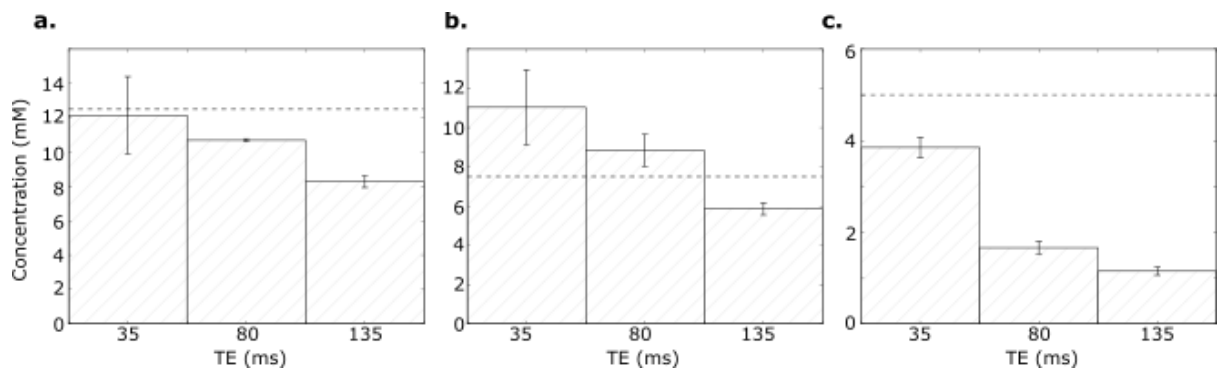
Figure 4-20: Metabolite concentrations corrected for T2 relaxation for a) Glu (12.5 mM), b) mI (7.5 mM) and c) Lac (5 mM) in the braino phantom. Dashed line represents the phantom concentration.

91
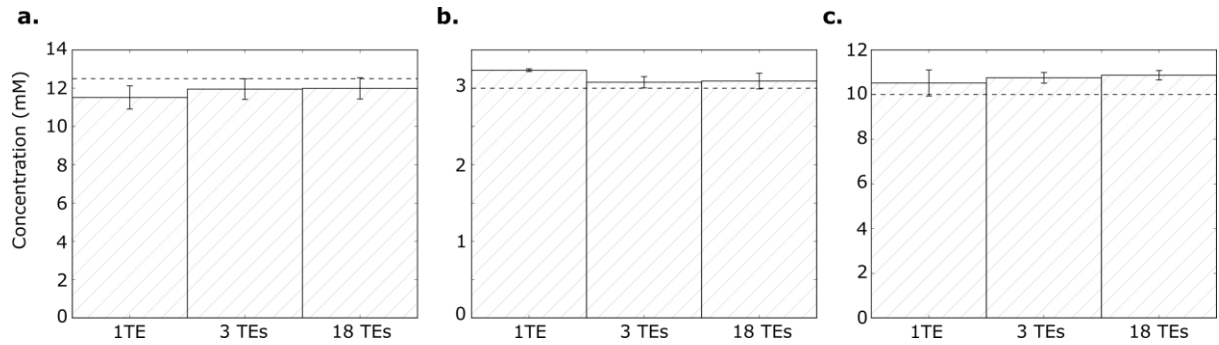
Figure 4-21: Mean ± SEM concentration estimated from one TE (35 ms), three TEs (35, 80 and 135 ms) and 18 TEs (42 to 297 ms, 15 ms spacing between TEs) for a) NAA, b) Cho and c) Cr in the braino phantom. The dashed line represents the phantom concentration. Metabolite concentrations have been corrected for T2 relaxation using T2 estimates from 18 TEs (n = 4).

Figure 4-14 shows the estimates of NAA, Cho and Cr in the braino phantom from 35 ms PRESS, a mean estimate from 3 TEs (35 ms, 80 ms and 135 ms) and the mean estimated from 18 TEs (42 ms – 297 ms). There was not a significant difference between the three values for any of the metabolites.

Figure 4-15 shows the estimates of Glu and mI in the braino phantom from 35 ms PRESS, a mean estimate from 3 TEs (35 ms, 80 ms and 135 ms) and the mean estimated from 18 TEs (42 ms – 297 ms). The mean estimates of Glu and mI using 3 TEs were significantly different when T2s were estimated using 2 TEs instead of 18 TEs.
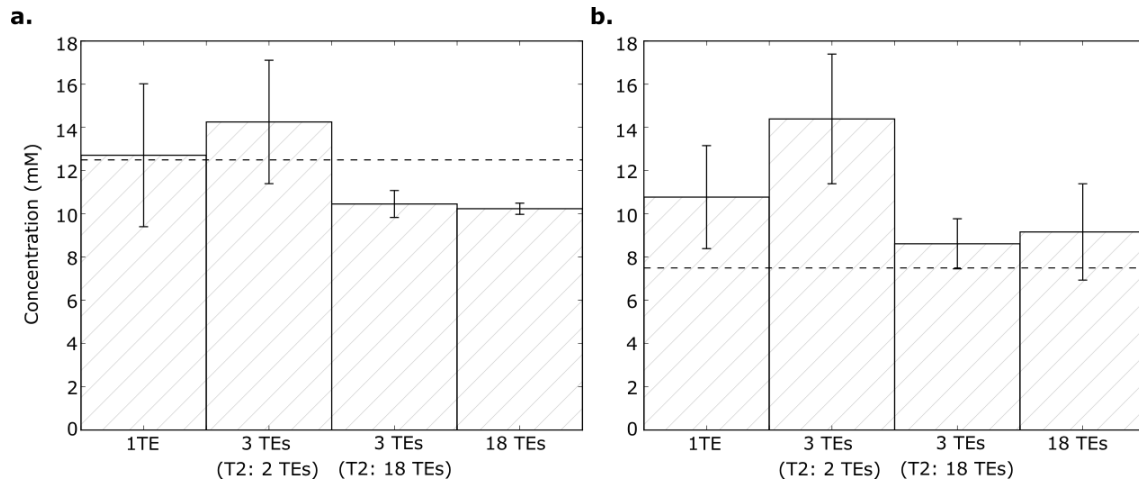
Figure 4-22: Mean ± SEM concentration estimated from one TE (35 ms), three TEs (35, 80 and 135 ms) and 18 TEs (42 to 297 ms, 15 ms spacing between TEs) for a) Glu and b) mI in the braino phantom. The dashed line represents the phantom concentration. 1 TE and 18 TEs have been corrected for T2 relaxation using T2s estimated from 18 TEs. 3 TEs have been corrected for T2 relaxation using concentrations corrected using 2 TEs (T2: 2 TEs) and 18 TEs (T2: 18 TEs) (n=4).

Metabolite concentrations corrected for T2 relaxation were comparable at 35 ms, 80 ms and 135 ms for NAA, Cho and Cr in the braino phantom. The mean estimates from 35 ms short-TE MRS, from 3 TEs and from 18 TEs were similar for these three metabolites, with minimal difference between the concentrations estimated from 3 TEs and 18 TEs. The concentration estimates of coupled metabolites varied significantly with echo time with concentration estimates also affected by how the metabolite T2 relaxation was measured.

4.3.2.3 The Effect of Intravoxel Heterogeneity and Metabolite Concentrations Corrected for T2 Relaxation in Volunteers

Voxels placed in volunteers were segmented to determine the amount of grey matter, white matter and cerebrospinal fluid (CSF) in the voxel. Metabolite concentrations were corrected for both water content differences and T2 relaxation. Figure 4-16 shows the estimated NAA concentration at various TEs, corrected for T2 relaxation in various ways. Approximately 18% of the voxel was CSF.
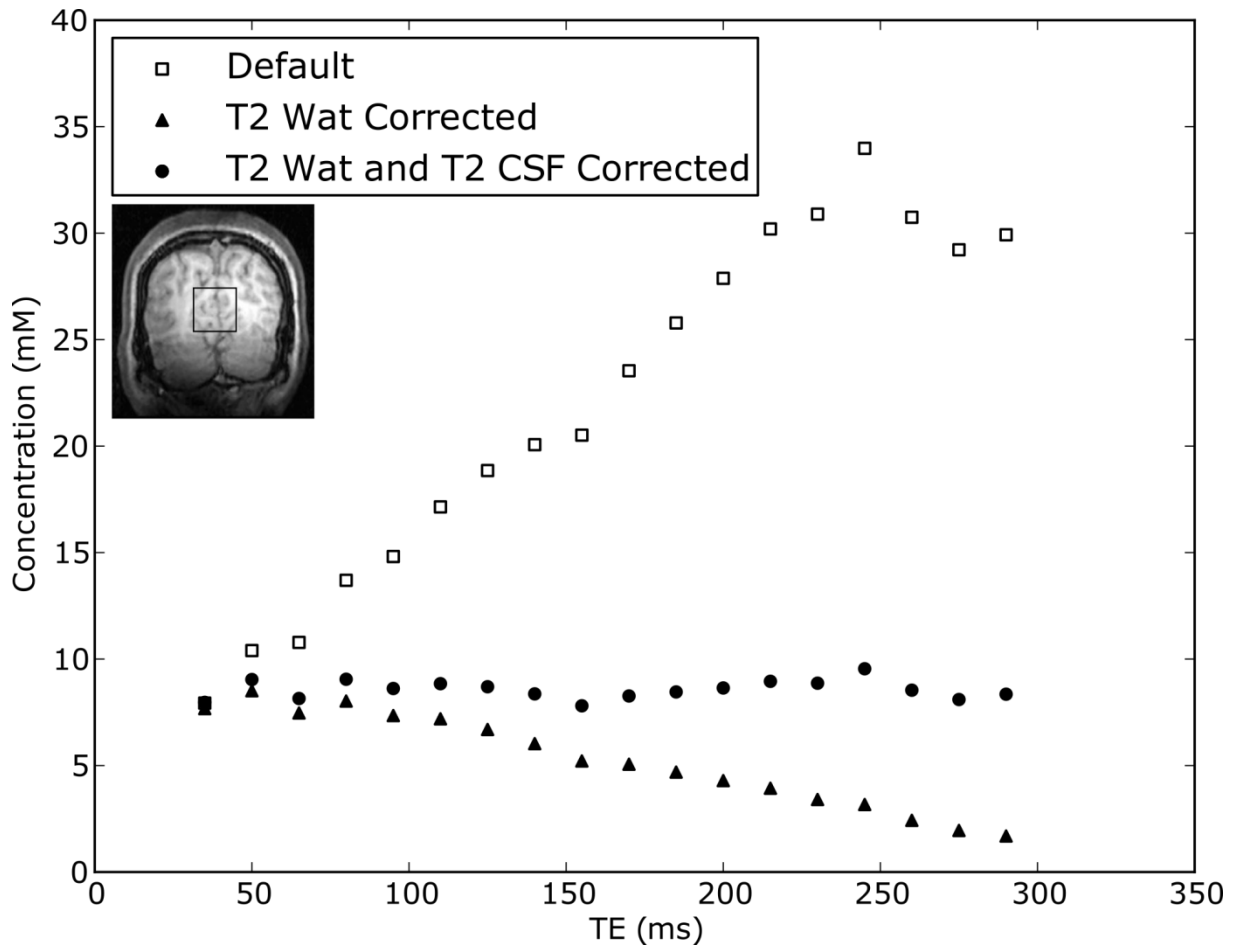
Figure 4-23: Metabolite concentration of NAA quantified at various echo times. 18% of the voxel was CSF. Default concentrations had only the TARQUIN default T2 correction applied, T2 Wat Corrected were corrected assuming a monoexponential water decay whilst T2 Wat and T2 CSF corrected were corrected for GM, WM and CSF T2 and water content differences.

Metabolite concentrations corrected using default TARQUIN settings steadily increased with echo time. Conversely, metabolite concentrations corrected for metabolite T2 relaxation and assuming a single T2 for water decreased with echo time. When metabolite concentrations were corrected for metabolite T2 relaxation times, as well as for GM, WM and CSF components, a stable metabolite concentration was observed when determined at different echo times. This was true for tNAA, tCho and tCr in all volunteers.

4.3.3 Summary of Findings

The T2 relaxation time of metabolites with large singlets without significant spectral overlap estimated from 2 TEs were comparable with those estimated from 18 TEs in both phantom and volunteer. Similarly, the T2 estimates of water from 2 TEs and 18 TEs were also comparable; however, a non-monoexponential signal decay was observed for water in vivo and intravoxel heterogeneity should be accounted for when estimating metabolite concentrations at long TEs. The influence of long-T2 components in the water decay can be minimised by using a maximum TE of 135 ms. For coupled metabolites, the T2 estimates from 2 TEs were not consistent with those from 18 TEs. Furthermore, the relaxation-corrected concentrations of coupled metabolites were significantly different at the three TEs examined.

4.4 Discussion

In this chapter, a combination of simulations, phantom and volunteer data have been used to assess the accuracy of metabolite quantification. Simulations were used to assess how changes in experimental conditions affect quantification accuracy while investigating the effects of spectral overlap and echo time choice have on quantification.

4.4.1 Simulations

Three spectral model systems were investigated using simulations. A brain model system, based on the braino phantom, containing some of the major brain metabolites; a model system containing Glu, Gln and NAA; and a model of GPC, PCh, mI and Gly. The second and third model systems were chosen as changes in Glu and Gln, and in mI and Gly, can lead to contrasting clinical outcomes and the pairs of metabolites have spectra which overlap.

Simulated spectra were constructed for the three model systems at three echo times to investigate how the J-evolution of coupled metabolites affects metabolite quantification. Echo times of 35 and 135 ms were chosen because of their common use in clinical practice, whilst an echo time of 80 ms – which has been proposed for measurement of Glu (Schubert et al., 2004a) – would allow for the decay of short-T2 macromolecule and lipid components in vivo.

Results of the simulations showed that the main determinant of quantification accuracy was data quality rather than echo time choice. The mean concentration estimates became more accurate as SNR increased and were more accurate in spectra simulated with narrow line widths.

The RMS percentage errors of multiplets were consistently larger than those of metabolites with large singlets, which is likely due to inherent differences in SNR for multiplets, while the SD and RMS percentage error of Gly was greater than that of other metabolites. The RMS percentage error of Gly was smallest at TE 80 ms and this is likely due to the reduction of the overlapping mI resonance at this TE. Of the three echo times investigated, the mean concentration of Glu was most accurate at 35 ms but with a considerably smaller SD and RMS percentage errors at 135 ms. For Gln the RMS percentage errors were smallest at 135 ms and largest at 35 ms. An echo time of 80 ms was least accurate for both Glu and Gln estimation. This is in contrast to previous simulation studies which have suggested 80 ms for improved quantification of Glu (Hancu, 2009) and Gln (Hancu and Port, 2011).

Whilst the current study had a 1:1 ratio of Glu:Gln, Hancu investigated a 10:4.5 ratio with a higher amount of NAA. While a 10:4.5 ratio may be typical of normal brain, the ratio can

vary considerably in pathology (Davies et al., 2008a; Panigrahy et al., 2006). A 1:1 ratio was therefore chosen to investigate overlap with comparable resonance intensities. The Glu signal intensity differences between these studies is the most likely cause of the discrepancies between these studies. Another key difference was the inclusion of a macromolecular baseline in the Hancu studies which is likely to affect Glu measurement at 35 ms.

Interestingly, the standard deviations of metabolite concentrations were consistently smaller at FWHM 7 Hz compared with 3 Hz. Whilst the standard deviations were smaller at 7 Hz, the mean concentrations were typically less accurate than those with smaller linewidths. While the reason for this is unclear, this has also been observed in a similar study at 4 T, and could be attributed to an increase in signal area following line broadening (Bartha, 2007).

Previous investigations into the influence of experimental conditions have shown the importance of high SNR and narrow linewidths for quantification precision at 1.5 T (Bartha et al., 2000; Kanowski et al., 2004) and 4 T (Bartha, 2007), while estimates of the precision of GABA measurements at 3 T have been previously been presented (Near et al., 2013). This chapter presents values for the precision of NAA, Cho and Cr which indicate that individual concentration estimates of these metabolites are reliable to within 10% at SNRs of 15 and above. For metabolites which present as multiplets or single peak resonances with considerable overlap, such as Gly, GPC and PCh, an SNR greater than 25 would be required for quantification at this level of accuracy on a case-by-case basis. Accuracy of within 10% for coupled metabolites would likely require a spectrum SNR in the region of 40 and above at typical in vivo concentrations, given reports at 4 T (Bartha, 2007). However, this prediction is

predicated on the presence of a large single peak in the spectrum and metabolite-specific SNRs for accurate quantification of coupled metabolites have not been investigated.

The results presented in this chapter could be used to help power future sample sizes. For cohort studies, the mean metabolite concentrations are likely to be accurate regardless of echo time choice, providing the sample size is large enough. However, while the SNRs and linewidths chosen for the simulations are comparable to those seen in clinical data, they do not represent the full range observed clinically. Future work should therefore establish at what SNRs and linewidths the accuracy of quantification completely breaks down.

The use of idealised conditions has inevitably meant there are limitations to this work. As the purpose of this work was to assess the effect of J-coupling evolution with echo time on quantification, T2 relaxation and baseline effects which would be present in vivo were not included in the simulations. Though the presence of macromolecules and lipids has been ignored, the models selected may provide a surrogate indication of their effects as the equal ratio of Glu:Gln and Gly:mI intensities allow for inferences of the effect of spectral overlap to be made. This is likely reflected in the increased errors associated with multiplets, Gly, GPC and PCh when compared with those of NAA, tCho and Cr. The presence of a baseline may therefore affect coupled resonance or metabolites at low concentrations more than prominent singlets. Fitting routines such as TARQUIN can model the baseline either using experimentally acquired data or as individual measurements; both of these methods provide reproducible concentrations and resonances with a high SNR are likely to be determined accurately even with overlap with the presence of a baseline.

Asymmetric non-Gaussian lineshapes and lineshapes distorted by eddy currents were not modelled in this data. While these effects can affect quantification methods which do not allow freedom in the fitting routines (Wilson et al., 2011), lineshapes can be improved when processing the data by applying either eddy current correction or by performing lineshape correction (De Graaf et al., 1990). Heavily distorted lineshapes are rare and can be excluded through visual inspection of the data, the influence of linewidth and SNR is therefore more pertinent for the majority of acquired spectra.

Signals from outside the intended region of interest can be excited due to slice selection and chemical shift errors. These errors will lead to small errors in the overall metabolic profile of the region of interest and knowledge of the voxel profile can help identify the influence of any such contamination. The use of small voxels and pulse sequences such as LASER which minimise chemical shift errors can render the influence of these effects small in comparison to that of SNR and linewidth.

A further limitation is that the simulated spectra were constructed using the same process that TARQUIN simulates its basis sets with. The simulations therefore do not account for incomplete or inaccurate prior knowledge that can arise in experimentally acquired data. Chemical shift displacement errors are likely to be the most significant unmodelled effect. Chemical shift displacement errors will lead to the simulation of inaccurate basis models for coupled metabolites which will lead to inaccurate quantification, however they can be corrected for by using experimentally acquired basis sets. Phantom and volunteer data were therefore acquired to investigate what effect unmodelled experimental factors can have on quantification.

4.4.2 Phantom and Volunteer Studies

One such factor is T2 relaxation which should be accounted for in metabolite quantification.

The T2 relaxation time was estimated in phantoms using 2 TEs and using 18 TEs. The mean T2 relaxation times were estimated from a monoexponential fit and the two values were comparable. A multi-exponential decay was observed in the water signal of volunteers in vivo. This effect was attributed to the presence of CSF and an increase in the amount of CSF was associated with greater multi-exponential behaviour.

The influence of CSF on a biexponential signal decay was investigated using a mathematically constructed water decay signal. CSF has a much longer T2 than tissue water and the disparity in signal decays becomes more pronounced as TE increases. The effect of CSF can therefore be minimised by estimating the T2 relaxation with a final TE of 135 ms and shorter.

The T2 relaxation times of metabolites were estimated using 2 TEs (35 ms and 135 ms) and using 18 TEs for NAA, Cho and Cr. The estimated mean T2 relaxation times were similar. Following the earlier simulation study, this is likely due to the high signal of the NAA, Cho and Cr peaks. This suggests that estimating the T2 relaxation time of these metabolites from data collected at the short and long TEs commonly used in clinical practice is a valid approach.

The concentration of tNAA, tCho and tCr were estimated at echo times of 35 ms, 80 ms and 135 ms in the braino phantom and volunteer. The mean metabolite concentrations corrected for T2 relaxation times were similar at each TE, indicating that concentrations can likely be estimated accurately at each of the echo times providing a reasonable T2 estimate is available.

The T2 relaxation times of the coupled metabolites Glu, mI and Lac were also estimated using the 2 TE and 18 TE approaches. In each case, the mean T2 relaxation times were significantly different between the two methods. Whilst simulations have shown the J-evolution of metabolites with echo time does not appear to affect metabolite quantification as much as data quality, it does appear to influence T2 estimation. This is likely due to a combination of the inherently lower SNR of multiplets compared with singlets and small errors in the signal fitting at multiple echo times compounding when estimating T2 values. The true metabolite signal will not exactly match the simulated one in the basis set for a number of experimental reasons. Careful selection of appropriate echo times and acquisition protocol is required for accurate evaluation of the T2 relaxation time of coupled metabolites (Ganji et al., 2012b; Madan et al., 2015b; Xin et al., 2008a).

Consistent with the simulated analysis, a greater variation in metabolite concentrations was observed for multiplets compared to singlets between the three echo times of 35, 80 and 135 ms. The errors associated with the concentrations measured in phantoms were larger than those seen in the simulations. In volunteers the estimated concentrations varied significantly for mI and Glu depending on the echo time that data was acquired at. These errors could be due to inaccurate T2 relaxation times. This could also be attributed to small differences in the basis set compared with the experimental spectrum leading to significant errors. Differences in the temperature and pH can lead to changes in spectral appearance, while the chemical shift displacement artefact can also affect the acquired spectrum. The chemical shift displacement artefact is a likely cause of the signal and T2 variation of lactate in the braino phantom.

The use of multiple echo times to estimate metabolite concentrations was investigated. There was not a significant difference in the measurement of NAA, Cho or Cr using mean estimates from one, three and 18 TE acquisitions. There was a significant difference in the mean concentration estimates of Glu and mI from 3 TEs when different T2 relaxation time values were used, illustrating the importance of accurate T2 relaxation times for metabolite quantification. The use of two TEs has previously been shown to improve the classification accuracy in paediatric brain tumours (Vicente et al., 2013), however it did not improve the accuracy of metabolite quantification in phantoms in our experiments. A logical extension to this study would be to use an experimentally acquired basis set to quantify phantom data. However, this would not remove all of the problems associated with obtaining an accurate basis set for in vivo studies as tissue conditions will vary.

4.5 Conclusions

This study has used a combination of simulations, phantoms and volunteer data to investigate the accuracy of metabolite quantification at different echo times. Simulated spectra demonstrated that while the mean concentration estimate of a cohort is generally accurate to within 10% within the parameters of current quality control criteria. Quantification accuracy is improved with high SNR and narrow line widths. The precision of any single measurement is highly dependent on SNR. Concentration estimates for metabolites with large single peak resonances, such as NAA, Cho and Cr, are likely reliable to within 10% of the true value with SNR levels of 15 and above. However, for metabolites with spectroscopy dominated by multiplets, an overall spectrum SNR greater than 25 with further investigation needed to determine metabolite-specific SNRs required for accurate quantification of multiplets. Additional spectral overlap did not significantly affect the

accuracy of metabolite quantification of multiplets; however, measurement of Gly, GPC and PCh – metabolites which completely overlap with other metabolites and are predominantly large single peaks – was less accurate.

The simulations did not identify a single optimal echo time for metabolite quantification of all metabolites. There was a significant difference in the metabolite concentration estimates in phantoms and in vivo depending on TE choice. Correction for T2 relaxation effects was demonstrated to be important for accurate metabolite quantification. The T2 relaxation time of water and metabolites with large single peak resonances can be estimated from two echo times; however, T2 estimates for multiplets will require careful protocol design.

The use of short-TEs is recommended for future studies as they will reduce the influence of T2 relaxation on quantification and have inherently higher SNR. The use of reasonable T2 estimates is required to correct for relaxation effects. In cases where these are not available, these can be measured from two echo times to keep the acquisition time to within a clinically acceptable timeframe. In particular, the measurement of water T2 is rapid due to its very high natural abundance and could be added to all in vivo studies.

5. VARIATION OF T2 RELAXATION TIMES IN PAEDIATRIC BRAIN TUMOURS AND THEIR EFFECT ON METABOLITE QUANTIFICATION AT 1.5 TESLA

5.1 Introduction

Brain tumours are the most common solid tumours in children and a significant cause of morbidity and mortality. 1H magnetic resonance spectroscopy (MRS) provides a non-invasive means of profiling the chemical composition of brain tumours, providing prognostic and diagnostic biomarkers which can be used for tumour classification (Davies et al., 2008; Vicente et al., 2013) and for monitoring treatment response (Quon et al., 2011). As quantitative metabolite biomarkers start to be proposed for clinical decision making in individual patients (Wilson et al., 2014, 2013), accurate measurement becomes of increasing importance.

MRS is typically implemented clinically by adhering to an agreed protocol and comparing the results to those obtained using the same protocol. Whilst metabolite levels can be reported as ratios, quantification is typically performed by fitting to a set of metabolite basis functions and concentrations are calculated with reference to an unsuppressed water signal (R. Kreis et al., 1993).

Popular analysis packages, LCModel (Provencher, 1993) and TARQUIN (Wilson et al., 2011), are often used for metabolite quantification, assuming T2 relaxation times typical of normal brain in their calculations. However, relaxation times are sensitive to microenvironment and have been shown to change with pathology (Isobe et al., 2002; Li et al., 2008; Madan et al., 2015; Sijens and Oudkerk, 2002). In the previous major studies of brain tumours using MRS, further correction for the differences in T2 relaxation between brain tumours and healthy

brain has not been performed and the effects of T2 relaxation variation have been assumed to be small at short-TE (Davies et al., 2008; Panigrahy et al., 2006; Vicente et al., 2013).

The use of longer TEs for metabolite quantification has been proposed recently (Choi et al., 2013; Napolitano et al., 2013; Schubert et al., 2004), however, T2 relaxation times are known to have a significant effect on concentration determination at long-TEs (Yamamoto et al., 2015, Chapter 4) and correction for T2 relaxation has been shown to have a significant effect on metabolite ratios at 3T (Li et al., 2008). Accurate water and metabolite T2 relaxation times are therefore likely to be required for reliable metabolite quantification. With the emergence of various acquisition protocols, it is becoming increasingly important to explore the effects of relaxation on quantification at various echo times.

In a recent multi-center study of paediatric brain tumours (Vicente et al., 2013), reporting concentrations measured at both short and long-TE, there was a large difference between the concentrations measured at the two echo times. Though a recent study has examined the effect of using long-TEs for quantification using LCModel (Yamamoto et al., 2015), the influence of varying T2 relaxation times on brain tumour quantification at short-TE has not been formally assessed.

Whilst previous studies of adult brain tumours have shown significant differences in both water and metabolite T2 relaxation times (Isobe et al., 2002; Li et al., 2008; Madan et al., 2015; Sijens and Oudkerk, 2002), T2 relaxation in childhood brain tumours has not been extensively studied to date. Investigation of relaxation times in the paediatric population is of particular importance as metabolite T2 relaxation times in normal brain have been shown to change with age (Kirov et al., 2008). In addition, for brain tumours, specific studies in

children are required since the tumours are histologically and biologically different from their adult counterparts (Gilheeney and Kieran, 2012; Merchant et al., 2010). Further differences arise in the incidence of brain tumours, with low grade gliomas and medulloblastoma occurring more frequently in children than in adults.

Measuring T2 formally is challenging since acquisition protocols require multiple echo times and this leads to long acquisition times. This issue is particularly pertinent to the study of children where long scans are poorly tolerated. However, protocols using two echo times have been implemented clinically (Sijens and Oudkerk, 2002; Vicente et al., 2013). Furthermore, the T2 relaxation times of NAA, Cho, Cr and water, estimated from two TEs (35 and 135 ms), were shown to be comparable with those estimated using more TEs at longer echo times in Chapter 4. A protocol using two echo times therefore has the potential to estimate the T2 values of metabolites and water whilst keeping acquisition times within reasonable limits.

In this chapter, metabolite and water T2 relaxation times in apparently normal brain and childhood brain tumours have been retrospectively calculated from data collected at both short and long-TE with the aim of establishing how the relaxation properties of major metabolites vary and the effect this has on metabolite quantification.

5.2 Methods

5.2.1 Patients
Two cohorts were retrospectively selected from patients where single-voxel MRS had been performed prior to treatment between September 2006 and July 2011. The first cohort consisted of 31 children with brain tumours. This tumour group was comprised of four

diffuse intrinsic pontine gliomas (4 male, mean age 11.4 years), 10 medulloblastomas (6 male and 4 female, mean age 6.1 years) and 17 pilocytic astrocytomas (9 male and 8 female, mean age 7.4 years).

Comparison was made with a second cohort consisting of 24 children (18 male and 6 female, mean age 6.4 years) with normal-appearing MRI and MRS. These children had undergone investigation for a suspected metabolic disorder which was subsequently ruled out. All patients were under 16 years of age and informed parental consent and research ethics approval was obtained.

5.2.2 MRS Acquisition

MRS was acquired using a Siemens Symphony Magnetom NUM4 1.5 T scanner following conventional imaging. The standard imaging set of T1-weighted, T2-weighted and T1-weighted images post contrast administration was used to delineate the tumour margins. Cubic voxels of side length 1.5 cm or 2 cm were placed entirely within the solid component of the tumour avoiding any cyst or necrosis and point-resolved spectroscopy (PRESS) was performed. Cubic voxels of side length 2 cm were placed in the basal ganglia and parietal white matter in the cohort with normal-appearing MRI and MRS. Water suppressed data were acquired with 128 repetitions from the larger voxels and 256 repetitions from the smaller ones. For all scans, a TR time of 1500 ms was used and data were acquired at both short (30 ms) and long (135 ms) TE. Water unsuppressed MRS data were also acquired with 4 repetitions as a concentration reference at both TEs.

5.2.3 Processing and Analysis

Raw spectroscopy data were automatically processed using TARQUIN v 4.3.8 (Wilson et al., 2011b). TARQUIN models experimental data as a linear combination of simulated basis

signals. To extract metabolite concentrations, the fitted signal amplitudes â are scaled by two factors: W_{att} and W_{conc}.

The W_{att} parameter accounts for the reduction of the water signal relative to metabolite signals due to differences in T2 relaxation at a given TE and is defined as $W_{att} = [exp(-TE/T2_{water}) / exp(-TE/T2_{metabolite})]$. This parameter is used to adjust the metabolite concentrations to be independent of TE and will give the correct value if $T2_{water}$ and $T2_{metabolite}$ are known accurately. W_{conc} denotes the assumed water concentration for a given tissue type and is used to scale â to the amplitude of the unsuppressed water signal. W_{conc} and W_{att} are assumed as 35880 mM and 0.7 respectively by TARQUIN as default.

Tumour spectra were referenced to the total choline signal to account for frequency drift, while normal brain spectra were referenced to a combination of total choline-creatine-NAA-lipids. MRS was quantified using the internal basis set 1H brain + Gly, Cit, Glth. Due to significant spectral overlap at 1.5 T, the following metabolites were combined in the subsequent analysis: Gln + Glu = Glx; NAA + NAAG = tNAA; Cr + PCr = tCr and GPC + PCh = tCho.

T2 Measurement

T2 relaxation times were estimated by fitting TARQUIN estimates of signal amplitude â (Wilson et al., 2011b) for each metabolite from the two echo times to a monoexponential function.

Concentration Calculation

To assess the importance of accurate T2 relaxation times for metabolite quantification, metabolite concentrations corrected using various combinations of measured and literature

T2 values were compared. The following terms are used for the various methods of obtaining the T2 values. Tissue type refers to pilocytic astrocytoma, medulloblastoma or normal brain.

Individual water (IW) correction uses the T2 relaxation time of water measured as part of the MRS acquisition for that case.

Individual metabolite (IM) correction uses the case's estimated metabolite T2 values where the metabolite could be quantified accurately at both echo times. Where a metabolite T2 could not be estimated for a case, the tissue's mean average T2 value from the rest of the cases in the study was used for tNAA, tCho and tCr and a metabolite T2 of 300 ms was assumed for all other metabolites.

Average water (AW) correction uses the average T2 relaxation time of water obtained from the cases in the study with the same tissue type.

Average metabolite (AM) correction uses the average T2 relaxation time for the metabolites obtained from the cases in the study with the same tissue type for NAA, tCho, Cr and Tau and a metabolite T2 of 300 ms for all other metabolites.

Literature water (LW) T2 relaxation times were taken to be 174.5 ms in both brain tumour types and 88.6 ms in normal brain (Isobe et al., 2002).

Literature metabolite (LM) T2 values of 368.8, 205.3 and 265.4 ms were used for tNAA, tCr and tCho respectively in healthy brain (Isobe et al., 2002). In both brain tumour types, the T2 values used for tNAA, tCr and tCho were 227.5, 196.3 and 275.3 ms. A T2 of 300 ms was assumed for all other metabolites.

The term default is used for concentrations estimated using TARQUIN's default W_{att} value of 0.7. This value is based on TE = 30 ms data collected in adults at 1.5 T and assumes T2 relaxation times typical of white matter.

Metabolite concentrations quantified at short-TE were corrected for relaxation effects by calculating case-specific W_{att} values using IM and IW T2 values. These values are assumed to be the best estimates of the metabolite values and all other methods are compared against these with the root mean square (rms) differences being reported.

Quality Control

MRS data were required to have a water linewidth (full-width-at-half maximum, FWHM) < 15 Hz and signal-to-noise ratio ≥ 4. Spectra were reviewed for quality by two expert spectroscopists. Short- and long-TE spectra were assessed to identify metabolites present at both echo times for inclusion in the T2 analysis.

Statistics

One-way ANOVA tests were used to analyze the mean T2 relaxation times and metabolite concentrations for the four tissue groups and paired Mann-Whitney U tests were performed. Statistical significance was declared for $P < 0.05$. A Mann-Whitney U test was chosen ahead of a Student's t-test as it is more conservative for small sample sizes (Fay and Proschan, 2010).

5.3 Results

Following quality control, a total of 26 tNAA (10 pilocytic astrocytomas, 5 medulloblastoma, 16 normal), 36 tCr (8 pilocytic astrocytomas, 9 medulloblastoma, 16 normal), 38 tCho (11 pilocytic astrocytomas, 9 medulloblastoma, 16 normal) could be reliably measured across all

tissue types. Figure 5-1 shows example pilocytic astrocytoma and medulloblastoma spectra.

Figure 5-2 shows example basal ganglia and white matter spectra.
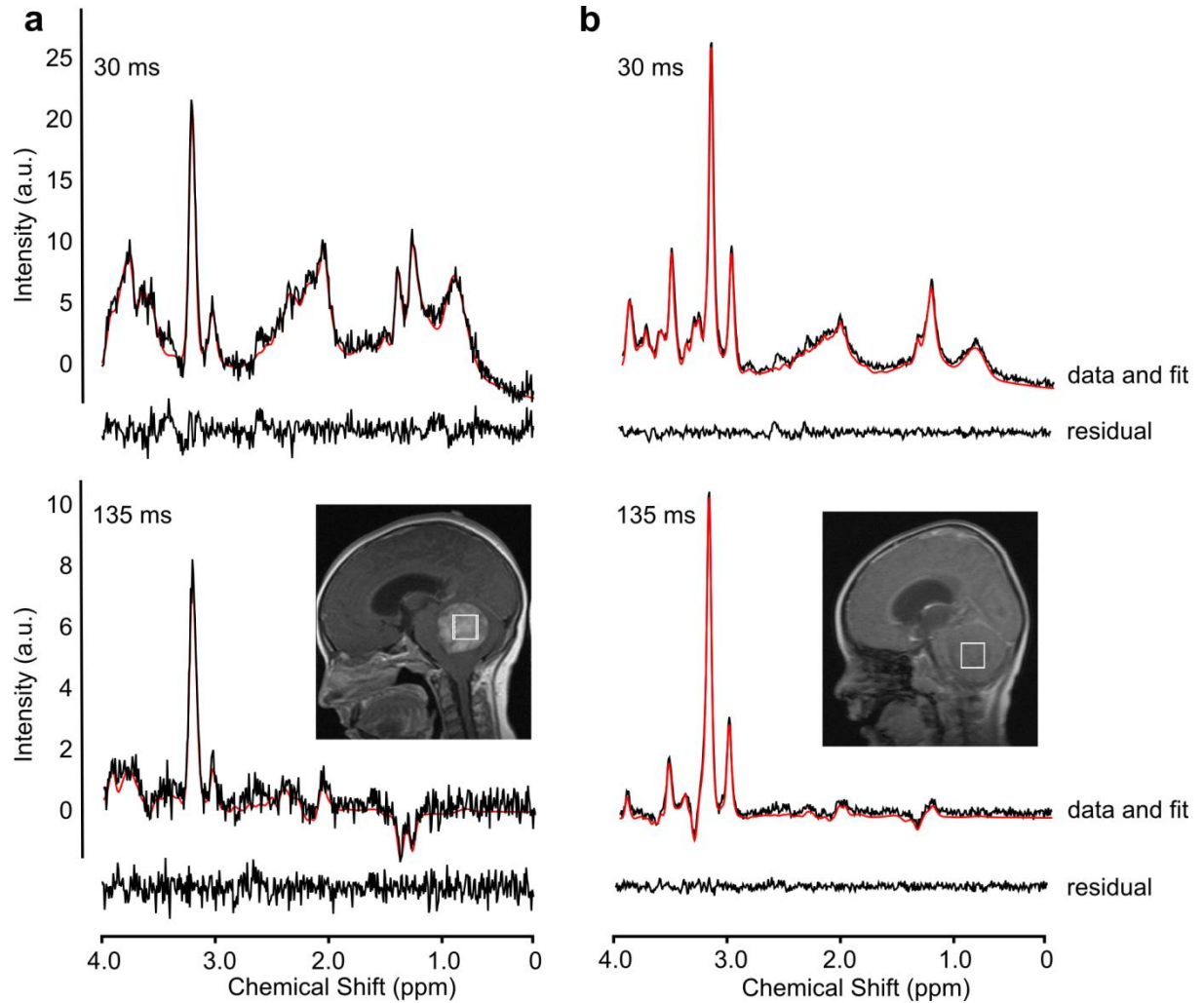
Figure 5-1: Example spectra from a) pilocytic astrocytoma and b) medulloblastoma at short and long-TE with TARQUIN fits (red) and fit residuals shown beneath the spectra
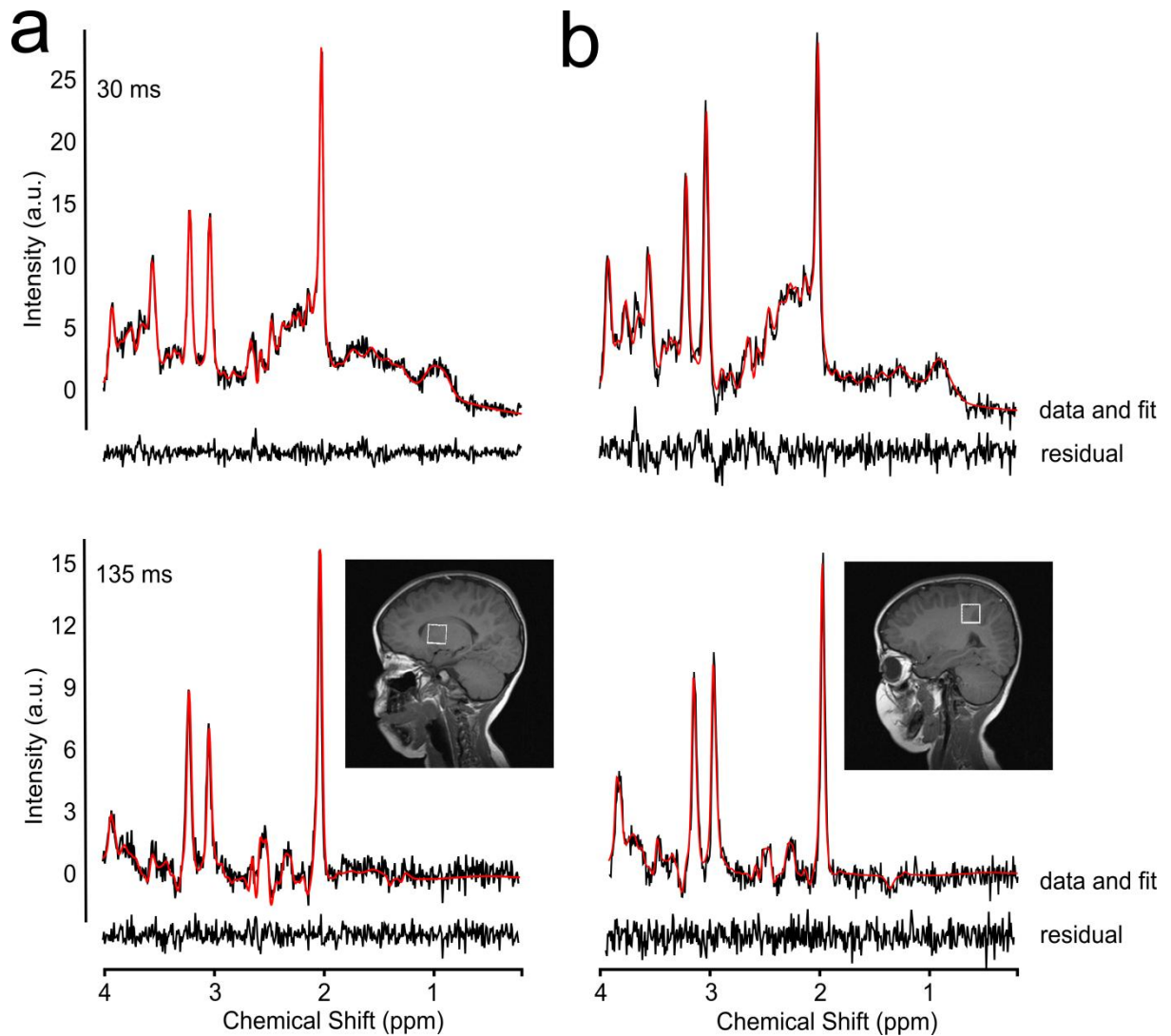
Figure 5-2: Example spectra from a) basal ganglia and b) white matter at short and long-TE with TARQUIN fits (red) and fit residuals shown beneath the spectra

5.3.1 T2 Results

	T2 Relaxation Time (ms)							
	PA		MB		WM		BG	
	Mean ± SD	n	Mean ± SD	n	Mean ± SD	n	Mean ± SD	n
tNAA	191 ± 56	10	333 ± 124	5	423 ± 113	14	436 ± 140	16
tCho	372 ± 176	11	587 ± 143	9	313 ± 154	15	344 ± 122	14
tCr	217 ± 65	8	305 ± 51	9	237 ± 72	10	225 ± 78	16
Water	181 ± 35	11	123 ± 45	10	90 ± 9	15	86 ± 8	16

Table 5-1: Estimated T2 relaxation times (ms) in pilocytic astrocytoma (PA), medulloblastoma (MB), basal ganglia (BG) and white matter (WM).
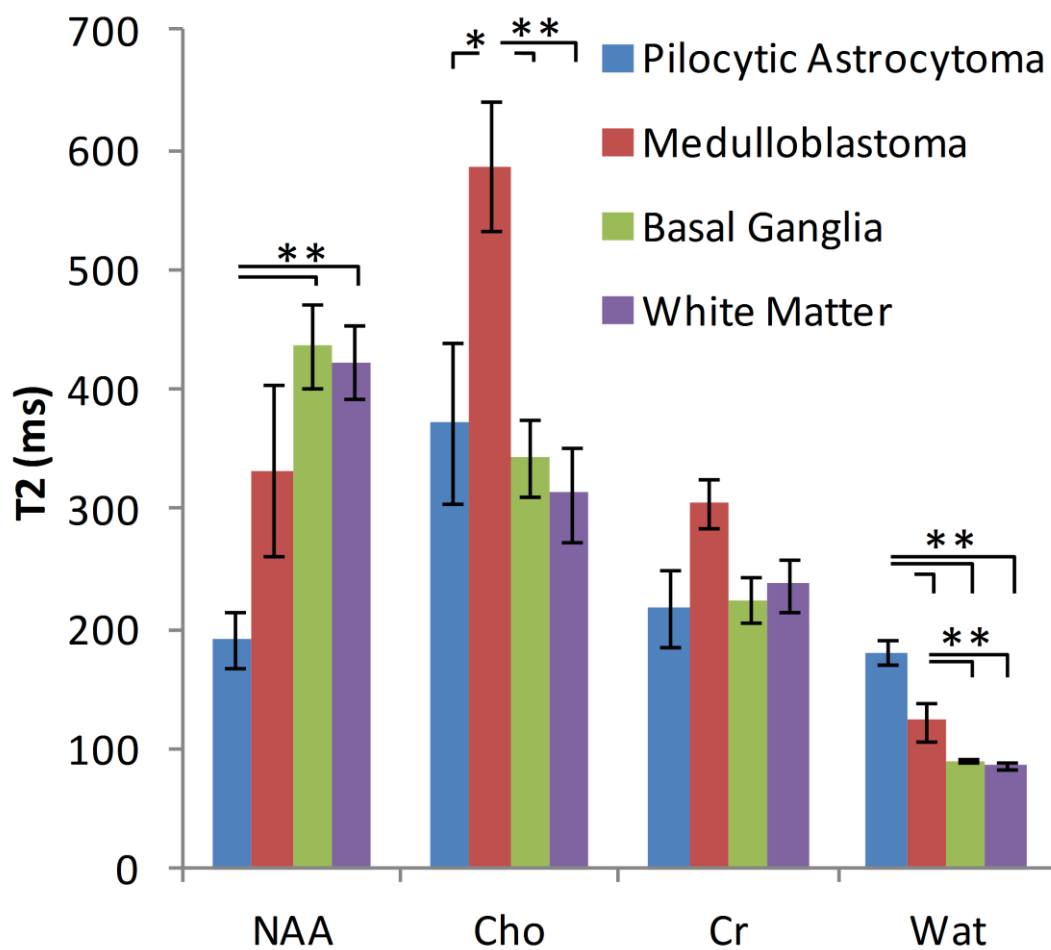
Figure 5-3: Mean (standard error) T2s of tNAA, tCho, tCr, Tau, Glx and water for pilocytic astrocytomas, medulloblastomas, basal ganglia and normal white matter. *P < 0.05, ** P < 0.001

T2 values for metabolites and water are represented in Figure 5-3 with the values given in Table 5-1. tCho was significantly longer in medulloblastomas compared to pilocytic astrocytoma (Mann-Witney U-test, P = 0.04) and compared to white matter (Mann-Witney U-test, P < 0.001) and basal ganglia (Mann-Witney U-test, P < 0.001). The T2 relaxation time of tNAA was significantly shorter in pilocytic astrocytomas compared to white matter (Mann-Witney U-test, P < 0.001) and basal ganglia (Mann-Witney U-test, P < 0.001).

The T2 relaxation times of tissue water in pilocytic astrocytomas 181 ± 35 ms, diffuse intrinsic pontine glioma 133 ± 25 ms and medulloblastomas 123± 45 ms were found to be

significantly longer than in white matter 90 ± 9 ms and basal ganglia 86 ± 8 ms (Mann-Witney U-test, $P = 10^{-6}$) in all cases). The T2 relaxation time of water was significantly longer in pilocytic astrocytomas than in medulloblastoma and diffuse intrinsic pontine gliomas (Mann-Witney U-test, $P = 0.001$).

The mean W_{att} values, calculated using the mean tissue water and metabolite T2 relaxations times, were 0.95, 0.85 and 0.80 for pilocytic astrocytomas, medulloblastomas and normal brain respectively at TE= 30ms. There was no correlation between T2 relaxation times and age in normal brain for water or any of the metabolites.

5.3.2 Metabolite Concentrations Corrected for T2 Relaxation Times

Table 5-2 shows the mean metabolite concentrations in the different tissue types, corrected for water (IW) and metabolite T2 (IM) relaxation. The concentration of tNAA (Mann-Witney U-test, $P = 10^{-23}$), tCr ($P = 10^{-6}$), GABA ($P = 10^{-5}$), Glu ($P = 10^{-7}$) and Glx ($P = 10^{-6}$) were significantly lower in tumours compared to normal brain, whilst Lac ($P = 10^{-4}$) was significantly higher in tumours. The concentration of tCho ($P = 10^{-5}$), Tau ($P = 10^{-4}$), Glth ($P = 10^{-4}$), Gly ($P = 0.02$) and tCr ($P = 0.03$) were significantly higher in medulloblastomas compared to pilocytic astrocytomas whilst Glc ($P = 0.01$) was higher in pilocytic astrocytomas compared to medulloblastomas. All significant differences in concentration levels that were observed in the fully corrected data were also present when concentrations were estimated using default TARQUIN settings. Classification accuracy of paediatric brain tumours was not improved when using fully-corrected metabolite concentrations.

5.3.3 Concentration Correction Comparisons

Metabolite concentrations were measured and adjusted using various combinations of T2 values as detailed in the methods section. Mean metabolite concentrations corrected using

default T2 values and short-TE MRS and long-TE MRS corrected for the prolonged echo time

of 135 ms using default T2 values are given in Table 5-3 and Table 5-4 respectively.

	Concentration (mmol/kg)								
	ANOVA all groups (*P* value)	Pilocytic Astrocytomas		Medulloblastomas		Pilocytic astrocytoma vs medulloblastoma (*P* value)	Normal		Normal vs all tumours (*P* value)
		Mean	SD	Mean	SD		Mean	SD	
tNAA	10^{-22}	1.63 ±	0.66	1.28 ±	1.35	0.52	7.44 ±	4.45	10^{-23}
tCho	10^{-10}	1.18 ±	0.39	5.53 ±	2.24	< 0.001	1.62 ±	0.64	< 0.01
tCr	10^{-6}	0.85 ±	0.61	3.73 ±	2.28	< 0.05	5.69 ±	2.10	10^{-6}
Lac	10^{-4}	1.35 ±	0.59	4.03 ±	2.47	0.06	0.32 ±	0.97	10^{-4}
Ala	0.09	0.29 ±	0.36	0.30 ±	0.46	0.63	0.12 ±	0.17	< 0.05
Glu	10^{-6}	2.58 ±	1.01	3.15 ±	0.95	0.81	6.05 ±	2.47	10^{-7}
Gln	0.43	2.64 ±	1.59	2.04 ±	1.80	0.69	1.71 ±	1.48	0.22
ml	0.16	1.12 ±	1.14	3.08 ±	3.13	0.32	3.48 ±	3.72	0.17
Tau	10^{-5}	0.65 ±	0.47	4.39 ±	2.19	< 0.01	0.98 ±	1.23	< 0.05
Glc	0.08	3.04 ±	1.37	1.13 ±	1.08	< 0.01	2.40 ±	1.23	0.32
GABA	10^{-4}	0.47 ±	0.32	1.46 ±	1.52	< 0.05	2.93 ±	0.81	10^{-5}
Glth	< 0.05	0.27 ±	0.42	1.36 ±	0.84	< 0.01	0.68 ±	0.60	0.78
Gly	10^{-5}	0.33 ±	0.54	4.15 ±	1.87	< 0.01	0.42 ±	0.62	0.06
Scy	< 0.01	0.00 ±	0.00	0.65 ±	0.51	< 0.05	0.19 ±	0.14	0.34
Glx	10^{-5}	5.22 ±	2.59	5.20 ±	2.75	0.42	7.75 ±	3.95	10^{-6}

Table 5-2: Estimated metabolite concentrations (mmol/kg) of pilocytic astrocytomas, medulloblastomas and normal brain, corrected for individually estimated water and metabolite T2 relaxation times.

When averaged over all metabolites and all tissue types, the mean metabolite concentrations calculated using the default T2 relaxation times and short echo time MRS were underestimated by 26% compared to the mean concentrations determined using the IW and IM relaxation times (Mann-Whitney U-test, $P = 10^{-5}$).

When averaged over all metabolites, the mean metabolite concentrations using the default T2 relaxation times and short echo time MRS were underestimated by 37% in pilocytic astrocytomas, by 16% in medulloblastomas and by 16% in normal brain, compared to the mean concentrations determined using the IW and IM relaxation times.

The mean concentrations measured using LW, LM T2 relaxation times were not significantly different from concentrations corrected using IW, IM T2 values.

	Concentration (mmol/kg)							
	Pilocytic Astrocytomas			Medulloblastomas			Normal	
	Mean		SD	Mean		SD	Mean		SD
tNAA	1.09	±	0.47	0.96	±	0.85	6.53	±	2.68
tCho	0.85	±	0.22	4.90	±	2.01	1.40	±	0.37
tCr	0.58	±	0.34	3.14	±	1.87	4.74	±	1.30
Lac	1.01	±	0.43	3.36	±	2.02	0.28	±	0.85
Ala	0.22	±	0.28	0.25	±	0.37	0.11	±	0.15
Glu	1.95	±	0.79	2.64	±	0.78	5.25	±	1.92
Gln	1.99	±	1.18	1.71	±	1.50	1.52	±	1.35
ml	0.85	±	0.89	2.58	±	2.63	2.95	±	2.55
Tau	0.49	±	0.35	3.68	±	1.85	0.81	±	1.05
Glc	2.29	±	1.01	0.95	±	0.91	2.06	±	1.07
GABA	0.35	±	0.24	1.22	±	1.29	2.59	±	0.75
Glth	0.20	±	0.32	1.14	±	0.70	0.60	±	0.53
Gly	0.25	±	0.40	3.47	±	1.56	0.39	±	0.56
Scy	0.00	±	0.00	0.54	±	0.43	0.17	±	0.13
Glx	3.94	±	1.97	4.35	±	2.28	6.78	±	3.27

Table 5-3: Metabolite concentrations (mmol/kg) of pilocytic astrocytomas, medulloblastomas and normal brain, estimated using TARQUIN's default settings at short TE.

	Concentration (mmol/kg)					
	Pilocytic Astrocytomas		Medulloblastomas		Normal	
	Mean	SD	Mean	SD	Mean	SD
tNAA	0.39 ±	0.21	0.62 ±	0.23	5.81 ±	0.96
tCho	0.41 ±	0.13	4.15 ±	1.82	1.13 ±	0.17
tCr	0.26 ±	0.09	2.29 ±	1.18	3.43 ±	0.88
Lac	0.46 ±	0.24	1.38 ±	0.74	0.39 ±	0.28
Ala	0.06 ±	0.08	0.61 ±	0.77	0.03 ±	0.08
Glu	0.32 ±	0.24	0.50 ±	0.56	2.68 ±	1.07
Gln	0.31 ±	0.23	0.83 ±	0.38	0.69 ±	0.80
ml	0.52 ±	0.56	8.47 ±	4.01	3.64 ±	1.65
Tau	0.63 ±	0.79	2.65 ±	1.61	0.78 ±	0.48
Glc	1.78 ±	3.87	0.00 ±	0.00	0.95 ±	1.18
GABA	0.21 ±	0.09	1.40 ±	1.37	1.86 ±	0.52
Glth	0.17 ±	0.06	0.39 ±	0.31	0.42 ±	0.24
Gly	0.35 ±	0.57	1.89 ±	1.31	0.33 ±	0.35
Scy	0.13 ±	0.21	0.44 ±	0.33	0.14 ±	0.12
Glx	0.64 ±	0.47	1.34 ±	0.94	3.37 ±	1.86

Table 5-4: Metabolite concentrations (mmol/kg) of pilocytic astrocytomas, medulloblastomas and normal brain, estimated using TARQUIN's default W_{att} having allowed for a TE of 135 ms.

5.3.4 Estimated Errors in Metabolite Concentrations Calculated using Various T2 values

The percentage rms difference of the metabolite concentrations from the values determined using the individually measured water (IW) and metabolite (IM) T2 relaxation times are presented in Table 5-5.

At short-TE, average rms differences of 6.3% from the individually-corrected concentrations were found when the IW T2 values (with LM or AM) were used. At long-TE differences of 27% were found.

The percentage rms difference observed at short-TE was significantly smaller than at long-TE (22% vs. 53%; Mann-Witney U-test, $P = 10^{-26}$) across all tissue types and for all T2 correction

methods. The percentage rms differences were significantly smaller when the IW T2 were used compared with the other methods of T2 water correction (16% vs. 24%; Mann-Witney U-test, $P = 10^{-16}$) across all tissue types.

	Medulloblastomas				
	Default	LM, LW	AM, AW	LM, IW	AM, IW
Short TE Singlets	18.8	14.8	5.9	5.1	4.5
Long TE Singlets	50.6	63.7	25.9	22.9	19.7
	Pilocytic Astrocytomas				
	Default	LM, LW	AM, AW	LM, IW	AM, IW
Short TE Singlets	34.5	27.9	26.9	9.8	10.1
Long TE Singlets	78.0	79.5	78.7	41.4	41.8
	Normal Brain				
	Default	LM, LW	AM, AW	LM, IW	AM, IW
Short TE Singlets	13.1	5.5	5.1	4.4	4.2
Long TE Singlets	70.5	24.3	22.7	19.8	18.6

Table 5-5: The root mean square percentage difference between metabolite concentrations corrected using different combinations of T2 relaxation times (see Methods and Materials) compared to the corrected concentration using the patient's measured T2 values (IM, IW): Key: L – literature; A – average; I – individual; M – metabolite; W – water.

5.4 Discussion

In this study, T2 relaxation times of metabolites and water have been estimated in childhood brain tumours and metabolite concentrations corrected for relaxation effects are reported. The importance of T2 relaxation times for quantification has also been assessed.

In previous major studies of metabolite concentrations in brain tumours (Davies et al., 2008; Howe et al., 2003; Panigrahy et al., 2006; Vicente et al., 2013), no correction for the differences in T2 relaxation times of brain tumours and healthy brain was performed. A water attenuation factor of 0.7 is applied to the data by default in LCModel and TARQUIN. This value is calculated using data collected at 1.5 T in healthy adult brain assuming an echo

time of 30 ms and is not suitable for quantification of long-TE data. In this study, concentrations measured without further correction for the differences in relaxation were typically underestimated by approximately 25% at short-TE.

This is the first study that has reported metabolite concentrations corrected for T2 relaxation effects in paediatric brain tumours. Whilst there are differences between the concentrations corrected for water and metabolite T2 and the default T2 values, the main features in the metabolite profiles reported for medulloblastomas and pilocytic astrocytomas in children have been substantiated (Davies et al., 2008; Panigrahy et al., 2006; Vicente et al., 2013). tNAA, tCr, Glu, and Glx were all significantly reduced in tumours compared to healthy controls, while Lac was significantly increased in tumours compared with normal brain. Concentrations of tCho, tCr, Glth, Tau and Gly were all significantly higher in medulloblastomas compared to pilocytic astrocytomas; however Glc was significantly higher in pilocytic astrocytomas when compared to medulloblastomas. While previous studies have assessed the influence of T2 relaxation on metabolite ratios (Li et al., 2008) and quantification at long-TE (Yamamoto et al., 2015), this study has assessed the variation in relaxation time in paediatric brain tumours and normal brain and the effect on metabolite quantification. The relative importance of water and metabolite T2 relaxation times has also been assessed.

The T2 relaxation time of tissue water was found to have a greater effect on concentration measurements than the T2 relaxation time of metabolites. Due to the high SNR of the water signal, an additional multi-TE acquisition to measure the T2 of water can be implemented with a scan time of less than a minute and is recommended to improve the accuracy of

metabolite quantification. However, if water T2 values for individual cases are not available, then the mean values for the relevant tissue type should be used.

At long-TE, the rms percentage differences from concentrations corrected for both IW and IM T2 relaxation were larger than at short-TE, suggesting that accurate metabolite T2 values are of more importance at long echo times than at short. This is as expected since signal losses due to T2 relaxation effects increase with echo time and hence inaccurate T2 estimation will lead to greater errors in concentration determination at longer echo times. Use of short echo times, reduces the errors due to poor T2 estimates and this should be taken into consideration where concentration determination is important. Since no significant differences in the T2 measurements were detected between tissue types for the majority of metabolites, T2 values determined from normal brain could reasonably be used in determining concentrations for tumours. More accurate values are likely to be obtained if metabolite specific T2s are used, although this is somewhat more challenging to implement. It should be recognized that even with this correction, errors will increase with echo time and that errors can be large for individual cases.

A number of studies have reported T2 relaxation times of adult brain tumours at 1.5 (Isobe et al., 2002; Sijens and Oudkerk, 2002) and 3 T (Li et al., 2008; Madan et al., 2015), however relaxation times in paediatric brain tumours have been relatively unexplored. Consistent with observations of prolonged water T2 in adult brain tumours, the T2 relaxation time of water was found to be significantly longer in tumours than normal brain and in pilocytic astrocytomas compared to medulloblastomas and diffuse intrinsic pontine gliomas. The long T2 in brain tumours is consistent with the high signal seen on T2 weighted imaging

compared with grey matter and corresponds to the high water content, especially in pilocytic astrocytomas. No correction has been made for variations of water tissue content in keeping with previous studies of brain tumours and it is not known what error this will introduce on concentration measurements. However voxels were placed entirely within the solid component of the tumour to exclude all cystic components.

The T2 of tCho was found to be significantly longer in medulloblastomas compared to pilocytic astrocytomas. Previous reports of tCho T2 in brain tumours have been variable, with tCho T2 observed to be longer in brain tumours compared to normal brain at 3T (Li et al., 2008; Madan et al., 2015) but shorter in a prior 1.5T study (Sijens and Oudkerk, 2002). Previous studies have observed differences in the T2 relaxation times of tNAA (Isobe et al., 2002) and tCr (Isobe et al., 2002; Madan et al., 2015) in tumours compared to healthy controls, but no significant differences were observed in our study. The reason for the long T2 of tCho in medulloblastoma is uncertain. However, the resonance at 3.20 ppm is composed mainly of PCh in medulloblastomas and GPC in gliomas (Albers et al., 2005; Wilson et al., 2009a), while free choline can also contribute significantly to the tCho peak in medulloblastomas. The prolonged T2 of tCho in medulloblastomas may therefore be due to the difference in T2 values between these metabolites, with a longer PCh T2 being consistent with its lower molecular weight relative to GPC, and could reflect different environments for choline metabolites in the two tumour types

Previous studies of the T2 relaxation time of tCr have indicated there may be differences in the T2 relaxation of the methyl and methylene groups (Deelchand et al., 2012; Ganji et al., 2012). Whilst the whole tCr spectrum is fitted in the analysis, a correction term is included

which corresponds to a resonance at 3.91 ppm to allow for attenuation of this signal following water suppression and the tCr T2 may therefore be biased towards the 3.02 ppm methyl group resonance.

NAA is typically only present at low concentrations in pilocytic astrocytomas and very low concentrations in medulloblastomas. However, it is unlikely that the signal is from surrounding brain since voxels were placed entirely within the tumor margins and NAA has been observed previously in ex vivo analysis of these tumours with HRMAS (Wilson et al., 2009a). The significantly lower T2 in pilocytic astrocytomas compared with normal brain would be consistent with some of the signal around 2ppm being from a macromolecular component, although it is not sufficiently low for this to explain the entire signal (Tamrazi et al., 2016).

A bias towards overestimated metabolite T2 relaxation times may have been introduced due to exclusion of cases where the signal could not be accurately fitted at the longer echo time. The relatively short range of TE values used may also have led to an overestimation of metabolite T2 values (Brief et al., 2005). Brief et al recommended T2 estimation with a maximum TE of 800 ms; however, acquiring MRS at TE 800 ms would add considerable time to the protocol as the NSA would need to be increased to obtain data of a suitable SNR.

A limitation of this retrospective study is that only two TEs have been used to evaluate T2 relaxation times. The use of multiple TEs will improve the accuracy of T2 estimation by reducing the influence of poorly determined metabolite concentrations. However, in Chapter 4, metabolite and water T2 relaxation times estimated from two TEs and estimated from 18 TEs (maximum TE 290 ms) were comparable in phantom and volunteer data for

NAA, Cho, Cr and water and justifies the dual TE protocol approach. This was not true for coupled metabolites, however, and the T2 relaxation times of coupled metabolites were therefore not estimated in this study. For optimal evaluation of the relaxation times of coupled metabolites appropriate TE values should be determined following evaluation of the J-evolution of metabolite signals as overlap of chemically inequivalent species will have an effect on the apparent T2 of MRS peaks (Xin et al., 2008). However, the optimal TE values vary between metabolites and using additional TEs is prohibitively time consuming for routine tumour evaluation in a clinical environment. If a dual echo time acquisition is to be used, the optimum pair of values is not currently known. A shorter TE than 30 ms was not possible using PRESS due to the RF power requirements of this pulse sequence (Zhu and Barker, 2011). While the increased SNR associated with using a shorter final TE than 135 ms could allow more cases to be assessed, the use of a shorter TE could increase the influence of the baseline on T2 estimation and this would require assessment. Estimation of water T2 values requires a much shorter acquisition due to its high signal intensity and could readily be included as part of the routine protocol.

Whilst the effects of T2 on metabolite determination have been investigated, no attempt has been made to correct for T1 saturation effects. In clinical studies, a TR of 1500-2000 ms is typically used to maximize the signal acquired in an acceptable timeframe, with 1500 ms being commonly used in paediatric single voxel spectroscopy studies at 1.5T (Davies et al., 2008; Panigrahy et al., 2006; Vicente et al., 2013). This relative consistency of acquisition should provide comparability of data between studies. Furthermore, a previous study of relaxation effects in adult brain tumours found no significant differences in the T1 between

metabolites or between tissue types (Sijens and Oudkerk, 2002), implying that metabolite values may be comparable even if a different TR is used.

5.5 Conclusions

T2 relaxation times of water and metabolites vary between tissue types in children. Using a short echo time and correcting for T2 effects with the best values available reduce inaccuracies due to T2 variability. The T2 relaxation time of water had a greater influence on metabolite quantification than the T2 relaxation time of metabolites. Estimation of tissue water T2 is quick due to its high natural abundance and the use of case-specific water T2 values is preferable for correction of relaxation effects.

Further evaluation of the T2 relaxation times is needed using an appropriate set of TEs for coupled metabolites. The T2 relaxation time of tissue water should also be assessed in paediatric brain tumours at other field strengths. T2 values themselves are a measure of molecular environment and provide an additional means of investigating and characterizing tissue.

6. METABOLITE QUANTIFICATION AT 3 T OF PAEDIATRIC BRAIN TUMOURS AND CONGENITAL ADRENAL HYPERPLASIA

6.1 Introduction

Chapter 5 established that the use of appropriate estimates of the T2 relaxation time of water was the most important factor for accurate metabolite quantification at 1.5 T. The mean metabolite concentrations for the cohort were not significantly different when literature, rather than case-specific, relaxation times were used to correct for relaxation effects. On a case by case basis, however, the root mean square percentage difference from the concentration corrected using case-specific water and metabolite T2 relaxation times were significantly smaller when case-specific water relaxation times were used rather than values obtained from the literature.

With magnetic field strengths of 3 T and greater becoming more common in clinical practice there is now an interest in establishing how changes in field strength affect quantification. Previous comparisons of T2 relaxation times in normal brain have shown that the T2 relaxation times of water (Gelman et al., 1999; Wansapura et al., 1999) and metabolites (Barker et al., 2001; Mlynárik et al., 2001) are significantly reduced at 3 T compared with 1.5 T. The correction factor used to correct for relaxation effects is based on the ratio of two exponentials, representing water and metabolite, and shorter relaxation times could have a significant effect.

Variation of T2 relaxation times with field strength and its effect on metabolite quantification in paediatric brain tumours has not been formally assessed. The additional time required to formally estimate metabolite relaxation times can be prohibitive in a clinical setting. The T2 relaxation time of water, however, can be measured in less than a minute by collecting unsuppressed water spectra at multiple echo times. This chapter uses this approach to estimate the T2 relaxation time of water in paediatric brain tumours and in patients with congenital adrenal hyperplasia (CAH).

CAH is an inherited recessive disease which is typically treated with steroids. Treatment with steroids is known to increase water absorption (McKay and Cidlowski, 2003) and this could be reflected by changes in the T2 relaxation time of water. Furthermore, it is not currently known if CAH is associated with changes in T2 relaxation times.

The purpose of this chapter is to introduce a clinical protocol which is designed to quickly obtain the T2 relaxation times of water. This protocol is used to estimate the T2 relaxation time of water at 3 T in normal brain, paediatric brain tumours and in CAH. The effect on metabolite quantification due to variation of metabolite and water T2 relaxation times at 3 T is also assessed.

6.2 Methods and Materials

6.2.1 Paediatric Brain Tumours
Data Acquisition

MRS was acquired using a Phillips Achieva 3 T scanner following conventional imaging. The standard imaging set of T1-weighted, T2-weighted and T1-weighted images post contrast administration was used to delineate the tumour margins. Cubic voxels of side length 1.5 cm

or 2 cm were placed inside the tumour and point-resolved spectroscopy (PRESS) was performed. MRS was acquired at a short echo time using a TR of 2000 ms was used and a TE 38-41 ms. Water suppressed data were acquired with 128 repetitions from the larger voxels and 192 repetitions from the smaller ones. Water unsuppressed MRS data were also acquired with 4 repetitions as a concentration reference.

Age	Sex	Diagnosis	VOI	Treatment
9.36	F	PA	15mm	Pre-Treatment
9.74	M	PA	20mm	Chemotherapy
1.66	M	PA	20mm	Chemotherapy
8.03	F	PA	15mm	Resected
5.82	F	PA	15mm	Resection
1.40	F	OPG	15mm	Chemotherapy
1.40	F	OPG	15mm	Chemotherapy
5.17	F	OPG (NF1)	15mm	Pre-Treatment
4.91	M	OPG	20mm	Resected, Chemotherapy
7.31	F	OPG (NF1)	20mm	Chemotherapy
6.48	M	OPG	15mm	Resected, Chemotherapy, Radiotherapy
12.67	M	DIPG	20mm	Radiotherapy
8.00	M	DIPG	15mm	Radiotherapy
8.14	M	DIPG	15mm	Radiotherapy
0.50	M	DIPG	15mm	Radiotherapy
8.51	M	Medulloblastoma	15mm	Pre-Treatment

Table 6-1: Age, sex, tumour type, voxel size and treatment details of the paediatric brain tumour cohort.

The patient details are presented in Table 6-1. In addition to the short-TE MRS, a multi-TE water sequence was collected. The multi-TE water sequence collected water unsuppressed MRS data from 18 echo times spaced every 15 ms from an initial TE of 42 ms to a final TE of 297 ms. Data were collected using a TR of 2000 ms and one repetition was collected per TE.

Data Processing

Metabolite concentrations were initially quantified with TARQUIN v4.3.8 using the internal basis set 1H brain + Cit, Glth, Gly. The water attenuation parameter, W_{att}, was set to 1 and the water concentration was assumed to be 43300 mM, the same as grey matter.

T2 Estimation

Following the results of Chapter 4, the first five points of the multi-TE water were fitted to a monoexponential decay to minimise the influence of long-T2 components when estimating the T2 relaxation time of water. The T2 relaxation time of water was also estimated by fitting the first (TE = 42 ms) and seventh (TE = 132 ms) points to a monoexponential to compare the effect of fitting using multiple echo times with T2s estimated from short and long-TE

Quantification

The metabolite concentrations were multiplied by the calculated W_{att} to obtain metabolite concentrations corrected for T2 relaxation.

The effect of the T2 relaxation time of water on metabolite quantification at 3 T was estimated by using different values for the T2 relaxation time of water. The T2 relaxation times used were as follows: case-specific T2 relaxation times, estimated from the first 5 points of the multi-TE water; adult glioma values of 145 ms for low grade gliomas and 155 ms for high grade gliomas taken from the literature (Madan et al., 2015a). Due to the similar appearance of paediatric brain tumours and grey matter on T2-weighted imaging, comparison was also made using the T2 of grey matter, 100 ms (Stanisz et al., 2005). Pilocytic astrocytomas (PAs) and optic pathway gliomas (OPGs) were assumed to be low

grade gliomas while anaplastic astrocytomas and diffuse intrinsic pontine gliomas (DIPGs) were assumed to be high grade gliomas.

Metabolite T2 relaxation times were assumed to be similar to adult brain tumours and were set as 256 ms, 285 ms and 168 ms for tNAA, tCho and tCr respectively (Madan et al., 2015a). A T2 of 250 ms was assumed for all other metabolites, with the exception of lipids and macromolecules which were assumed to have a T2 of 60 ms.

The metabolite concentrations estimated using GM and adult glioma T2 relaxation times were compared to the metabolite concentrations estimated using case-specific T2 relaxation times for water. The mean and rms percentage difference of GM and adult glioma-corrected concentrations from concentrations corrected using case-specific values were estimated.

Statistics

The T2 relaxation time of water as estimated using the first 5 points of the multi-TE water and using the first and seventh points, and the mean percentage difference between T2 relaxation correction methods were compared using a Student's t-test. An ANOVA was used to compare the mean values of the T2 relaxation times of each tumour type, and the mean metabolite concentrations for each tumour type. A Student's t-test was used to compare mean values where ANOVA $P < 0.05$.

6.2.2 Congenital Adrenal Hyperplasia
Patients

The CAH study consisted of two cohorts. The first cohort contained 17 females with CAH due to 21-hydroxylase deficiency (mean age 32.7 years). Comparison was made with a second cohort consisting of 17 healthy female controls (mean age 28.6 years).

Data Acquisition

MRS was acquired in both cohorts using a Phillips Achieva 3 T scanner following conventional imaging. The standard imaging set of T1-weighted, T2-weighted and T1-weighted images post contrast administration was used to delineate the tumour margins. Cubic voxels of side length 2 cm were placed in parietal white matter and the temporal lobe. In all cases MRS was acquired using PRESS with TR 2000 ms and collected at short (37-41 ms) and long (135 ms) TE. Water suppressed data were acquired with 128 repetitions from the larger voxels and 192 repetitions from the smaller ones. Water unsuppressed MRS data were also acquired with 4 repetitions as a concentration reference. A multi-TE water scan was also acquired as before.

Data Processing

A T1-weighted image was segmented using FSL to determine the GM, WM and CSF composition of the voxel. Metabolite concentrations were initially quantified with TARQUIN v4.3.8 using the internal basis set 1H brain + Glth, Cit, Gly. The water attenuation parameter, W_{att}, was set to 1 and the water concentration was assumed to be that of pure water, 55556 mM, in accordance with (Gasparovic et al., 2006a)

T2 Estimation

The metabolite signal amplitudes were fitted to a monoexponential decay curve to estimate the T2 relaxation times of metabolites. The T2 relaxation time of water was estimated by fitting the first five TEs of the multi-TE water to a monoexponential. To avoid bias from voxels containing large amounts of CSF, the T2 relaxation time of water was only measured in voxels containing less than 5% CSF as determined by segmentation. The results and discussion that justify this choice are presented in Chapter 4.

Quantification

The reported metabolite concentrations were corrected for relaxation effects following the method detailed by Gasparovic et al (Gasparovic et al., 2006b).

Three combinations of metabolite and water T2 relaxation times were used to assess the influence of relaxation on quantification. The combinations were as follows:

LM, LW: This combination assumed literature values for metabolites (LM) (Träber et al., 2004b) and for GM, WM and a CSF T2 of 1300 ms (LW) (Stanisz et al., 2005).

LM, IW: This combination assumed literature values for metabolites (LM) a value of 1300 ms for CSF. The T2 relaxation times of GM and WM were assumed to be equal and a case-specific water T2 relaxation time, as measured from the multi-TE water, was used (IW).

IM, IW: This combination used the estimated case-specific T2 relaxation times for tNAA, tCho and tCr (IM). A T2 relaxation time of 1300 ms was used for CSF. The T2 relaxation times of GM and WM were assumed to be equal and a case-specific water T2 relaxation time, as measured from the multi-TE water, was used (IW).

Student's t-tests were used to compare T2 relaxation times between tissue types. Statistical

significance was declared for *P* < 0.05.

6.3 Results

6.3.1 T2 Relaxation Times and Metabolite Concentration Correction in Paediatric Brain Tumours

The T2 relaxation time of water was estimated from the multi-TE water in PAs, OPGs, DIPGs

and medulloblastoma (Figure 6-1). An ANOVA determined that the mean T2 relaxation times

were significantly different (*P* = 0.02).
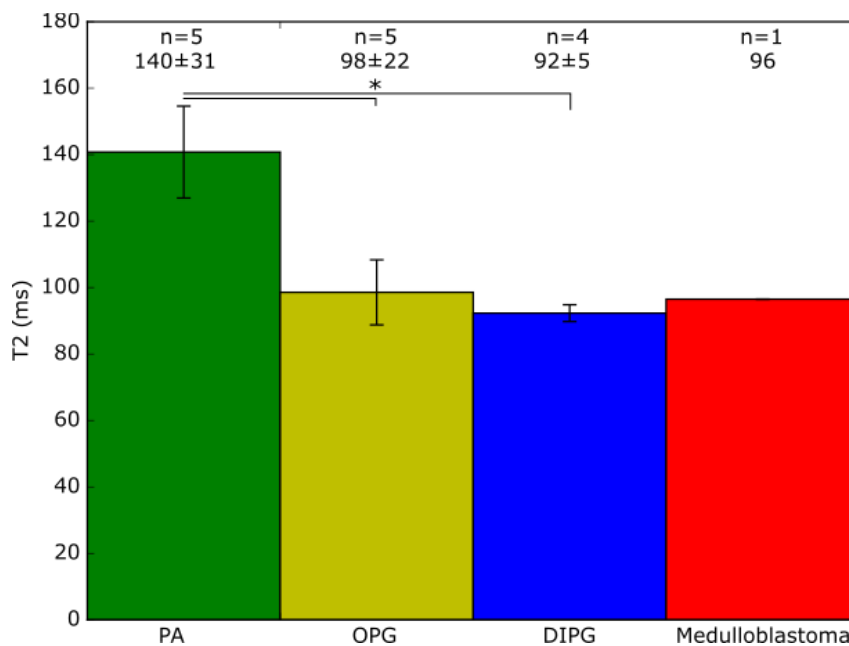
Figure 6-1: Mean water T2 relaxation times ± SEM in pilocytic astrocytomas (PA), optic pathway gliomas (OPG), diffuse intrinsic pontine gliomas (DIPG) and medulloblastoma (MB). * *P* < 0.05

The mean T2 relaxation time of PAs was significantly longer than the mean T2 relaxation

times of OPG and DIPG (Student's t-test, *P* = 0.04 and 0.02 respectively).The mean T2

relaxation time of water in pilocytic astrocytomas was significantly shorter at 3T compared with 1.5T (Student's t-test, $P < 0.01$).

The T2 relaxation times of water as estimated using the first 5 points and as estimated using only the first and seventh points (TEs 42 and 132 ms) were compared. Over the whole patient cohort, there was not a significant difference between the two values (Student's t-test, $P = 0.98$). No significant differences were found for PAs (Student's t-test, $P = 0.88$), OPGs (Student's t-test, $P = 0.95$) or DIPGs (Student's t-test, $P = 0.96$). Though some cases exhibited multi-exponential behaviour, there was not a significant difference between the T2 relaxation times estimated using the first 5 points and estimated using only the first and seventh points for these cases.

The metabolite concentrations of the gliomas in the cohort were corrected using case-specific water T2 relaxation times. These concentrations were compared to concentrations which had been corrected using the T2 relaxation time of water in grey matter and corrected using the T2 relaxation time of low and high grade adult gliomas. The mean percentage difference and the root mean square (rms) percentage differences are given in Table 6-2.

	GM	Adult Glioma T2s
Mean Percentage Difference	-0.9%	10.7%
Rms Percentage Difference	8.6%	13.7%

Table 6-2: Mean percentage difference and rms percentage difference of concentrations corrected using grey matter water and adult glioma T2 relaxation times when compared to concentrations corrected using case-specific T2 relaxation times.

The percentage difference from the concentrations corrected using case-specific T2 relaxation times was significantly smaller when the water T2 relaxation time was assumed to be that of GM rather than that of adult gliomas (Student's t-test, $P = 10^{-13}$). There was not,

however, a difference in the mean concentrations when case-specific water T2 relaxation times were used compared with concentrations corrected assuming GM T2 relaxation times for the water T2 (Student's t-test, P = 0.93) or adult glioma T2 relaxation times for the water T2 (Student's t-test, P = 0.24).

The mean percentage difference and rms percentage differences of metabolite concentrations corrected for T2 relaxation effects using adult glioma water T2 relaxation times compared with metabolite concentrations corrected using case-specific water relaxation times are show in Table 6-3 for 1.5 and 3 T.

	1.5 T	3 T
Mean Percentage Difference	0.0%	10.7%
Rms Percentage Difference	2.9%	13.7%

Table 6-3: Mean percentage difference and rms percentage difference at 1.5 (from Chapter 5) and 3T of concentrations corrected using adult glioma T2 relaxation times from concentrations corrected using case-specific T2 relaxation times for water and literature values for metabolites.

The percentage difference was significantly smaller at 1.5 T than at 3 T (Student's t-test, P = 10^{-15}).

Mean metabolite concentrations for PAs, OPGs and DIPGs corrected using case-specific T2 relaxation times are presented in Table 6-4.

	PA			OPG			DIPG			MB
	Mean		SD	Mean		SD	Mean		SD	Conc.
NAA	2.47	±	1.81	2.61	±	1.63	2.33	±	1.54	1.94
Cho	2.79	±	0.86	2.95	±	0.94	2.63	±	0.25	3.84
Cr	4.73	±	2.39	5.06	±	2.08	4.74	±	1.82	5.03
Glu	4.06	±	2.88	4.16	±	1.88	5.16	±	2.58	2.09
Gln	2.01	±	1.88	1.64	±	1.63	4.55	±	1.86	4.73
ml	5.63	±	6.29	3.77	±	2.59	4.90	±	4.55	3.21
Lac*	0.55	±	0.74	0.48	±	0.34	2.60	±	0.79	0.91
Tau	1.19	±	2.37	0.14	±	0.28	0.79	±	0.96	1.85
Ala	0.17	±	0.10	0.18	±	0.21	0.77	±	0.82	1.17
Asp**	1.11	±	2.16	4.98	±	1.58	8.83	±	1.96	14.49
Cit	0.53	±	0.29	0.75	±	0.50	0.93	±	0.64	0.92
GABA	0.24	±	0.33	1.51	±	2.43	2.49	±	1.73	0.00
Glc	1.75	±	1.49	2.46	±	2.36	1.48	±	1.41	3.82
Glth	0.80	±	0.72	0.91	±	0.41	0.51	±	0.51	0.91
Gly	1.84	±	2.24	1.92	±	1.04	1.88	±	0.68	10.08
Scy	0.29	±	0.53	0.07	±	0.09	0.02	±	0.04	0.00
TLM09	6.01	±	3.56	5.08	±	3.89	4.45	±	1.88	7.10
TLM13	13.42	±	6.83	12.76	±	5.14	19.62	±	8.35	21.17
TLM20	13.20	±	3.31	10.06	±	5.36	11.09	±	3.33	8.54

Table 6-4: Mean ± standard deviation (SD) metabolite concentrations for pilocytic astrocytomas (PAs, n=5), optic pathway gliomas (OPGs, n=5) and diffuse intrinsic pontine gliomas (DIPGs, n=4) and medulloblastoma (MB, n=1). Metabolite concentrations have been corrected using case-specific T2 relaxation times for water and adult glioma T2 relaxation times for tNAA, tCho and tCr. Lipids and macromolecules were assumed to have a metabolite T2 of 60 ms whilst 250 ms was assumed for all other metabolites. * ANOVA $P < 0.01$, ** $P < 0.001$.

Lac was significantly higher in DIPGs compared with OPGs (Student's t-test, $P < 0.01$) and PAs (Student's t-test, $P < 0.01$). Similarly, Asp was significantly higher in DIPGs compared with OPGs (Student's t-test, $P = 0.02$) and PAs (Student's t-test, $P < 0.01$), whilst Asp was also higher in OPGs compared with PAs (Student's t-test, $P = 0.02$).

6.3.2 T2 Relaxation Times and Metabolite Concentration Correction in CAH
T2 Relaxation Times

T2 relaxation times were estimated for the temporal lobe and parietal white matter in

patients with CAH and healthy controls. The T2 relaxation times are shown in Figure 6-2.
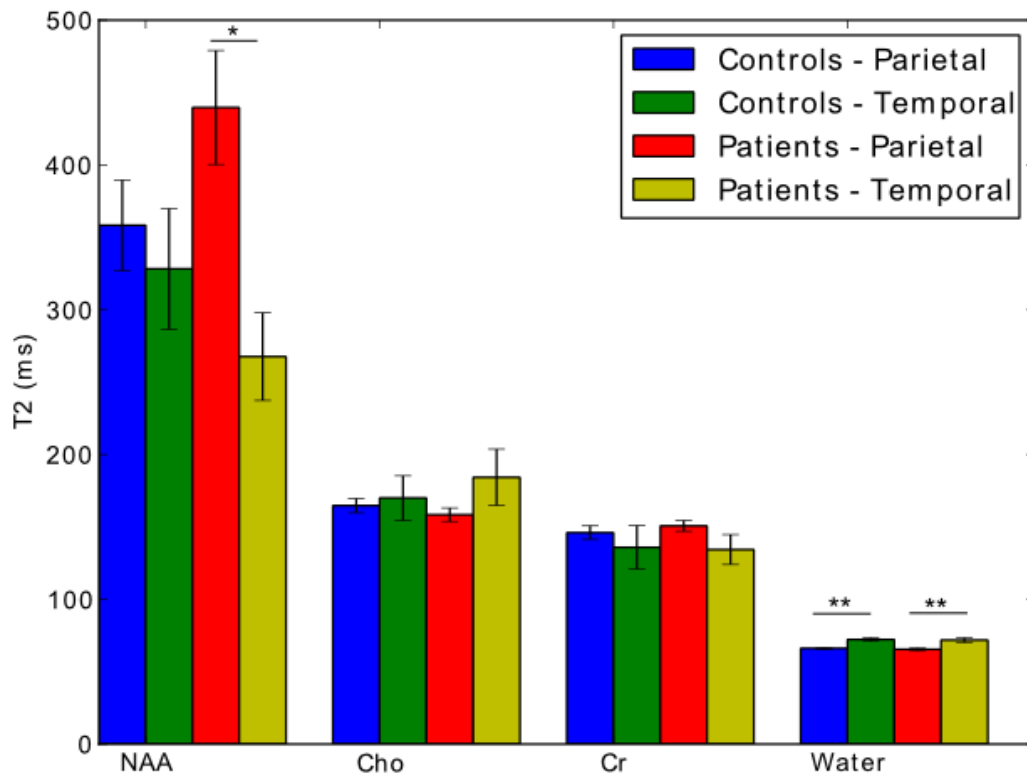
Figure 6-2: Mean T2 relaxation times ± SEM for NAA, Cho, Cr and tissue water from voxels
placed in parietal white matter and the temporal lobe in healthy controls and patients with
CAH. * $P < 0.05$, ** $P < 0.01$.

The T2 of NAA was significantly longer in CAH parietal white matter compared with CAH

temporal lobe (Student's t-test, t = 2.65, P = 0.02). The T2 of tissue water in the parietal

white matter of controls was significantly shorter compared with the T2 in the temporal lobe

of controls (t = 4.91, P = 0.0001) and CAH patients (t = 3.79, P = 0.002). The T2 of tissue

water was significantly longer in the temporal region than in parietal white matter of CAH

patients (t = 3.64, P = 0.005).

Metabolite Concentrations Corrected for Relaxation Effects

The metabolite and water T2 relaxation times were used to correct for relaxation effects and are shown in Figure 6-3.
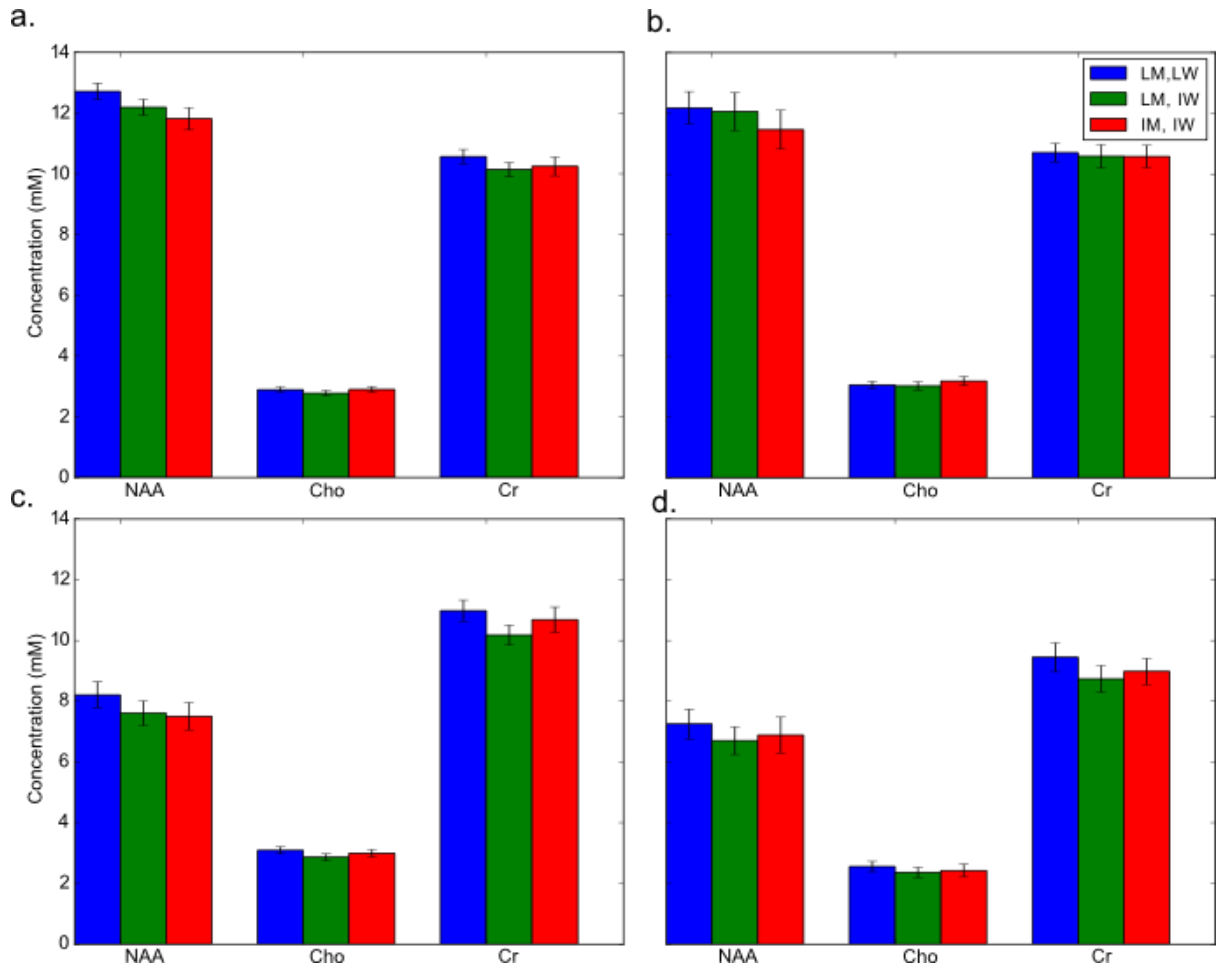
Figure 6-3: Mean metabolite concentrations ±SEM for a) healthy parietal, b) CAH parietal, c) healthy temporal, d) CAH temporal. Metabolite concentrations were corrected for relaxation effects using various combinations of T2 relaxation times: literature T2 values for metabolites and CSF and a case-specific measured T2 for grey and white matter which were assumed to be equal (LM, IW); and case-specific measured T2 relaxation times for metabolites and water with grey matter and white matter assumed to have equal T2 relaxation times (IM, IW).

There were no significant changes in metabolite concentration when case-specific T2 relaxation times were used to correct for relaxation effects. Table 6-5 shows the percentage difference from metabolite concentrations corrected for using literature values, assumed to

be the gold standard, for metabolite concentrations corrected for using case-specific T2

relaxation times. Table 6-6 shows the rms percentage difference.

PD	Default	LM, LW	LM, IW	AM, AW	AM, IW
Controls	-9.46	2.41	-0.19	-0.81	-0.87
Patients	-9.78	1.41	0.48	-0.20	-0.67

Table 6-5: Percentage Difference from IM, IW in congenital adrenal hyperplasia and healthy controls. Key: IM: Individual Metabolite T2, IW: Individual Water T2, LM: Literature MetaboliteT2, LW: Literature Water T2, AM: cohort Average Metabolite T2, AW: cohort Average Water T2.

RMS	Default	LM, LW	LM, IW	AM, AW	AM, IW
Controls	11.77	5.09	4.51	3.72	3.72
Patients	12.09	5.77	4.57	4.66	3.34

Table 6-6: RMS Percentage Difference from IM, IW in congenital adrenal hyperplasia and healthy controls. Key: IM: Individual Metabolite T2, IW: Individual Water T2, LM: Literature MetaboliteT2, LW: Literature Water T2, AM: cohort Average Metabolite T2, AW: cohort Average Water T2.

6.4 Discussion

In this study, multi-TE water data has been used to estimate the T2 relaxation times of water

in pathology and the effect of changes in the T2 relaxation on quantification has been

assessed at 3 T.

The T2 relaxation time of PA, none of which were found in the optic pathway, was

significantly longer than those of both OPG and DIPG. The T2 relaxation times of optic

pathway glioma, diffuse intrinsic pontine glioma and medulloblastoma were similar to that

of grey matter at 3T. These findings are consistent with T2-weighted imaging, where OPGs,

DIPGs and medulloblastoma tend to have a similar appearance to grey matter. Conversely,

PAs, which are often cystic, are typically associated with areas of high intensities on T2-

weighted images.

Consistent with reports in normal brain (Gelman et al., 1999; Wansapura et al., 1999), the T2 relaxation time of water was significantly shorter in paediatric gliomas at 3 T compared with 1.5 T. There is little published data about the T2 relaxation time of water in paediatric brain tumours and a formal comparison of T2 relaxation time changes with field strength has not been performed in adult tumour populations. However, published relaxation times at 1.5 (Isobe et al., 2002) and 3 T (Madan et al., 2015a) in adults indicate that this may be true in adults too. The T2 relaxation times for OPGs and DIPGs estimated in this study are not consistent with the higher T2 values seen in adult cohorts.

T2 relaxation times were estimated from the first five points of the multi-TE water to minimise the potential influence of long-T2 components, for example from CSF or cystic components, on the water signal (consult Chapter 4 for further details). T2 relaxation times were also estimated from the first and seventh points, TEs 42 and 132 ms respectively. Whilst a slight difference in T2 relaxation times estimated by the two methods was noted for cases where the water signal decay was not monoexponential, the difference was small and the difference between the two methods was not significant. This finding adds further weight to the use of two TEs for estimating T2 relaxation times, as was used in the paediatric brain tumour study at 1.5 T detailed in chapter 5. Whilst it is not necessary to collect more than two echo times to estimate the T2 relaxation time of water, the additional echo times allow an assessment of whether the relaxation of water is mono- or multi-exponential. In the cases in this study where the decay was not mono-exponential, the T2-weighted imaging indicated that multiple components were present in the voxel. Collecting multiple echo times could therefore provide information about the voxel composition, in particular the amount of CSF present (Kreis et al., 1993), without a significant additional time penalty.

The effect of T2 relaxation time differences on metabolite quantification in paediatric brain tumours was investigated by correcting for relaxation effects using different T2 relaxation times. The rms percentage difference, from concentrations corrected using case-specific T2 values, was largest when adult glioma T2 values were used compared with the use of GM T2s. This is consistent with most paediatric brain tumours appearing similar to GM on T2-weighted imaging. Though differences were observed on a case-by-case basis, there was not a significant difference in the mean concentrations estimated for either the whole patient cohort or for individual tumour types. This effect could be due to the small sample sizes available for individual tumour types. The mean and rms percentage differences were larger at 3 T compared with 1.5 T. This is likely due to the shorter relaxation times at 3 T and suggests that if quantified MRS is to be used for clinical decision making, then case-specific T2 relaxation times should be used.

T2 relaxation times of water and metabolites were also estimated in congenital adrenal hyperplasia. It was hypothesised that the treatment patients with CAH with steroids could lead to changes in the T2 relaxation time of water, however there was only a trend towards changes in water T2 relaxation times in this study. The only T2 relaxation time differences observed were between the T2 relaxation times of water in the parietal and mesial temporal lobe. These differences reflect the differing amounts of grey and white matter found in these locations.

Quantification of MRS data was using various combinations of T2 relaxation times was assessed. There was not a significant difference in the mean metabolite concentrations estimated when case-specific relaxation times were used compared with the use of

literature values. Furthermore, the mean and rms percentage differences were small. This indicates that it is not necessary to correct for relaxation effects using case-specific values unless there is compelling evidence that there are significant changes in T2 relaxation times.

There are a number of limitations to this study. The water contents and relaxation times of normal brain are well studied, meaning accurate quantification of normal brain MRS presents a straightforward task if the amounts of GM, WM and CSF are known. Accurate quantification of brain tumours, however, presents a more difficult problem. MRS investigations of paediatric brain tumours often use the concentration of water in GM as a concentration reference, however the water concentration of paediatric brain tumours is not well known. Furthermore, while segmentation of normal brain is a relatively simple task, segmentation of paediatric brain tumours is complicated by the microcystic nature of some tumour types and varying appearance of tumours on T2 imaging. Whilst accurate quantification of tumour MRS would account for changes in water content, as well as T2 relaxation, an investigation of water content is beyond the scope of this work. Similarly, an analysis of the metabolite T2 relaxation times and of T1 relaxation in brain tumours would add significant time to the scanning session which is not feasible in a paediatric clinical setting.

The paediatric brain tumour cohort investigated is also not ideal. The heterogeneous cohort used consists of patients undergoing various treatments and it is not known what effect treatment will have on T2 relaxation times. The statistical power of this study is also limited by the small numbers of each tumour type available.

6.5 Conclusions

A quick, one-minute sequence has been introduced which can measure the T2 relaxation time of water with a scan time of less than a minute. The tissue water T2 relaxation times of paediatric brain tumours are shorter at 3 T than at 1.5 T. The RMS percentage differences were larger at 3 T when compared with 1.5 T. Case-specific water T2 relaxation times are therefore recommended if metabolite concentrations are to be used for clinical decision making. However, for analysis of cohorts, appropriate literature T2 relaxation times can be used. The water and metabolite T2 relaxation times were not significantly changed in congenital adrenal hyperplasia when compared with healthy controls. The use of case-specific water or metabolite T2 relaxation times did not significantly change metabolite quantifications in CAH or normal brain. In normal brain and CAH there was a RMS percentage difference of approximately 5% when concentrations corrected using case-specific values were compared with concentrations corrected using literature values. Future work should investigate potential changes in the metabolite T2 relaxation times of paediatric brain tumours at 3 T and what affect this might have on the accuracy of metabolite quantification.

7. JPRESS

7.1 Introduction

Short and long echo time spectroscopy, as conventionally used in MRS investigations, provides a convenient vehicle for visually identifying changes in the metabolites NAA, Cho, Cr and Lac compared with normal brain. With prominent singlets without substantial spectral overlap, tNAA, tCho and tCr can be readily identified at all echo times whilst the inverted Lac doublet at long TE allows unambiguous identification. However, unambiguous assignment of a number of coupled metabolites presents a challenging task due to crowded spectra.

MRS is often analysed by fitting the whole spectrum to a range of metabolites using prior knowledge. In large cohorts of paediatric tumours, a number of other metabolites, such as Glu (Davies et al., 2008a), Gln (Wilson et al., 2013), Gly (Davies et al., 2010a, 2008a), mI (Harris et al., 2008a; Panigrahy et al., 2006; Peet et al., 2007), Tau (Davies et al., 2008a; Kovanlikaya et al., 2005; Panigrahy et al., 2006), have emerged as being important in paediatric brain tumours, a finding confirmed by ex vivo analysis (Wilson et al., 2009b). However whilst visual inspection alone can identify changes in tNAA, tCho and tCr, visual identification of Glu, Gln, Gly, mI, Tau is more difficult. These metabolites are typically present in smaller concentrations or are coupled metabolites that are difficult to identify due to the crowded regions they occupy in the spectrum (Govindaraju et al., 2000).

Various methods have been proposed for identification of these metabolites; however there are limited options available that have the potential to identify all metabolites. optimised PRESS sequences for Gly (Choi et al., 2011a) and Glu (Schubert et al., 2004b), spectral editing for Gly (Choi et al., 2008) and mI (Choi et al., 2005; Kim et al., 2004), TE-averaging for Gly

(Prescot et al., 2006) and Glu (Hurd et al., 2004), CT-PRESS for Glu (Mayer and Spielman, 2005) and difference spectroscopy for Glu, Gln and mI (Snyder et al., 2010). These methods have limitations, however, with spectral editing providing limited information about other metabolites, optimised sequences resulting in significant signal loss and TE-averaging sacrificing the information available from J-evolution.

Another option, commonly used in vitro, is J-resolved spectroscopy, a two dimensional spectroscopy technique which is called JPRESS when used in vivo (Ryner et al., 1995; Thomas et al., 2003, 1996). JPRESS is acquired by collecting PRESS spectra at multiple echo times, retaining the chemical shift information typical of conventional one dimensional spectroscopy in F1, the x-dimension, and indirectly encoding the scalar coupling information for each metabolite in F2, the y-dimension. This spreads coupled metabolites into two dimensions, allowing identification of metabolites using the known chemical shift and scalar coupling constants for each metabolite based on their position in the spectrum (Govindaraju et al., 2000).

A number of limitations have hindered the adoption of JPRESS in a clinical setting. JPRESS is associated with long acquisition times, with literature studies often over 20 minutes long (Nagarajan et al., 2010; Soeiro-de-Souza et al., 2015; Thomas et al., 2003). A long scan duration is not typically feasible in routine clinical practice where advanced MR techniques typically follow the standard clinical MRI investigation. Of the reported literature studies with an acquisition time less than 20 minutes (Furuyama et al., 2012; Lin et al., 2014; Sarma et al., 2014; Weaver et al., 2015), two studies utilise compressed sensing (Furuyama et al., 2012; Sarma et al., 2014) to collect data in 12 minutes, while another requires a large voxel

size of size 4 x 4 x 4 cm which is impractical in a paediatric brain tumour cohort to collect

data in 9.6 minutes (Weaver et al., 2015). The shortest reported acquisition time is 8

minutes and 32 seconds which was reported by Lin et al, however children with paediatric

brain tumours do not tolerate long scan times well and a further reduction in acquisition

time would be welcome in this cohort.

Visualisation of the data requires postprocessing techniques which are not commercially

available on clinical scanners, limiting its utility to radiologists. Quantification of the data also

presents a problem. Whilst robust fitting routines are available for 1D spectroscopy, the

options available for JPRESS are limited and are tailored to specific acquisition protocols

(Fuchs et al., 2014; Schulte and Boesiger, 2006). Peak area integration presents an imprecise

method for determining metabolite concentrations. A final option available for

quantification of JPRESS data is to extract the spectroscopy data from each echo time and

analyse using conventional 1D fitting packages.

In this chapter, an acquisition protocol and processing pipeline is developed and optimised

for use in paediatric brain tumours on a clinical 3T scanner. As children do not tolerate long

imaging sessions well, the acquisition protocol was optimised to collect clinically useful data

within 6 minutes. Use of the protocol is then demonstrated in four paediatric brain tumours.

7.2 Methods

7.2.1 Protocol Development and Optimisation

7.2.1.1 Protocol Development
A braino phantom containing 12.5 mM N-acetylaspartate, 12.5 mM glutamate, 10 mM

creatine, 7.5 mM myo-Inositol, 5 mM lactate, 3 mM choline was scanned. 1 g of sodium

azide was added to each phantom as a biocide to prevent the growth of bacterial organisms.

1 mL/L of gadolinium was added to each phantom as a relaxation agent to shorten the T1

relaxation time. The pH of all phantoms was adjusted to 7.2 in line with healthy tissue.

Details of the protocol are presented in Table 7-1.

	TR (ms)	Starting TE	NSA/TE	TE spacing	#TEs
Volunteer 1	2000	36	16	10	16
Volunteer 2	2000	36	8	10	32
Volunteer 3	2000	36	16	10	64
Volunteer 4	2000	36	8	15	30
Braino Phantom	2000	36	8	5	128

Table 7-1: Acquisition protocols in phantom and volunteer for JPRESS protocol and processing development.

Informed consent was obtained from 3 healthy adults (2 males and 1 female) with a mean

age of 25 ± 2 years. A 30x30x30mm voxel was placed in occipitoparietal grey matter and

scans were performed. All scans were performed with TR = 2000 ms and starting echo time

TE_1 = 36ms with NSA = 8 or 16 whilst equal-spacing of either 10 or 15 ms was used to collect

16, 30, 32 or 64 free induction decays. Full details of the protocols used on volunteers are

listed in Table 7-1.

7.2.1.2 Postprocessing Development
The raw data for each experiment was transferred to a personal computer and processed

using code written in-house in Python. The water component of the free induction decays

was removed using Hankel singular value decomposition and the baseline was corrected for

any displacement to reduce interference. Baseline displacement correction is performed by

taking the average value of a region of the spectrum containing only noise and no signal and

subsequently subtracting this value from the spectrum.

Estimates of the water peak position in the water suppressed spectra, ref, were collected

from the TARQUIN analysis and were used to correct for frequency drift effects by

multiplying each point, k, of the FID by $\exp(-2\pi i \times ref \times k \times (128/2000))$.

To optimise the visualised spectrum, the combined TARQUIN fits for the tNAA, tCho and tCr

singlets at the final echo time were duplicated and converted into FIDs to simulate additional

echo times up to a final TE of 500 ms. A penalty of 0.9 was applied to each successive echo

time to simulate T2 relaxation effects. The data was then apodised in both dimensions using

a squared sine bell filter and Fourier transformed in two dimensions.

7.2.2 JPRESS of Paediatric Brain Tumours

7.2.2.1 MRS Acquisition

Four patients with paediatric brain tumours were investigated Table 7-2. Informed parental

consent was acquired and JPRESS investigation followed conventional imaging.

Age (years)	Sex	Tumour Type
9.8	Male	Medulloblastoma
10.6	Male	Diffuse Intrinsic Pontine Glioma (DIPG)
8.2	Male	Pilocytic Astrocytoma
6.5	Female	Optic Pathway Glioma

Table 7-2: Patient details of paediatric brain tumour patients studied with JPRESS.

JPRESS was collected from cubic voxels of size 30 x 30 x 30 mm for all cases using the final

optimised protocol and processing steps. A repetition time of 2000 ms was used with a

starting TE of 42 ms and 15 ms spacing between echo times. 8 averages were acquired per

echo time for a total acquisition time of 6 minutes. The starting TE of 42 ms was chosen as

this was the minimum echo time that that could be achieved with all possible voxel orientations.

PRESS with an echo time of 35 ms, TR of 2000 ms and 128 averages was also collected from the medulloblastoma and DIPG cases.

7.2.2.2 Metabolite Quantification

Metabolite concentrations were calculated by extracting the 1D FIDs associated with each echo time and writing them into a DICOM file using Python code developed in house. The DICOM files were processed with TARQUIN using the brain + Glth basis set for healthy volunteers and the brain + Glth, Gly, Cit basis set for brain tumour patients.

T2 relaxation times were estimated for water and metabolites and metabolite concentrations were corrected for relaxation effects. The reported concentration is the mean of all estimated corrected concentrations from TEs 35-140 ms for that metabolite. A full description of metabolite quantification and correction for relaxation effects is provided in Chapter 2.

7.2.2.3 JPRESS Visualisation

To visualise the data the 2D Fourier transformed matrix was displayed as a contour plot in magnitude mode. Lower and upper bounds were used to ensure that the spectra remained free of noise. Spectral quality was determined through visual inspection of the display for artifacts. The thresholds of the display were further optimised to ensure that all desired peaks were present and fully resolved.

The protocol and processing pipeline is shown in Figure 7-1.
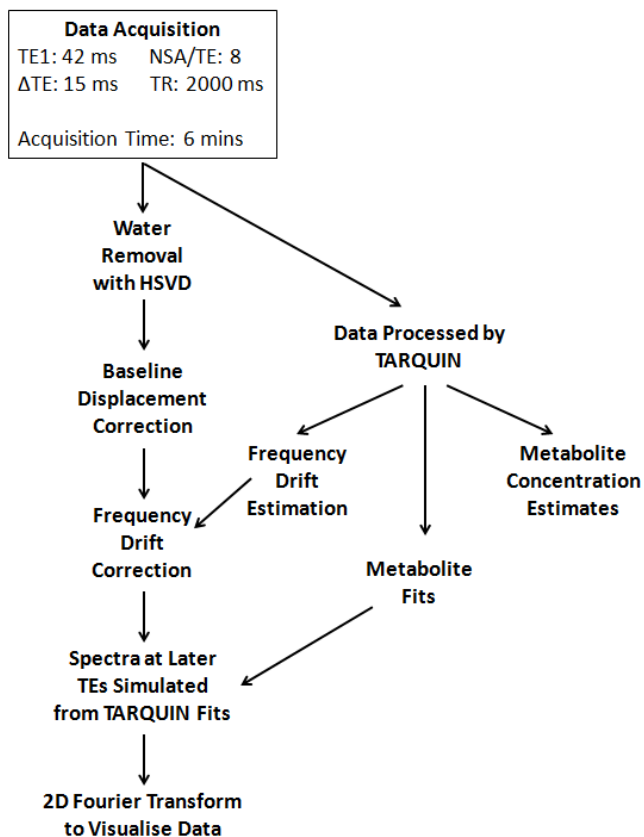
Figure 7-1: Optimised acquisition protocol and processing pipeline for JPRESS.

7.3 Results

7.3.1 Protocol Optimisation

Acquisition parameters were varied to optimise the protocol. The effect of changing the

spacing between successive echo times is shown in Figure 7-1. How changing the number of

echo times collected is shown in Figure 7-2. Figure 7-3 shows how the choice of final echo

time affects the resolution of the spectrum.

Changing the increments between successive echo times had no effect on the quality of the

spectrum (Figure 7-1). Changing the echo time spacing only has the effect of changing the

spectral width of F1. The relationship between echo time spacing and spectral width is given by spectral width = 1 /(TE spacing). All metabolites present in the braino phantom and visible in volunteer spectra were within a range of ± 30 Hz, which corresponds to an echo time spacing of 15 ms.
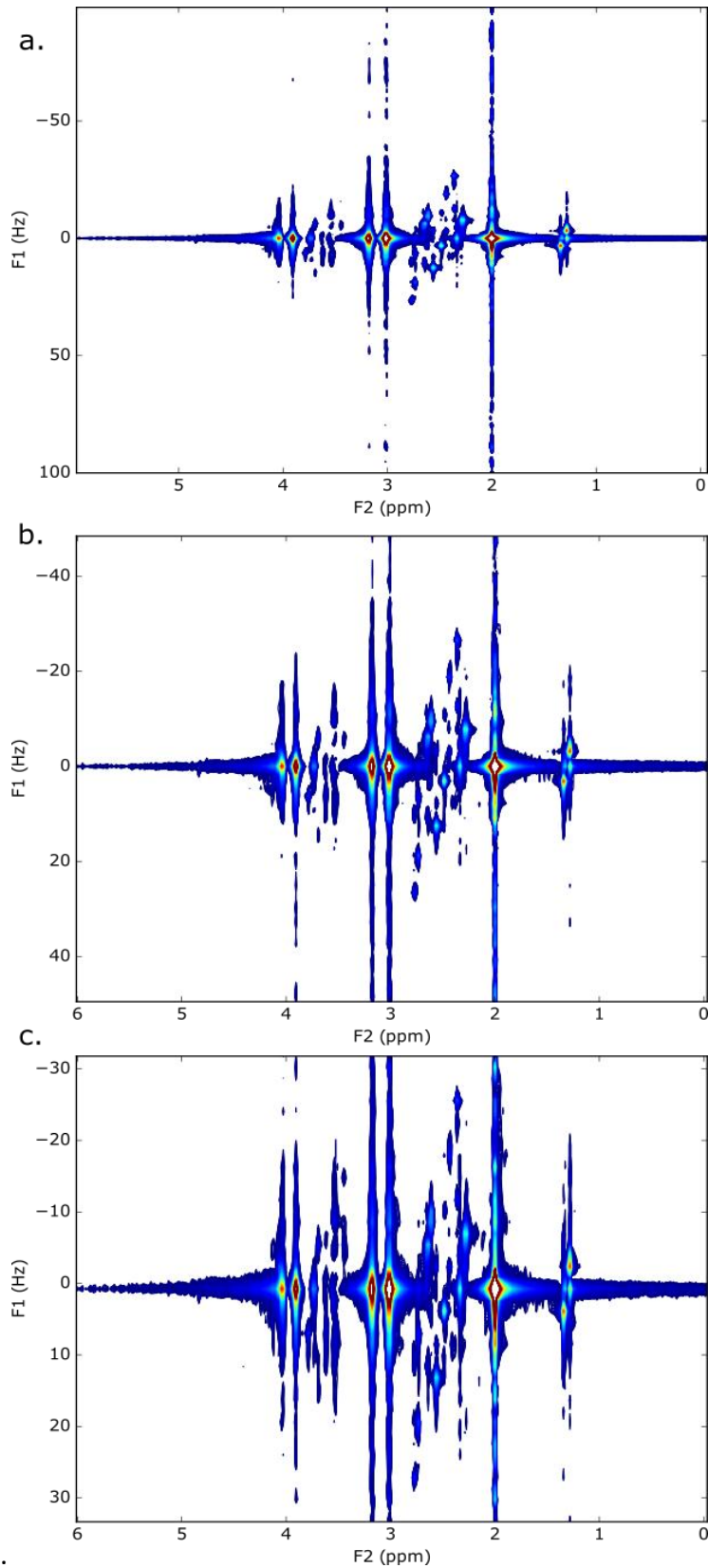
Figure 7-2:JPRESS spectrum of braino phantom with a) Echo time spacing of 5 ms. b) Echo time spacing of 10 ms. c) Echo time spacing of 15 ms.

The effect of collecting a larger number of echo times was assessed in Figure 7-2. Visual inspection shows that the two spectra are comparable. The final echo time sampled, rather than the number of echo times collected, appears to have a greater effect on visualisation of the 2D data (Figure 7-3). When the final echo time is not long enough, the coupled metabolites have not completely modulated or completely decayed and the spatial resolution is poor.
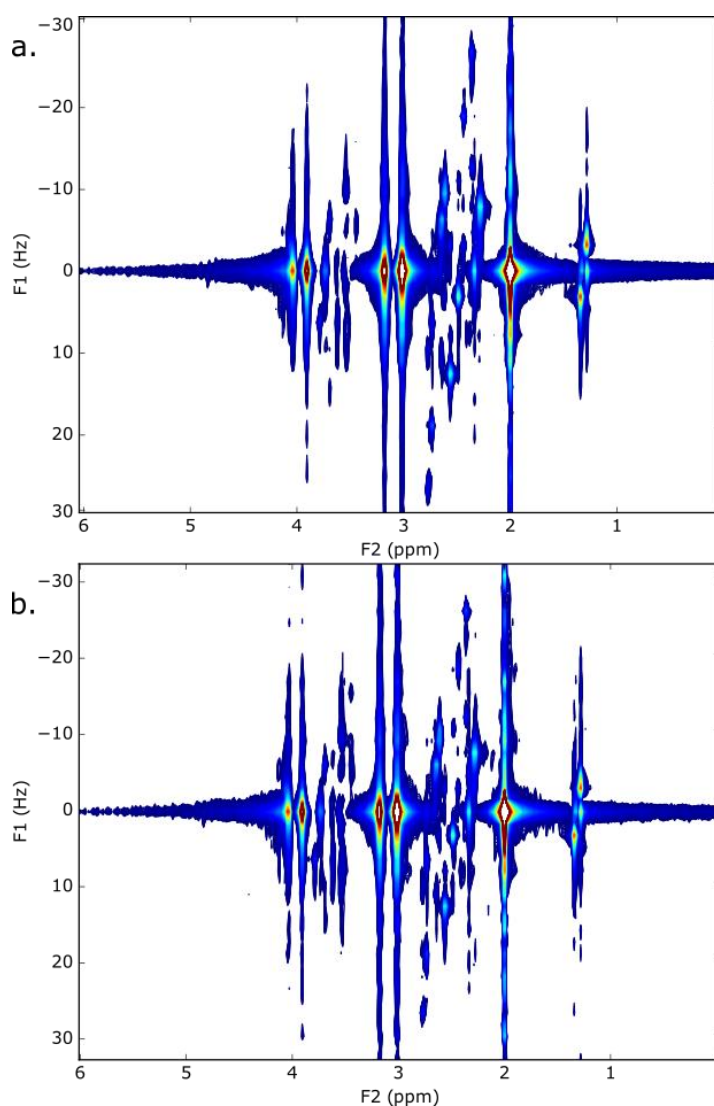
Figure 7-3: JPRESS spectrum of braino phantom with a) 55 TEs collected with a spacing of 5 ms between echo times and b) 19 TEs collected with a spacing of 5 ms between echo times. Both spectra had a final TE of 315 ms. a) Has been magnified to show the same spectral range as b).
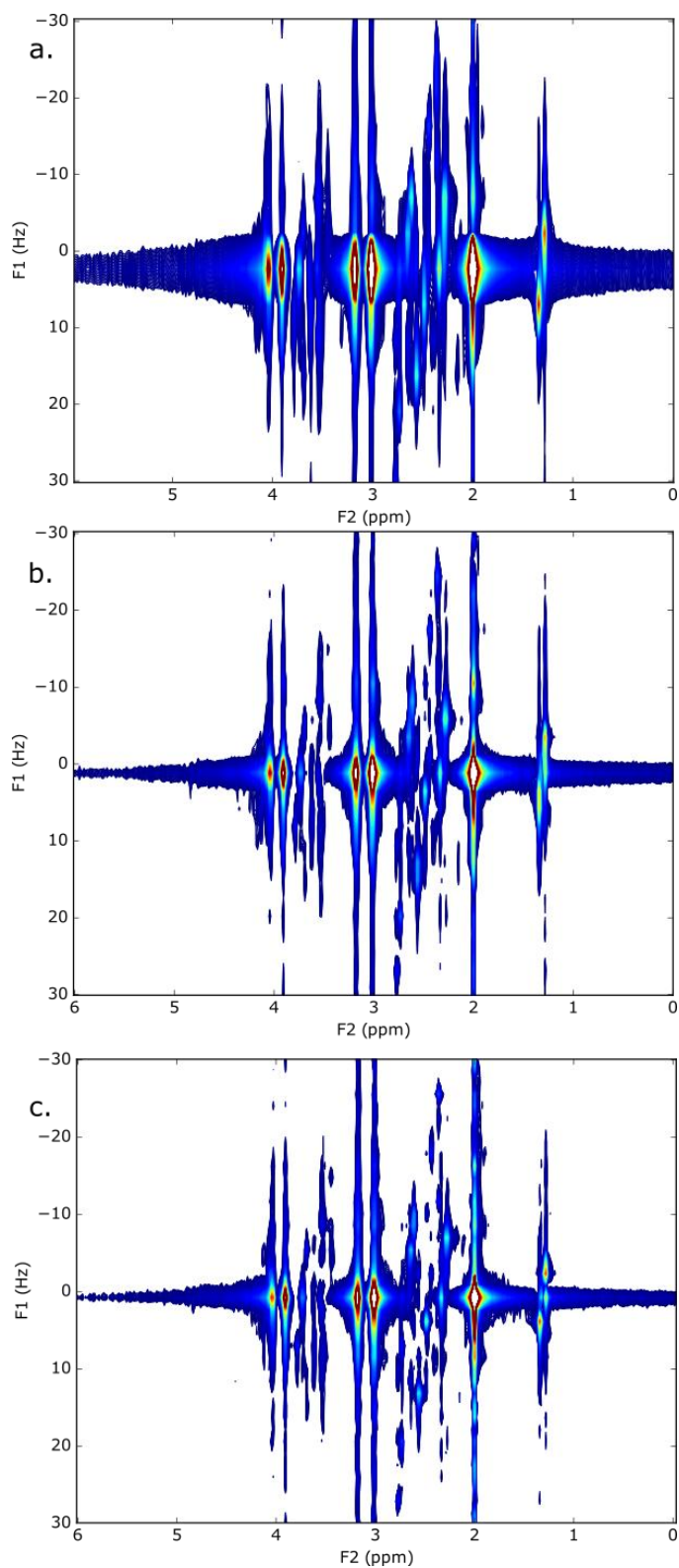
Figure 7-4: JPRESS spectra with a) 43 TEs collected with a spacing of 5 ms between echo times, final TE = 246 ms; b) 43 TEs collected with a spacing of 10 ms between echo times, final TE = 456 ms and c) 43 TEs collected with a spacing of 15 ms between echo times, final TE =666 ms. a) and b) have been magnified to show the same spectral range as c).

7.3.2 Processing Optimisation
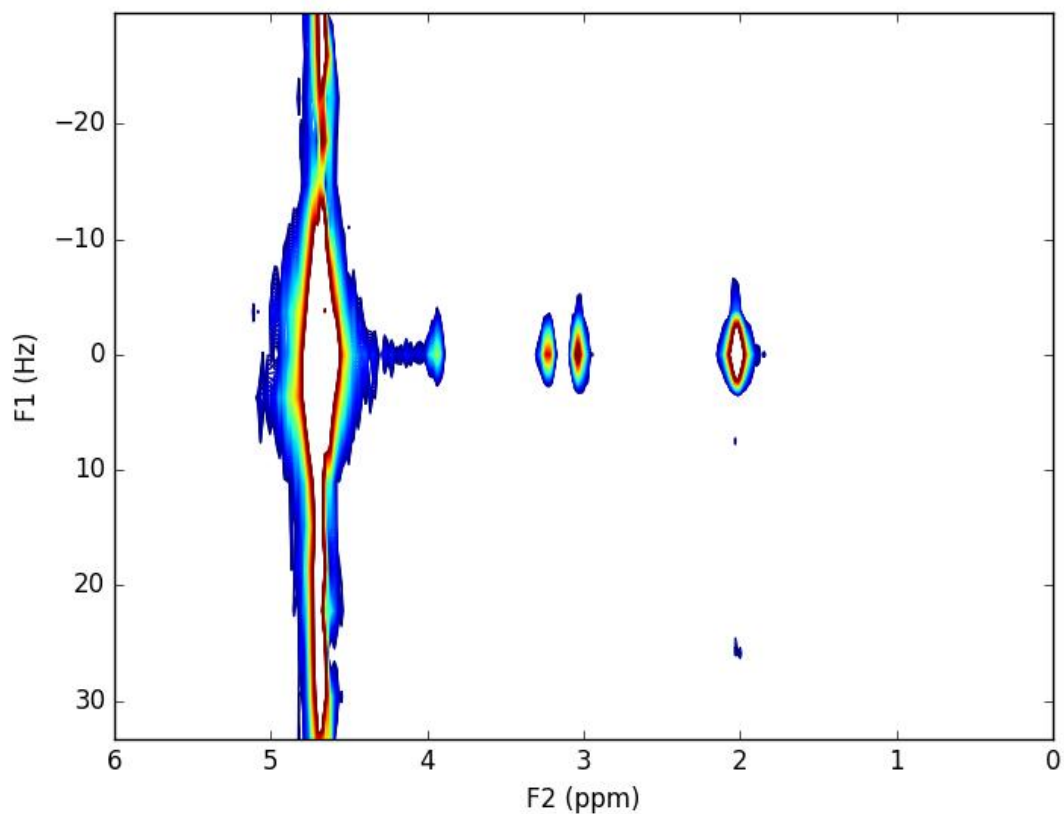
Figure 7-5: An example braino phantom JPRESS spectrum with the residual water signal still present.

The intensity of the residual water signal greatly outweighed the intensity of coupled metabolite peaks (Figure 7-5). The relative intensity differences meant that a number of the resonance peaks of Glu and mI were effectively reduced into the noise of the 2D contour plots and could not be identified.   Removal of the residual water using the HSVD algorithm enabled detection of lower intensity resonances from coupled metabolites to be identified.
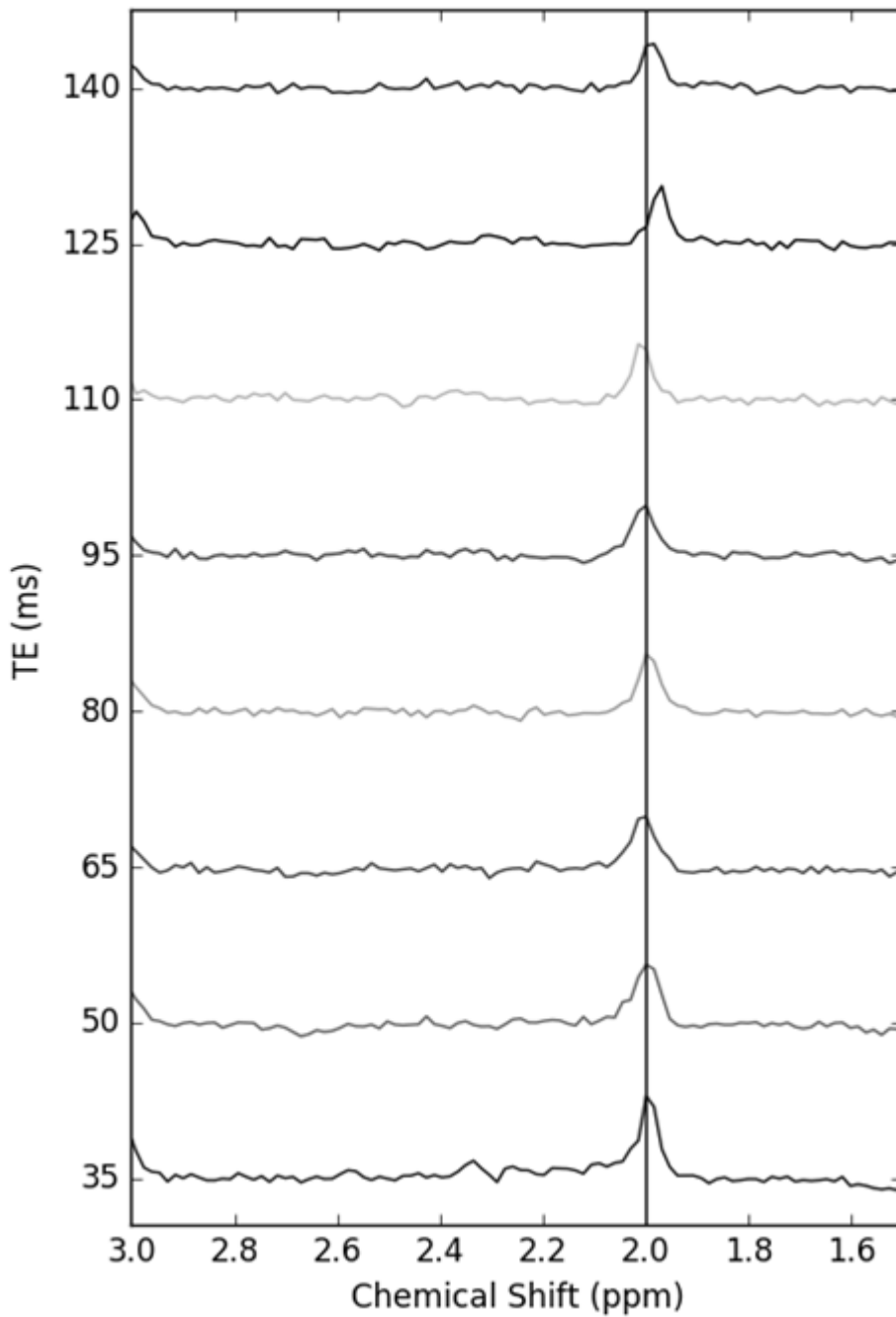
Figure 7-6: Stack plot of NAA peak position at various echo times in a healthy volunteer.

Figure 7-6 shows the position of the NAA at various echo times. The position of the peak altered due to frequency drift. This led to truncation artifacts above the tNAA, tCho and tCr singlets and wider peak intensities on the 2D plot.
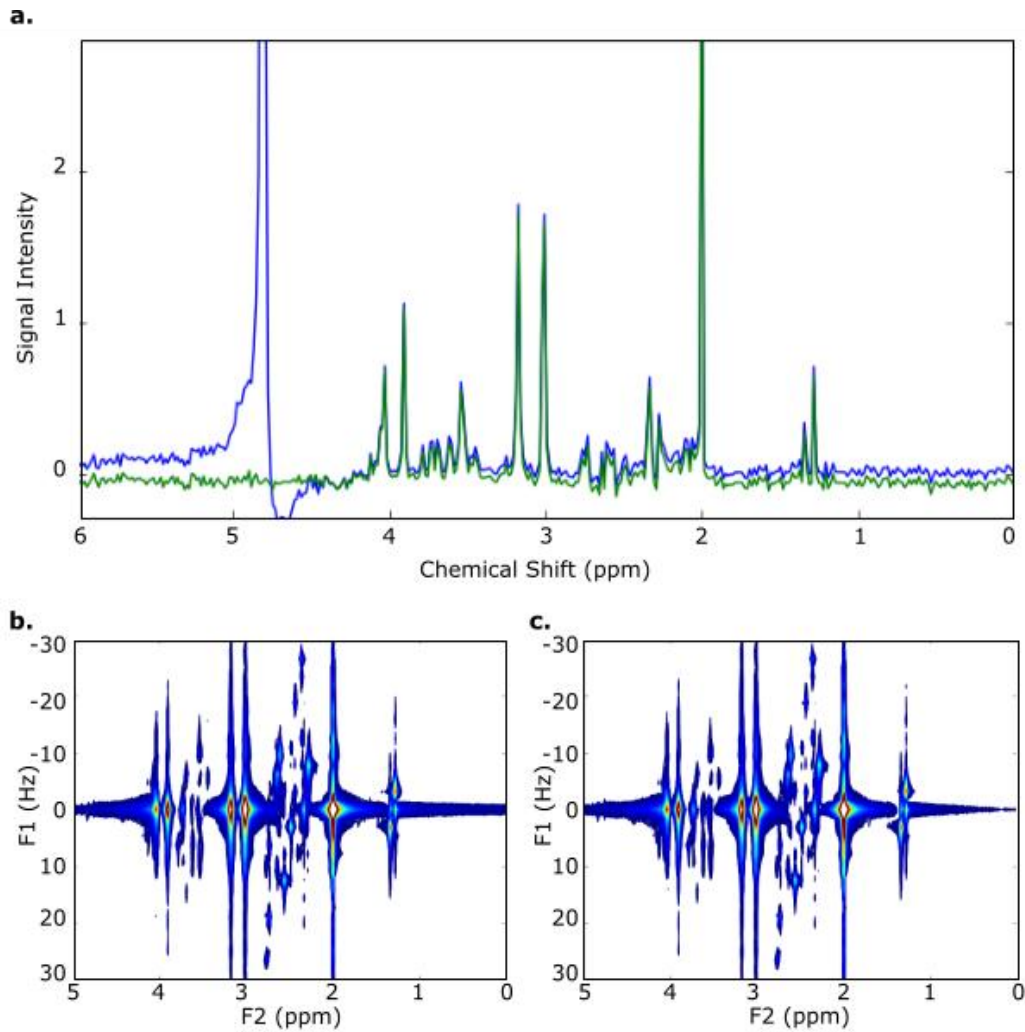
Figure 7-7: a) MRS data without residual water (green) and with the residual water (blue). Removal of the residual displaced the baseline of each TE'S spectrum. This created a large band across 0 Hz in b) the JPRESS spectrum. Aligning the baseline of each TE reduced the effect of the 0 Hz baseline in c) the JPRESS spectrum

Removal of the residual water peaks displaced the baseline of the 1D MRS (Figure 7-6). The

band created at 0 Hz in the JPRESS spectrum complicated determination of low intensity

peaks in the region of 0 Hz.
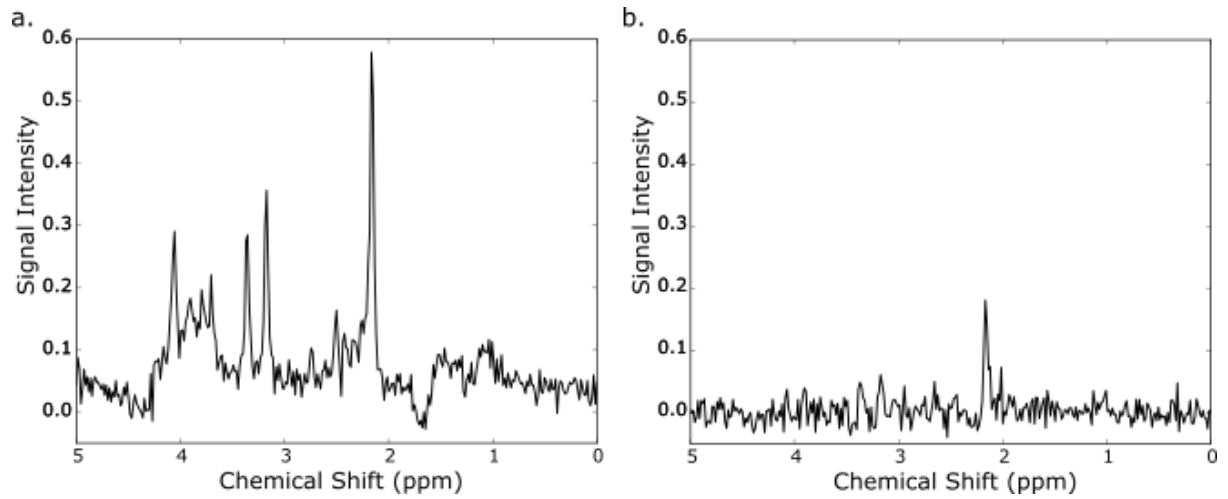
Figure 7-8: a) MRS collected at TE = 35 ms and b) MRS collected at TE = 295 ms in healthy volunteer.

All coupled metabolites had decayed into the noise by an echo time of 295 ms, with only tNAA, tCho and tCr observable in volunteers (Figure 7-7).

The optimised protocol is demonstrated on phantom data in Figure 7-8.
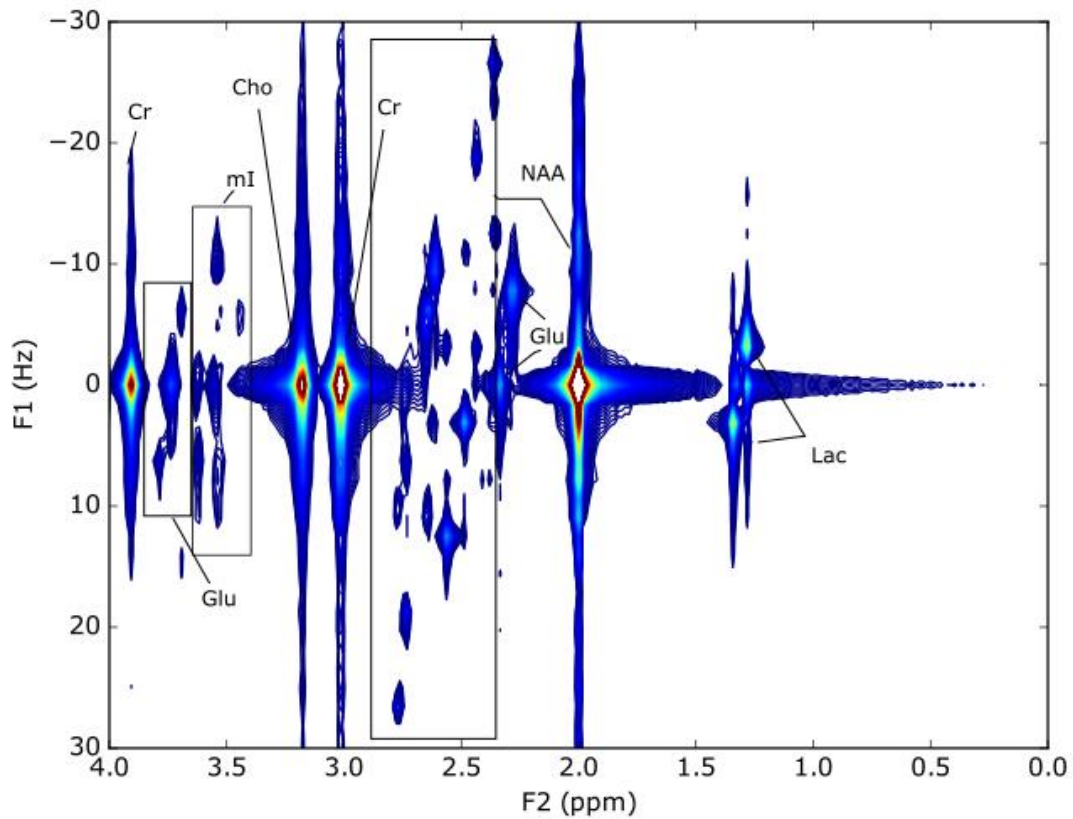
Figure 7-9: Magnified JPRESS and peak assignments for braino phantom.

7.3.4 JPRESS in Healthy Volunteers

JPRESS was collected from a healthy volunteer using ideal acquisition parameters for NSA

and maximum TE with an acquisition time of 35 minutes (Figure 7-8). The JPRESS spectrum

was compared with phantom JPRESS data and with simulated JPRESS spectra to assign

metabolite peaks.
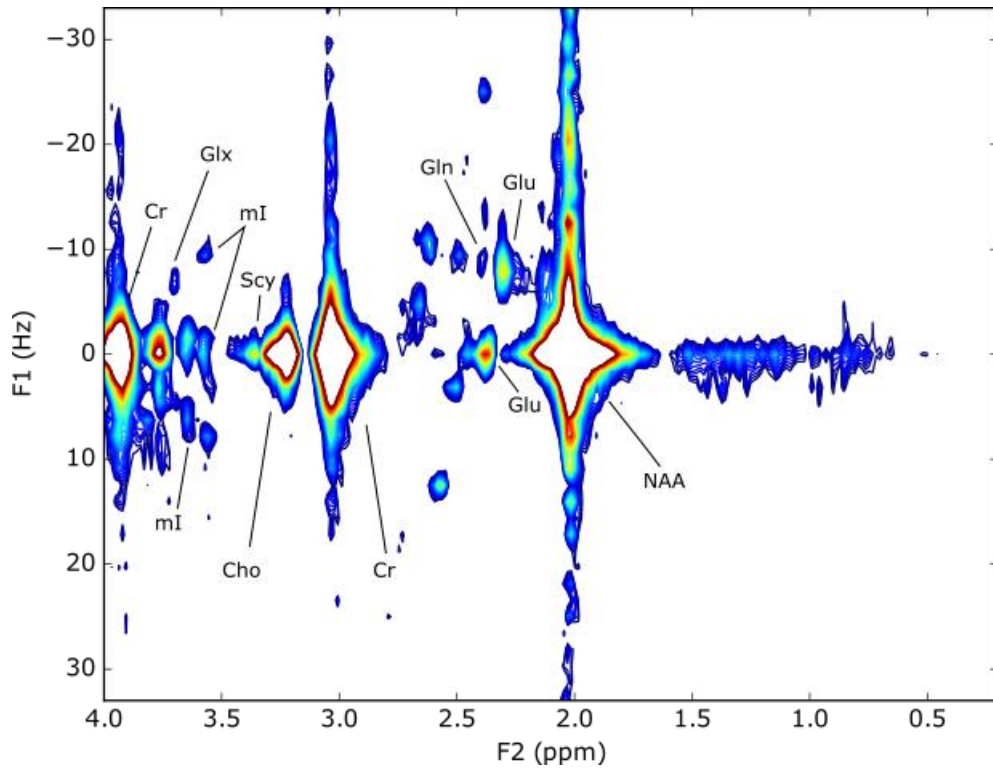
Figure 7-8: Magnified JPRESS of normal brain in healthy volunteer and peak assignments. JPRESS was collected with 16 NSA/TE and 64 TEs with 10 ms spacing from TE 35 ms to TE 655 ms. The acquisition time was 35 minutes.
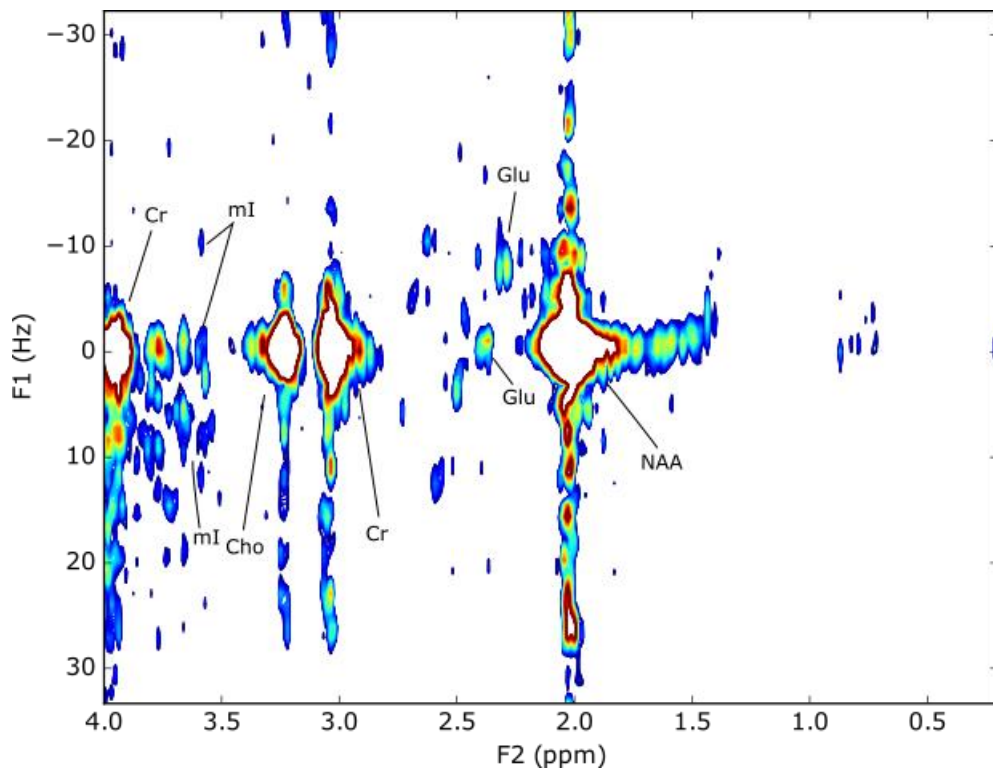
Figure 7-9: Final JPRESS protocol following protocol and processing optimisation. The acquisition time was 6 minutes.

Figure 8 shows the optimised final protocol following optimisation of the protocol and following all postprocessing steps. This reduced the acquisition time to 6 minutes with all metabolites were well resolved.

7.3.5 JPRESS in Paediatric Brain Tumours

Figure 7-10 shows the JPRESS spectrum and a short-TE 35 ms PRESS spectrum collected in the same scanning session of a medulloblastoma. The position of JPRESS resonance peaks can be described by their J-coupling (Hz) values and chemical shift (ppm) positions on the F1 and F2 axes respectively. The JPRESS spectrum contained a resonance at 3.54 ppm, 0 Hz, this resonance is most consistent with glycine and no myo-Inositol cross peaks were observed.

The JPRESS spectrum also contained resonances at 3.40 ppm, 0 Hz and at 3.34 ppm, -7 Hz. The resonance at 3.40 ppm, 0 Hz was twice as large as the resonance at 3.34 ppm, - 7 Hz. The JPRESS spectrum of Tau was simulated and the corresponding resonances at 3.40 ppm, 0 Hz and 3.34 ppm, - 7 Hz had equal intensities. TARQUIN fits to the 35 ms PRESS did not assign any peaks to mI The apparent doublet at 3.4 ppm was not well fitted by TARQUIN. The lactate doublet and lipid peak at 1.3 ppm were well separated in JPRESS.
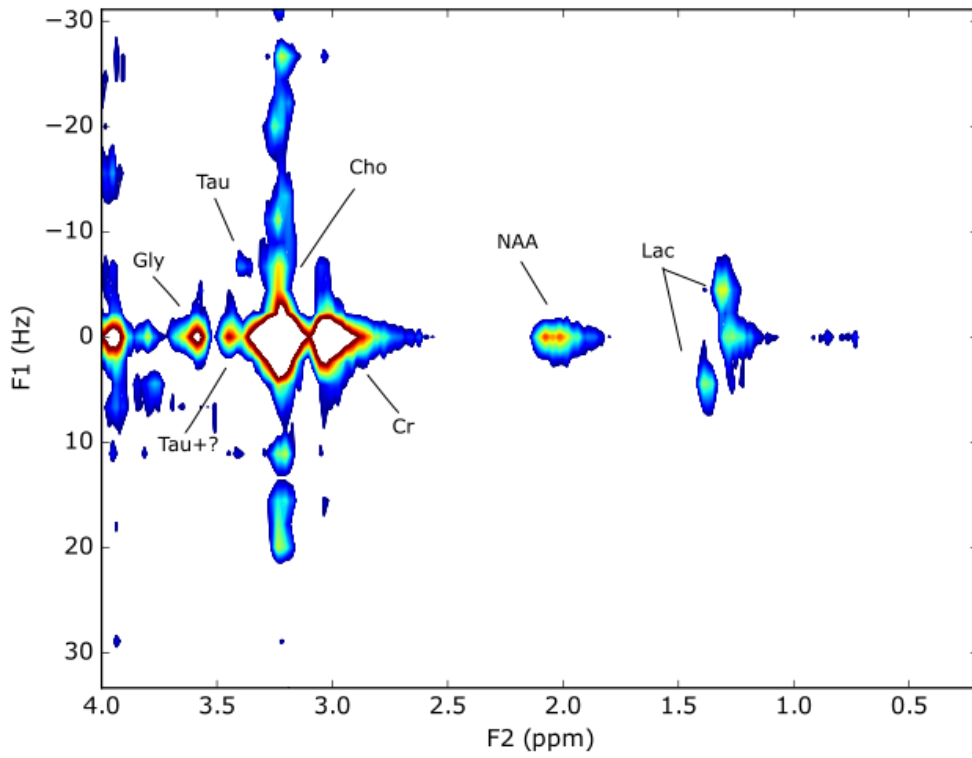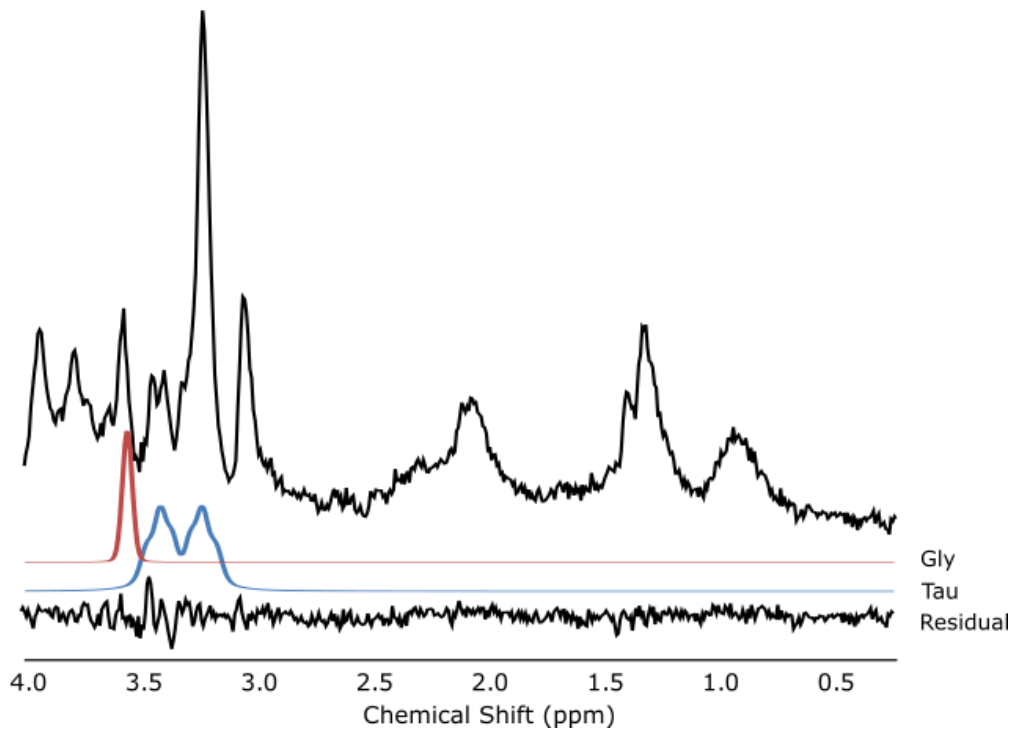
Figure 7-10: a) JPRESS spectrum of medulloblastoma, b) 35 ms PRESS of medulloblastoma collected in the same session. TARQUIN residual and fits for Gly and Tau included.

a.
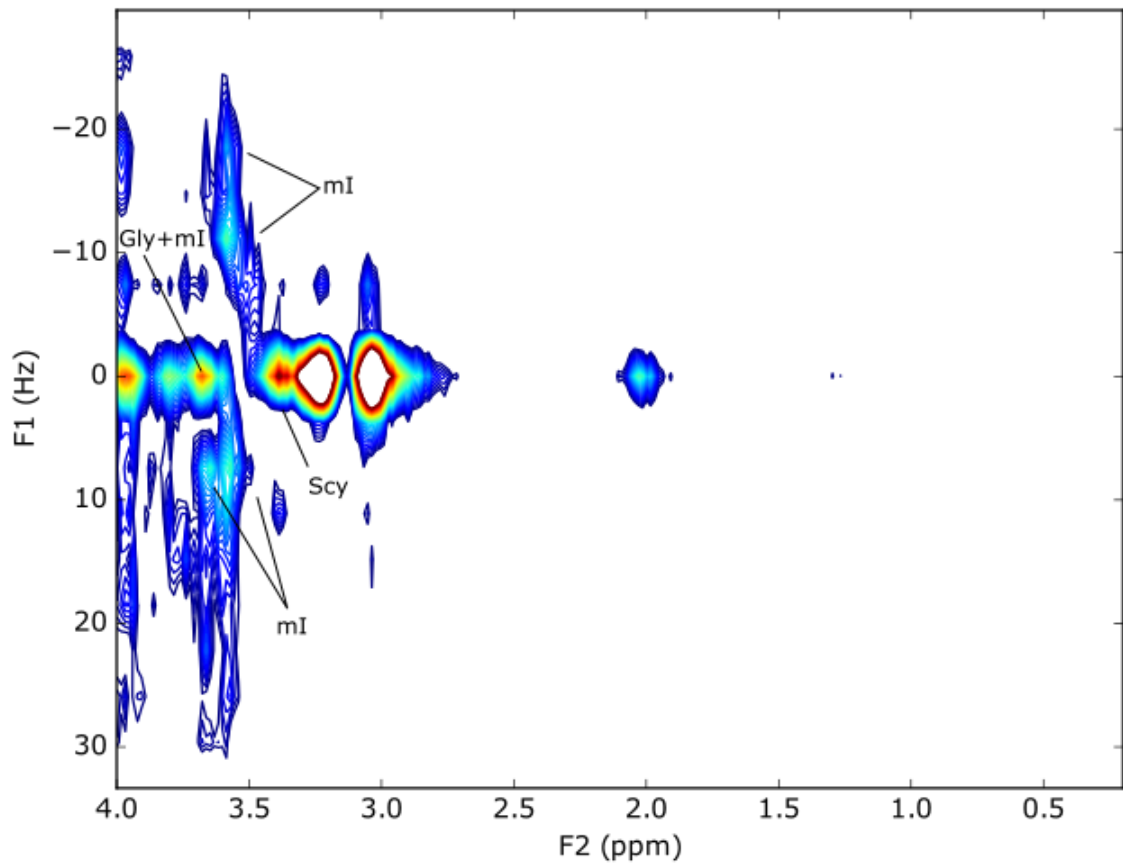
b.
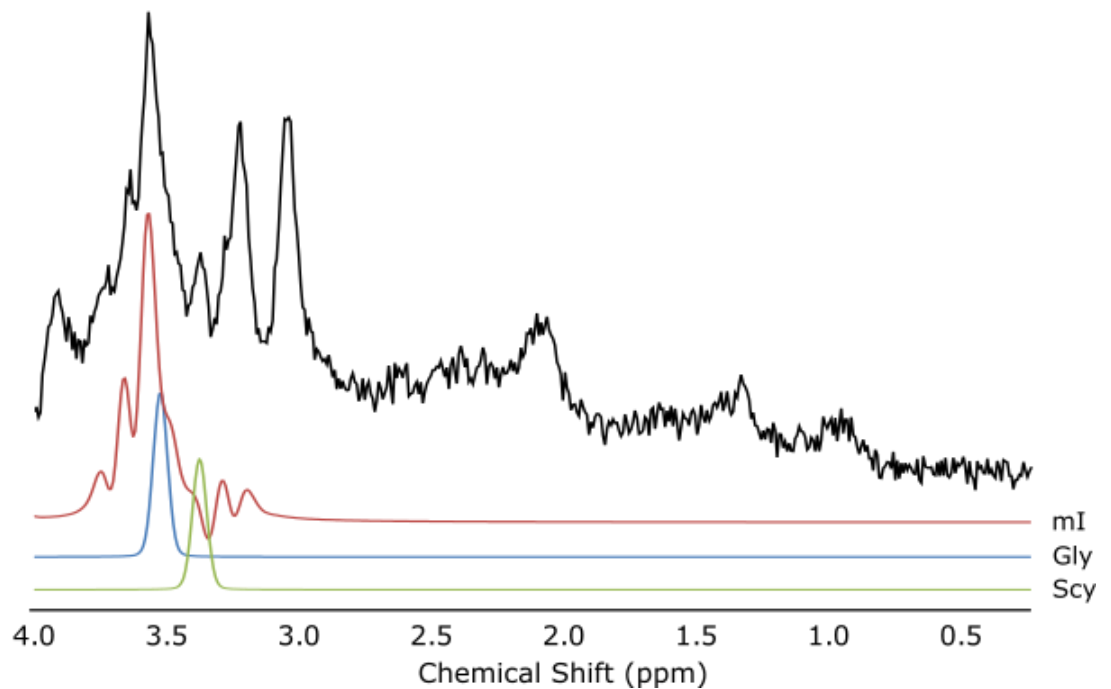
Figure 7-11: a) JPRESS spectrum of pilocytic astrocytoma, b) 1D MRS extracted from the pilocytic astrocytoma JPRESS dataset with a TE of 42 ms. TARQUIN fits for mI, Gly and Scy included.

Figure 7-11 shows the JPRESS spectrum and the extracted short-TE (42 ms) MRS of a pilocytic astrocytoma. The TARQUIN fit of the TE 42 ms estimated resonances from Gly and mI of approximately equal intensity at a chemical shift of 3.54 ppm. The intensities of the peaks at 3.54 ppm, 0 Hz and 3.54 ppm, -11 Hz are approximately equal. The SNR of the extracted 42 ms PRESS spectrum was 12.8.
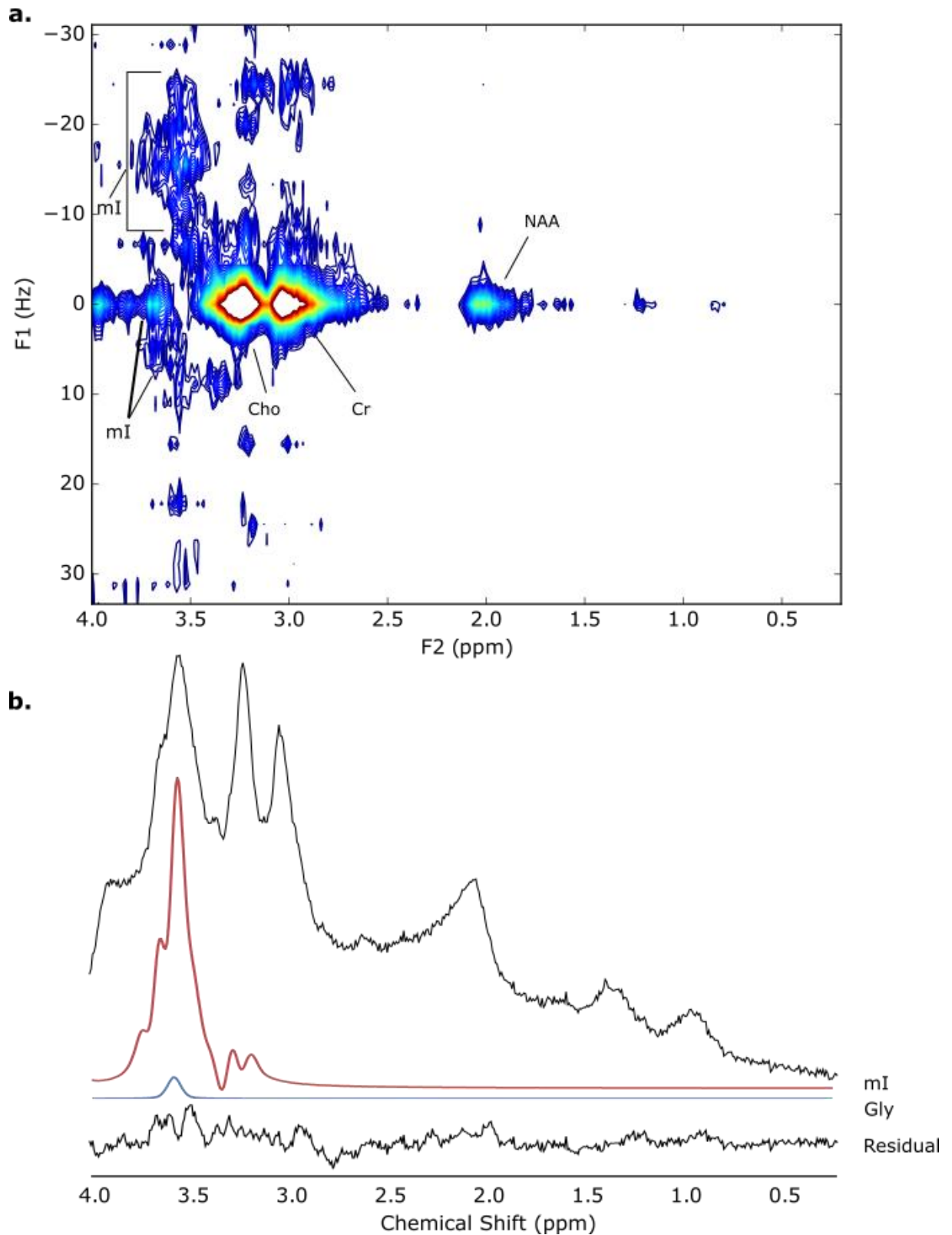
Figure 7-12: JPRESS spectrum of diffuse intrinsic pontine gliomas (DIPG), b) 35 ms PRESS of DIPG collected in the same session. TARQUIN residual and fits for mI and Gly included.

The JPRESS and short-TE PRESS spectra of a DIPG are shown in Figure 7-12. The resonances between -20 Hz and 10 Hz at approximately 3.54 ppm are most consistent with mI

	Concentration (mM)			
	Medulloblastoma		DIPG	
	PRESS	JPRESS	PRESS	JPRESS
tNAA	0.86	1.70	1.66	1.86
tCho	3.97	3.72	1.67	2.09
tCr	6.29	6.54	5.88	5.74
Glu	3.54	0.75	1.27	0.72
Gln	4.80	1.94	0.80	2.99
mI	0.00	1.49	13.05	7.34
Gly	5.19	3.38	0.51	0.45
Tau	9.02	5.45	0.00	2.42
Glx	8.34	2.68	2.07	3.71

Table 7-3: Metabolite concentrations (mM) of medulloblastoma and diffuse intrinsic pontine glioma (DIPG) estimated by 35 ms PRESS and JPRESS.

Table 7-3 shows the estimated concentrations for a range of metabolites as determined by

35 ms PRESS and JPRESS.

7.4 Discussion

This study presents a clinical protocol for JPRESS which can acquire clinical data in a 6 minute

timeframe. The protocol was optimised for visual detection of metabolites with a boundary

condition of a 6 minute acquisition time, rather than for explicit metabolite quantification.

The protocol parameters were optimised to produce a suitable protocol with a 6 minute

scan time. A substantial time reduction was achieved by collecting data with 8 NSA/TE rather

than 16, after visual inspection of phantom and volunteer spectra indicated that Glu, Gln and

mI could still be identified when collecting fewer averages. The spacing between echo times

was optimised to ensure the spectral width of the y-dimension, related to the J-coupling

values of metabolites, was large enough to allow detection of all metabolite peaks. The

protocol was optimised using a braino phantom and volunteer data. All metabolites in the

braino phantom and volunteer data fell within a range of ± 30 Hz. Spectral width is inversely proportional to echo time spacing and consequently an of 15 ms was used in the protocol. While it is possible that metabolites of small concentrations may fall out of this spectral range, it is not expected due to the published chemical shifts and coupling constants for brain metabolites (Govindaraju et al., 2000). Furthermore, it is also not likely that these metabolites would be observable in the 2D spectrum, given the low quantities they would be present in compared to more prominent metabolites like tNAA, tCho and tCr.

The number of echo times and the final echo time collected were also assessed. These two concepts are inextricably linked after determining the optimal final echo time and will be discussed in tandem. The final echo time collected had a greater bearing on the visualisation of the spectrum and the final echo time and had a considerable effect on resolution of coupled metabolites. By keeping the number of echo times constant, but varying the echo time spacing, it was determined that the final echo time should be long enough for coupled metabolites to have both undergone complete J-evolution, to improve the resolution of the spectrum (Edden and Barker, 2011), and to have completely decayed into the noise to avoid unwanted artefacts in the spectrum. Coupled metabolites have a reported in vivo T2 relaxation time of the order of approximately 180-200 ms (Ganji et al., 2012c) and a final echo time of 290 ms was sufficient for good resolution of coupled metabolites in phantom and in vivo data.

A number of postprocessing steps were utilised to improve visualisation of the data. Though coupled metabolites had typically decayed into the noise by an echo time of 290 ms, the tNAA, tCho and tCr singlets were typically still present. As such, spectra at longer echo times

were simulated by duplicating the combined fit to the tNAA, tCho and tCr singlets at 290 ms

and applying a relaxation penalty to effectively simulate the collection of longer echo times.

This had an effect analogous to the zero filling of a 1D spectrum to artificially improve

resolution. There was no benefit conferred by simulating past the point where singlets

would also have effectively decayed into the noise.

The intensity of the residual water peak in the spectrum dominated the JPRESS spectrum.

With the residual peak still present in the FID, typically only the tNAA, tCho and tCr singlets

had sufficient intensity to be detected using JPRESS. The residual water peak was removed

using the HSVD algorithm (Barkhuijsen et al., 1987) and enabled visualisation of the lower

intensity resonances of coupled metabolites. Removal of the residual water peak altered the

'height' of the extracted 1D MRS baseline. Variation in the baseline height among echo times

reduced the resolution of the spectrum and reduced the ability to identify smaller

resonances at J = 0 Hz. Frequency drift of the spectrum due to magnetic field

inhomogeneities also reduced the resolution of the spectrum and created truncation

artifacts above high intensity resonances.

At typical clinical field strengths ≤ 3 T, unambiguous detection of coupled resonances can be

hampered by severe spectral overlap with neighbouring metabolites. While this problem is

reduced at higher field strengths, which have improved spectral resolution and higher SNR

(Bartha, 2007; Snyder and Wilman, 2010), MRS methods which can improve detection of key

metabolites such as Tau, Glu, Gln and mI would be welcome. Various methods have been

proposed for optimised identification of coupled metabolites such as optimised-TE (Choi et

al., 2012; Snyder and Wilman, 2010) and spectral editing (Choi et al., 2008, 2005; Snyder et

al., 2010), however these methods are typically metabolite-specific which null surrounding resonances and reduce the information that can be extracted from an acquisition. A two-dimensional method that retains all metabolite information by spreading coupled metabolite resonances into a second dimension was therefore chosen. Of the most common 2D MRS techniques, JPRESS was chosen ahead of L-COSY (Thomas et al., 2003) as it was available on our clinical 3 T MR system without modification and is CE-marked. JPRESS also offers the facility to extract the short and long-TE 1D MRS spectra that the radiologists at Birmingham Children's Hospital were already familiar with interpreting which aided its translation into a clinical setting.

The JPRESS protocol presented in this study acquires data in approximately 6 minutes. When compared to the shortest reported JPRESS study time of 8 minutes 32 seconds (Lin et al., 2014), the protocol duration presented in this chapter was primarily reduced by collecting data at fewer TEs (18 vs 32). This reduction in TEs was achieved by increasing the step size between TEs from 10 ms to 15 ms, which still enabled all metabolites to be observed in the spectrum, and by choosing a final TE which ensured coupled metabolites had both undergone full J-modulation and T2 decay.

The main Glu and mI resonances that were observed in the braino phantom were also observed in healthy volunteers in the optimised protocol. However, a number of the NAA cross-peaks associated with the aspartate moiety were not observed in the in vivo spectrum. This is likely due to the limits of SNR in vivo with this protocol; however, the missing cross-peaks could also be a result of motion and the effects of motion on the spectrum warrants further investigation.

While a 6 minute acquisition time appears suitable for detection of novel metabolite biomarkers, it may not be best suited for metabolite quantification, particularly in the case of the coupled metabolites. In this study, metabolites were quantified as a series of 1D experiments and corrected for T2 relaxation effects. A more sophisticated analysis method, ProFit, is available which fits the full 2D spectrum using prior knowledge (Schulte and Boesiger, 2006). ProFit was designed for analysis data with smaller increments between echo times, however, and was therefore not used in this study.

A JPRESS spectrum was acquired in four paediatric brain tumour cases. The signal to noise of the DIPG was low and no meaningful conclusions could be made from the OPG. The diffuse resonances at approximately 3.50 ppm between -25 Hz and 15 Hz have been assigned to mI. While the resolution of this feature is poor, its appearance is consistent with mI peaks present in the phantom; though the reason for the relatively poor signal in comparison to the phantom is unclear, one possible explanation for this is motion during the acquisition.

In medulloblastoma, the 35 ms PRESS analysed with TARQUIN assigned the peak at 3.54 ppm to Gly and determined that no mI was present in the spectrum. The acquired JPRESS spectrum was compared with a simulated mI JPRESS spectrum and the characteristic peaks off 0 Hz in the F1 dimension were not present in the acquired spectrum. This confirms TARQUIN's assignment. The JPRESS spectrum contained resonances at 3.40 ppm, 0 Hz and a resonance at 3.34 ppm, -7 Hz. The corresponding resonances in the 35 ms PRESS spectrum were assigned to Tau by TARQUIN, however this region of the spectrum was not completely fitted. The corresponding Tau JPRESS spectrum had equal intensities for these two

resonances and this suggests that one of the peaks was not included in the basis set. It is not known what this peak might be.

In pilocytic astrocytoma, comparison of the JPRESS spectrum with the extracted 1D MRS at 42 ms verified the identification of scyllo-Inositol in the TARQUIN fit to the 1D data. The TARQUIN fit also suggested a considerable amount of Gly was present in the voxel. The intensities of the resonances at 3.54 ppm, 0 Hz and 3.54 ppm, -11 Hz in the JPRESS spectrum were approximately equal, however simulations of Gly and mI indicated that, if Gly was present in the spectrum, the resonance at 3.54 ppm, 0 Hz would be higher. The number of averages, 8, collected for the 42 ms spectrum was small. It is possible that a TARQUIN fit of a standard short-TE PRESS sequence with 128 averages would have led to a different TARQUIN fit. However, the SNR of the extracted spectrum was 12.8 and this would typically pass quality control. This suggests that JPRESS could be a potential method for discriminating between Gly and mI.

While the JPRESS protocol has the potential to collect clinically useful data, there are a number of significant limitations to it. A voxel size of 30 x 30 x 30 mm was required to collect data with sufficient SNR. This voxel size is large by spectroscopic standards, with voxel sizes ranging from 13 x 13 x 13 mm to 20 x 20 x 20 mm more common in a clinical setting, however this JPRESS protocol could be suitable for brain tumours which have not been resected.

Even with a 30 x 30 x 30 mm, SNR still presented a slight issue for the less cellular tumours assessed with JPRESS. SNR could be improved by increasing the number of averages collected per echo time, however this would have a considerable impact on the scan

duration which would render it unsuitable for clinical use where scanning time for functional imaging is limited.

Despite reducing the scan duration to 6 minutes, limited scanning time will still affect its clinical uptake. While JPRESS has the potential to identify or confirm the presence of novel metabolite biomarkers, as evidenced by the medulloblastoma example, confirmation of metabolite assignment is difficult. JPRESS spectra are complex and can be difficult to interpret by the untrained eye and processing packages which confirm metabolite assignment are not available to radiologists. With scanning time limited and little confirmed benefit for either metabolite identification or quantification, conventional short and long-TE MRS is likely to remain the popular choice for clinical use.

7.5 Conclusions
A clinical JPRESS protocol has been developed which has the potential to help identify novel metabolite biomarkers by utilising the MRS J-evolution of coupled metabolites with TE. For JPRESS to enter routine clinical use, robust and improved quantification over conventional one dimensional MRS would need to be demonstrated and postprocessing packages will need development for use by radiologists

8. CONCLUSIONS AND FUTURE WORK

Metabolite concentration estimates have been established as fundamental biomarkers of disease and prognosis in a research setting. There is increasing interest in validating the use of metabolite concentrations for clinical decision making. A number of acquisition protocols and quantification techniques exist and the choice of these will affect the estimated concentration values. The aim of this thesis was to address how echo time choice and T2 relaxation affect the accuracy of metabolite quantification.

With increasing interest in using metabolite concentrations for patient management, the influence of echo time choice on metabolite quantification was assessed in chapter 4. Conventional short and long-TEs of 35 and 135 ms and an intermediate echo time of 80ms were assessed using a combination of simulations, phantoms and volunteer data. Though exploiting the J-evolution of metabolites can improve the accuracy of metabolite quantification, no single TE consistently estimates all metabolite concentrations most accurately in either simulations or phantom data. Echo time choice should therefore be guided by the clinical question being addressed by MRS.

Instead the accuracy of any one individual measurement is predominantly determined by the quality of the data given appropriate postprocessing techniques. tNAA, tCho and tCr can be measured to within <10% of their actual value for SNRs of 15 and above. Accurate measurement of the less prominent Glu, Gln, mI, Gly only approaches an accuracy of within 10 % when the spectrum's SNR is 25 and above for concentrations commonly found in vivo.

The macromolecular baseline which would be present in vivo was not modelled in this work. While this would not typically affect measurements at echo times of 80 and 135 ms, where baseline interference is reduced due to T2 relaxation, inclusion of macromolecular baselines typical of both normal brain and pathology would be an interesting extension to this work. Future work should also investigate quantification of more complex spectra with concentrations typical of brain tumours. An assessment of the limits of MRS quantification and how very poor SNRs and linewidths affect quantification accuracy should also be performed.

T2 relaxation times were estimated from two protocols in Chapter 4. The T2 estimates of NAA, Cho, Cr and water are comparable when estimated from two TEs (35 and 135 ms) and from 18 TEs, however T2 estimation of coupled metabolites is challenging even with multiple TEs. While the long-T2 components in the water signal influence the T2 estimation of water, this is minimised by using a maximum TE of 135 ms.

Chapter 5 presented a retrospective study of paediatric brain tumour MRS collected from two echo times at 1.5 T. The T2 relaxation times of water and metabolites are significantly different between normal brain and tumour and between different tumour types. The difference in the T2 relaxation times of tumour and normal brain significantly affects metabolite concentrations and the T2 relaxation time of water has a greater effect on metabolite quantification than that of metabolites. Correction for T2 relaxation is particularly important for MRS collected at long-TE. The use of case-specific T2 relaxation times may therefore be necessary for accurate metabolite quantification at long-TE.

A multi-TE water scan is introduced in chapter 6 which was used to estimate the T2 relaxation time of water with an acquisition time of one minute. The T2 relaxation time of water in paediatric brain tumours is significantly shorter at 3 T compared with 1.5 T. Correction using case-specific values may be of more importance as field strength increases in paediatric brain tumours. The T2 relaxation times of tNAA, tCho and tCr were estimated in congenital adrenal hyperplasia (CAH). The root mean square percentage difference between concentrations corrected using case-specific metabolite T2 values and those corrected using literature values is less than 5%, implying that case-specific T2 correction is not required in CAH.

Metabolite T2 relaxation times were not assessed in paediatric brain tumours at 3 T and this should form the basis of future work. Variation in the T2 relaxation times of coupled metabolites should also be assessed at both 1.5 and 3 T.

Spectral overlap of metabolites makes unambiguous identification of coupled metabolites difficult at 3 T. In chapter 7 a clinical protocol for JPRESS was presented which can acquire clinically useful data with an acquisition time of 6 minutes which represents a substantial reduction in scan time and makes acquisition feasible for clinical use. JPRESS was acquired in four paediatric brain tumour cases and can aid discrimination between myo-Inositol and glycine. Acquisition of JPRESS could therefore provide early metabolite biomarkers of prognosis and this warrants further investigation. Future work should focus on assessing the accuracy of metabolite quantification of JPRESS.

To summarise, the data quality of MRS was found to affect the accuracy of metabolite quantification more than spectral overlap and echo time choice. T2 relaxation times were

found to vary significantly between field strengths and between normal brain and pathology. The use of case-specific water T2 relaxation times significantly affected metabolite quantification at both 1.5 and 3 T. Further work is required to investigate potential variation of metabolite T2 relaxation times in paediatric brain tumours at 3 T and how variation might affect metabolite quantification. The use of short echo times will improve spectral SNR and reduce the influence of T2 relaxation; however, the effect of baseline interference on metabolite quantification accuracy requires further investigation. The T2 relaxation time of water is quick to measure and is recommended for accurate metabolite quantification.

The 2D spectroscopy technique JPRESS was developed for clinical investigation of paediatric brain tumours. While JPRESS can aid the detection and assignment of novel metabolite biomarkers of diagnosis and prognosis, there is currently no evidence to suggest it currently should replace conventional short or long-TE PRESS for metabolite quantification.

REFERENCES

Adalsteinsson, E., Sullivan, E.V., Kleinhans, N., Spielman, D.M., Pfefferbaum, A., 2000. Longitudinal decline of the neuronal marker N-acetyl aspartate in Alzheimer's disease. Lancet Lond. Engl. 355, 1696–1697.

Albers, M.J., Krieger, M.D., Gonzalez-Gomez, I., Gilles, F.H., McComb, J.G., Nelson, M.D., Blüml, S., 2005. Proton-decoupled 31P MRS in untreated pediatric brain tumors. Magn. Reson. Med. 53, 22–29. doi:10.1002/mrm.20312

Auning, E., Kjærvik, V.K., Selnes, P., Aarsland, D., Haram, A., Bjørnerud, A., Hessen, E., Esnaashari, A., Fladby, T., 2014. White matter integrity and cognition in Parkinson's disease: a cross-sectional study. BMJ Open 4, e003976. doi:10.1136/bmjopen-2013-003976

Barker, P.B., Hearshen, D.O., Boska, M.D., 2001. Single-voxel proton MRS of the human brain at 1.5T and 3.0T. Magn. Reson. Med. 45, 765–769. doi:10.1002/mrm.1104

Barkhuijsen, H., de Beer, R., van Ormondt, D., 1987. Improved algorithm for noniterative time-domain model fitting to exponentially damped magnetic resonance signals. J. Magn. Reson. 1969 73, 553–557. doi:10.1016/0022-2364(87)90023-0

Bartha, R., 2007. Effect of signal-to-noise ratio and spectral linewidth on metabolite quantification at 4 T. NMR Biomed. 20, 512–521. doi:10.1002/nbm.1122

Bartha, R., Drost, D.J., Menon, R.S., Williamson, P.C., 2000. Comparison of the quantification precision of human short echo time (1)H spectroscopy at 1.5 and 4.0 Tesla. Magn. Reson. Med. 44, 185–192.

Bartha, R., Smith, M., Rupsingh, R., Rylett, J., Wells, J.L., Borrie, M.J., 2008. High field (1)H MRS of the hippocampus after donepezil treatment in Alzheimer disease. Prog. Neuropsychopharmacol. Biol. Psychiatry 32, 786–793. doi:10.1016/j.pnpbp.2007.12.011

Barton, S.J., Howe, F.A., Tomlins, A.M., Cudlip, S.A., Nicholson, J.K., Bell, B.A., Griffiths, J.R., 1999. Comparison of in vivo 1H MRS of human brain tumours with 1H HR-MAS spectroscopy of intact biopsy samples in vitro. Magma N. Y. N 8, 121–128.

Biomarkers Definitions Working Group., 2001. Biomarkers and surrogate endpoints: preferred definitions and conceptual framework. Clin. Pharmacol. Ther. 69, 89–95. doi:10.1067/mcp.2001.113989

Birch, R., Peet, A.C., Arvanitis, T.N., Wilson, M., 2015. Sensitivity encoding for fast 1H MR spectroscopic imaging water reference acquisition. Magn. Reson. Med. 73, 2081–2086. doi:10.1002/mrm.25355

Birch, R., Peet, A.C., Dehghani, H., Wilson, M., 2016. Influence of macromolecule baseline on (1) H MR spectroscopic imaging reproducibility. Magn. Reson. Med. doi:10.1002/mrm.26103

Bleyer, W.A., 1999. Epidemiologic impact of children with brain tumors. Childs Nerv. Syst. ChNS Off. J. Int. Soc. Pediatr. Neurosurg. 15, 758–763. doi:10.1007/s003810050467

Blüml, S., Margol, A.S., Sposto, R., Kennedy, R.J., Robison, N.J., Vali, M., Hung, L.T., Muthugounder, S., Finlay, J.L., Erdreich-Epstein, A., Gilles, F.H., Judkins, A.R., Krieger, M.D., Dhall, G., Nelson, M.D., Asgharzadeh, S., 2015. Molecular subgroups of

medulloblastoma identification using noninvasive magnetic resonance spectroscopy. Neuro-Oncol. nov097. doi:10.1093/neuonc/nov097

Blüml, S., Panigrahy, A., Laskov, M., Dhall, G., Krieger, M.D., Nelson, M.D., Finlay, J.L., Gilles, F.H., 2011. Elevated citrate in pediatric astrocytomas with malignant progression. Neuro-Oncol. 13, 1107–1117. doi:10.1093/neuonc/nor087

Bottomley, P.A., 1987. Spatial localization in NMR spectroscopy in vivo. Ann. N. Y. Acad. Sci. 508, 333–348.

Brief, E.E., Whittall, K.P., Li, D.K.B., MacKay, A.L., 2005. Proton T2 relaxation of cerebral metabolites of normal human brain over large TE range. NMR Biomed. 18, 14–18. doi:10.1002/nbm.916

Brooks, W.M., Friedman, S.D., Gasparovic, C., 2001. Magnetic resonance spectroscopy in traumatic brain injury. J. Head Trauma Rehabil. 16, 149–164.

Bull, J.G., Saunders, D.E., Clark, C.A., 2012. Discrimination of paediatric brain tumours using apparent diffusion coefficient histograms. Eur. Radiol. 22, 447–457. doi:10.1007/s00330-011-2255-7

Cancer Research UK, 2015. Children's cancer statistics [WWW Document]. Cancer Res. UK. URL http://www.cancerresearchuk.org/health-professional/cancer-statistics/childrens-cancers (accessed 8.4.16).

Cai, K., Singh, A., Roalf, D.R., Nanga, R.P.R., Haris, M., Hariharan, H., Gur, R., Reddy, R., 2013. Mapping glutamate in subcortical brain structures using high-resolution GluCEST MRI. NMR Biomed. 26, 1278–1284. doi:10.1002/nbm.2949

Cao, Y., Tsien, C.I., Nagesh, V., Junck, L., Ten Haken, R., Ross, B.D., Chenevert, T.L., Lawrence, T.S., 2006. Survival prediction in high-grade gliomas by MRI perfusion before and during early stage of RT [corrected]. Int. J. Radiat. Oncol. Biol. Phys. 64, 876–885. doi:10.1016/j.ijrobp.2005.09.001

Castillo, M., Kwock, L., Mukherji, S.K., 1996. Clinical applications of proton MR spectroscopy. Am. J. Neuroradiol. 17, 1–15.

Cavassila, S., Deval, S., Huegen, C., van Ormondt, D., Graveron-Demilly, D., 2001. Cramér–Rao bounds: an evaluation tool for quantitation. NMR Biomed. 14, 278–283. doi:10.1002/nbm.701

Cavassila, S., Deval, S., Huegen, C., van Ormondt, D., Graveron-Demilly, D., 2000. Cramér-Rao Bound Expressions for Parametric Estimation of Overlapping Peaks: Influence of Prior Knowledge. J. Magn. Reson. 143, 311–320. doi:10.1006/jmre.1999.2002

Choi, C., Bhardwaj, P.P., Seres, P., Kalra, S., Tibbo, P.G., Coupland, N.J., 2008. Measurement of glycine in human brain by triple refocusing 1H-MRS in vivo at 3.0T. Magn. Reson. Med. 59, 59–64. doi:10.1002/mrm.21450

Choi, C., Ganji, S., Hulsey, K., Madan, A., Kovacs, Z., Dimitrov, I., Zhang, S., Pichumani, K., Mendelsohn, D., Mickey, B., Malloy, C., Bachoo, R., DeBerardinis, R., Maher, E., 2013. A comparative study of short- and long-TE 1H-MRS at 3T for in-vivo detection of 2-hydroxyglutarate in brain tumors. NMR Biomed. 26, 1242–1250. doi:10.1002/nbm.2943

Choi, C., Ganji, S.K., DeBerardinis, R.J., Dimitrov, I.E., Pascual, J.M., Bachoo, R., Mickey, B.E., Malloy, C.R., Maher, E.A., 2011a. Measurement of glycine in the human brain in vivo by 1H-MRS at 3T: Application in brain tumors. Magn. Reson. Med. Off. J. Soc. Magn. Reson. Med. Soc. Magn. Reson. Med. 66, 609–618. doi:10.1002/mrm.22857

Choi, C., Ganji, S.K., DeBerardinis, R.J., Hatanpaa, K.J., Rakheja, D., Kovacs, Z., Yang, X.-L., Mashimo, T., Raisanen, J.M., Marin-Valencia, I., Pascual, J.M., Madden, C.J., Mickey, B.E., Malloy, C.R., Bachoo, R.M., Maher, E.A., 2012. 2-hydroxyglutarate detection by magnetic resonance spectroscopy in IDH-mutated patients with gliomas. Nat. Med. 18, 624–629. doi:10.1038/nm.2682

Choi, C., Ogilvie, C.J., Malykhin, N., Ngo, J.T.V., Hartfeil, M.A.W., Coupland, N.J., 2005. Detection of the myo-inositol 4.06-ppm resonance by selective J rewinding: application to human prefrontal cortex in vivo. Magn. Reson. Med. 54, 1536–1540. doi:10.1002/mrm.20688

Cohen, A., Holmen, S., Colman, H., 2013. IDH1 and IDH2 Mutations in Gliomas. Curr. Neurol. Neurosci. Rep. 13, 345. doi:10.1007/s11910-013-0345-4

Crawford, F.W., Khayal, I.S., McGue, C., Saraswathy, S., Pirzkall, A., Cha, S., Lamborn, K.R., Chang, S.M., Berger, M.S., Nelson, S.J., 2009. Relationship of pre-surgery metabolic and physiological MR imaging parameters to survival for patients with untreated GBM. J. Neurooncol. 91, 337–351. doi:10.1007/s11060-008-9719-x

Dang, L., White, D.W., Gross, S., Bennett, B.D., Bittinger, M.A., Driggers, E.M., Fantin, V.R., Jang, H.G., Jin, S., Keenan, M.C., Marks, K.M., Prins, R.M., Ward, P.S., Yen, K.E., Liau, L.M., Rabinowitz, J.D., Cantley, L.C., Thompson, C.B., Vander Heiden, M.G., Su, S.M., 2009. Cancer-associated IDH1 mutations produce 2-hydroxyglutarate. Nature 462, 739. doi:10.1038/nature08617

Davies, N.P., Wilson, M., Harris, L.M., Natarajan, K., Lateef, S., Macpherson, L., Sgouros, S., Grundy, R.G., Arvanitis, T.N., Peet, A.C., 2008a. Identification and characterisation of childhood cerebellar tumours by in vivo proton MRS. NMR Biomed. 21, 908–918. doi:10.1002/nbm.1283

Davies, N.P., Wilson, M., Natarajan, K., Sun, Y., MacPherson, L., Brundler, M.-A., Arvanitis, T.N., Grundy, R.G., Peet, A.C., 2010a. Non-invasive detection of glycine as a biomarker of malignancy in childhood brain tumours using in-vivo 1H MRS at 1.5 tesla confirmed by ex-vivo high-resolution magic-angle spinning NMR. NMR Biomed. 23, 80–87. doi:10.1002/nbm.1432

De Graaf, A.A., Van Dijk, J.E., BoéE, W.M.M.J., 1990. Quality: quantification improvement by converting lineshapes to the lorentzian type. Magn. Reson. Med. 13, 343–357. doi:10.1002/mrm.1910130302

De Stefano, N., Airas, L., Grigoriadis, N., Mattle, H.P., O'Riordan, J., Oreja-Guevara, C., Sellebjerg, F., Stankoff, B., Walczak, A., Wiendl, H., Kieseier, B.C., 2014. Clinical relevance of brain volume measures in multiple sclerosis. CNS Drugs 28, 147–156. doi:10.1007/s40263-014-0140-z

Deelchand, D.K., Henry, P.-G., Uğurbil, K., Marjańska, M., 2012. Measurement of transverse relaxation times of J-coupled metabolites in the human visual cortex at 4 T. Magn. Reson. Med. 67, 891–897. doi:10.1002/mrm.23080

Descamps, M., Hyare, H., Stebbing, J., Winston, A., 2008. Magnetic resonance imaging and spectroscopy of the brain in HIV disease. J. HIV Ther. 13, 55–58.

Dodgshun, A.J., Maixner, W.J., Hansford, J.R., Sullivan, M.J., 2016. Low rates of recurrence and slow progression of pediatric pilocytic astrocytoma after gross-total resection: justification for reducing surveillance imaging. J. Neurosurg. Pediatr. 17, 569–572. doi:10.3171/2015.9.PEDS15449

Dufour, C., Beaugrand, A., Pizer, B., Micheli, J., Aubelle, M.-S., Fourcade, A., Couanet, D., Laplanche, A., Kalifa, C., Grill, J., Dufour, C., Beaugrand, A., Pizer, B., Micheli, J., Aubelle, M.-S., Fourcade, A., Couanet, D., Laplanche, A., Kalifa, C., Grill, J., 2011. Metastatic Medulloblastoma in Childhood: Chang's Classification Revisited, Metastatic Medulloblastoma in Childhood: Chang's Classification Revisited. Int. J. Surg. Oncol. Int. J. Surg. Oncol. 2012, 2012, e245385. doi:10.1155/2012/245385, 10.1155/2012/245385

Edden, R.A.E., Barker, P.B., 2011. If J doesn't evolve, it won't J-resolve: J-PRESS with bandwidth-limited refocusing pulses. Magn. Reson. Med. Off. J. Soc. Magn. Reson. Med. Soc. Magn. Reson. Med. 65, 1509–1514. doi:10.1002/mrm.22747

Eisenhauer, E.A., Therasse, P., Bogaerts, J., Schwartz, L.H., Sargent, D., Ford, R., Dancey, J., Arbuck, S., Gwyther, S., Mooney, M., Rubinstein, L., Shankar, L., Dodd, L., Kaplan, R., Lacombe, D., Verweij, J., 2009. New response evaluation criteria in solid tumours: revised RECIST guideline (version 1.1). Eur. J. Cancer Oxf. Engl. 1990 45, 228–247. doi:10.1016/j.ejca.2008.10.026

Ellingson, B.M., Bendszus, M., Boxerman, J., Barboriak, D., Erickson, B.J., Smits, M., Nelson, S.J., Gerstner, E., Alexander, B., Goldmacher, G., Wick, W., Vogelbaum, M., Weller, M., Galanis, E., Kalpathy-Cramer, J., Shankar, L., Jacobs, P., Pope, W.B., Yang, D., Chung, C., Knopp, M.V., Cha, S., van den Bent, M.J., Chang, S., Al Yung, W.K., Cloughesy, T.F., Wen, P.Y., Gilbert, M.R., 2015. Consensus recommendations for a standardized Brain Tumor Imaging Protocol in clinical trials. Neuro-Oncol. 17, 1188–1198. doi:10.1093/neuonc/nov095

Fangusaro, J., 2012. Pediatric High Grade Glioma: a Review and Update on Tumor Clinical Characteristics and Biology. Front. Oncol. 2. doi:10.3389/fonc.2012.00105

Fay, M.P., Proschan, M.A., 2010. Wilcoxon-Mann-Whitney or t-test? On assumptions for hypothesis tests and multiple interpretations of decision rules. Stat. Surv. 4, 1–39. doi:10.1214/09-SS051

Fetit, A.E., Novak, J., Peet, A.C., Arvanitis, T.N., 2015. Three-dimensional textural features of conventional MRI improve diagnostic classification of childhood brain tumours. NMR Biomed. 28, 1174–1184. doi:10.1002/nbm.3353

Fisher, S.K., Novak, J.E., Agranoff, B.W., 2002. Inositol and higher inositol phosphates in neural tissues: homeostasis, metabolism and functional significance. J. Neurochem. 82, 736–754.

Fjell, A.M., McEvoy, L., Holland, D., Dale, A.M., Walhovd, K.B., Alzheimer's Disease Neuroimaging Initiative, 2013. Brain changes in older adults at very low risk for Alzheimer's disease. J. Neurosci. Off. J. Soc. Neurosci. 33, 8237–8242. doi:10.1523/JNEUROSCI.5506-12.2013

Frahm, J., Bruhn, H., Gyngell, M.L., Merboldt, K.D., Hänicke, W., Sauter, R., 1989. Localized high-resolution proton NMR spectroscopy using stimulated echoes: Initial applications to human brain in vivo. Magn. Reson. Med. 9, 79–93. doi:10.1002/mrm.1910090110

Fuchs, A., Boesiger, P., Schulte, R.F., Henning, A., 2014. ProFit revisited. Magn. Reson. Med. 71, 458–468. doi:10.1002/mrm.24703

Furuyama, J.K., Wilson, N.E., Burns, B.L., Nagarajan, R., Margolis, D.J., Thomas, M.A., 2012. Application of compressed sensing to multidimensional spectroscopic imaging in human prostate. Magn. Reson. Med. 67, 1499–1505. doi:10.1002/mrm.24265

Gan, G., Haas-Kogan, D., 2010. Low-Grade Gliomas, in: Gupta, N., Banerjee, A., Haas-Kogan, D. (Eds.), Pediatric CNS Tumors, Pediatric Oncology. Springer Berlin Heidelberg, pp. 1–35.

Ganji, S.K., Banerjee, A., Patel, A.M., Zhao, Y.D., Dimitrov, I.E., Browning, J.D., Brown, E.S., Maher, E.A., Choi, C., 2012a. T2 measurement of J-coupled metabolites in the human brain at 3T. NMR Biomed. 25, 523–529. doi:10.1002/nbm.1767

García-Gómez, J.M., Luts, J., Julià-Sapé, M., Krooshof, P., Tortajada, S., Robledo, J.V., Melssen, W., Fuster-García, E., Olier, I., Postma, G., Monleón, D., Moreno-Torres, A., Pujol, J., Candiota, A.-P., Martínez-Bisbal, M.C., Suykens, J., Buydens, L., Celda, B., Van Huffel, S., Arús, C., Robles, M., 2009. Multiproject-multicenter evaluation of automatic brain tumor classification by magnetic resonance spectroscopy. Magma N. Y. N 22, 5–18. doi:10.1007/s10334-008-0146-y

Garwood, M., DelaBarre, L., 2001. The Return of the Frequency Sweep: Designing Adiabatic Pulses for Contemporary NMR. J. Magn. Reson. 153, 155–177. doi:10.1006/jmre.2001.2340

Gasparovic, C., Song, T., Devier, D., Bockholt, H.J., Caprihan, A., Mullins, P.G., Posse, S., Jung, R.E., Morrison, L.A., 2006a. Use of tissue water as a concentration reference for proton spectroscopic imaging. Magn. Reson. Med. 55, 1219–1226. doi:10.1002/mrm.20901

Geethanath, S., Baek, H.-M., Ganji, S.K., Ding, Y., Maher, E.A., Sims, R.D., Choi, C., Lewis, M.A., Kodibagkar, V.D., 2012. Compressive sensing could accelerate 1H MR metabolic imaging in the clinic. Radiology 262, 985–994. doi:10.1148/radiol.11111098

Gelman, N., Gorell, J.M., Barker, P.B., Savage, R.M., Spickler, E.M., Windham, J.P., Knight, R.A., 1999. MR imaging of human brain at 3.0 T: preliminary report on transverse relaxation rates and relation to estimated iron content. Radiology 210, 759–767. doi:10.1148/radiology.210.3.r99fe41759

Gilheeney, S.W., Kieran, M.W., 2012. Differences in molecular genetics between pediatric and adult malignant astrocytomas: age matters. Future Oncol. Lond. Engl. 8, 549–558. doi:10.2217/fon.12.51

Goodden, J., Pizer, B., Pettorini, B., Williams, D., Blair, J., Didi, M., Thorp, N., Mallucci, C., 2014. The role of surgery in optic pathway/hypothalamic gliomas in children. J. Neurosurg. Pediatr. 13, 1–12. doi:10.3171/2013.8.PEDS12546

Govindaraju, V., Young, K., Maudsley, A.A., 2000. Proton NMR chemical shifts and coupling constants for brain metabolites. NMR Biomed. 13, 129–153.

Graaf, R.A. de, 2007. In Vivo NMR Spectroscopy: Principles and Techniques, 2nd Revised edition edition. ed. Wiley-Blackwell, Chichester, West Sussex, England ; Hoboken, NJ.

Grill, J., Puget, S., Andreiuolo, F., Philippe, C., MacConaill, L., Kieran, M.W., 2012. Critical oncogenic mutations in newly diagnosed pediatric diffuse intrinsic pontine glioma. Pediatr. Blood Cancer 58, 489–491. doi:10.1002/pbc.24060

Guillevin, R., Menuel, C., Taillibert, S., Capelle, L., Costalat, R., Abud, L., Habas, C., De Marco, G., Hoang-Xuan, K., Chiras, J., Vallée, J.-N., 2011. Predicting the outcome of grade II

glioma treated with temozolomide using proton magnetic resonance spectroscopy. Br. J. Cancer 104, 1854–1861. doi:10.1038/bjc.2011.174

Gujar, S.K., Maheshwari, S., Björkman-Burtscher, I., Sundgren, P.C., 2005. Magnetic resonance spectroscopy. J. Neuro-Ophthalmol. Off. J. North Am. Neuro-Ophthalmol. Soc. 25, 217–226.

Haase, A., Frahm, J., Hänicke, W., Matthaei, D., 1985. 1H NMR chemical shift selective (CHESS) imaging. Phys. Med. Biol. 30, 341–344.

Hancu, I., 2009. Optimized glutamate detection at 3T. J. Magn. Reson. Imaging JMRI 30, 1155–1162. doi:10.1002/jmri.21936

Hancu, I., Port, J., 2011. The case of the missing glutamine. NMR Biomed. 24, 529–535. doi:10.1002/nbm.1620

Hargrave, D., Chuang, N., Bouffet, E., 2008. Conventional MRI cannot predict survival in childhood diffuse intrinsic pontine glioma. J. Neurooncol. 86, 313–319. doi:10.1007/s11060-007-9473-5

Haris, M., Cai, K., Singh, A., Hariharan, H., Reddy, R., 2011. In vivo mapping of brain myo-inositol. NeuroImage 54, 2079–2085. doi:10.1016/j.neuroimage.2010.10.017

Harris, L.M., Davies, N.P., Macpherson, L., Lateef, S., Natarajan, K., Brundler, M.-A., Sgouros, S., English, M.W., Arvanitis, T.N., Grundy, R.G., Peet, A.C., 2008a. Magnetic resonance spectroscopy in the assessment of pilocytic astrocytomas. Eur. J. Cancer Oxf. Engl. 1990 44, 2640–2647. doi:10.1016/j.ejca.2008.08.012

Harris, L.M., Davies, N.P., Macpherson, L., Lateef, S., Natarajan, K., Brundler, M.-A., Sgouros, S., English, M.W., Arvanitis, T.N., Grundy, R.G., Peet, A.C., 2008b. Magnetic resonance spectroscopy in the assessment of pilocytic astrocytomas. Eur. J. Cancer Oxf. Engl. 1990 44, 2640–2647. doi:10.1016/j.ejca.2008.08.012

Hipp, S.J., Steffen-Smith, E., Hammoud, D., Shih, J.H., Bent, R., Warren, K.E., 2011. Predicting outcome of children with diffuse intrinsic pontine gliomas using multiparametric imaging. Neuro-Oncol. 13, 904–909. doi:10.1093/neuonc/nor076

Hore, P.J., 1989. Nuclear Magnetic Resonance. Oxford University Press, U.S.A., Oxford ; New York.

Howe, F.A., Barton, S.J., Cudlip, S.A., Stubbs, M., Saunders, D.E., Murphy, M., Wilkins, P., Opstad, K.S., Doyle, V.L., McLean, M.A., Bell, B.A., Griffiths, J.R., 2003. Metabolic profiles of human brain tumors using quantitative in vivo 1H magnetic resonance spectroscopy. Magn. Reson. Med. 49, 223–232. doi:10.1002/mrm.10367

Hurd, R., Sailasuta, N., Srinivasan, R., Vigneron, D.B., Pelletier, D., Nelson, S.J., 2004. Measurement of brain glutamate using TE-averaged PRESS at 3T. Magn. Reson. Med. 51, 435–440. doi:10.1002/mrm.20007

Isobe, T., Matsumura, A., Anno, I., Yoshizawa, T., Nagatomo, Y., Itai, Y., Nose, T., 2002. Quantification of cerebral metabolites in glioma patients with proton MR spectroscopy using T2 relaxation time correction. Magn. Reson. Imaging 20, 343–349.

Julià-Sapé, M., Coronel, I., Majós, C., Candiota, A.P., Serrallonga, M., Cos, M., Aguilera, C., Acebes, J.J., Griffiths, J.R., Arús, C., 2012. Prospective diagnostic performance evaluation of single-voxel 1H MRS for typing and grading of brain tumours. NMR Biomed. 25, 661–673. doi:10.1002/nbm.1782

Just, M., Thelen, M., 1988. Tissue characterization with T1, T2, and proton density values: results in 160 patients with brain tumors. Radiology 169, 779–785. doi:10.1148/radiology.169.3.3187000

Kanowski, M., Kaufmann, J., Braun, J., Bernarding, J., Tempelmann, C., 2004. Quantitation of simulated short echo time 1H human brain spectra by LCModel and AMARES. Magn. Reson. Med. 51, 904–912. doi:10.1002/mrm.20063

Kantarci, K., 2013. Magnetic resonance spectroscopy in common dementias. Neuroimaging Clin. N. Am. 23, 393–406. doi:10.1016/j.nic.2012.10.004

Kantarci, K., Boeve, B.F., Wszolek, Z.K., Rademakers, R., Whitwell, J.L., Baker, M.C., Senjem, M.L., Samikoglu, A.R., Knopman, D.S., Petersen, R.C., Jack, C.R., 2010. MRS in presymptomatic MAPT mutation carriers. Neurology 75, 771–778. doi:10.1212/WNL.0b013e3181f073c7

Kantarci, K., Jack, C.R., Xu, Y.C., Campeau, N.G., O'Brien, P.C., Smith, G.E., Ivnik, R.J., Boeve, B.F., Kokmen, E., Tangalos, E.G., Petersen, R.C., 2000. Regional metabolic patterns in mild cognitive impairment and Alzheimer's disease: A 1H MRS study. Neurology 55, 210–217.

Kantarci, K., Knopman, D.S., Dickson, D.W., Parisi, J.E., Whitwell, J.L., Weigand, S.D., Josephs, K.A., Boeve, B.F., Petersen, R.C., Jack, C.R., 2008. Alzheimer disease: postmortem neuropathologic correlates of antemortem 1H MR spectroscopy metabolite measurements. Radiology 248, 210–220. doi:10.1148/radiol.2481071590

Keeler, J., 2010. Understanding NMR Spectroscopy, 2nd Revised edition edition. ed. Wiley-Blackwell, Chichester, U.K.

Kelly, J.P., Weiss, A.H., 2013. Detection of tumor progression in optic pathway glioma with and without neurofibromatosis type 1. Neuro-Oncol. 15, 1560–1567. doi:10.1093/neuonc/not120

Khayal, I.S., Crawford, F.W., Saraswathy, S., Lamborn, K.R., Chang, S.M., Cha, S., McKnight, T.R., Nelson, S.J., 2008. Relationship Between Choline and Apparent Diffusion Coefficient in Patients With Gliomas. J. Magn. Reson. Imaging JMRI 27, 718–725. doi:10.1002/jmri.21288

Kim, H., Wild, J.M., Allen, P.S., 2004. Strategy for the spectral filtering of myo-inositol and other strongly coupled spins. Magn. Reson. Med. 51, 263–272. doi:10.1002/mrm.10697

Kirov, I.I., Fleysher, L., Fleysher, R., Patil, V., Liu, S., Gonen, O., 2008a. Age dependence of regional proton metabolites T2 relaxation times in the human brain at 3 T. Magn. Reson. Med. 60, 790–795. doi:10.1002/mrm.21715

Koh, D.M., Thoeny, H.C. (Eds.), 2010. Diffusion-Weighted MR Imaging, Medical Radiology. Springer Berlin Heidelberg, Berlin, Heidelberg.

Kovanlikaya, A., Panigrahy, A., Krieger, M.D., Gonzalez-Gomez, I., Ghugre, N., McComb, J.G., Gilles, F.H., Nelson, M.D., Blüml, S., 2005. Untreated pediatric primitive neuroectodermal tumor in vivo: quantitation of taurine with MR spectroscopy. Radiology 236, 1020–1025. doi:10.1148/radiol.2363040856

Kreis, R., 2016. The trouble with quality filtering based on relative Cramér-Rao lower bounds. Magn. Reson. Med. 75, 15–18. doi:10.1002/mrm.25568

Kreis, R., Ernst, T., Ross, B.D., 1993. Absolute Quantitation of Water and Metabolites in the Human Brain. II. Metabolite Concentrations. J. Magn. Reson. B 102, 9–19. doi:10.1006/jmrb.1993.1056

Kreis, R., Ernst, T., Ross, B.D., 1993. Development of the human brain: In vivo quantification of metabolite and water content with proton magnetic resonance spectroscopy. Magn. Reson. Med. 30, 424–437. doi:10.1002/mrm.1910300405

Krishnan, K.R.R., Charles, H.C., Doraiswamy, P.M., Mintzer, J., Weisler, R., Yu, X., Perdomo, C., Ieni, J.R., Rogers, S., 2003. Randomized, placebo-controlled trial of the effects of donepezil on neuronal markers and hippocampal volumes in Alzheimer's disease. Am. J. Psychiatry 160, 2003–2011. doi:10.1176/appi.ajp.160.11.2003

Krishnatry, R., Zhukova, N., Guerreiro Stucklin, A.S., Pole, J.D., Mistry, M., Fried, I., Ramaswamy, V., Bartels, U., Huang, A., Laperriere, N., Dirks, P., Nathan, P.C., Greenberg, M., Malkin, D., Hawkins, C., Bandopadhayay, P., Kieran, M.W., Manley, P.E., Bouffet, E., Tabori, U., 2016. Clinical and treatment factors determining long-term outcomes for adult survivors of childhood low-grade glioma: A population-based study. Cancer 122, 1261–1269. doi:10.1002/cncr.29907

Lange, T., Dydak, U., Roberts, T.P.L., Rowley, H.A., Bjeljac, M., Boesiger, P., 2006. Pitfalls in Lactate Measurements at 3T. Am. J. Neuroradiol. 27, 895–901.

Levitt, M.H., 2008. Spin Dynamics: Basics of Nuclear Magnetic Resonance, 2nd Revised edition edition. ed. Wiley-Blackwell, Chichester, England ; Hoboken, NJ.

Li, Y., Srinivasan, R., Ratiney, H., Lu, Y., Chang, S.M., Nelson, S.J., 2008. Comparison of T1 and T2 metabolite relaxation times in glioma and normal brain at 3 T. J. Magn. Reson. Imaging JMRI 28, 342–350. doi:10.1002/jmri.21453

Lin, M., Kumar, A., Yang, S., 2014. Two-Dimensional J-Resolved LASER and Semi-LASER Spectroscopy of Human Brain. Magn. Reson. Med. Off. J. Soc. Magn. Reson. Med. Soc. Magn. Reson. Med. 71, 911–920. doi:10.1002/mrm.24732

Listernick, R., Ferner, R.E., Liu, G.T., Gutmann, D.H., 2007. Optic pathway gliomas in neurofibromatosis-1: controversies and recommendations. Ann. Neurol. 61, 189–198. doi:10.1002/ana.21107

Llufriu, S., Kornak, J., Ratiney, H., Oh, J., Brenneman, D., Cree, B.A., Sampat, M., Hauser, S.L., Nelson, S.J., Pelletier, D., 2014. Magnetic resonance spectroscopy markers of disease progression in multiple sclerosis. JAMA Neurol. 71, 840–847. doi:10.1001/jamaneurol.2014.895

Louis, D.N., Perry, A., Reifenberger, G., von Deimling, A., Figarella-Branger, D., Cavenee, W.K., Ohgaki, H., Wiestler, O.D., Kleihues, P., Ellison, D.W., 2016. The 2016 World Health Organization Classification of Tumors of the Central Nervous System: a summary. Acta Neuropathol. (Berl.) 131, 803–820. doi:10.1007/s00401-016-1545-1

Madan, A., Ganji, S.K., An, Z., Choe, K.S., Pinho, M.C., Bachoo, R.M., Maher, E.M., Choi, C., 2015a. Proton T2 measurement and quantification of lactate in brain tumors by MRS at 3 Tesla in vivo. Magn. Reson. Med. 73, 2094–2099. doi:10.1002/mrm.25352

Marcus, K., Astrakas, L., Zurakowski, D., Zarifi, M., Mintzopoulos, D., Poussaint, T., Anthony, D., De Girolami, U., Black, P., Tarbell, N., Tzika, A., 2007. Predicting survival of children with CNS tumors using proton magnetic resonance spectroscopic imaging biomarkers. Int. J. Oncol. doi:10.3892/ijo.30.3.651

Mayer, D., Spielman, D.M., 2005. Detection of glutamate in the human brain at 3 T using optimized constant time point resolved spectroscopy. Magn. Reson. Med. 54, 439–442. doi:10.1002/mrm.20571

McKay, L.I., Cidlowski, J.A., 2003. Physiologic and Pharmacologic Effects of Corticosteroids.

McRobbie, D.W., Moore, E.A., Graves, M.J., Prince, M.R., 2007. MRI from Picture to Proton, 2 edition. ed. Cambridge University Press, Cambridge, UK ; New York.

Merchant, T.E., Pollack, I.F., Loeffler, J.S., 2010. Brain tumors across the age spectrum: biology, therapy, and late effects. Semin. Radiat. Oncol. 20, 58–66. doi:10.1016/j.semradonc.2009.09.005

Miller, B.L., Moats, R.A., Shonk, T., Ernst, T., Woolley, S., Ross, B.D., 1993. Alzheimer disease: depiction of increased cerebral myo-inositol with proton MR spectroscopy. Radiology 187, 433–437. doi:10.1148/radiology.187.2.8475286

Minati, L., Aquino, D., Bruzzone, M.G., Erbetta, A., 2010. Quantitation of normal metabolite concentrations in six brain regions by in-vivo 1H-MR spectroscopy. J. Med. Phys. Assoc. Med. Phys. India 35, 154–163. doi:10.4103/0971-6203.62128

Mlynárik, V., Gruber, S., Moser, E., 2001. Proton T_1 and T_2 relaxation times of human brain metabolites at 3 Tesla: METABOLITE T_1 AND T_2 IN HUMAN BRAIN AT 3 T. NMR Biomed. 14, 325–331. doi:10.1002/nbm.713

Mok, W., Chow, T.W., Zheng, L., Mack, W.J., Miller, C., 2004. Clinicopathological Concordance of Dementia Diagnoses by Community Versus Tertiary Care Clinicians. Am. J. Alzheimers Dis. Other Demen. 19, 161–165.

Mukherji, S.K. (Ed.), 1998. Clinical Applications of MR Spectroscopy. Wiley-Blackwell, New York.

Mullins, P.G., Chen, H., Xu, J., Caprihan, A., Gasparovic, C., 2008. Comparative reliability of proton spectroscopy techniques designed to improve detection of J-coupled metabolites. Magn. Reson. Med. 60, 964–969. doi:10.1002/mrm.21696

Murphy, P.S., Rowland, I.J., Viviers, L., Brada, M., Leach, M.O., Dzik-Jurasz, A.S.K., 2003. Could assessment of glioma methylene lipid resonance by in vivo (1)H-MRS be of clinical value? Br. J. Radiol. 76, 459–463. doi:10.1259/bjr/16316438

Murphy, P.S., Viviers, L., Abson, C., Rowland, I.J., Brada, M., Leach, M.O., Dzik-Jurasz, A.S.K., 2004. Monitoring temozolomide treatment of low-grade glioma with proton magnetic resonance spectroscopy. Br. J. Cancer 90, 781–786. doi:10.1038/sj.bjc.6601593

Nagarajan, R., Gomez, A.M., Raman, S.S., Margolis, D.J., McClure, T., Thomas, M.A., 2010. Correlation of endorectal 2D JPRESS findings with pathological Gleason scores in prostate cancer patients. NMR Biomed. 23, 257–261. doi:10.1002/nbm.1446

Napolitano, A., Kockenberger, W., Auer, D.P., 2013. Reliable gamma aminobutyric acid measurement using optimized PRESS at 3 T. Magn. Reson. Med. 69, 1528–1533. doi:10.1002/mrm.24397

Near, J., Andersson, J., Maron, E., Mekle, R., Gruetter, R., Cowen, P., Jezzard, P., 2013. Unedited in vivo detection and quantification of γ-aminobutyric acid in the occipital cortex using short-TE MRS at 3 T. NMR Biomed. 26, 1353–1362. doi:10.1002/nbm.2960

Nicolin, G., Parkin, P., Mabbott, D., Hargrave, D., Bartels, U., Tabori, U., Rutka, J., Buncic, J.R., Bouffet, E., 2009. Natural history and outcome of optic pathway gliomas in children. Pediatr. Blood Cancer 53, 1231–1237. doi:10.1002/pbc.22198

O'Connor, J.P.B., Aboagye, E.O., Adams, J.E., Aerts, H.J.W.L., Barrington, S.F., Beer, A.J., Boellaard, R., Bohndiek, S.E., Brady, M., Brown, G., Buckley, D.L., Chenevert, T.L., Clarke, L.P., Collette, S., Cook, G.J., deSouza, N.M., Dickson, J.C., Dive, C., Evelhoch, J.L., Faivre-Finn, C., Gallagher, F.A., Gilbert, F.J., Gillies, R.J., Goh, V., Griffiths, J.R., Groves, A.M., Halligan, S., Harris, A.L., Hawkes, D.J., Hoekstra, O.S., Huang, E.P., Hutton, B.F., Jackson, E.F., Jayson, G.C., Jones, A., Koh, D.-M., Lacombe, D., Lambin, P., Lassau, N., Leach, M.O., Lee, T.-Y., Leen, E.L., Lewis, J.S., Liu, Y., Lythgoe, M.F., Manoharan, P., Maxwell, R.J., Miles, K.A., Morgan, B., Morris, S., Ng, T., Padhani, A.R., Parker, G.J.M., Partridge, M., Pathak, A.P., Peet, A.C., Punwani, S., Reynolds, A.R., Robinson, S.P., Shankar, L.K., Sharma, R.A., Soloviev, D., Stroobants, S., Sullivan, D.C., Taylor, S.A., Tofts, P.S., Tozer, G.M., van Herk, M., Walker-Samuel, S., Wason, J., Williams, K.J., Workman, P., Yankeelov, T.E., Brindle, K.M., McShane, L.M., Jackson, A., Waterton, J.C., 2016. Imaging biomarker roadmap for cancer studies. Nat. Rev. Clin. Oncol. doi:10.1038/nrclinonc.2016.162

Office for National Statistics, 2016. Cancer Registration Statistics, England: 2014 [WWW Document]. URL http://www.ons.gov.uk/peoplepopulationandcommunity/healthandsocialcare/conditionsanddiseases/bulletins/cancerregistrationstatisticsengland/2014 (accessed 7.28.16).

Opstad, K.S., Ladroue, C., Bell, B.A., Griffiths, J.R., Howe, F.A., 2007. Linear discriminant analysis of brain tumour (1)H MR spectra: a comparison of classification using whole spectra versus metabolite quantification. NMR Biomed. 20, 763–770. doi:10.1002/nbm.1147

Opstad, K.S., Wright, A.J., Bell, B.A., Griffiths, J.R., Howe, F.A., 2010. Correlations between in vivo (1)H MRS and ex vivo (1)H HRMAS metabolite measurements in adult human gliomas. J. Magn. Reson. Imaging JMRI 31, 289–297. doi:10.1002/jmri.22039

Orphanidou-Vlachou, E., Vlachos, N., Davies, N.P., Arvanitis, T.N., Grundy, R.G., Peet, A.C., 2014. Texture analysis of T1 - and T2 -weighted MR images and use of probabilistic neural network to discriminate posterior fossa tumours in children. NMR Biomed. 27, 632–639. doi:10.1002/nbm.3099

Oz, G., Alger, J.R., Barker, P.B., Bartha, R., Bizzi, A., Boesch, C., Bolan, P.J., Brindle, K.M., Cudalbu, C., Dinçer, A., Dydak, U., Emir, U.E., Frahm, J., González, R.G., Gruber, S., Gruetter, R., Gupta, R.K., Heerschap, A., Henning, A., Hetherington, H.P., Howe, F.A., Hüppi, P.S., Hurd, R.E., Kantarci, K., Klomp, D.W.J., Kreis, R., Kruiskamp, M.J., Leach, M.O., Lin, A.P., Luijten, P.R., Marjańska, M., Maudsley, A.A., Meyerhoff, D.J., Mountford, C.E., Nelson, S.J., Pamir, M.N., Pan, J.W., Peet, A.C., Poptani, H., Posse, S., Pouwels, P.J.W., Ratai, E.-M., Ross, B.D., Scheenen, T.W., Schuster, C., Smith, I.C.P., Soher, B.J., Tkáč, I., Vigneron, D.B., Kauppinen, R.A., MRS Consensus Group, 2014. Clinical proton MR spectroscopy in central nervous system disorders. Radiology 270, 658–679. doi:10.1148/radiol.13130531

Oz, G., Iltis, I., Hutter, D., Thomas, W., Bushara, K.O., Gomez, C.M., 2011. Distinct neurochemical profiles of spinocerebellar ataxias 1, 2, 6, and cerebellar multiple

system atrophy. Cerebellum Lond. Engl. 10, 208–217. doi:10.1007/s12311-010-0213-6

Packer, R.J., Zhou, T., Holmes, E., Vezina, G., Gajjar, A., 2013. Survival and secondary tumors in children with medulloblastoma receiving radiotherapy and adjuvant chemotherapy: results of Children's Oncology Group trial A9961. Neuro-Oncol. 15, 97–103. doi:10.1093/neuonc/nos267

Padovani, L., André, N., Constine, L.S., Muracciole, X., 2012. Neurocognitive function after radiotherapy for paediatric brain tumours. Nat. Rev. Neurol. 8, 578–588. doi:10.1038/nrneurol.2012.182

Pajtler, K.W., Witt, H., Sill, M., Jones, D.T.W., Hovestadt, V., Kratochwil, F., Wani, K., Tatevossian, R., Punchihewa, C., Johann, P., Reimand, J., Warnatz, H.-J., Ryzhova, M., Mack, S., Ramaswamy, V., Capper, D., Schweizer, L., Sieber, L., Wittmann, A., Huang, Z., van Sluis, P., Volckmann, R., Koster, J., Versteeg, R., Fults, D., Toledano, H., Avigad, S., Hoffman, L.M., Donson, A.M., Foreman, N., Hewer, E., Zitterbart, K., Gilbert, M., Armstrong, T.S., Gupta, N., Allen, J.C., Karajannis, M.A., Zagzag, D., Hasselblatt, M., Kulozik, A.E., Witt, O., Collins, V.P., von Hoff, K., Rutkowski, S., Pietsch, T., Bader, G., Yaspo, M.-L., von Deimling, A., Lichter, P., Taylor, M.D., Gilbertson, R., Ellison, D.W., Aldape, K., Korshunov, A., Kool, M., Pfister, S.M., 2015. Molecular Classification of Ependymal Tumors across All CNS Compartments, Histopathological Grades, and Age Groups. Cancer Cell 27, 728–743. doi:10.1016/j.ccell.2015.04.002

Panigrahy, A., Blüml, S., 2009. Neuroimaging of pediatric brain tumors: from basic to advanced magnetic resonance imaging (MRI). J. Child Neurol. 24, 1343–1365. doi:10.1177/0883073809342129

Panigrahy, A., Borzage, M., Blüml, S., 2010a. BASIC PRINCIPLES AND CONCEPTS UNDERLYING RECENT ADVANCES IN MRI OF THE DEVELOPING BRAIN. Semin. Perinatol. 34, 3–19. doi:10.1053/j.semperi.2009.10.001

Panigrahy, A., Krieger, M.D., Gonzalez-Gomez, I., Liu, X., McComb, J.G., Finlay, J.L., Nelson, M.D., Gilles, F.H., Blüml, S., 2006. Quantitative short echo time 1H-MR spectroscopy of untreated pediatric brain tumors: preoperative diagnosis and characterization. AJNR Am. J. Neuroradiol. 27, 560–572.

Panigrahy, A., Nelson, M.D., Blüml, S., 2010b. Magnetic resonance spectroscopy in pediatric neuroradiology: clinical and research applications. Pediatr. Radiol. 40, 3–30. doi:10.1007/s00247-009-1450-z

Parihar, V.K., Limoli, C.L., 2013. Cranial irradiation compromises neuronal architecture in the hippocampus. Proc. Natl. Acad. Sci. 110, 12822–12827. doi:10.1073/pnas.1307301110

Peet, A.C., Arvanitis, T.N., Leach, M.O., Waldman, A.D., 2012. Functional imaging in adult and paediatric brain tumours. Nat. Rev. Clin. Oncol. 9, 700–711. doi:10.1038/nrclinonc.2012.187

Peet, A.C., Lateef, S., MacPherson, L., Natarajan, K., Sgouros, S., Grundy, R.G., 2007. Short echo time 1 H magnetic resonance spectroscopy of childhood brain tumours. Childs Nerv. Syst. ChNS Off. J. Int. Soc. Pediatr. Neurosurg. 23, 163–169. doi:10.1007/s00381-006-0206-4

Penner, J., Rupsingh, R., Smith, M., Wells, J.L., Borrie, M.J., Bartha, R., 2010. Increased glutamate in the hippocampus after galantamine treatment for Alzheimer disease.

Prog. Neuropsychopharmacol. Biol. Psychiatry 34, 104–110.
doi:10.1016/j.pnpbp.2009.10.007

Pirzkall, A., McGue, C., Saraswathy, S., Cha, S., Liu, R., Vandenberg, S., Lamborn, K.R., Berger, M.S., Chang, S.M., Nelson, S.J., 2009. Tumor regrowth between surgery and initiation of adjuvant therapy in patients with newly diagnosed glioblastoma. Neuro-Oncol. 11, 842–852. doi:10.1215/15228517-2009-005

Poudel, G.R., Stout, J.C., Domínguez D, J.F., Salmon, L., Churchyard, A., Chua, P., Georgiou-Karistianis, N., Egan, G.F., 2014. White matter connectivity reflects clinical and cognitive status in Huntington's disease. Neurobiol. Dis. 65, 180–187. doi:10.1016/j.nbd.2014.01.013

Posse, S., Otazo, R., Dager, S.R., Alger, J., 2013. MR spectroscopic imaging: principles and recent advances. J. Magn. Reson. Imaging JMRI 37, 1301–1325. doi:10.1002/jmri.23945

Prescot, A.P., Frederick, B. deB, Wang, L., Brown, J., Jensen, J.E., Kaufman, M.J., Renshaw, P.F., 2006. In vivo detection of brain glycine with echo-time-averaged 1H magnetic resonance spectroscopy at 4.0 T. Magn. Reson. Med. 55, 681–686. doi:10.1002/mrm.20807

Preul, M.C., Caramanos, Z., Collins, D.L., Villemure, J.G., Leblanc, R., Olivier, A., Pokrupa, R., Arnold, D.L., 1996. Accurate, noninvasive diagnosis of human brain tumors by using proton magnetic resonance spectroscopy. Nat. Med. 2, 323–325.

Provencher, S.W., 2001a. Automatic quantitation of localized in vivo 1H spectra with LCModel. NMR Biomed. 14, 260–264.

Provencher, S.W., 1993. Estimation of metabolite concentrations from localized in vivo proton NMR spectra. Magn. Reson. Med. 30, 672–679.

Puget, S., Philippe, C., Bax, D.A., Job, B., Varlet, P., Junier, M.-P., Andreiuolo, F., Carvalho, D., Reis, R., Guerrini-Rousseau, L., Roujeau, T., Dessen, P., Richon, C., Lazar, V., Le Teuff, G., Sainte-Rose, C., Geoerger, B., Vassal, G., Jones, C., Grill, J., 2012. Mesenchymal transition and PDGFRA amplification/mutation are key distinct oncogenic events in pediatric diffuse intrinsic pontine gliomas. PloS One 7, e30313. doi:10.1371/journal.pone.0030313

Quon, H., Brunet, B., Alexander, A., Murtha, A., Abdulkarim, B., Fulton, D., Smerdely, M., Johnson, M., Urtasun, R., Patel, S., Ghosh, S., Roa, W., 2011. Changes in serial magnetic resonance spectroscopy predict outcome in high-grade glioma during and after postoperative radiotherapy. Anticancer Res. 31, 3559–3565.

Raschke, F., Jones, T.L., Barrick, T.R., Howe, F.A., 2014. Delineation of gliomas using radial metabolite indexing. NMR Biomed. 27, 1053–1062. doi:10.1002/nbm.3154

Ray, K.J., Larkin, J.R., Tee, Y.K., Khrapitchev, A.A., Karunanithy, G., Barber, M., Baldwin, A.J., Chappell, M.A., Sibson, N.R., 2016. Determination of an optimally sensitive and specific chemical exchange saturation transfer MRI quantification metric in relevant biological phantoms. Nmr Biomed. 29, 1624–1633. doi:10.1002/nbm.3614

Risacher, S.L., Saykin, A.J., 2013. Neuroimaging biomarkers of neurodegenerative diseases and dementia. Semin. Neurol. 33, 386–416. doi:10.1055/s-0033-1359312

Rodriguez Gutierrez, D., Awwad, A., Meijer, L., Manita, M., Jaspan, T., Dineen, R.A., Grundy, R.G., Auer, D.P., 2014. Metrics and textural features of MRI diffusion to improve

classification of pediatric posterior fossa tumors. AJNR Am. J. Neuroradiol. 35, 1009–1015. doi:10.3174/ajnr.A3784

Rorden, C., Brett, M., 2000. Stereotaxic display of brain lesions. Behav. Neurol. 12, 191–200.

Rumboldt, Z., Camacho, D.L.A., Lake, D., Welsh, C.T., Castillo, M., 2006. Apparent diffusion coefficients for differentiation of cerebellar tumors in children. AJNR Am. J. Neuroradiol. 27, 1362–1369.

Rupsingh, R., Borrie, M., Smith, M., Wells, J.L., Bartha, R., 2011. Reduced hippocampal glutamate in Alzheimer disease. Neurobiol. Aging 32, 802–810. doi:10.1016/j.neurobiolaging.2009.05.002

Ryner, L.N., Sorenson, J.A., Thomas, M.A., 1995. 3D localized 2D NMR spectroscopy on an MRI scanner. J. Magn. Reson. B 107, 126–137.

Sarma, M.K., Nagarajan, R., Macey, P.M., Kumar, R., Villablanca, J.P., Furuyama, J., Thomas, M.A., 2014. Accelerated Echo-Planar J-Resolved Spectroscopic Imaging in the Human Brain Using Compressed Sensing: A Pilot Validation in Obstructive Sleep Apnea. AJNR Am. J. Neuroradiol. 35, S81–S89. doi:10.3174/ajnr.A3846

Schubert, F., Gallinat, J., Seifert, F., Rinneberg, H., 2004a. Glutamate concentrations in human brain using single voxel proton magnetic resonance spectroscopy at 3 Tesla. NeuroImage 21, 1762–1771. doi:10.1016/j.neuroimage.2003.11.014

Schulte, R.F., Boesiger, P., 2006. ProFit: two-dimensional prior-knowledge fitting of J-resolved spectra. NMR Biomed. 19, 255–263. doi:10.1002/nbm.1026

Seymour, Z.A., Panigrahy, A., Finlay, J.L., Nelson, M.D., Blüml, S., 2008. Citrate in Pediatric CNS Tumors? Am. J. Neuroradiol. 29, 1006–1011. doi:10.3174/ajnr.A1018

Sijens, P.E., Oudkerk, M., 2002. 1H chemical shift imaging characterization of human brain tumor and edema. Eur. Radiol. 12, 2056–2061. doi:10.1007/s00330-001-1300-3

Simister, R.J., Woermann, F.G., McLean, M.A., Bartlett, P.A., Barker, G.J., Duncan, J.S., 2002. A Short-echo-time Proton Magnetic Resonance Spectroscopic Imaging Study of Temporal Lobe Epilepsy. Epilepsia 43, 1021–1031. doi:10.1046/j.1528-1157.2002.50701.x

Smith, S.A., Levante, T.O., Meier, B.H., Ernst, R.R., 1994. Computer Simulations in Magnetic Resonance. An Object-Oriented Programming Approach. J. Magn. Reson. A 106, 75–105. doi:10.1006/jmra.1994.1008

Smith, S.M., 2002. Fast robust automated brain extraction. Hum. Brain Mapp. 17, 143–155. doi:10.1002/hbm.10062

Smith, S.M., Jenkinson, M., Woolrich, M.W., Beckmann, C.F., Behrens, T.E.J., Johansen-Berg, H., Bannister, P.R., De Luca, M., Drobnjak, I., Flitney, D.E., Niazy, R.K., Saunders, J., Vickers, J., Zhang, Y., De Stefano, N., Brady, J.M., Matthews, P.M., 2004. Advances in functional and structural MR image analysis and implementation as FSL. NeuroImage 23 Suppl 1, S208-219. doi:10.1016/j.neuroimage.2004.07.051

Smyth, M.D., Rubin, J., 2010. Ependymoma, in: Gupta, N., Banerjee, A., Haas-Kogan, D. (Eds.), Pediatric CNS Tumors, Pediatric Oncology. Springer Berlin Heidelberg, pp. 67–87.

Snyder, J., Thompson, R.B., Wilman, A.H., 2010. Difference spectroscopy using PRESS asymmetry: application to glutamate, glutamine, and myo-inositol. NMR Biomed. 23, 41–47. doi:10.1002/nbm.1424

Snyder, J., Wilman, A., 2010a. Field strength dependence of PRESS timings for simultaneous detection of glutamate and glutamine from 1.5 to 7T. J. Magn. Reson. San Diego Calif 1997 203, 66–72. doi:10.1016/j.jmr.2009.12.002

Snyder, J., Wilman, A., 2010b. Field strength dependence of PRESS timings for simultaneous detection of glutamate and glutamine from 1.5 to 7T. J. Magn. Reson. San Diego Calif 1997 203, 66–72. doi:10.1016/j.jmr.2009.12.002

Soeiro-de-Souza, M.G., Henning, A., Machado-Vieira, R., Moreno, R.A., Pastorello, B.F., da Costa Leite, C., Vallada, H., Otaduy, M.C.G., 2015. Anterior cingulate Glutamate–Glutamine cycle metabolites are altered in euthymic bipolar I disorder. Eur. Neuropsychopharmacol. 25, 2221–2229. doi:10.1016/j.euroneuro.2015.09.020

Soher, B., Semanchuk, P., Todd, D., Steinberg, J., Young, K., 2011. VeSPA: Integrated applications for RF pulse design, spectral simulation and MRS data analysis. Presented at the ISMRM, Montreal, Quebec, Canader.

Squitieri, F., Cannella, M., Simonelli, M., Sassone, J., Martino, T., Venditti, E., Ciammola, A., Colonnese, C., Frati, L., Ciarmiello, A., 2009. Distinct brain volume changes correlating with clinical stage, disease progression rate, mutation size, and age at onset prediction as early biomarkers of brain atrophy in Huntington's disease. CNS Neurosci. Ther. 15, 1–11. doi:10.1111/j.1755-5949.2008.00068.x

Stanisz, G.J., Odrobina, E.E., Pun, J., Escaravage, M., Graham, S.J., Bronskill, M.J., Henkelman, R.M., 2005. T1, T2 relaxation and magnetization transfer in tissue at 3T. Magn. Reson. Med. 54, 507–512. doi:10.1002/mrm.20605

Stebbins, G.T., Murphy, C.M., 2009. Diffusion tensor imaging in Alzheimer's disease and mild cognitive impairment. Behav. Neurol. 21, 39–49. doi:10.3233/BEN-2009-0234

Steffen-Smith, E.A., Shih, J.H., Hipp, S.J., Bent, R., Warren, K.E., 2011a. Proton magnetic resonance spectroscopy predicts survival in children with diffuse intrinsic pontine glioma. J. Neurooncol. 105, 365–373. doi:10.1007/s11060-011-0601-x

Stoessl, A.J., 2012. Neuroimaging in the early diagnosis of neurodegenerative disease. Transl. Neurodegener. 1, 5. doi:10.1186/2047-9158-1-5

Sturrock, A., Laule, C., Wyper, K., Milner, R.A., Decolongon, J., Dar Santos, R., Coleman, A.J., Carter, K., Creighton, S., Bechtel, N., Bohlen, S., Reilmann, R., Johnson, H.J., Hayden, M.R., Tabrizi, S.J., Mackay, A.L., Leavitt, B.R., 2015. A longitudinal study of magnetic resonance spectroscopy Huntington's disease biomarkers. Mov. Disord. Off. J. Mov. Disord. Soc. 30, 393–401. doi:10.1002/mds.26118

Tamrazi, B., Nelson, M.D., Blüml, S., 2016. MRS of pilocytic astrocytoma: The peak at 2 ppm may not be NAA. Magn. Reson. Med. doi:10.1002/mrm.26374

Tate, A.R., Underwood, J., Acosta, D.M., Julià-Sapé, M., Majós, C., Moreno-Torres, A., Howe, F.A., van der Graaf, M., Lefournier, V., Murphy, M.M., Loosemore, A., Ladroue, C., Wesseling, P., Luc Bosson, J., Cabañas, M.E., Simonetti, A.W., Gajewicz, W., Calvar, J., Capdevila, A., Wilkins, P.R., Bell, B.A., Rémy, C., Heerschap, A., Watson, D., Griffiths, J.R., Arús, C., 2006. Development of a decision support system for diagnosis and grading of brain tumours using in vivo magnetic resonance single voxel spectra. NMR Biomed. 19, 411–434. doi:10.1002/nbm.1016

Taylor, M.D., Northcott, P.A., Korshunov, A., Remke, M., Cho, Y.-J., Clifford, S.C., Eberhart, C.G., Parsons, D.W., Rutkowski, S., Gajjar, A., Ellison, D.W., Lichter, P., Gilbertson, R.J., Pomeroy, S.L., Kool, M., Pfister, S.M., 2012. Molecular subgroups of

medulloblastoma: the current consensus. Acta Neuropathol. (Berl.) 123, 465–472. doi:10.1007/s00401-011-0922-z

Thomas, M.A., Hattori, N., Umeda, M., Sawada, T., Naruse, S., 2003. Evaluation of two-dimensional L-COSY and JPRESS using a 3 T MRI scanner: from phantoms to human brain in vivo. NMR Biomed. 16, 245–251. doi:10.1002/nbm.825

Thomas, M.A., Ryner, L.N., Mehta, M.P., Turski, P.A., Sorenson, J.A., 1996. Localized 2D J-resolved 1H MR spectroscopy of human brain tumors in vivo. J. Magn. Reson. Imaging JMRI 6, 453–459.

Tisell, A., Leinhard, O.D., Warntjes, J.B.M., Lundberg, P., 2013. Procedure for quantitative 1H magnetic resonance spectroscopy and tissue characterization of human brain tissue based on the use of quantitative magnetic resonance imaging. Magn. Reson. Med. 70, 905–915. doi:10.1002/mrm.24554

Träber, F., Block, W., Lamerichs, R., Gieseke, J., Schild, H.H., 2004a. 1H metabolite relaxation times at 3.0 tesla: Measurements of T1 and T2 values in normal brain and determination of regional differences in transverse relaxation. J. Magn. Reson. Imaging 19, 537–545. doi:10.1002/jmri.20053

K., Brandt, J., Bassett, S.S., Redgrave, G.W., Margolis, R.L., van Zijl, P.C.M., Barker, P.B., Ross, C.A., 2012. Brain metabolite alterations and cognitive dysfunction in early Huntington's disease. Mov. Disord. Off. J. Mov. Disord. Soc. 27, 895–902. doi:10.1002/mds.25010

Vaidya, K., Smee, R., Williams, J.R., 2012. Prognostic factors and treatment options for paediatric ependymomas. J. Clin. Neurosci. Off. J. Neurosurg. Soc. Australas. 19, 1228–1235. doi:10.1016/j.jocn.2012.02.006

Veech, R.L., 1991. The metabolism of lactate. NMR Biomed. 4, 53–58.

Vicente, J., Fuster-Garcia, E., Tortajada, S., García-Gómez, J.M., Davies, N., Natarajan, K., Wilson, M., Grundy, R.G., Wesseling, P., Monleón, D., Celda, B., Robles, M., Peet, A.C., 2013. Accurate classification of childhood brain tumours by in vivo ^{1}H MRS - a multi-centre study. Eur. J. Cancer Oxf. Engl. 1990 49, 658–667. doi:10.1016/j.ejca.2012.09.003

Wansapura, J.P., Holland, S.K., Dunn, R.S., Ball, W.S., 1999. NMR relaxation times in the human brain at 3.0 tesla. J. Magn. Reson. Imaging JMRI 9, 531–538.

Weaver, K.E., Richards, T.L., Logsdon, R.G., McGough, E.L., Minoshima, S., Aylward, E.H., Kleinhans, N.M., Grabowski, T.J., McCurry, S.M., Teri, L., 2015. Posterior Cingulate Lactate as a Metabolic Biomarker in Amnestic Mild Cognitive Impairment. BioMed Res. Int. 2015. doi:10.1155/2015/610605

Wilson, M., Cummins, C.L., MacPherson, L., Sun, Y., Natarajan, K., Grundy, R.G., Arvanitis, T.N., Kauppinen, R.A., Peet, A.C., 2013. Magnetic resonance spectroscopy metabolite profiles predict survival in paediatric brain tumours. Eur. J. Cancer 49, 457–464. doi:10.1016/j.ejca.2012.09.002

Wilson, M., Davies, N.P., Brundler, M.-A., McConville, C., Grundy, R.G., Peet, A.C., 2009a. High resolution magic angle spinning 1H NMR of childhood brain and nervous system tumours. Mol. Cancer 8, 6. doi:10.1186/1476-4598-8-6

Wilson, M., Davies, N.P., Grundy, R.G., Peet, A.C., 2009b. A quantitative comparison of metabolite signals as detected by in vivo MRS with ex vivo 1H HR-MAS for childhood brain tumours. NMR Biomed. 22, 213–219. doi:10.1002/nbm.1306

Wilson, M., Gill, S.K., MacPherson, L., English, M., Arvanitis, T.N., Peet, A.C., 2014. Noninvasive detection of glutamate predicts survival in pediatric medulloblastoma. Clin. Cancer Res. Off. J. Am. Assoc. Cancer Res. 20, 4532–4539. doi:10.1158/1078-0432.CCR-13-2320

Wilson, M., Reynolds, G., Kauppinen, R.A., Arvanitis, T.N., Peet, A.C., 2011a. A constrained least-squares approach to the automated quantitation of in vivo ^{1}H magnetic resonance spectroscopy data. Magn. Reson. Med. 65, 1–12. doi:10.1002/mrm.22579

Xin, L., Gambarota, G., Mlynárik, V., Gruetter, R., 2008b. Proton T2 relaxation time of J-coupled cerebral metabolites in rat brain at 9.4 T. NMR Biomed. 21, 396–401. doi:10.1002/nbm.1205

Yamamoto, T., Isobe, T., Akutsu, H., Masumoto, T., Ando, H., Sato, E., Takada, K., Anno, I., Matsumura, A., 2015a. Influence of echo time in quantitative proton MR spectroscopy using LCModel. Magn. Reson. Imaging 33, 644–648. doi:10.1016/j.mri.2015.01.015

Zacharoulis, S., Moreno, L., 2009. Ependymoma: an update. J. Child Neurol. 24, 1431–1438. doi:10.1177/0883073809339212

Zhang, Y., Brady, M., Smith, S., 2001. Segmentation of brain MR images through a hidden Markov random field model and the expectation-maximization algorithm. IEEE Trans. Med. Imaging 20, 45–57. doi:10.1109/42.906424

Zhu, H., Barker, P.B., 2011. MR Spectroscopy and Spectroscopic Imaging of the Brain. Methods Mol. Biol. Clifton NJ 711, 203–226. doi:10.1007/978-1-61737-992-5_9